Tectonic and Sea Level Control on the Transport and Depositional Processes in a Siliciclastic Sedimentary Basin. Insights from the Ganges-Brahmaputra Delta, Bengal Basin, Bangladesh.

Dissertation for the Doctoral Degree in Natural Sciences

(Dr. rer. nat.)

in the Faculty of Geosciences at the University of Bremen

submitted by

Luisa Palamenghi

April 2012

- Gutachter -

Prof. Dr. Volkhard Spiess

Prof. Dr. Till Hanebuth

Declaration

Name: Luisa Palamenghi
Address: Vor Dem Steintor 138
28203, Bremen

Herewith I declare that

I. This document and the accompanying data has been composed by myself, and describes my own work

II. Material from the published or unpublished work of others, which is referred to in the dissertation, is credited to the author in the text.

III. This work has not been submitted for any other degree.

Bremen, 30th April 2012

…….
(Signature)

~Acknowledgements~

This work was done within the Project ‘‘SO-188-Bengal Sea Level’’, funded by the German Ministry of Education and Science (BMBF), Grant no. 03G0188A and the DFG project ‘‘Bengal Shelf IODP’’, Grant no. SP296/31-1. An additional extension on the funding was kindly offered by the Family Support within the framework of the GLOMAR Bremen International Graduate School for Marine Science funded by the DFG under the Excellence Initiative by the German federal and state governments to promote science and research at German Universities.

The constant, constructive and sometime even strenuous support and assistance received from Prof. Dr. V. Spiess and from Dr. T. Schwenk has helped me to understand, not only the relevance of this study in terms of its academic importance, but also to contextualize it within a broader vision. The comprehension they had and the encouragement I received with respect to the delay due to the birth of my son Nico is praiseworthy. I sincerely thank them.

My critical perspective on scientific questions and the learning processes to answer them has enormously benefitted of the experience and extraordinary education of Dr. H.-R. Kudrass.

Prof. Dr. C. France-Lanord, member of my Glomar Committee, has helped me to finalize my results adding interesting and stimulating hints for reflection and research.

I am very grateful to the members and colleagues of the Research Group Marine Technology and Environmental Research of the Geosciences Department of the Bremen University. Thanks to those who are still here and to who is gone. A friendly and collaborative atmosphere has always permitted to pass from a PhD to the next one, like a baton in a relay, the knowledge collected in the many years of data acquisition, processing and interpretation.

A special mention goes also to Dr. S. Mulitza that rejected my application for another PhD position but, like a keystone, he spontaneously introduced me to my future supervisors. Thank you very much.

Thanks also to the several generations of PhDs, Post Docs and friends that have populated my stay in this city, Bremen, a big harbour that welcomed us all and let us go with no regrets having added a great and luminous chapter to our life.

Not a single moment my motivation failed thanks to the love of my parents and of my son,
this PhD Thesis is dedicated to them.

~Abstract~

Climate, tectonic and sea level changes are the primary drivers for sedimentary basin dynamics at any time and space scale. Their frequency and cyclicity is far from being completely understood especially due to their mutual interaction which makes it very hard to distinguish between the cause and the effect of the observed phenomenology. One of the greatest scientific challenge emerged in the 21st Century is the urgent need to quantify the anthropogenic impact on natural systems as it has been claimed to be equally a primary driver or even locally overwhelming the natural factors.

This study will focus on the tectonic and sea level changes impact on a sedimentary basin and will examine in detail the events succession within sedimentary sequences. This is made in the perspective of building robust boundary conditions for modelling of future scenario, of constraining events with high geo-hazard impact and of implement for environmental sustainable integrated management of the coastal zones.

The case study presented in this PhD Thesis is the Ganges-Brahmaputra Delta, which feeds the Bengal Basin since the Eocene under the effect of the monsoon climate, the convergent tectonic setting and sea level oscillations. This mega-delta is unanimously considered in great peril as lying just few meters above sea level and associated with the India-Eurasia subduction zone. The project is part of a long term cooperation between the University of Bremen and the BGR, Hannover, which existed since 1993 and resulted in four expeditions with the R/V Sonne to the Bay of Bengal. In the study, an integrated approach of source-to-sink reconstruction of the depositional history of siliciclastic sequences was carried out. In particular, the sedimentary record has been evaluated on different time scales from decades to millennia. Beyond the relevance of the study area, the results could be of great help in the understanding the forcing controlling passive continental margins and their terrestrial sediment sources.

For the achievement of these purposes, seismo-acoustic data mainly collected during the SO188-2 Expedition (2006) were analyzed. The data has been processed, interpreted using the basic principles of sequence stratigraphy and integrated with previously collected sedimentological data to obtain new insights in the process stratigraphy of the two major deposition elements on the Bengal Shelf, the Ganges-Brahmaputra subaqueous delta and the Swatch of No Ground shelf canyon. In addition it has been studied: the compaction trends due to the burial overpressure, the tectonic subsidence, the shoreline and shelf break trajectories.

A robust chrono-stratigraphic framework has been developed using the existing seismostratigraphic models for system tract identification based on a global sea curve with centennial to millennial resolution. The response of the depositional system to different sea level stands and the migration of

the shelf depocentre through last glacial-interglacial cycle (123-0 ka) could be identified. A substantial asymmetric distribution is found in a multi-source ramp setting build-up by the contemporaneous formation of a mid- to shelf margin delta on the eastern Bengal Shelf and the channelization of turbidity currents through the canyon in the west.

In general, the tectonic subsidence has been evaluated in the order of 0.175 m/ka during last glacial-interglacial cycle. The lithostatic stress caused by the sedimentation of the last glacial-interglacial cycle composite sequence (10-35 m) has produced as much accommodation as the thickness of the sequence but the additional accommodation caused by the overburden pressure within the sequence is of maximum 0.4 m. Since sea level variations are not sufficient to explain the imbalance of the depocentre distribution on the shelf, the obtained values are applied to rebound shoreline- and shelf break depths. The western shelf has indeed degenerated and no bypass occurred through this threshold but in the canyon. Sediment bypass across the eastern shelf break occurred within a normal shoreline regression. Additionally, the results show that the receiving morphological reliefs of the Bengal Basin are all dipping toward the west with a increasing slope angle during the last glacial-interglacial cycle, which may possibly indicate active elevation of the eastern Bengal Shelf close to the continent-ocean margin.

Concerning the creation of the shelf canyon Swatch of No Ground, the data analysis suggests, that this canyon developed because shelf channels (subaerial or subaqueous) sufficiently persisted in time and optimally located in space, and thereby become chronically entrenched due to the continuous vertical shelf accretion beside. Active tectonic processes on the Bengal Shelf might have contributed to the initial formation and consolidation of the Swatch of No Ground canyon as a preferential conduit toward the Bengal Fan by keeping a knick point constantly located close or at the canyon head. This could have diverted the drainage during falling and low sea level stands from the western shelf toward the canyon as observed in the paleo-drainage reconstruction.

High-resolution analysis of the modern submarine Ganges-Brahmaputra Delta reveal that transparent Units (TUs) are the most prominent, continuously traceable architectural elements within the sigmoidal clinoform. TUs are interpreted to be formed by liquefaction flows generated by earthquakes and could be related to the historical well known major earthquakes which occurred in 1762, 1897 and 1950. Using the TUs as time marks it could be shown that the mean annual storage rates have been significantly decreased within the last _300 years from 22% down to 13.8% of the present total annual fluviatile suspension supply to the delta. However, the decrease is mainly focused on the eastern part of the submarine delta. This asymmetry is also manifested in the clinoform shapes, the eastern foreset beds are grading toward a convex shape whereas the western foreset beds are grading toward a concave clinoform. The decreased mean annual storage rate in the eastern clinoform is probably significantly induced by the decline in monsoon precipitation over the last centuries. The

asymmetry of foreset deposition suggests that the whole depocentre of the fluvial sediment load is shifting toward the western subaqueous delta and to the Swatch of No Ground Canyon and, thereby, increasing the export to the deep-sea fan.

~Zusammenfassung~

Klima, Tektonik und Meeresspiegelschwankungen sind die wichtigsten kontrollierenden Faktoren der Dynamik von Sedimentbecken auf allen Zeit- und Raumskalen. Ihre Frequenz und Zyklizität sind bei weitem noch nicht vollständig verstanden, da es durch die herrschenden Wechselwirkungen schwierig ist, zwischen Ursachen und Wirkungen der beobachteten Phänomene zu unterscheiden. Eine der größten wissenschaftlichen Herausforderungen des 21. Jahrhunderts ist die Quantifizierung des anthropogenen Einflusses auf natürliche Systeme, da vermutetet wird, dass diese genauso wichtig sein können wie natürliche Kontrollfaktoren, oder diese zumindest lokal dominieren können.

Diese Arbeit konzentriert sich auf den Einfluss von Tektonik und Meeresspiegel auf Sedimentbecken, um dabei die Abfolge von Ereignissen innerhalb von Sedimentsequenzen im Detail herauszuarbeiten. Eine Motivation dabei ist auch, robuste Randbedingungen für Zukunftsmodelle zu bestimmen, die sich insbesondere mit dem Einfluss von Geo-Risiken und der Entwicklung von nachhaltigem Küstenzonen-Management beschäftigen.

Die hier präsentierte Fallstudie befasst sich mit dem Ganges-Brahmaputra Delta, welches das Bengal Becken seit dem Eozän auffüllt. Dieser Prozess ist stark beeinflusst vom Monsun-Klima, der konvergenten Tektonik und den Meeresspiegelschwankungen. Heute sieht sich dieses Mega-Delta unzweifelhaft einer großen Gefährdung ausgesetzt, da es nur wenige Meter über dem Meeresspiegel und nahe an der Indien-Eurasien Subduktionszone liegt. Das wissenschaftliche Projekt, welches sich mit diesen Fragen beschäftigt, ist Teil einer langjährigen Kooperation zwischen der Universität Bremen und der BGR, Hannover, die seit 1993 existiert und von vier Ausfahrten mit der FS Sonne in den Golf von Bengalen begleitet wurde. Innerhalb dieser Studie wurde ein integrierter Ansatz gewählt, um eine "Source-to-Sink" Rekonstruktion der Depositionsgeschichte der siliklastischen Sequenzen durchzuführen. Insbesondere wurde das sedimentäre Archiv auf unterschiedlichen Zeitskalen von Dekaden bis Millennien untersucht. Über die Relevanz für das Arbeitsgebiet hinaus sollen die Ergebnisse zum grundsätzlichen Verständnis der Kontrollfaktoren von passiven Kontinentalrändern und ihrer terrestrischen Quellen beitragen.

Um diese Ziele zu erreichen, wurde ein seismo-akustischer Datensatz untersucht, der hauptsächlich auf der Fahrt SO 188-2 (2006) gesammelt wurde. Die Daten wurden prozessiert und dann interpretiert, in dem die Grundprinzipien der Sequenzstratigraphie angewandt wurden. Vorliegende sedimentologische Ergebnisse wurden integriert, um neue Erkenntnisse über die Stratigraphie der wichtigsten Depositionsorte auf dem Bengal Schelf zu erlangen, nämlich dem submarinen Delta und

dem Schelfcanyon "Swatch of No Ground". Weiterhin wurden die Kompaktionstrends, die tektonische Subsidenz sowie Küstenlinien- und Schelfkanten-Trajektorien untersucht.

Ein robuster chrono-stratigraphischer Rahmen wurde entwickelt, in dem die existierenden seismostratigraphischen Modelle zur Identifikation von Ablagerungsräumen basierend auf einer globalen Meeresspiegelkurve benutzt wurden, und zwar mit einer zeitlichen Auflösung von Jahrhunderten bis Millennien. Die Reaktion des depositionalen Systems auf unterschiedliche Meeresspiegel und die Migration von Schelfdepozentren während des letzten Glazial-Interglazialzyklus wurde analysiert. Dabei zeigte sich eine asymmetrische Verteilung dergestalt, dass sich auf dem östlichen Schelf ein Delta vom mittleren Schelf bis zur Schelfkante entwickelt hat, während auf dem westlichen Schelf der Sedimenttransport durch den Canyon kanalisiert wurden.

Die Abschätzung der tektonischen Subsidenz ergab generell einen Wert von ca. 0,175 m/ka für den letzten Glazial-Interglazialzyklus. Der lithostatische Druck, der durch die Ablagerung innerhalb dieses Zyklus erzeugt wurde, kreierte letztendlich einen zusätzlichen Akkomodationsraum von höchsten 0,4 m. Da die Meeresspiegelschwankungen allein nicht ausreichen, die Konfiguration der Depositionszentren auf dem Schelf zu erklären, wurden die ermittelten Werte angewandt um die Tiefen von Küstenlinien und Schelfkanten zu korrigieren. Dabei zeigte sich, dass der westliche Schelf in der Tat degenerierte und der Sedimentabfluss durch den Canyon erfolgen musste, während auf dem östlichen Schelf der Sedimentfluss über die Schelfkante innerhalb einer normalen Regression erfolgte. Zusätzliche erbrachten die Berechnungen, dass die jeweiligen Oberflächen des Bengal Beckens nach Westen geneigt waren, wobei diese Neigung während des letzten Glazial-Interglazialzyklus verstärkt wurde. Dies könnte durch eine rezente tektonische Hebung des östlichen Schelfs, der nahe an der tektonischen Kontinent-Ozean Grenze liegt, erklärt werden.

Die Analyse der Daten vom Schelfcanyon weisen darauf hin, dass dieser Canyon sich entwickelt hat, weil die Position von Schelfkanälen (submarin oder subaerisch) sich über die Zeit räumlich nicht verändert hat, und sich somit dieser Einschnitt durch das kontinuierliche Anwachsen des Schelfes neben dem Einschnitt immer weiter vertieft hat. Aktive tektonische Prozesse auf dem Bengal Schelf mögen zur Initiation und Konsolidierung des Canyons beigetragen haben, da sich wahrscheinlich eine Knickpunkt konstant an der Stelle des oberen Canyon Ende befunden hat. Dies könnte dann zur beobachteten Trennung der Drainage auf dem Schelf während des fallenden und tiefsten Meeresspiegelstandes beigetragen haben.

Die hochauflösende Analyse des modernen submarinen Ganges-Brahmaputra Delta erbrachte, dass transparente Einheiten (TUs) die wichtigsten, kontinuierlich verfolgbaren Strukturelemente innerhalb der sigmoidalen Klinoformen sind. Diese TUs wurden interpretiert als das Ergebnis kurzzeitiger Sedimentverflüssigung, die durch Erbeben ausgelöst wurde, und konnten den historisch bekannten Erdbeben von 1762, 1897 und 1950 zugeordnet werden. Mittels der TUs als Zeitmarken konnte gezeigt werden, dass die mittlere jährliche Ablagerungsrate während der letzten 300 Jahre

kontinuierlich zurück gegangen ist, und zwar von 22% auf 13% der heutigen vollständigen Suspensionsfracht, die zum Delta transportiert wird. Diese Abnahme konzentriert sich auf das östliche Delta. Auch die Gestalt der Klinoformen zeigt eine Asymmetrie, im östlichen Delta entwickeln sie eine mehr konvexe Form, während sie im westlichen Delta zu einer mehr konkaven Form tendieren. Während der Rückgang der mittleren jährlichen Ablagerung wahrscheinlich durch eine Abnahme der Monsunregen Intensität über die letzten Jahrhunderte verursacht wurde, zeigt die beobachtete Asymmetrie, dass das gesamte Depositionszentrum des fluvialen Inputs nach Westen in Richtung Canyon wandert, und somit der Export der Sedimente zum Tiefseefächer zunimmt.

~ Chapter 1~
Introduction

1.1. The challenge

Climate, tectonic, sea level variations and their mutual interaction are the primary factors controlling the transport and depositional processes within sedimentary basins but the severe alterations in the land- and sea-scapes produced by the athropogenic stress have risen the need to quantify its relative importance (IPCC, 2007). The separation and quantification of the 'natural' and human impacts is a challenge because of the complexity of their interaction (Wang and Hejazi, 2011) where humans are indeed part of Nature and actually one of Its maximum expression in term of species evolution and adaptation to the surrounding environment (Darwin, 1859).

The environmental sustainability will rest heavily on policies and programmes that promote integrated and co-ordinated development at a basin scale for conservation and production goals, and comprehensive protection against erosion from river flow anomalies and sea-water actions that combines structural with human and institutional capability building measures (Du and Zhang, 2000; Inam et al., 2003; Li et al., 2004b; Thanh et al., 2004; Saito, 2005; Wolanski, 2007; Woodroffe et al., 2006).

In order to discern the cause and the effect of the observed phenomenology and to improve predictive capability for future changes due the system drivers (Nicholls et al., 2007; Syvitsky 2009) it has become of fundamental importance a comprehensive understanding of the 'natural' component and the resistance and resilience capability of the basins to perturbations, especially human-induced ones.

The study of past high resolution sedimentary archives is therefore a precious tool to monitor areas or regions where the anthropogenic impact is suspected to have caused significant modifications. Once established a robust framework for sedimentary basin evolution through time scale comparable to those of the human impact such as days, months, years, decades, centuries and millennia it will be possible to observe diversion or re-enforcement of the expected 'natural' behaviour in an integrated vision (Vörösmarty et al., 2000; Cruz et al., 2007).

1.1 Sedimentary basin vulnerability

Potential global vulnerability of natural and human interacting systems addressed in great peril are the deltas and estuaries of the great rivers and particularly the Mega-Deltas coastal zone of the East, South and South-East Asia (Fig. 1.1.). The alluvial and deltaic plains of the Tigri-Eufrates, Indus, Ganges-Brahmaputra, Irrawaddy, Chao Phraya, Mekong, Red River, Pearl River, Yellow River and the Yangtze support the live hood of millions of people destined to grow in the near future (Ericson et al., 2006; Woodroffe et al., 2006). Natural accommodation created by the tectonic and sea level

variations makes space available to the huge sediment supply derived by the Himalaya and Tibetan Massif accelerated by the weathering of the monsoon climate. Since the industrial revolution in the late Eighteen Century, rates of global sea level rise are progressively exciding the space made available by the 'natural' controlling factors (Syvitzky et al., 2009) and projected values are very likely to result in significant losses of coastal land, ecosystems, infrastructures and economic activities like agriculture, aquaculture and industrial plants (Cruz et al., 2007). In addition to this, sea level intrusion due to sea level rise in the low lying deltaic and alluvial plain will worsen the effects of the storm surge inundation with severe consequences on the temporal or permanent population dislocation and water acidification for irrigation porpoises. Due to reduced drainage capacity of river's fresh water during monsoon floods, as a side effects possible insurgence of cholera epidemy (Han and Webster, 2002; Cruz et al., 2007) may occur in the country side but more dangerously in the Megacities which have developed in the Mega-Deltas (Fig. 1.1.) such as Tianjin ($12x10^6$ inhabitants) grown along the Hai River, which connects to the Yellow and Yangtze Rivers via the Grand Canal; Shanghai on the Yangtze Delta ($23x10^6$ inhabitants); Guangzhou on the Pearl River Delta ($12x10^6$ inhabitants); Bangkok on the Chao Phraya Delta ($14x10^6$ inhabitants); Dhaka at the confluence of the Ganges-Brahmaputra ($16x10^6$ inhabitants); and Karachi close to the Indus Delta ($20x10^6$ inhabitants).

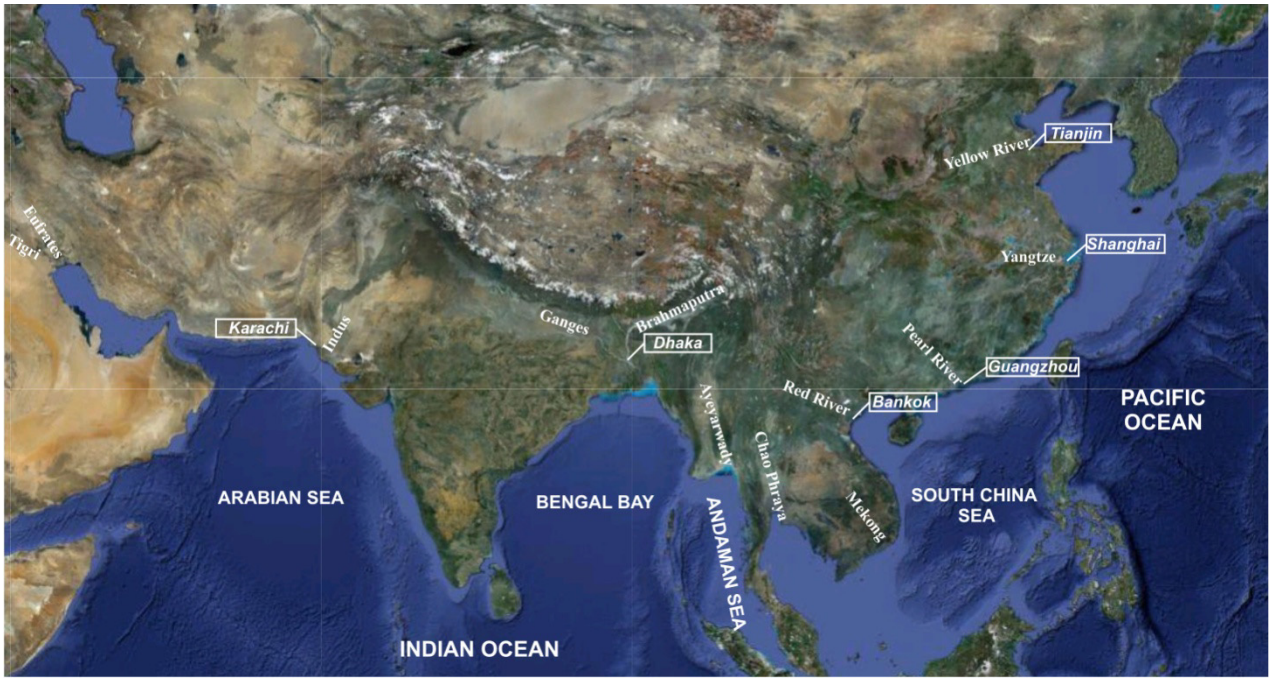

Figure 1.1. Regional map of the Megadeltas coastal zone of the East, South and South-East Asia and of the Megacities which have grown in the delta or in their vicinity (Google Earth, 2012).

Human activities had altered the stream flows directly by affecting the hydrological processes or indirectly by disturbing the climate variables. The direct human impacts on stream flow include land

use change (Schilling et al., 2010; Arrigoni et al., 2010), dam construction and reservoir operation (Rossi et al., 2009), and surface water and groundwater withdrawal and return flow (Weiskel et al., 2007; Wang and Cai, 2010). Human impacts on climate can operate at various spatial scales. For example, at the global scale, human-induced elevated CO^2 emissions contribute to global warming, while at the regional and local scale, irrigation and urbanization may alter precipitations and heat flow (Kustu et al., 2011; Wang and Hejazi, 2011).

Growing evidence suggests the ocean-atmosphere system that controls the global climate can lurch from one state to another. Certain threshold events may become more probable and non-linear changes and surprises should be anticipated, even if they cannot be predicted with a high degree of confidence. Abrupt or unexpected changes pose great challenges to the ability to adapt and can thus increase sedimentary basins vulnerability to significant impacts (Preston et al., 2006).

The spotlight in climate research is shifting from gradual to rapid or abrupt change. There is some risk that a catastrophic collapse of the ice sheet could occur over a couple of centuries if polar water temperatures warm by a few degrees. Scientists suggest that such a risk has a probability of between 1 and 5% (Alley, 2002). Because of this risk, as well as the possibility of a larger than expected melting of the Greenland Ice Sheet, a recent study estimated that there is a 1% chance that global sea level could rise by more than 4 metres in the next two centuries (Hulbe and Payne, 2001). The best estimates of sea level variations indicate however a net rise that lies closer to 2 mm yr^{-1} but local and regional rates may differ being significantly higher from the global mean (Peltier, 2001).

1.3. Principles of Stratigraphy

In a sedimentary basin the description of lithified and unlithified bodies based on their inherent properties and the sediment bodies organization into distintive and mappable units is called statigraphy and is fundamental to establish their distribution, relationship in space and their succession in time, and to interpret geologic history.

Process stratigraphy is the science of the recognition and interpretation of the genetic structures of stratigraphy and its aim is to understand the driving mechanism for the range of stratigraphic architecture found in sedimentary basins. The history of process stratigraphy dates back to the mid-1900s when stratigraphic successions were recognized to be divisible into sedimentary packages separated by uncomformities of inter-regional extent and that landward and seaward shifts of the shoreline were controlled by the relative magnitude of the rate of sea level change and rate of subsidence (Sloss, 1950, 1962, 1963).

In a first instance it was over estimated the role of eustasy (Fig. 1.2) or the global sea level measured from the sea surface to a fixed datum (Haq et al., 1987; Wilgus et al., 1988). The overwhelming estimate of the role of eustasy was reconsidered in the late 1980s (Miall et al., 1991, 1992) and the

new key idea of accommodation was introduced as the space made available for sediment to accumulate (Jervey, 1988).

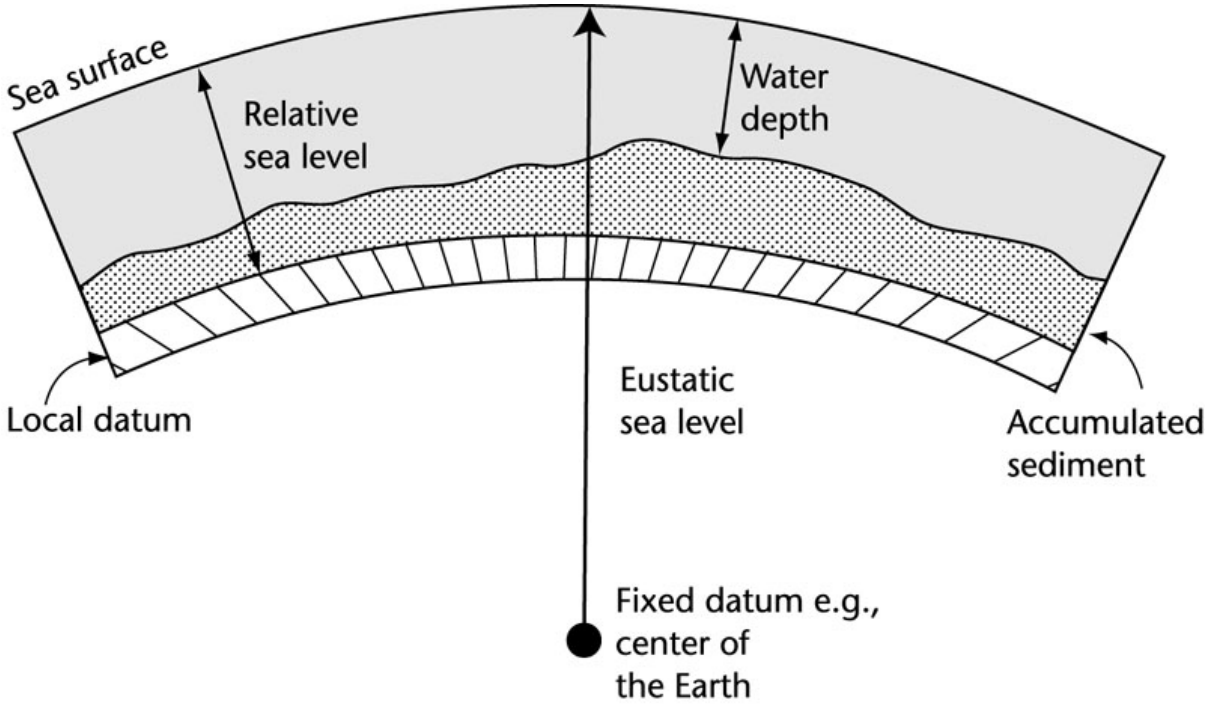

Figure 1.2. Definition of terms used in process stratigraphy: eustatic sea level, relative sea level and water depth (after Jervey 1988; Emery and Meyers 1996; Allen and Allen, 2005)

Sediment fluxes may underfill, fill or overfill such space but according to the fact that sediment can only accumulate long term up a base level, either being base level a graded stream profile on land or a graded shelf profile on a continental shelf, a change in accommodation ΔA is equal to

$$\Delta A = \Delta E + \Delta S + \Delta C \quad (1.1)$$

where E is eustasy, S is subsidence and C is compaction. A change in water depth ΔW con therefore be written as

$$\Delta W = \Delta A - \Delta D = (\Delta E + \Delta S + \Delta C) - \Delta D \quad (1.2)$$

where ΔD is the amount of sediment deposited (Allen and Allen, 2005). Sediment cannot accumulate for long time above the base level, and consequently sediment may be bypassed downstream or into deeper water. High sediment supply in a basin with adequate accommodation will cause sedimentary facies to aggrade. If sediment supply is less then accommodation, the facies belt will degrade. If sediment supply exceeds the available accommodation, facies belt will prograde.

1.3.1 Autigenic and allogenic control on transport and depositional processes

The stratigraphic architecture of a sedimentary basin comprehends an integrated geomorphic system that from the source denudational areas (mountain ranges, hill tracts, altiplanes, etc.) results in a flux to depositional sink areas on land (colluvial, alluvial and deltaic planes) and offshore (shoreface, continental shelf, slope and deep sea fan) until the maximum distal reaches the mean of sediment transport can achieve. For any given elevation of the source area and of the body of water into which the river debouches, fluvial systems tend to develop a dynamic equilibrium in the form of a graded longitudinal profile (Miall, 1996). This equilibrium profile is achieved when the river is able to transport its sediment load without aggradation or degradation of the channel (Leopold and Bull, 1979; Pirmez et al., 2000). Any stress exerted on this integrated system will alter the equilibrium profile.

Sedimentation is controlled by a combination of autigenic and allogenic stresses which determines the distribution of depositional elements within a depositional system, as well as the large scale stacking pattern of depositional systems within a sedimentary basin (Catuneanu, 2009). Autogenic processes or internal control (self-induced avulsion in fluvial and deep water environment, oversteepening, etc) are particularly important at sub-depositional system scale. Allogenic or external control includes tectonic, sea level, climate and anthropogenic impact. Tectonic is commonly equated with basin subsidence but crustal cooling, crustal loading, water depth changes and sediment compaction also contribute to the total subsidence and need to be equally computed by applying the opportune corrections (Watts and Ryan, 1976; Allen and Allen, 2005). Eustatic fluactuations of global sea level are controlled by both tectonic and climate mechanism over various time scales (Table 1). Global middle and high frequency climate changes are controlled by orbital motion of the Earth (Hays et al., 1976; Imbrie, 1982) commonly termed Milankovitch cycles and astronomical forces with different frequencies (Table 1.1.). Tectonic processes play also an important role on the longer time scales such as the formation of thrust-fold belts that may act as barriers for atmospheric circulation. Allogenic control provides the common platform that connects and synchronizes the depositional trend recorded at any given time in all environments established within a sedimentary basin and allows developing sequence stratigraphic models at a basin scale. A fundamental application of the stratigrafic models is the facies predictability, initially developed for oil industry practitioners but in this study it will be applied for academic porpoises.

1.3.2. Seismostratigraphy: cycles and events

Stratigraphy makes use of systematic branches defined on the basis of the property of the lithified and unlithified bodies they analize (Table 1.2.).

A major breakthrough was the use of seismic reflection surveys which uses the principles of sound propagation to investigate the Earth surface and subsurface. By measuring the time elapsed from the signal emission to the signal return, two way travel time, TWT, it can be derived the thickness of the units at a resolution that depends on the intensity of the initial signal.
The higher frequency the signal will have, the better the individual strata or events will be resolved. Low frequency emissions will produce a deeper image of the sedimentary structure to the detriment of

Table 1.1. Tectonic, orbital and astronomic controls on eustatic fluctuations (Vail et al., 1977; Miall et al., 2000; Catuneanu, 2006)

Hierarchical order	Duration (Ma)	Cause
1st	200-400	TECTONIC: formation and break up of supracontinets
2nd	10-100	TECTONIC: Volume changes in mid-oceanic spreading centres
3rd	1-10	TECTONIC: regional plate kinematics
4th	0.1-1	ORBITAL FORCING: eccentricity
5th	0.01-0.1	ORBITAL FORCING: obliquity, precession
5th	0.001-0.01	ASTRONOMICAL BANDS: sun spot cycles, nutation cycle
7th	0.0001-0.001	CALENDAR BANDS: seasons, earth-moon interactions

resolution. A reliable chronostratigraphic interpretation of a basin fill depends on the type, amount and quality of the available data which will contribute to understand the distribution and nature of the sedimentary facies in term of geological processes operating at a specific time. In this study the general principles of seismic stratigraphy will be applied, and sequence stratigraphy integrated with precedent studies on biostratigraphy will be used to ground truth the analyzed sections.
A crucial point in seismostratigraphic studies is therefore the investigated time scale(s). Humans are adapted to daily and yearly cycles. Graduable and predictable cycles (tides, seasons, etc) that dominate the daily life can experience unpredictable, sudden and potentially catastrophic events (pe. storms, floods, draughts, earthquakes, volcanic eruptions, meteorite impacts). The perception at a global or local scale depends on the extension and duration of the imaged sections. Cycles are described as sinuous curves with certain periodicities and more or less uniform amplitudes. Thus they can be extrapolated from modern data into the past unless periods are too long to be actuallistically measured. Events, in contrast, are not only aperiodic; they also occur in varying amplitude, the larger

Table 1.2. Branches of process stratigraphy

Discipline	Property
Lithostratigraphy	Lithology
Biostratigraphy	Fossils
Magnetostratigraphy	Magnetic polarity
Chemostratigraphy	Chemical properties
Chronostratigraphy	Absolute ages
Allostratigraphy	Discontinuities
Seismic stratigraphy	Seismic data
Sequence stratigraphy	Depositional trends

the rarer. Onto geological spans, the open scale of intensities implies an element of nonuniformitariasm (Seilacher, 1991). Consequently from the megasequences enclosing stratigraphic sequences deposited during distinct phases of plate motion, to the smallest units of stratigraphy relevance in terms of space or time, a depositional sequence is a coherent packet of strata genetically related and which can be traced for considerable distance across a basin. Depositional sequences have chronostratigraphic significance because they were deposited during a time interval limited by the time ages of the upper and lower boundary, or sequence boundaries, where these boundaries have not been affected by erosive events (Mitchum et al., 1977). Where regional erosive events (unconformity) mark the onset or the end of a depositional sequence, the age range is reduced.

Depositional sequences can be subdivided into smaller units of stratigraphy that have distinct stacking pattern of chronostratigraphic increments, the system tracts (Van Wagoner et al., 1988). The major shifts in the depocentre along and across the basin during a cycle (parasequences) could be traced back to his origin from the interaction of the relative sea level change and rate of total subsidence (Eq. 1). The total subsidence in a sedimentary basin is an ubiquitary control on accommodation whereas the impact of sea level becomes more significant in the downstream portions and in the marine (or lacustrine) environment. The landward most position the shoreline can achive is a fundamental position trough a cycle and represent the inflection of the sinuousidal curve. In the present day 2012 orbital and astronomical cycle the Planet Earth is at a maximum of eccentricity (100 ka) and sun spot activity (11 a), at the end of a precession cycle (20 ka) and in the middle of its obliquity orbit (40 ka). It is still unclear if the inflection at the maximum of the global sea level cycle has been passed or not.

1.4 Main objectives of this study

The dominant signal for the late Pleistocene (0.91-0 Ma) are glacial-interglacial variations of 100 ky and amplitude of 50 m (variations in height of 100 m). Before present day interglacial, the previous one occurred 123 ka ago (Waelbroeck et al., 2003). Within this cycle, total subsidence (tectonic+compaction), sea level and climate have altered exerting distinctive type of stress on the Mega-Deltas coastal zone of the East, South and South-East Asia.

Envisaging future and fruitful cooperation with similar studies for environmental sustainability, geohazard prevention and modelling prediction, in an integrated coastal management for the East, South and South-East Asia affected by the monsoon climate and related to the same regional tectonic, the main focus of this thesis will be the Ganges Brahmaputra Mega-Delta located in the Nation of Bangladesh (Fig. 1.1).

By mean of high and ultra high resolution seismo-acoustic data collected in several years since 1993 to 2006, the depositional sequence accumulated during last eccentricity cycle on the continental shelf offshore the Ganges Brahmaputra Megadelta will be analized in order to evaluate:

1) the depocentre shift on a continental shelf in response to different sea level stands

2) depocentre anomalous distribution along and across a continental shelf

3) the tectonic subsidence and its differential component on a continental shelf

4) the architecture of the depositional elements (subaqueous delta and shelf canyon) and of individual strata, if any, genetically related and which can be traced for considerable distance across the basin

1.4.1 Thesis Outline

This thesis includes (1) a review of the theoretical background and (2) on local peculiar transport and sedimentary conditions in the case study area, (3) the methods of the data acquisition and processing, and the set of formulas used in the calculation of the compaction trend and backstripping. The following chapters are presented in the form of manuscripts on the glacial-interglacial Cycle on the Bengal Shelf (4) and on the main shelf depositional elements, the Ganges-Brahmaputra subaqueous delta (5) and the Swatch of No Ground Canyon (6). **Chapter 5 was published in April 2011, in Volume 31 of the Continental Shelf Research Journal, pages 712-730.** Chapter 3 and 6 are in preparation for international peer-reviewed journals.

~ Chapter 2~

The case study: Bengal Basin

2.1 Location of the Ganges-Brahmaputra Mega-Delta

The source-to-sink system of the Himalayas-Bengal Basin-Bengal Fan is driven by the rivers Ganges and Brahmaputra which transport the worldwide greatest flow of sediment to the ocean. The Ganges River originates in the western Himalayas and it drains the southern slopes of the mountain chain. The Brahmaputra has its source in central Tibet; it follows the northern slope of the Himalayas and, after a westward sharp bend in the Assam Basin, it enters the Bangladesh alluvial plain. The Ganges is primarily a meandering river transporting mainly silt-clay-sized material in suspension, while the Brahmaputra is primarily a braided river with a bed load consisting predominantly of fine sand and silt (Coleman 1969). The Brahmaputra and the Ganges, named Jamuna and Padma in the Bengali language, converge 190 km inshore the coastline of Bangladesh and join the Meghna which drains the adjacent Sylhet Basin. The Meghna gives the name to the delta which lies at the north-eastern edge of the Bengal Bay (Fig. 2.1). It is a tide dominated delta and is formed by four major channels which feed a broad subaqueous delta on the Bengal Shelf. A deeply incised canyon, the Swatch of No Ground Delta Front Through, intersects the Bengal Shelf and form a preferential conduit for sediment delivery to the Deep Sea Bengal Fan (Currey et al., 2003; Schwenk et al., 2005).

2.2. Structural Regional Geology

The Bengal Basin is a forearc basin located at the juncture of three interacting plates: the Indian shield, Burman Margin and Eurasian Plates.

Initial separation in Early Cretaceous of India from Australia and Antarctica was north-westward, but plate reorganization occurred in Late Cretaceous, perhaps about 90– 96 Ma, changing the direction to more northward (Curray et al., 1982; Veevers, 1982). Before the departure of India from Australia and Antarctica in the Early Cretaceous, South Tibet, and Siam-Burma-Malaysia- Sumatra Blocks had already spun off northward and had docked against Asia.

The three large continental masses were closely joined (Fig. 2.2.a), with ‘Greater India’ extending an unknown distance into the Tethys Sea. With the break-up, a continuous zone of subduction was established along the southern margin of the Asian and Tibetan Plates. The initial alignment of these subduction zones is speculative, but was probably about east–west or southeast–northwest. A zone of subduction in the margin of Asia continued farther south before the India–Asia collision (Fig. 2.2.b). During the collision process, India indented Asia, and Indochina and Southeast Asia were extruded eastward and southeastward. In Mid-Paleocene, about 59 Ma, soft collision occurred between the northwest corner of the Indian Shield and South Tibet (Fig. 2.2.b).

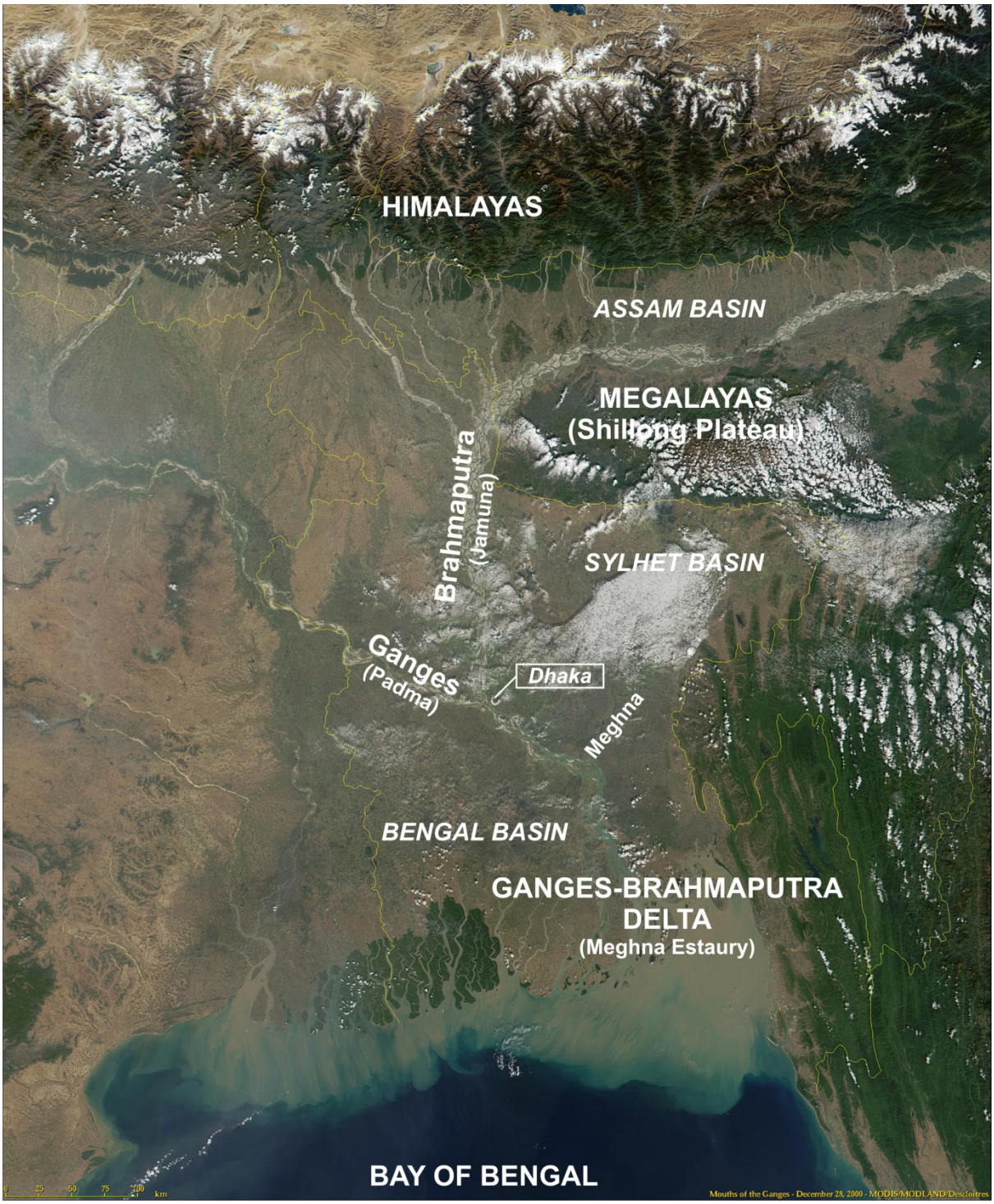

Figure 2.1. Satellite image (Modis-Modland, 28.12.2000) of the Bangladesh Country illustrating the Ganges-Brahmaputra Delta.major physiographic elements.

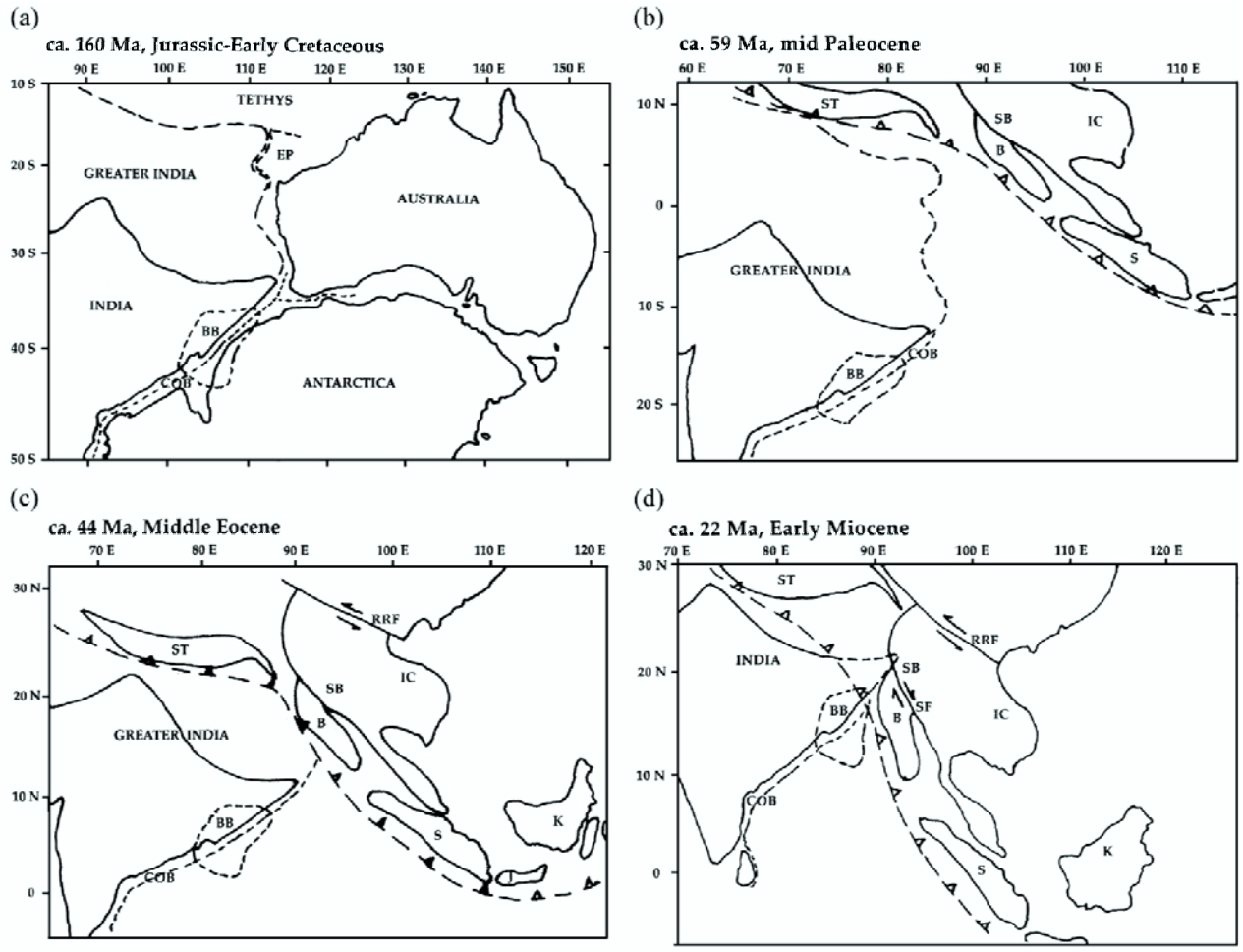

Figure 2.2. Plate reconstructions modified mainly from Lee and Lawver (1995) and Alam et al., 2003. EP=Exmouth Plateau; COB=continent ocean boundary; ST=South Tibet; B=Burma Block or IBA (Indo, Burma, Andaman); SB=SIBUMASU (Siam, Burma, Malaysia, Sumatra); IC=Indochina; S=Sumatra; BB=Bengal Basin; K=Kalimantan; J=Java; RRF=Red River Fault; SF=Sagaing Fault. (a) Eastern Gondwana fit of the margins of "Greater India", Australia and Antarctica. (b) Plate reconstruction at about 59 Ma, Mid-Paleocene, the start of "soft collision" between India and Southeast Asia. (c) About 44 Ma, Middle Eocene, the start of "hard collision" between India and South Asia. (d) About 22 Ma, Early Miocene, a time of major collision between India and South Tibet in the north and India and Burma in the east.

India underwent some CCW rotation from about 60–55 Ma (Klootwijk et al., 1992), at which time the suture was completely closed. Since then India passed obliquely into and/or under Asia. Tibet had previously docked against south Asia, which at that time lay farther south. Subsequent crustal shortening and tectonic escape, i.e. extrusion of Indochina, Southeast Asia and South China, created the indentation where India is now situated. During the 'soft collision', ca. 59–44 Ma, the northward or NNE motion of India continued, and was slowed perhaps by closing up formerly relatively between the other accreted terraines of South Asia (Chen et al., 1993). By Early Eocene, about 44 Ma, hard continent–continent collision related to the Himalayan orogeny commenced (Fig. 2.2.c). By this time the older sutures were more fully compressed. This was also a time of major plate reorganization in

the eastern Indian Ocean, when the Indian and Australian plates joined to form a single plate and the Australia–Antarctica separation started to accelerate. Some change in spreading direction also occurred and this was approximately the time when tectonic extrusion of the Burma and Siam-Burma-Malaysia- Sumatra Blocks and Indochina started (Tapponnier et al., 1982, 1986). The Bengal Basin became a remnant ocean basin (Ingersoll et al., 1995) (Fig. 2.2.d) at the beginning of Miocene because of the continuing oblique subduction of India beneath and southeast extrusion of Burma (West Burma Block) and the continent-ocean boundary passes offshore approximately down the axis of the upper part of the Swatch-of-no-Ground submarine canyon (Fig 2.2.).

The deformation front lies at the foot of the fold belt and it crops out at the continental slope offshore of eastern Myanmar and is coming ashore at the Ganges-Brahmaputra Delta (Fig. 2.3.). The NNW ongoing subduction of the Indian plate beneath Asia is estimated by GPS measurement 36 $mmyr^{-1}$ (Socquet, A. et al., 2006; Cummins, 2007). This ongoing subduction results in frequent earthquakes (Steckler et al, 2008) which concentrate on the plate boundaries at the eastern margin due to the combined effects of northward movement along the transform fault and eastward movement into the subduction zone (Cummins, 2007).

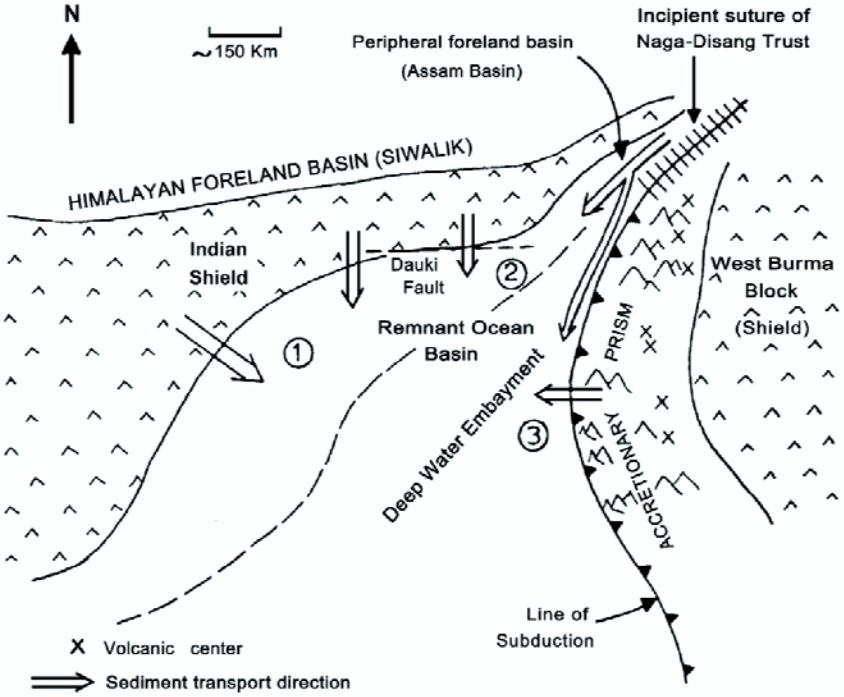

Figure 2.3. Schematic paleogeographic (Early Miocene) representation of the Bengal Basin and surroundings incorporating the plate tectonic model. The positions of the three tectonic provinces of the Bengal Basin are shown by encircled numbers: (1) The Stable Shelf, (2) The Central Deep Basin, and (3) The Chittagong–Tripura Fold Belt (Alam et al., 2002; Gani and Alam, 2002)

Different locations in the basin show spatially variable tectonic subsidence rates (Wiedecke et al., 1997; Goodbred and Kuehl, 2000a; Hübscher and Spiess, 2005).

The sediment repository preserved in the Bengal Basin is predominantly a huge delta complex fed by the coalesced Ganges and Brahmaputra rivers. It preserves a ca.16–22 km thick sequence of Cenozoic sediments (Curray & Moore, 1971; Curray, 1994; Gani & Alam, 1999; Uddin & Lundberg, 2004) distinct as geo-tectonic provinces (Alam et al., 2002): (1) The Stable Shelf; (2) The Central Deep Basin; and (3) The Chittagong–Tripura Fold Belt. From oldest to youngest stata, the Sylhet, Kopili, Bhuban, Bokabil, Tipam and Dupi Tila Formations, show facies evolution from marine through deltaic to fluvial environments (Najman 2012).

2.3. Climate and Oceanography

Oceanic surface circulation in the northern Bay of Bengal is driven by the seasonal migration of the Inter-Tropical Convergence Zone, ITCZ (Fig. 2.4.) During the summer monsoon, the N-NW displacement of the ITCZ generates a SW wind inducing an anticlockwise surface current. Transport of humid air from the sea to the inland originates intense precipitations in the drainage area of the Ganges and Brahmaputra. Vice versa, during winter, the ITCZ moves in a more equatorial position and the resulting NE monsoon induces a weaker clockwise oceanic current and dry conditions onshore. Premonsoon periods, during spring and autumn, coincide with tropical cyclones formation.

Figure 2.4. Satellite images of the Inter-Tropical Convergence Zone (ITCZ) which appears as a band of clouds consisting of showers, with occasional thunderstorms, that encircles the globe near the equator and of the Sidr cyclone that invested the costline of Bangladesh in 2007. The main parts of a tropical cyclone are the rainbands, the eye, and the eyewall. Air spirals in toward the center in a counter-clockwise pattern in the northern hemisphere (clockwise in the southern hemisphere), and out the top in the opposite direction. In the very center of the storm, air sinks, forming an "eye" that is mostly cloud-free.

The basic circulation is nearly barotropic and water temperatures are highest in the Arabian Sea and in the Bay of Bengal setting the conditions for the warm core generation of tropical cyclones (Fig. 2.4.). Being pushed from the south by wind stress and funnelled by the triangular shape at the head of the bay, cyclones have landfall in the northern Orissa, West Bengal, Bangladesh and part of northern Myanmar often causing dramatic storm surge (Murty et al., 1992).

Equatorial wind variability rather than river run-off is responsible for a positive sea level anomaly of 0,1-0,25 m in the coastal region and 0,05-0,15 cm in the interior bay from May to September (Han and Webster, 2002).

Coastal waters respond to semi-diurnal tidal forcing. Maximum amplitudes of 5 m are registered in the eastern estuary. In the western channels lower amplitudes coincide with a net export of river waters. The Sunderban mangrove forest is tidally dominated with tide differences of about 2 m. The lower delta plain is less than 3 m above sea level and saline water from the Bay of Bengal penetrates 100 km or more inland along the distributary channels during the dry season. In the offshore region, amplitude decreases from 0,8 in the topset beds to 0,5 m in the foreset-bottomset (Murty and Henry, 1983). It becomes negligible in the outer shelf. Sea level anomalies and high tides can intensify the amplitude of the storm surge impact on the coast (As-Salek and Yasuda, 2001).

Profiles of temperature, salinity and oxygen indicate a strong water mass stratification (Berner et al., 2003). Low salinity and temperate water originated by river run-off lies on top of warmer, saline and oxygen-poor water. Methane anomaly concentrations are found in the water column at -20 m and below -60 m water depth. The Swatch of No Ground is filled with anoxic water (Berner et al., 2003).

~ Chapter 3~

Material and Methods

3.1 Working areas

The majority of the data used in this study (Multichannel Seismic, Parasound Echosounder and Kongsberg Simrad EM 120 bathymetry) was collected during the R/V SONNE cruise 188 (Bengal Sea Level), the forth cruise with R/V Sonne to the Bay of Bengal. Previous cruises in 1994 (SO93, Bengal Fan) and 1997 (SO 125 and SO 126, Bengal Fan and Shelf) provided a first framework for many studies of the source-to-sink system Himalaya-Bengal Basin-Bengal Fan and for planning the targets of the new expedition. SO188-2 cruise took place from 01.07. to 31.07.2006 and new techniques and methods were used to achieve the overall objectives of reconstructing the process stratigraphy of the Bengal Basin by surveying different areas on the Bengal Shelf. The target areas (Fig. 2.4) and their associated objectives during the So188-2 Expeditions were:

Area 1. The subaqueous delta: investigate the sedimentary structure, evaluate the sediment budget and search for evidences of the anthropocene environmental changes.

Area 2. The Swatch of No Ground Canyon: the canyon floor potentially contains thick sequence (> 400 m) of laminated sediments representing a unique Holocene cyclone record. This record can be used to understand the linkages between tropical cyclone dynamics and future natural and anthropogenic climate variability. The canyon's head is addressed as a key determining factor for the architectural style of the deposits generated in deepwater environments and the reconstruction of the depositional history of siliciclastic sequences beyond the sea level stands. This could be of great help in the understanding of the tectonic and climatic forcing inherent to a continental margin and its terrestrial sediment source.

Area 3. The outer shelf and margin: regressive phases of the sea-level changes are recorded in a series of oolithic beach ridges on the middle shelf. Buried ridges are also known and they can be used as a time and depth marker to determine relative sea-level and in comparison with the global sea level the long-term subsidence of the shelf due to sediment loading and subduction tectonics.

Area 4. The Bengal Slope: the hemipelagic sediments of the northern Bay of Bengal are ideal to study the monsoonal precipitation changes during several glacial-interglacial cycles, as the surface salinity is determined by the freshwater input from Ganges and Brahmaputra. Several sites on the Bangladesh continental slope have been surveyed to establish an optimal location for the estimation of the runoff.

Area 5. The Upper Bengal Fan: the flux of terrigenous material from the shelf canyon and margin, has created a high-resolution archive containing data on the climatic conditions onshore and tectonic. Composition of the terrigenous material, of terrestrial organic compounds and marine biomarkers will particularly allow a high-resolution reconstruction of the Pleistocene monsoon dynamics.

The studied Areas in this PhD Thesis are 1, 2 and 3.

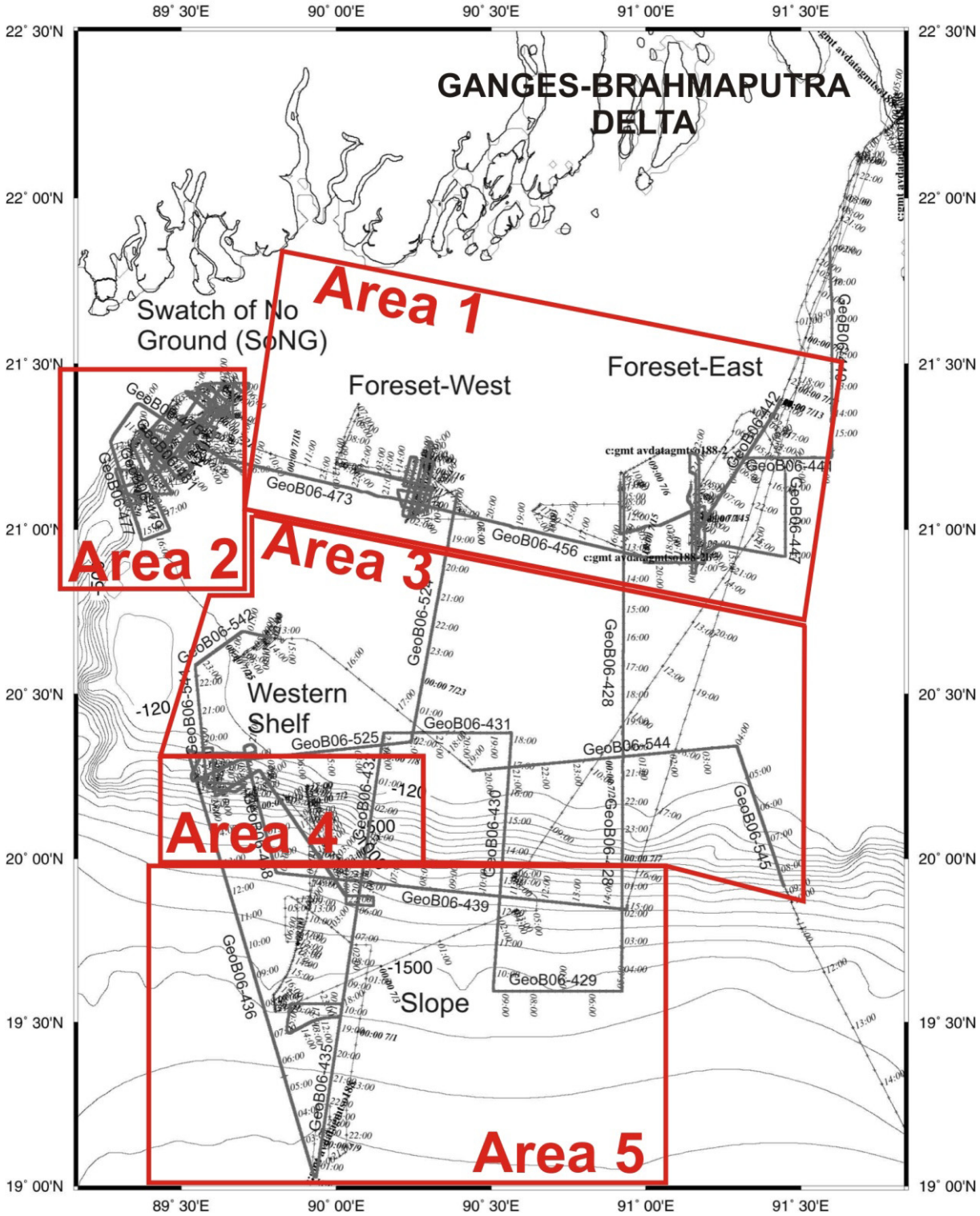

Figure 3.1. Cruise track and seismic profiles (thick gray lines) of SO 188-2.

3.2 Methods

3.2.1. Multi-Channel Seismic acquisition and processing

Two different Multi-Channel Seismic acquisition strategies (source and receiver sets) had been adopted to image the sedimentary structure according to the water depth:

-from 2000 to 15 m water depth. Source: 4,1 l GI Gun. Receiver: SYNTRON multichannel seismic streamer (96 channels, 600 m lenght)

-from 700 to 15 m water depth. Source: 0,4 l GI Gun. Receiver: especially designed 50 m long shallow water streamer (48 channels with spherical single hydrophones) that allows imaging of sedimentary deposits in shallow water depth with extremely high lateral resolution (von Lom-Keil et al., 2005).

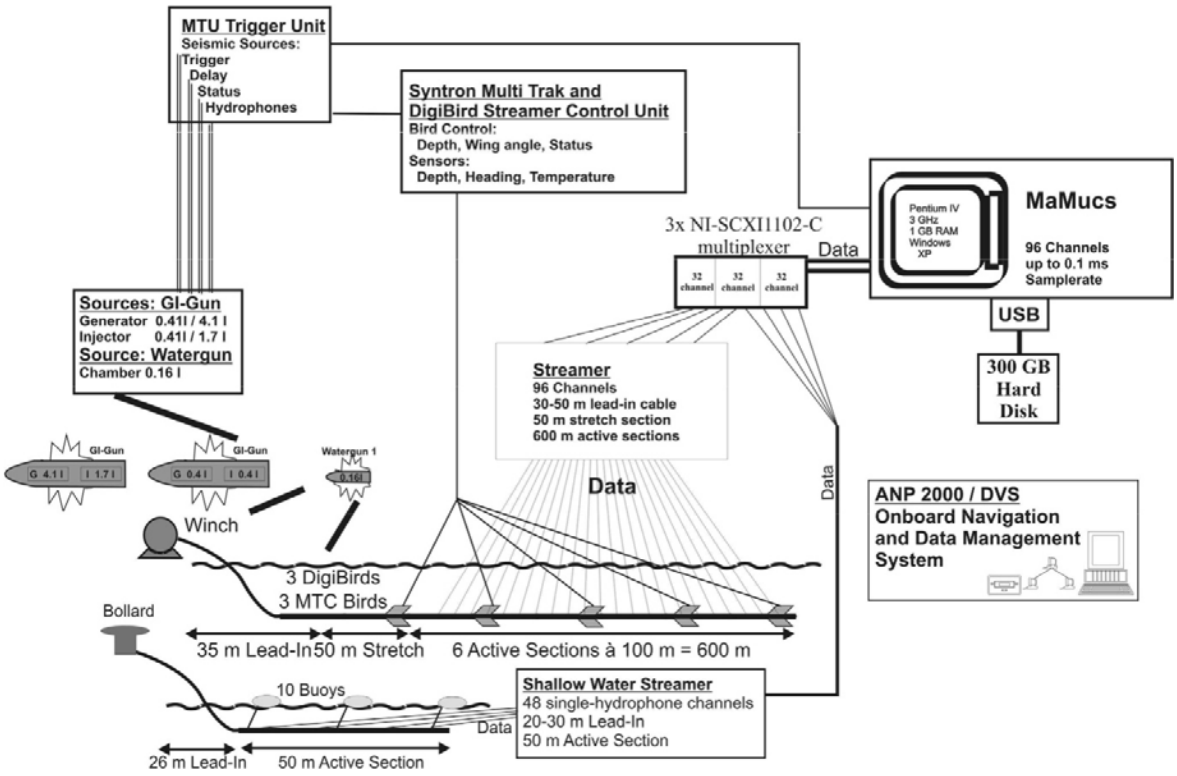

Figure 3.2 General outline of the Multichannel Seismic System used on SO 188-2.

The sound spectra generated from the 4.1 l and 0.4 l GI Guns provides a frequency ranging from 30 to 600 Hz. On some profiles the short and long streamer were used simultaneously and during these profiles the first 48 channels of the recording system were occupied by the shallow water streamer and the second 48 channels were occupied by the long streamer. The multiple and simultaneous acquisition of different frequency records gives the opportunity to create multi-frequency analysis of the sedimentary structure. The multi-frequency analysis will be detailed illustrated and deepened in Chapter 6.

Custom trigger unit controls the seismic sources and the Lead-In cable of the receivers were connected by extension cables to the custom data acquisition system (MaMucs) developed at the working group Marine Technology/Environmental Research at the University of Bremen. MaMucs consists of a Pentium IV based PC (3 GHz, 1GB RAM, Windows XP) with three NI6052E 16bit AD-Converters. Each ADC is connected to a 32 channel multiplexer (NI-SCXI1102-C) with onboard pre-amplification and anti-alias filter. Data were recorded with a sampling rate of 125 μs or 250 μs over intervals of 3-4 seconds.

The MCS data, collected and stored in hard disk in the form of demultiplexed SeGY format, were in first instance geo-referenced with GPS and GLONASS data from high quality navigation systems. The MCS was then processed with normal procedure for MCS stacking and migration (Yilmaz, 1991) using the Vista seismic processing software package. It is however worth to mention some processing and time consuming exceptions due to the very shallow water depth of acquisition. While in deep water environment the velocity analysis for stacking is a minor step and in the majority of the cases requests only a constant stacking velocity, in very variable and shallow water depths it becomes of fundamental importance. Therefore each profile was supplied with multiple velocity spectra for stacking as derived by the two main frequencies emitted. Another peculiar procedure to improve the image quality was a channel sort ordered despiking and filtering. The shallow water depth indeed produced a very imbalanced amplitude decay and signal-noise ratio, therefore, despiking and signal filters threshold applicable to the first receivers inline in the streamer, where too tight or inappropriate for the middle and last hydrophones. Channel and offset dependent filters where defined for each profile to obtain the best preservation of traces to maintain a good fold for stacking with 2.5 m to 5 m CMP binning distance. Before stack, a manual post-processing static correction was often necessary to remove residual static induced by oceanic waves.

3.2.2 Parasound and EM 120 bathimetry acquisition and processing

The PARASOUND system, permanently installed on R/V SONNE, was used for sediment echosounding profiling. It utilizes the parametric effect, which produces additional frequencies through nonlinear acoustic interaction of finite amplitude waves. If two sound waves of high energy are emitted simultaneously at different frequencies (here 18 kHz and e.g. 22 kHz), a signal of the difference frequency (e.g. 4 kHz) is generated at sufficiently high primary amplitudes. The new signal component is traveling in a narrow emission cone of only 4° aperture within the original high frequency waves. The resulting footprint size of 7% of the water depth is much smaller than for conventional systems and both vertical and lateral resolution is significantly improved to 10 dm to 40 dm. The Parasound recorded data digitized by the ParaDigMa software (Spiess, 1993), were manually converted to the SEG-Y standard format to load them into the HIS, Kingdom Suite, interpretation software together with the MCS.

For bathymetric mapping the deep-water multi-beam echosounder EM120 (SIMRAD) was used. The system allows an accurate bathymetric mapping up to full ocean depth with the usage of receptors from 191 beams, with widths of 2° across track and 20° along track. Thus, the actual footprint of a single beam has a dimension of 1° by 2°. The achievable swath width on a flat bottom will normally be up to six times the water depth dependent on the character of the seafloor. The EM 120 multibeam is not reliable in less than 100 m water depth. The data processing was carried out with the MB System software. Procedures include trace editing and gridding with optimal spacing according to the depth and data quality.

The GMT software [Wessel and Smith, 1991] was used for displaying the bathymetry grid and seismic line locations.

3.2.3. Compaction trend

When older rocks become buried deeper, as a result are subjected to greater weight of the overlying sedimentary burden. The pressure caused by this burden will force grains to rearrange in closer state. The pore sizes in the rock are reduced and excess water is forced out. This is known as compaction. The study of diagenesis in general and compaction in particular is very important for anybody who is interested in sediments and sedimentary rocks. Compaction models, as models of variations of density and porosity with depth, are important in basic and applied studies of the Earth.

In geophysics compaction is any process by which sediment is reduced in dimensions due to the effects of loading. Compaction processes can be divided into two major categories: mechanical and chemical compaction processes.

Mechanical compaction produces mechanical rearrangement (reorientation and sliding) of grains, compression, bending and ductile grain deformation, and breakage of grains (grain crushing), due to increased overburden stress during burial. These processes are primarily dependent on the effective stress and geo-mechanical (e.g., compressibility) properties of the rocks. As a result, changes in sediment physical properties occur: the volume of pore space (porosity) decreases, and density and velocity increase.

Chemical compaction involves physico-chemical processes such as pressure solution and purely chemical processes such as cementation, grain coating (coating of minerals by a film of clay preventing cementation at grain contacts), and mineral transformation (transformation of minerals due to thermal or chemical instability).

Stress, temperature and rock composition are the controlling parameters for compaction.

Here it will be considered the stress and they follows the set of formulas that are used in experimental model built in the Chapther 4 and Appendix I to evaluate the compaction trend on the Bengal Shelf.

Stress is defined as the force per unit area:

$$\sigma = F/A \tag{3.3.}$$

In a sedimentary basin vertical stress, σ_v, at a depth z below the subsurface is equal to the weight of the overlying sediments and the water column between the sea level and the sea bottom (z_w):

$$\sigma_v = \rho_b g z + \rho_w g z_w \tag{3.4.}$$

where ρ_b is the average bulk density of the sediments, ρ_w is the density of the sea water, and g is the acceleration due to gravity.

Rocks are made of mineral grains with voids (pores) between them, usually filled with fluids. In normally pressured environments, the pore fluid is in equilibrium and it exerts hydrostatic pressure, Phy, in all directions, which is proportional to the height of the water column from the sea level to depth z:

$$Phy = \rho_w g z \tag{3.4.}$$

Since it acts in all directions, hydrostatic pressure of pore fluids partially compensates vertical stress caused by overlying sediments. In this case sediments at depth z are subjected to reduced vertical stress, more commonly referred as effective stress:

$$\sigma_{eff} = \sigma_v - Phy \tag{3.5.}$$
$$\sigma_{eff} = \rho_b g z + \rho_w g z_w - \rho_w g z$$
$$\sigma_{eff} = (\rho_b - \rho_w) g z + \rho_w g z_w$$

This relationship is known as Terzaghi's Law. Terzaghi was the first one to recognize that it is effective stress and not vertical stress that controls the porosity reduction of the sediments. Terzaghi's law holds in all types of normally consolidated sediments. But sometimes in low permeability rocks such as shales, pore fluid takes a long time to escape during compaction and this leads to development of an overpressured zone. In these zones pressure of the pore fluids exceeds hydrostatic pressure and causes reduction of the effective stress:

$$\sigma_{eff} < \sigma_v - Phy \tag{3.6.}$$

Porosity, φ, is expressed as the ratio of the volume of the voids and the total volume and can be measured empirically on sediment cores with Sonic or Density Logs and with Formation Density sondes. The gamma ray probe installed on the RV Sonne during the SO93 Expedition was a multi-sensor core logger Geotek (P. Schulheiss, Surrey, UK) with a 10 milli-curie Cesium 137 gamma source (Kudrass et al., 1994). It measures the natural radioactivity of formations naturally occurring. Since the gamma ray tool counts the number and estimates the energy of gamma ray particles emitted by radioactive decay, the passage of these particles through matter affects the tool readings. Less dense formation will appear to be slightly more radioactive, even if the radioactive material per unit volume is the same. Thus, there is a tendency of decreasing in gamma ray counts downhole due to sediment compaction.

Know ρ_b from the density log, given the grain density of the rock ρ_{ma} and the density of the fluids that fill the formation pores ρ_w, we can find the porosity, φ, as corresponding to:

$$\varphi = (\rho_b - \rho_{ma}) / (\rho_w - \rho_{ma}) \quad (3.7.)$$

Density logs were converted into porosity by using a grain density, ρ_{ma}, of 2.75 gcm^{-3} as calculated from the ODP 718 and 719 from the central and the distal end of the Bengal Fan in the Indian Ocean (Shipboard Scientific Party, 1989a, 1989b; Brusova, 2011).

In Appendix I there are the calculated compaction trend based gravity cores SO93-79, SO93-80SL, SO93-128SL ,SO93-105KL, SO93-83KL collected on the Bengal Shelf (Fig. 3.8) on each system tract and respectively on the FRST11 (81.5-32 ka), LST12 (32-19 ka), TST13 (19-7 ka) and HST14 (7-0 ka).

3.2.4. Backstripping

The porosity loss obeys to a form of negative exponential which produces an asymptotic low porosity with increasing depth, z, (Athy, 1930; Hedberg, 1936; Allen and Allen, 2005):

$$\varphi = \varphi_0 e^{-cz} \tag{3.8.}$$

Where c is a coefficient determining the slope of the φ-depth curve, z is the depth and φ_0 is the porosity at the surface. To calculate the thickness of a sediment layer at any time in the past, it is necessary to move the layer up the appropriate porosity depth curve: this equivalent to sequentially removing overlying sediments layers and allowing the layer of interest to decompact.

Consider a sediment layer at present depth of z_1 and z_2 which is to be moved vertically to new shallower depths $z_{1'}$ and $z_{2'}$. From equation (3.7.) the amount of water filled pore space V_w between depths z_1 and z_2 is simply the porosity integrated over the depth interval:

$$V_w = \int_{z1}^{z2} \Phi_0 e^{-cz} dz \tag{3.9.}$$

which on integration gives

$$V_w = \varphi_0/c \{\exp(-cz_1)-\exp(-cz_2)\} \tag{3.10.}$$

Since the total volume of the sediment layer (V_t) is the volume due to pore filling water (V_w) and the volume of the sediment (V_s)

$$V_s = V_t - V_w \tag{3.11.}$$

and from Eq. (3.9) considering a unit cross-sectional area,

$$z_s = z_2 - z_1 - \varphi_0/c \{\exp(-cz_1)-\exp(-cz_2)\} \tag{3.12.}$$

on decompaction the sediment volume remain the same, only the volume of water expanding. The height of the water in a unit area sedimentary column lying between depths z_1' and z_2' is from Eq. (3.9)

$$z_w' = \varphi_0/c \{\exp(-cz_1')-\exp(-cz_2')\} \tag{3.13.}$$

The new decompacted thickness of the sediment layer is the sum of the thickness due to the sediment grains (3.11) and that due to the water (3.12) that is,

$$z_2'-z_1'=z_s+z_w' \tag{3.14.}$$

which becomes

$$z_2'-z_1'= z_2-z_1- \varphi_0/c \{\exp(-cz_1)-\exp(-cz_2)\}+ \varphi_0/c \{\exp(-cz_1')-\exp(-cz_2')\} \tag{3.15.}$$

This is the general decompaction equation and its solution is by numeric iteration (Allen and Allen, 2005).

The sediment and water load above a horizon of interest is a sedimentary basin causes an isostatic effect so that the total subsidence observed is made of a tectonic driving force component and a sediment/water load component. Watts and Ryan (1976) were the first to propose the isolation of the tectonic driving force by removal of the isostatic effect sediment load and called the technique backstripping.

If the porosity, φ, of the sediment layer at its new depth is

$$\varphi = \varphi_0/c \{(\exp(-cz_1')-\exp(-cz_2')) / (z_2'-z_1')\} \tag{3.16.}$$

and the bulk density of the new sediment layer (ρ_b) depends on the porosity and the density of the sediment grain (ρ_{sg})

$$\rho_{b=} \varphi \rho_w + (1- \varphi) \rho_{sg} \tag{3.17.}$$

the bulk density of the entire sedimentary column (ρ_b) made up of i^{th} layers is

$$\overline{\rho_b}=\Sigma i \{ (\overline{\varphi_i} \rho_{w+} (1- \overline{\varphi_i}) \rho_{sgi}) / S \} z_i' \tag{3.18.}$$

where $\overline{\varphi_i}$ is the mean porosity of the i^{th} layer, ρ_{sgi} is the grain density of the same layer, z_i' is the thickness of the i^{th} layer and S is the total thickness of the column corrected for compaction as in Eq. 3.14.

The loading effect of sediment can treated as problem of local (Airy) isostatic balance. Where sediment is replacing a column of water,

$$Z= S(\rho_m - \overline{\rho_b} / \rho_m - \rho_w) \quad (3.19.)$$

where Z is the depth of the basement corrected for sediment load and ρ_m, $\overline{\rho_b}$ and ρ_w are mantle, mean sediment column and water densities.

Incorporating the various effects in Eq. (1.1) of paleo-bathimatry, eustatic sea-level change and sediment loading, gives the Airy compensated tectonic subsidence

$$Z = S(\rho_m - \overline{\rho_b} / \rho_m - \rho_w) - \Delta_{SL}(\rho_w / \rho_m - \rho_w) + (W_d - \Delta_{SL}) \quad (3.1.)$$

where Δ_{SL} is the paleo-sea level relative to present, and W_d is the paleo-water dept. This is the subsidence relative to a stationary datum (today's sea level) that would have occurred in an entirely water filled basin.

~ Chapter 4~

Reconstruction of the Drainage of the Ganges-Brahmaputra Paleo-Deltas on the Bengal Shelf during Last Glacial-Interglacial Cycle.

Luisa Palamenghi[1,2,*], Tilmann Schwenk[3], Volkhard Spiess[4], Hermann R. Kudrass[5]

1-3-4 Department of Geosciences, University of Bremen, Klagenfurter Str. 28359 Bremen, Germany.
1 lupala@uni-bremen.de, 3 tschwenk@uni-bremen.de, 4 vspiess@uni-bremen.de

2 GLOMAR — Bremen International Graduate School for Marine Sciences, University of Bremen, Leobener Str., 28359 Bremen, Germany

5 MARUM — Center for Marine Environmental Sciences, University of Bremen, Leobener Str., 28359 Bremen, Germany
kudrass@gmx.de

* corresponding author

4.1. Introduction

The exposure of continental shelves during Quaternary eustatic variations has played a primary role in shelf margin accretion (Posamentier and Vail 1988; Van Wagoner et al. 1990; Steel et al., 2006) but also during transgressions (Cattaneo and Steel, 2003) and high-stands (Burgess and Hovius, 1998; Muto and Steel, 2002) thick deposits emplaced too.

The space made available for sediment to deposit, the total accommodation, is however offered not only by the eustatic variations but also by the local subsidence and sediment compaction (Posamentier and Allen, 1999; Allen and Allen, 2005). The latter has to be adequately considered to be able to understand the results of complex pattern of subsidence rate such those of the Bengal Basin.

The Bengal Basin is predominantly a huge delta complex fed by the coalesced Ganges and Brahmaputra rivers where the relative contributions to the basin from the Himalaya, Burman margin, Indian craton and Shillong Plateau is under debate (Alam, 1991; Uddin and Lundberg, 1999, 2004; Gani and Alam, 2003; Najman et al., 2008; Najman et al., 2010). The Bengal Basin is mainly located in Bangladesh including the Bengal Shelf, (Fig. 4. 1) at the northern edge of the Bay of Bengal. The mean land elevation of Bangladesh, apart from the Chittangong Hill Tract, is exceptionally low. The Bengal Shelf is also very shallow extending almost 300 km offshore until the shelf break at depths of 90 to 140 mbsl (Fig. 4.1).

Bangladesh's climate is dominated by the monsoon seasonal cycle and the impounded water that accumulates during the summer monsoon season produces a large surface load (Steckler et al., 2010). The water load generates a strong seasonal deflection as large as 6 cm of the ground surface superimposed upon the long-term trend subsidence attributed to tectonics and, in some cases, groundwater extraction (Steckler et al., 2010). The determination of the tectonic subsidence on land is therefore requesting long term observation (Steckler et al., 2008).

The offshore tectonic subsidence on the Bengal Shelf is instead estimated 0.4 mm a^{-1} based on averages of Middle Pleistocene sequences (Hübscher and Spiess, 2005) but only 0.2 mm a^{-1} based on the fossil oolitic shoreline on the western Bengal Shelf related to the sea-level low stands of the Last Glacial Maximum (Wiedecke et al., 1998; Goodbred, 2003).

In order to reconcile the local offshore subsidence results, this study is aimed to experimentally estimate the possible contribution to the total accommodation offered by the early diagenitic process of sediment compaction at the dated well site BODC-3 (Maurin and Rangin, 2009) on the eastern Bengal Shelf (Fig. 4.1). In order to reconstruct the paleo-drainage corrected for the total subsidence, the obtained subsidence rate will be tested on the seismostartigraphic bounding surfaces of the last glacial-interglacial cycle at each major change in the sea level stand.

In time of expected sea level rise (IPCC, 2007) the understanding of the tectonic subsidence at a basin scale is of fundamental importance because it drives the geo-morphological slopes of the receiving

basin and consequently the basin capacity to drain the water in excess that accumulates during the summer monsoon. At higher sea level stands, the tidal effect may increase the landward penetration and may obstacle the fresh water flux, causing permanent flooding of the depressed areas with dramatic consequences on the population, its health and settlement and the national economic sustainment.

4.1.1 Eustasy

Through the Cenozoic, basin base level variations have drastically changed amplitude from greenhouse to icehouse conditions at the Plio-Pleistocene transition (Lisiecki & Raymo 2005; Naish and Wilson, 2009; Sømme et al., 2009). Within the Quaternary, high and low sea level stands had been initially associated to glacial-interglacial periods related to orbital obliquity forcing (40 ky). In coincidence with a global temperature minimum in SST records occurred 920 ka ago (Clark et al., 2006) at the intervening interglacial Marine Isotope Stage 23 being markedly colder than previous interglacial stages, eleven glaciations succeeded at a 100 ky periodicity driven by the eccentricity orbital cycle and produced base level variations of ~100 m (Imbrie et al. 1984, Martinson et al., 1987, Lambeck et al., 2002).

The understanding of the Paleogene stratigraphy of the Bengal Basin is far from being widely accepted, whereas the Neogene rocks, can be divided using biostratigraphy into three seismically distinct and regionally correlatable Megasequences (MS). MS1 extends to NN15-NN16 (ca. 2.5–3.9 Ma), MS2 to NN19-NN20 (ca. 0.4–1.9 Ma) and MS3 to present day (Table 2.1; Najman et al., 2010).

Within the MS3, the Middle-Pleistocene to Holocene sedimentary sub-sequence on the Bengal Shelf consists five 4^{th} order cycles composite sequences composed of rhythmic clinoform beds formed mostly during period of falling sea level stages interrupted by transgressive surfaces (Hubscher et al., 1998; Hübscher and Spiess, 2005; Palamenghi et al., 2011).

4.1.2 Subsidence

The Bengal Basin is a remnant ocean basin that filled since the Indian craton collided with the Eurasian and Burma Plates. In the Mid-Paleocene, about 59 Ma, a soft collision occurred between the northwest corner of the Indian Shield and South Tibet and continued until Early Eocene, about 44 Ma, when hard continent–continent collision commenced and caused to the Himalayan orogeny (Chen et al., 2003; Alam et al., 2003). The eastern limit of the Indian continental crust is unclear (Brunnschweiler, 1966 and 1974; Hutchison, 1989; Mitchell, 1989; Mukhopadhyay and Dasgupta, 1988; Acharyya, 1998;). The continent ocean boundary (COB) beneath the Bengal Basin could be located between the hinge zone of paleo shelf break of the Indian continent and pass offshore approximately down the axis of the upper part of the Swatch of No Ground submarine canyon (Fig.

4.1), deeply incised into the Bengal Shelf (Alam et al., 2003). The depth of the basement in the central deep Bengal Basin is very poorly constrained. A comparison of the crustal thickness and lower crustal velocities from inverse and forward modelling of refraction and wide-angle reflection east and west of the Eocene hinge zone, shows remarkable differences. The basement lies at 1.5 km depth in the westernmost Bengal Basin and 22 km in the easternmost Bengal Basin (Kaila et al., 1992; Reddy et al., 1998; Mitra et al., 2008).

According to the available time-depth conversion, the basement may lie 11.8 km at the BODC-3 well (Maurin and Rangin, 2009) located on the eastern Bengal Shelf margin at 144 mbsl (Fig 4.1).

Thrusting and folding of the Neogene rocks related to the ridge collision with the margin is present in the Chittagong Hill Tract (Fig. 4.1), which is deformed into a series of N–S trending folds and east dipping thrusts (Najman et al., 2010). Further south, the base of the Myanmar margin is covered by sedimentary duplexes uniformly trend uniformly nearly Northwest–Southeast (Maurin and Rangin, 2009).

The cooling of the lithosphere has been causing subsidence in all the large igneous provinces of the Indian Ocean during their development from subaerial exposure into shallow waters and finally to deep sea (Coffin and al., 1992). Origin and the age of the basement in the central deep Bengal Basin are uncertain and the thermal subsidence is therefore very difficult to constrain.

4.1.3 Compaction

In a sedimentary basin the lithostatic stress due to the weight of overburden sediment causes a rearrangement in a closer state where the pore sizes between grains are reduced. In submarine environments, the surface sediments are water saturated but the initial volume of any water saturated sediment with time will be reduced according to the fluid pressure in the pores and the grain-to-grain mechanical strength (Terzaghi, 1936; Terzaghi and Peck, 1948). Such volume reduction is expressed as porosity loss or compaction trends, which obey to a form of negative exponential function where porosity decreases asymptotically with increasing depth (Athy, 1930; Hedberg, 1936).

The compaction trend of the turbidites deposits drilled at ODP Site 718 (Leg 166) located in the central Indian Ocean at the distal end of the Bengal Fan (01°01.252’S, 81°24.065’E, 4730.2 mbsl) shows not much difference to compaction trends built with Hamilton’s sea-bottom velocities. The porosity decreases from 61.8 % at the surface with -2.07 coefficient (Shipboard Scientific Party, 1989b and 1989c; Brusova, 2011).

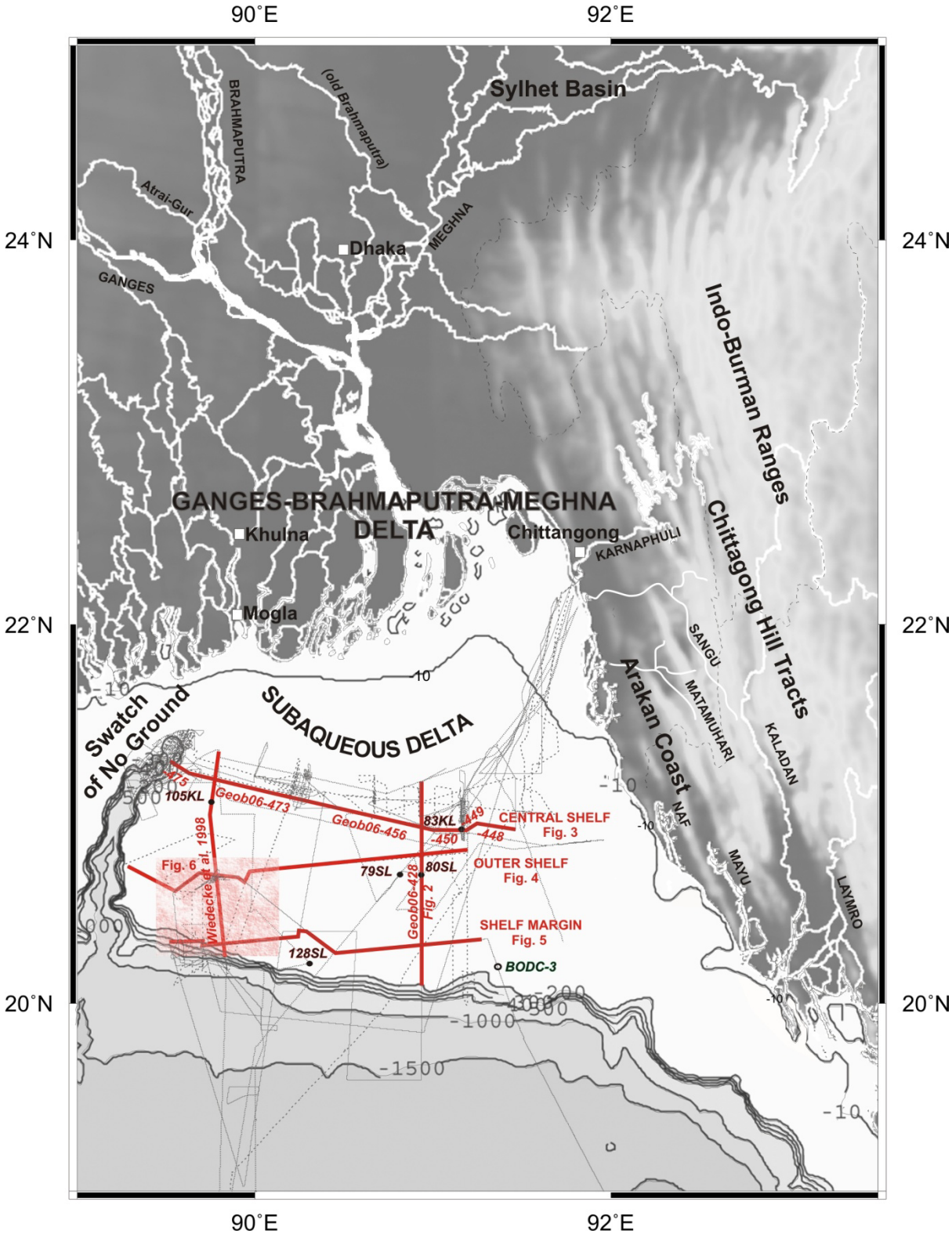

Figure 4.1. General map of the northern Bay of Bengal and location of the regional lines on the prodelta area of the modern subaqueous Ganges-Brahmaputra Delta, on the outer shelf and shelf margin. Bathymetric lines are plotted from the GEBCO-08 One Minute Grid.

4.2. Material and method

4.2.1. Sequence stratigraphy interpretation strategy

Acoustic data were collected using the parametric sediment echosounder Parasound during the expeditions SO93 in 1993, SO126 in 1996 and SO188 in 2006. Its reduced sediment penetration, especially in areas with the presence of sand, has been improved by carrying out a 2D Multichannel Seismic survey (60-180 Hz; 150-200 cm resolution) during the SO188 Expedition to integrate the seismic and acoustic data for a comprehensive interpretation. Regional dip and cross sections from the Bengal Shelf are investigated (Fig. 4.1) and the different acquisition strategies are integrated using the IHS KINGDOM software.

Table 2.1. Stratigraphic nomeclature in usage in this study and references

Name	Age (ka)	MIS	Ref.
HST14	0-7	1	
TST13	7-19		
LST12	19-32	2	
FRST11	32-81.5	3-4	
HST10	131-81.5	5	
TST9	135-131		
Mega-Sequence 3	135-1800		Uddin and Lundberg, 1999; Alam et al., 2003; Najman et al., 2010
Mega-Sequence 2	1800-2600		Uddin and Lundberg, 1999; Alam et al., 2003; Najman et al., 2010
Mega-Sequence 1	2600-5300 (?)		Uddin and Lundberg, 1999; Alam et al., 2003; Najman et al., 2010
Basal unit (Barail Fm. ?)	5300-39000 (?)		Alam et al., 2003

The MCS data are processes with the VISTA (Gedco Co.) seismic processing software package following conventional processing steps (Yilmaz, 1991). CMP binninig distance is usually 5 m but GeoB06-428 has requested a 10 m bin size to maintain an adequate fold. Time-depth conversion for thicknesses estimation was executed with a standard velocity of 1500 ms^{-1}.

The data were interpreted according to Hübscher and Spiess (2005) sequence stratigraphic model (Table 2.1). They adopted depositional sequence model IV (Hunt and Tucker 1992, Posamentier et al.

1992; Emery and Myers 1996; Hunt and Tucker 1995; Catuneanu et al., 2009), but in this research it is used the depositional sequence model II (Catuneanu et al., 2009) where the Sequence Boundaries (SBs) are bounded by subaerial unconformities and their marine correlative conformities taken at the base of forced regressive deposits (Posamentier and Allen 1999). Hübscher and Spiess (2005) did not identify any interglacial, it is therefore introduced a new nomenclature to accommodate them, so that the uppermost composite 4^{th} order sequence contains the system tracts: FRST 11, LST 12, TST 13 and HST 14 (Table 2.1). The time interval when they were deposited is defined based on the expected response of the sedimentary system to the sea level variations (Walbroek et al., 2002). These variations generate specific type of geometrical pattern (Posamentier et al., 1988; Van Wagoner, et al., 1988; Mitchum and Van Wagoner, 1991) and are correlated to the oxygen isotope stratigraphy following Prell et al. (1986) (Table 2.1).

4.2.2 Lithostratigraphic approch

The computation of paleo-thicknesses from recent thicknesses and the isolation of the loading-unloadig subsidence is a common practice (Watts and Ryann, 1976; refer to Chapter 3 for the set of equations). The backstripping is based on some simplifications: (1) the surface load is applied to an Airy-type crust behaving as would a vertical-sided prism, (2) it is assumed a steady subsidence of the basement, (3) a continuous sequence of sedimentation, and (4) no other source for thickness changes than compaction.

However, not only erosion, salt/mud diapirism, cementation and interlayered bedding (Springer, 1993) may invalidate the previous simplifications, but also it is widely known that changes in crustal thicknesses as well as dynamic tectonics may add significant contribution to the total subsidence (Allen and Allen, 2005). Nevertheless, the state-of-art of the structural geology and basin analysis on the central deep Bengal Basin is –especially due to the lack of scientific deep drillings- far away from being revealed.

This study is therefore a first attempt to constrain the loading-unloading subsidence on the submarine Ganges-Brahmaputra delta on the Bengal shelf. The porosity curves are derived from surface gravity cores (SO93-128SL, SO93-79SL, SO93-80SL) collected on the Bengal Shelf during the Cruise SO93. The time of deposition of these cores is derived from their seismostratigraphy. The wet bulk density has been measured onboard by a multi-sensor core logger (Geotek, P. Schultheiss, Surrey, UK) with a gamma-ray probe operating a 10 milli-curie Cs^{137} source. Density logs were converted into porosity by using a grain density of 2.75 gcm^{-3} (Brusova, 2011). The curves obtained are compared with the ODP 718 and 719 from the central and the distal end of the Bengal Fan in the Indian Ocean (Brusova, 2011).

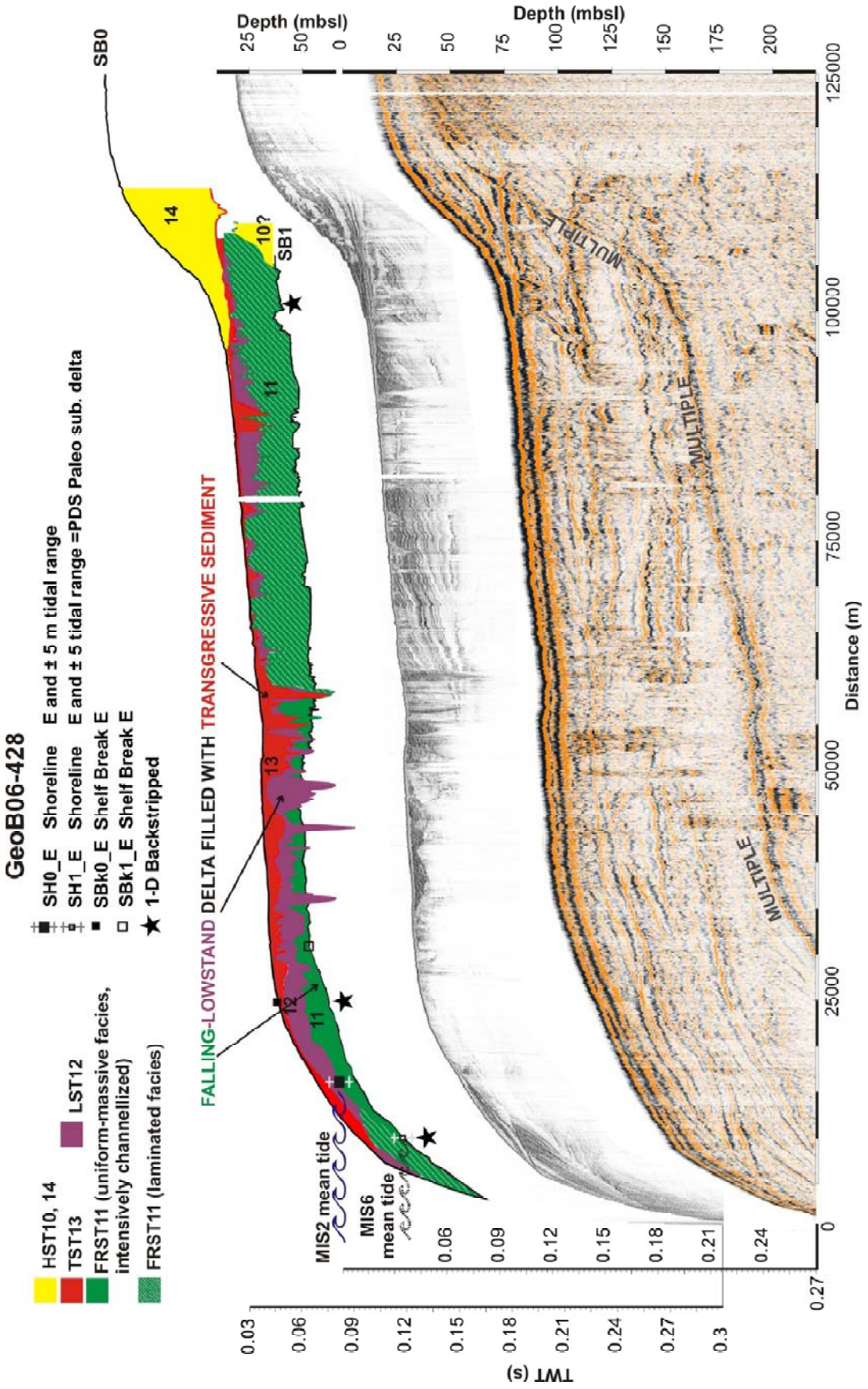

Figure 4.2. Interpreted NS regional dip section (MCS and Parasound) on the Bengal shelf (GeoB06-428).

4.3. Results

4.3.1. Sequence Boundaries

The sequence boundaries (SBs) are diachronous surfaces and while the Upper Sequence Boundary (SB0) is the seafloor (Fig. 4.2), the Lower Sequence Boundary (SB1) is identified by the integration of the Parasound dataset with the MCS profiles and is the base of the FRST11. The onset of FRST11 is set at the surface corresponding to the upper boundary of a stratified unit with typical concordant geometry present at the basin margin close to the Hatia Through and the SoNG eastern flank (Figs. 4.2 and 4.3). This unit has been attributed to the remnants of HST10 due very gentle downlap of the internal reflections on the upper boundary of the TST9 which resemble the downlap angle of the bottomset beds of the modern subaqueous delta in the prodelta area.

In SB0 and SB1 there are evidences of fossil shorelines (Figs. 4.4 and 4.5). Oolitic beach ridges on SB0 are exposed at the seafloor (Fig. 4.4). The beach ridges are lithified due to subaerial exposure (Wiedecke et al., 1998). The lithification causes attenuation of the Parasound signal penetration. From the shallower to the deepest ridge (Fig. 4.6), the surface morphology simplified from complex shoal of elevated multiple ridges and incised channels to simpler ridge with fewer crests and one or no channel. The seaward most ridge marks the position of the maximum sea level regression on SB0 (Fig. 4.6) and a dated core gives an age of ca. 24 ka to this set of beach ridges (Wiedecke et al., 1998; Goodbred, 2003).

Buried bar forms are present also at SB1 (Figs. 4.5 and 4.6), but the lithology of these ridges is not known. The frequent signal attenuation of Parasound while no signal loss in the seismic record may indicate lithification too (Fig. 4.5).

The paleo shoreline position is determined as a mean tidal level established in the infralittoral zone within the range of maximum and minimum tide (Rankey et al., 2011). The high tide level is taken at the crest top and the low tide level on the stoss sides at the base of the deepest beach ridge.

The SB0 maximum sea level regression is at 127.5 msbl ± ca. 2 m tidal range (Fig. 4.6). This ridge is not everywhere present and possibly has been eroded due to minor lithification. The deepest ridge at SB1 points out a possible shoreline at 163 mbsl but a tidal range of 5 m (Fig. 4.6).

None of the given depths is in agreement with the known depths for the maximum regression depth (Walbreok et al., 2002) during sea level low stands at MIS 2 (20 ka, 120 mbsl) and MIS 6 (132 ka, 125 mbsl) indicating they both need to be rebounded by the local subsidence.

4.3.2. FRST 11

The FRST11 filling of the morphologic relief of the receiving basin is composed of two distinct sedimentary bodies: a fan-shaped body on the central Bengal shelf that thins and terminates on the outer Bengal Shelf and an elongated longitudinal body on the continental margin (Fig. 4.7).

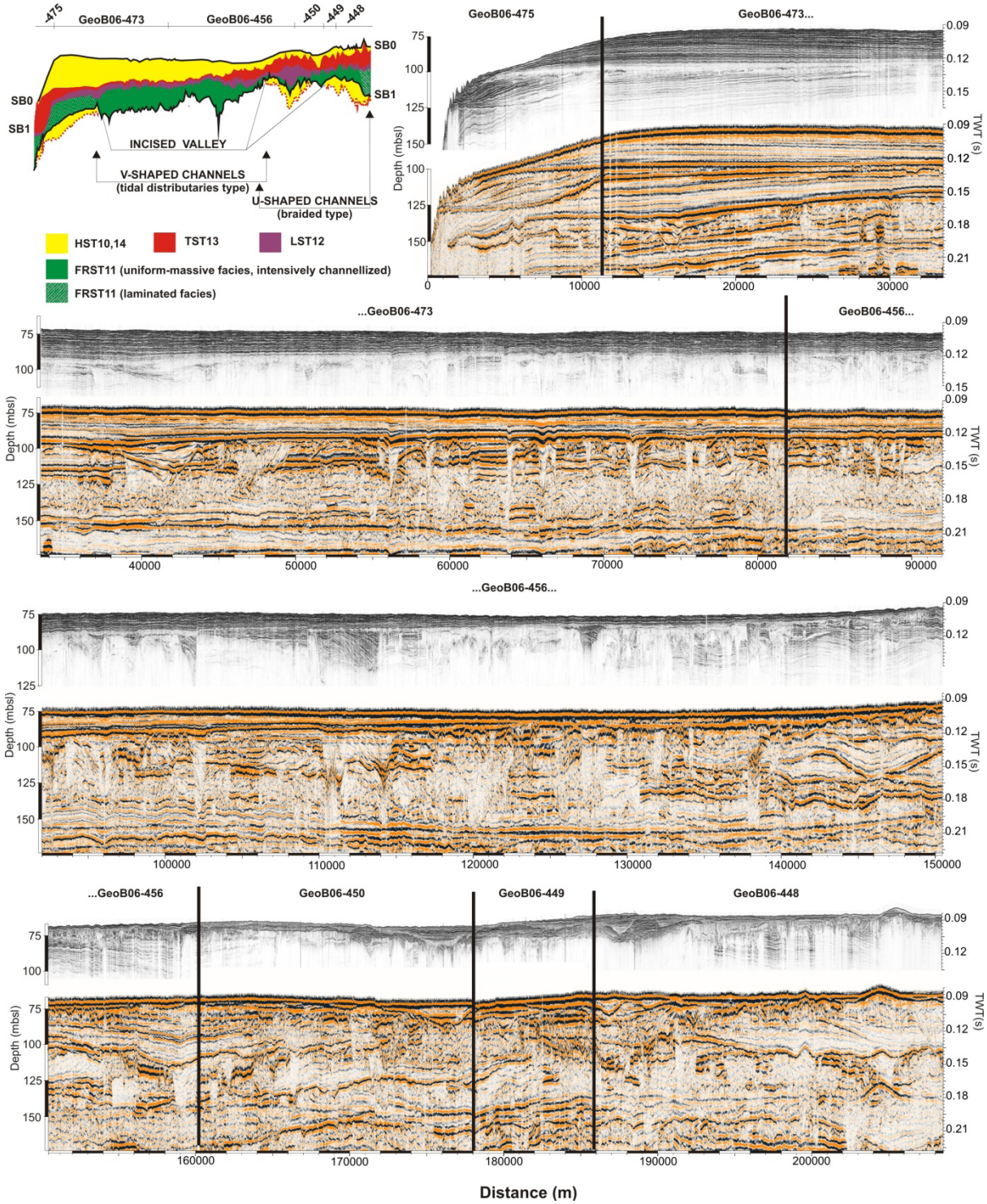

Figure 4.3. Interpreted EW regional cross section (MCS and Parasound) in the central Bengal Shelf composite by the GeoB06-448, -449, -450, -456 and 475. See Fig.4.1 for profiles location.

The FRST11 fan-shaped body on the central Bengal shelf is maximum 15-20 m thick (Fig. 4.7) and two seismo-acoustic facies typologies can be distinguished: stratified either in the MCS and Parasound record and a massive homogeneous facies with no penetration in the Parasound record that appears chaotic in the MCS with no signal loss (Fig. 4.2).

On the eastern outer Bengal Shelf the FRST11 is composed of a prograding sequence of stratified and massive-chaotic deposited beds. The stratified beds of FRST11 downlap on the SB1 with steeper incising angles moving seaward which gives the characteristic forced regressive oblique clinoform stacking pattern (Fig. 4.2). The topset beds of the oblique clinoform are truncated at their top and occasionally exposed at the surface (Fig. 4.2). The massive-chaotic facies extends further south (Figs. 4.4 and 4.5) and wide kilometre scale U-shaped valleys are incised tenths of metres locally eroding into the SB1 (Fig. 4.2).

In the western central Bengal Shelf the stacked oblique stratified clinoform beds of FRST11 are incised by numerous V-shaped channels in the order of tens to hundreds metres width and few metres deep (Fig. 4.3). The offlap breaks of the regressive sequence on the outer western shelf have become locus of oolitic ridges formation and the maximum seaward extent of the fan-shaped body is in the oolitic ridges region (Fig. 4.4).

The thickness of the elongated body on the continental margin is up to 15 m (Fig. 4.7) and it is composed of sigmoidal and convex clinoform beds occasionally erosive truncated (Fig. 4.5). This elongated body does not extend further offshore on the slope and pinches out approximately 300 mbsl.

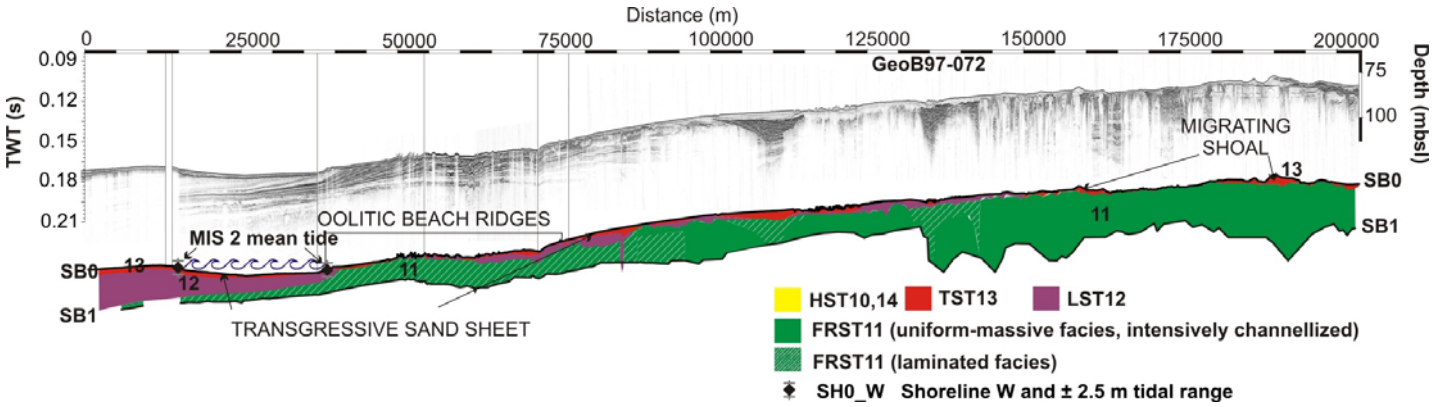

Figure 4.4. Interpreted EW regional cross section (MCS and Parasound) on the outer shelf composed of the GeoB97-072 and several other survey from SO126 and SO93 Expedition. See Fig. 4.1 for profiles location and Fig. 4.6 for shoreline tidal ranges.

4.3.3. LST12

The lower boundary of the LST12 corresponds to the maximum regressive surface that culminated in the Last Glacial Maximum end of base level fall. It would be the sequence boundary interpreted following the depositional model IV (Hunt and Tucker 1992; Hübscher and Spiess, 2005; Catuneanu et al., 2009). The lower boundary of the LST12 is erosive on the outer shelf and becomes concordant at the shelf margin, where LST12 is forming a series of saddle shaped or elongated bodies with stratified seimo-acoustic facies. The maximum thickness of the shelf margin depocentre is 10 m (Fig.

4.7) and the seismo-acoustic data show sigmoidal and convex clinoform beds that dowlap onto the FRST11 elongated body (Fig. 4.5).

In the western outer Bengal Shelf LST12 and FRST11 pinch out (Figs. 4.4 and 4.5) and there is no connection with the saddle and elongated bodies on the margin.

On the eastern outer Bengal Shelf, a lens with chaotic seismic facies is also present in the lower boundary region indicating reworking of the upper boundary of the FRST11 by wave action (Fig. 4.2).

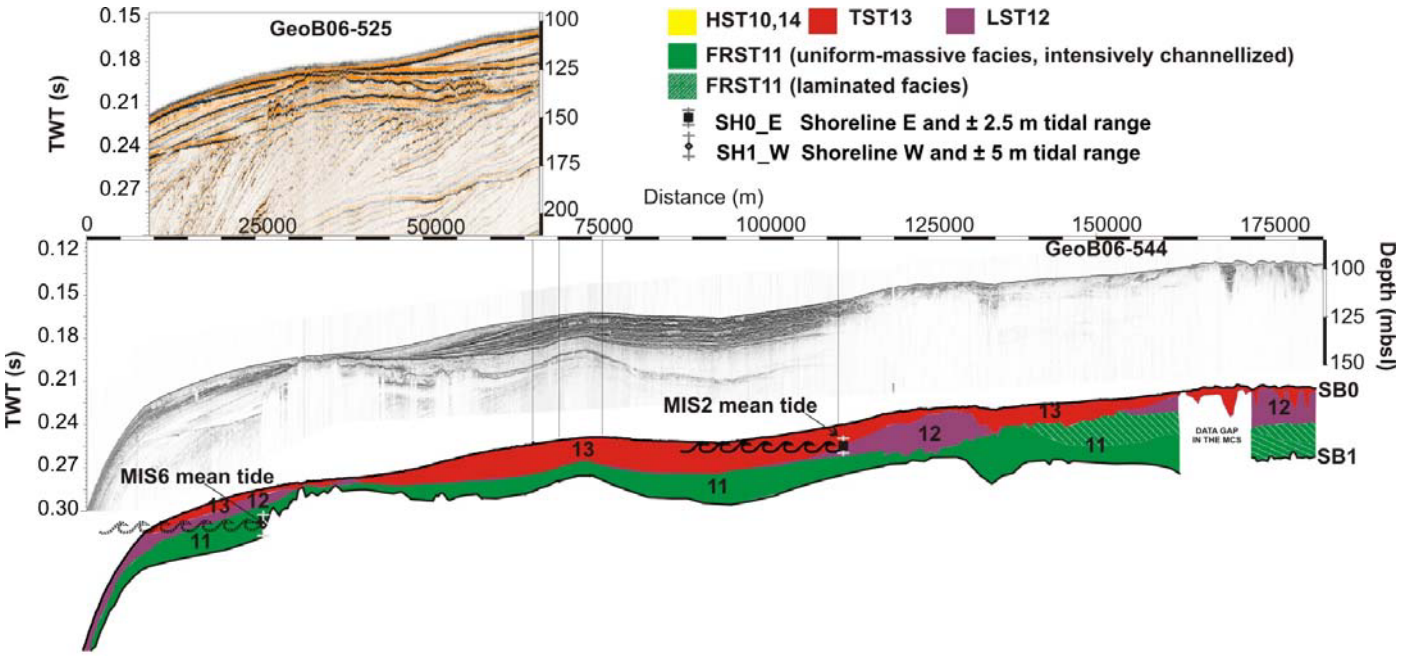

Figure 4.5. Interpreted EW regional cross section (MCS and Parasound) on the Bengal shelf margin composed of the GeoB06-525, -544 and several other surveys from SO188 Expedition. See Fig. 4.1 for profiles location and Fig. 4.6 for shoreline tidal ranges.

4.3.4. TST13

Several transgressive surfaces of erosion (TSEs) are encountered shelf wide and the deepest is the lower boundary of TST13. The V-shaped and U-shaped valleys are filled and truncated by TSEs (Figs. 2 and 3).

The upper boundary of TST13 is the SB0 until the seaward reaches of the prodelta area where it represents the receiving basin of the HST14. In the eastern Bengal Shelf there are some preserved morphological relieves: a series of five U-shaped channels distributed over 30 km and two ridges, 5 km large and 4 m high, with a NS alignment (Fig. 4.3).

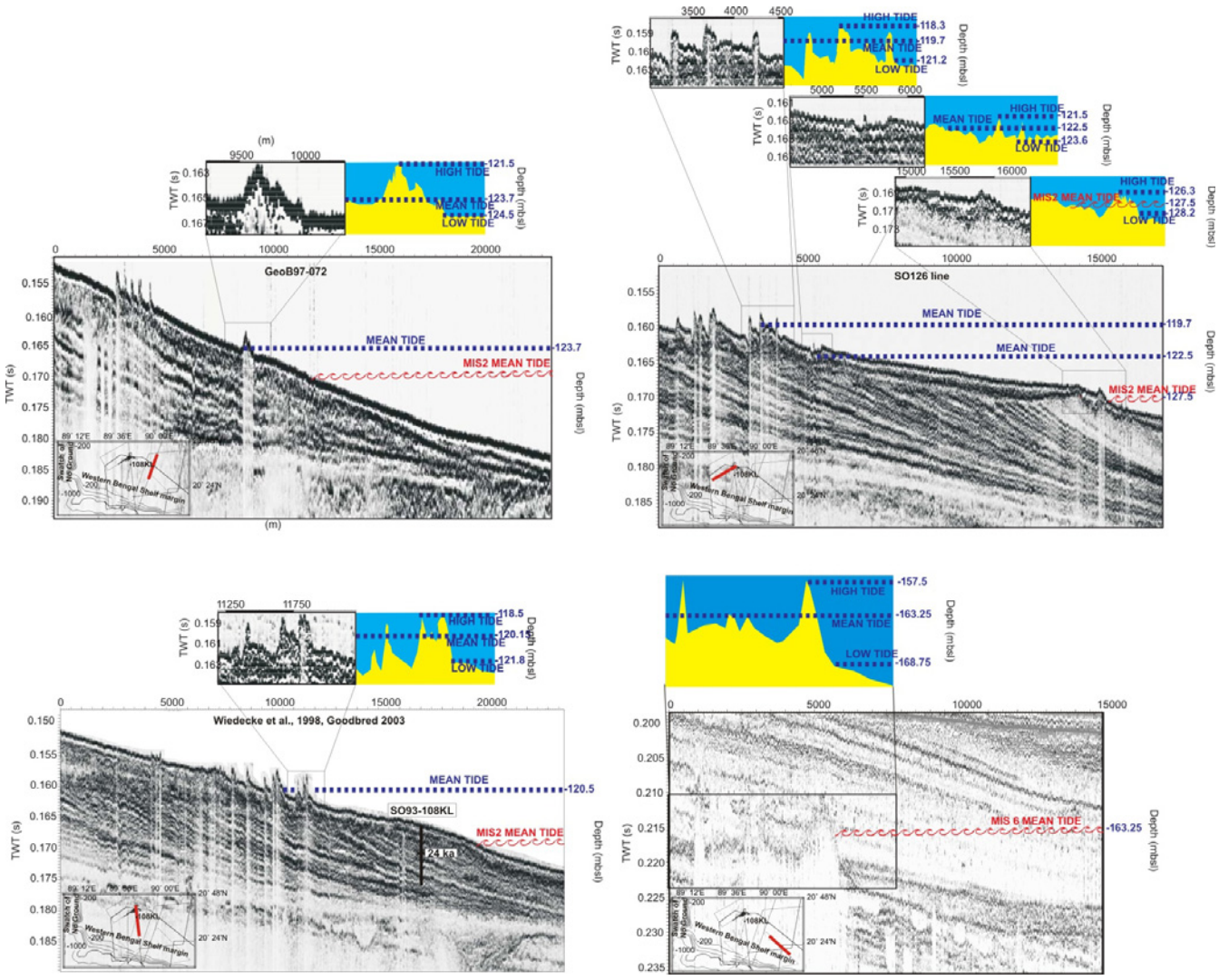

Figure 4.6. Examples of paleo shoreline positions identification from Parasound profiles located on the western Bengal Shelf. Profile location is shown in the insert at the lower leftcorner of the lines. See Fig. 4.1 for insert location. The mean tidal level is established in the infralittoral zone within the range of maximum and minimum tide. The Last Glacial Maximum and second-last glacial maximum (MIS 6) shoreline position is taken at the deepest of the encountered beach ridges.

The thickness of TST13 is mostly only few centimetres of trailing sand (Michels at al., 1998). Thicker deposits in the order of 5 m with a stratified seimo-acoustic facies are associated to filled structures (Fig. 4.7). Only a lobate body of more relevant thickness of 10-15 m is detected on the outer Bengal Shelf bounded on the west by the oolitic beach ridges and to the east by relief of acoustic transparent facies from LST12. The seimo-acoustic facies in the lobate body beds is stratified occasionally disrupted by small acoustic transparent lenses. The surface of the lobate body present evidences of erosion (Fig. 4.5).

4.3.5. HST14

The topset beds of the modern subaqueous delta extend several tens of km offshore the delta on the inner Bengal Shelf, but our data set is limited to water depth <-15 mbsl. The imaged portion of the stratigraphic sequence is maximum 70 m thick (Fig. 4.7) and has been divided into two sub-units: Sub-Unit 1 and Sub-Unit 2 (Palamenghi et al., 2011). Sub-Unit 1 is interpreted as a mixed sequence of bottomset and incoming foreset beds, and Sub-Unit 2 is composed of an individual sigmoidal clinoform building block of the prograding stratigraphic sequence of the Ganges–Brahmaputra subaqueous delta. Sub-Unit 1 was estimated to have been deposited between 4-7 ka and 0.2 ka ago. Sub-Unit 2 since the Ganges final convergence and confluence with the Brahmaputra ca. 300 years ago (Palamenghi et al., 2011).

4.3.6. Core location and sedimentary paleo-environment

The near surface sediment lithology is well described by sediment cores (80 SL, 79 SL, 128 SL, 105 KL and 83 KL) and the conversion from wet bulk density into dry bulk density and porosity is contained in Appendix I.

The cores contain all greenish gray terrigenous silt and clay, with occasional layers enriched in sand (Kudrass and Scientific Shipboard Party, 1994). Density and the negative exponential equation for the porosity trends are shown in Fig. 8.

4.3.6.1 SO93-80 SL

Core 80 SL is 6 m long and was collected 78 mbsl on the central Bengal Shelf (Fig. 4.1). 80 SL is laminated and contains at a depth of 287 cm a burrowed diffuse enrichment of fine sand with numerous benthic foraminifera, small shells and spines of echinoidea. The fauna of benthic foraminfera contains many Elphidium, Asterorotalia, Ammonia and some Triloculina, Spirococulina, Bolivina, Hoeglundina. No planktonic foraminfera were found. The core samples a clinoform sequence truncated at the topset (Fig. 4.2). This core was taken within FRST11 attributed (Hübscher and Spiess, 2005) to the falling period of MIS 4 and 3 (81.5-32 ka) that culminated at the Last Glacial, MIS 2. The truncation of the uppermost deposits might have been sub-aerially eroded or removed during the transgression. The depositional paleo-environment is however fully marine and is probably from a water depth of 20 to 30 m. (personal communication W. Weiss/BGR).

The mean density is 1.74 g cm^3 and surface porosity is 53% (Fig. 4.8).

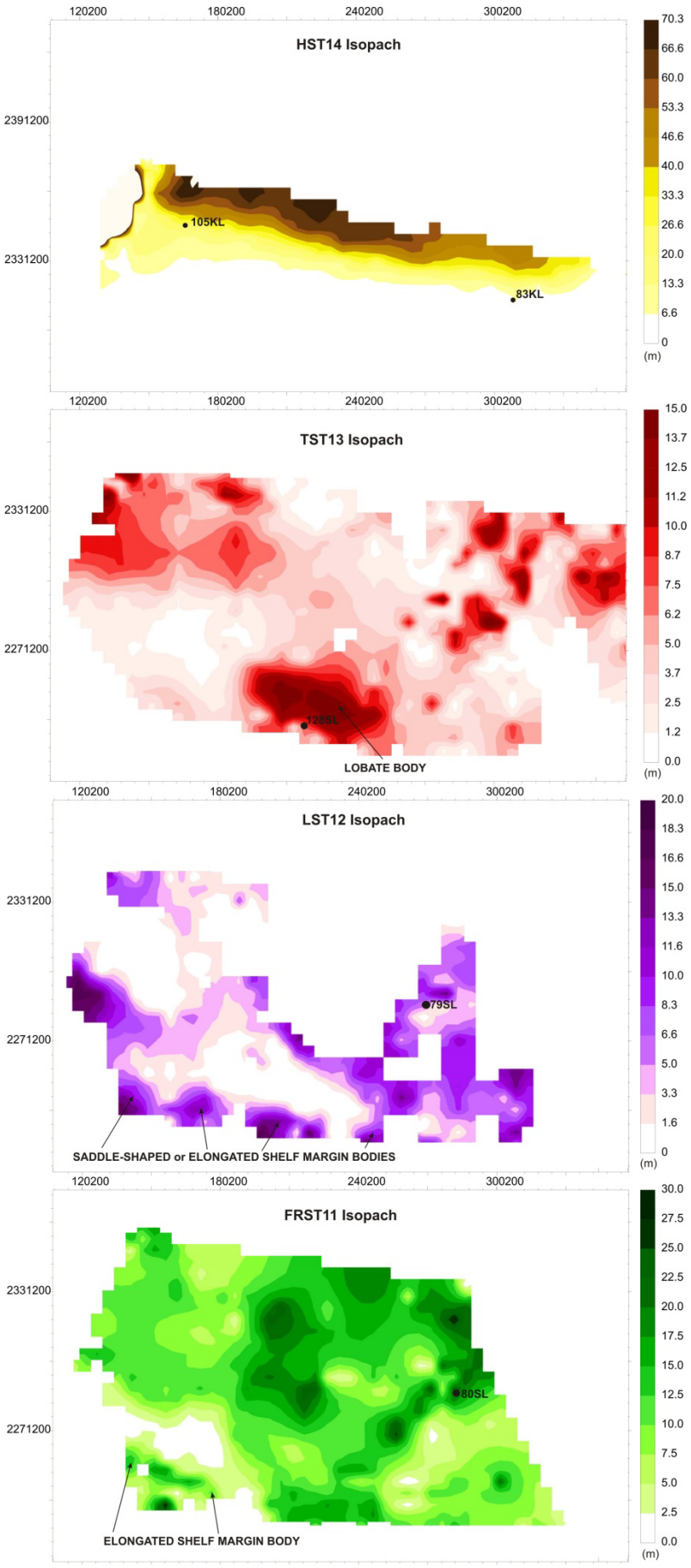

4.3.6.2. SO93-79 SL

Core 79 SL is 4 m long and was collected on the eastern outer Bengal Shelf at 87 mbsl (Fig. 4.1) and consists in the uppermost 40 cm of trailing sand and below overconsolidated mud with numerous thin layers of very fine sand with flaser bedding below (Kudrass et al., 1994: Michels et al., 1998). This area has been certainly sub-aerially exposed during maximum regression of MIS 2 (32-19 ka). The acoustic facies in the core vicinity is chaotic (Fig. 4.4) but the flaser bedding in 79SL suggests a tidal influence toward the end of base level fall in this area followed by the establishment of a fluviatile-deltaic environment. The overconsolidation is provoked by the drying up of the sediment during exposure suggesting this was probably an elevated area, pe. a levee or a river bank. The numerous evidences of reworking (Hübcher et al., 1998) such as erosive surfaces and migrating shoals (Fig. 4.4) however preclude from an unambiguous paleo-environmental reconstruction. The mean density is 1.71 g cm^{-3} and surface porosity is 59% (Fig. 4.8).

Figure 4.7. Isopach grids of the FRST11, LST12, TST13 and HST14 by using a velocity of 1500 m/s and compaction trend for the system tracts as derived from core SO93-105KL, SO93-83KL, SO93-128SL, SO93-79, SO93-80SL. For image clarity reasons the survey lines net used to create the grids is not shown, please refer to Figure 1 for survey lines distribution.

4.3.6.3. SO93-128 SL

In general, the majority of the deposits on the shelf associated to the sea level transgression (19-7 ka) consist of chaotic top layers from thin to severa1 centimeters thick of sandy mud with abundant shall debris or lateritic gravel.

Stratified transgressive deposits are detected instead in cut-and-fill structures in the central and outer Bengal Shelf and in the lobate body identified in TST13 on the outer Bengal Shelf (Fig. 4.7) where indeed the Core 128 SL has been collected (Fig. 4.5). Core 128 SL is 4.72 m long and was retrieved 145 mbsl. It consists, apart from the uppermost 5 cm of sand, of partly oxidized finely laminated mud, with burrows at the top (Kudrass et al., 1996). The presence of burrows indicats a well oxygenated environment at the time of deposition in contrast with the present day barren condition caused by an oxygen minimum zone (Berner et al., 2003). Bioturbation in present day is observed in the topset beds of the subaqueous delta but it becomes negligible in the forest and absent in the bottomset beds.

The typical mean density of the trailing sand is the higher of the sequence (1.76 g cm^{-3}) but the surface porosity, 55%, is lower due to high sand content. The mean density of 128SL core is 1.52 g cm^{-3} and surface porosity is 69% (Fig. 4.8).

4.3.6.4. SO93-107 KL and 83 KL

The 107 KL and 83 KL are 4.9 m and 5 m long respectively and have been collected in the bottomset of the modern subaqueous delta clinoform beds (HST14). The 107 KL core was taken 90 mbsl and the 83 KL at 74 mbsl. The cores were dated using gamma spectrometry and the nuclides ^{137}Cs, ^{228}Ra, ^{226}Ra, and ^{210}Pb. According to their sedimentation rate of 0.3 cm/yr and 1 cm/yr, the bases are ca. 1600 and 500 yrs old (Suckow et al., 2001).

They display regular horizontal bedding, but the relative sand content decrease in 107 KL (Michels et al., 1998).

The mean density of 107 KL and 83KL are 1.55 g cm^{-3} and 1.61 g cm^{-3} and their surface porosities are 65% and 64% respectively (Fig. 4.8).

4.3.7. Decompaction and backstripping of BODC-3 well

The compaction trend curve is based on an ideal stacked record composed by the sum of the cores in chronological order from the youngest to the oldest one. From the resulting porosity curve (Fig. 4.8) the loading subsidence has accounted for 6.2 km and compaction for 1.4 km. The remaining 4.2 km of accommodation in the 11.8 km sediment column (Maurin and Rangin, 2009) might be given by sea level variations plus an undefined amount derived from thermal subsidence.

When sedimentation rate started at the BODC-3 is unknown as the well do not extend further than the late Miocene. From the Eocene paleo-shelf break of the Indian continent, the margin has prograded

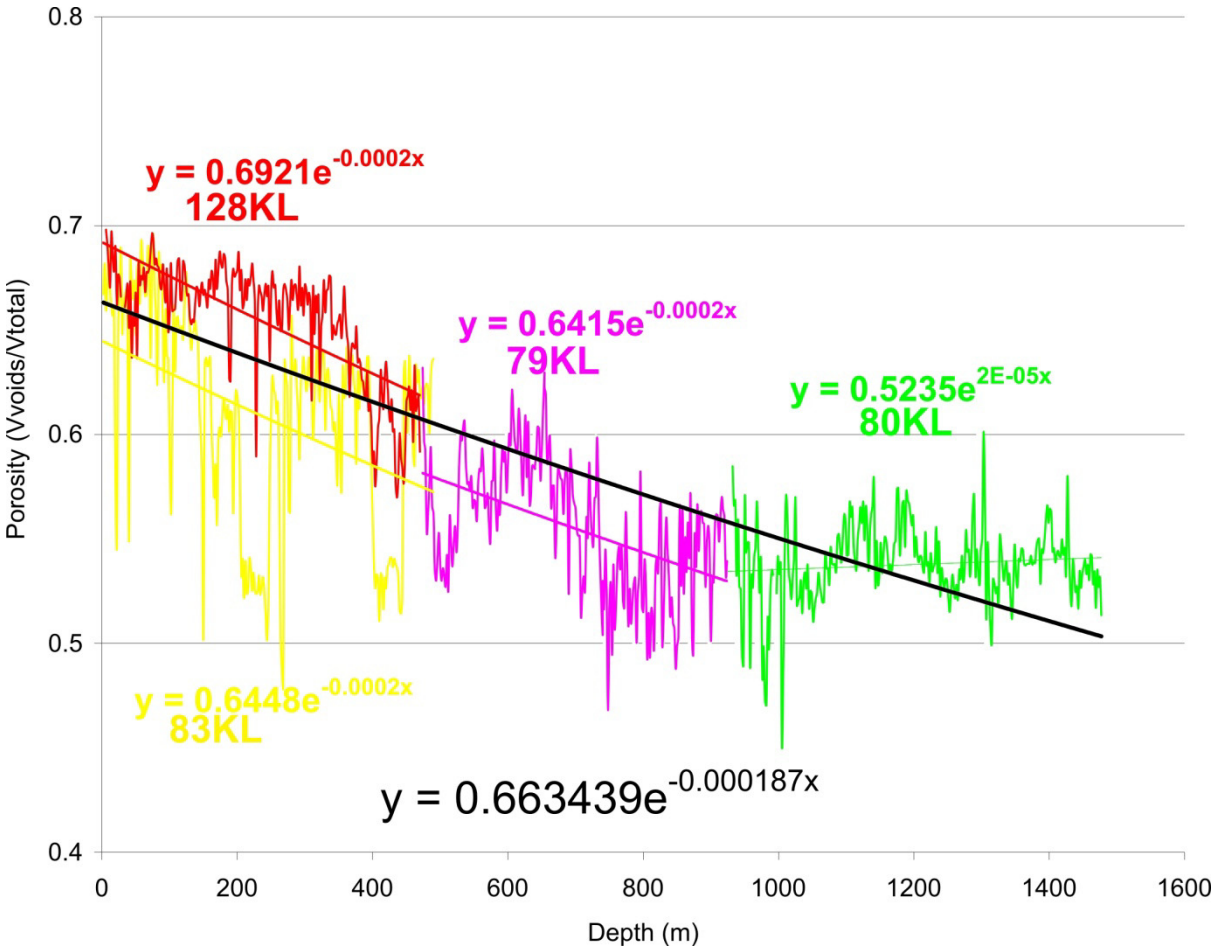

Figure 4.8. The stacked porosity profiles along the simplified chrono-stratigraphic succession is derived from the compaction trend of SO93-105KL, SO93-83KL, SO93-128SL, SO93-79, SO93-80SL.

more than 400 km offshore. The water depth during the soft collision of the Indian Craton with Eurasia is poorly constrained, however missing the mountain ranges as source for the sediments is expected only pelagic sedimentation load affecting the basement. During the Oligocene and Miocene eustatic variations, the margin has mostly prograded (Johnson and Alam, 1991; Alam et al., 2003), while the sea level has caused margin aggradation during the Pleistocene. It is expected active pelagic, emi-pelagic and/or turbiditic continuous sedimentation since the Oligocene.

Assuming the load becoming effective since the beguin of the Oligocene, the subsidence rate results 0.178 m/ka. The same exercise is repeated along two ideal transects on the eastern and western Bengal Shelf, at selected locations. The modern (SD) and the relict subaqueous delta (PSD), the

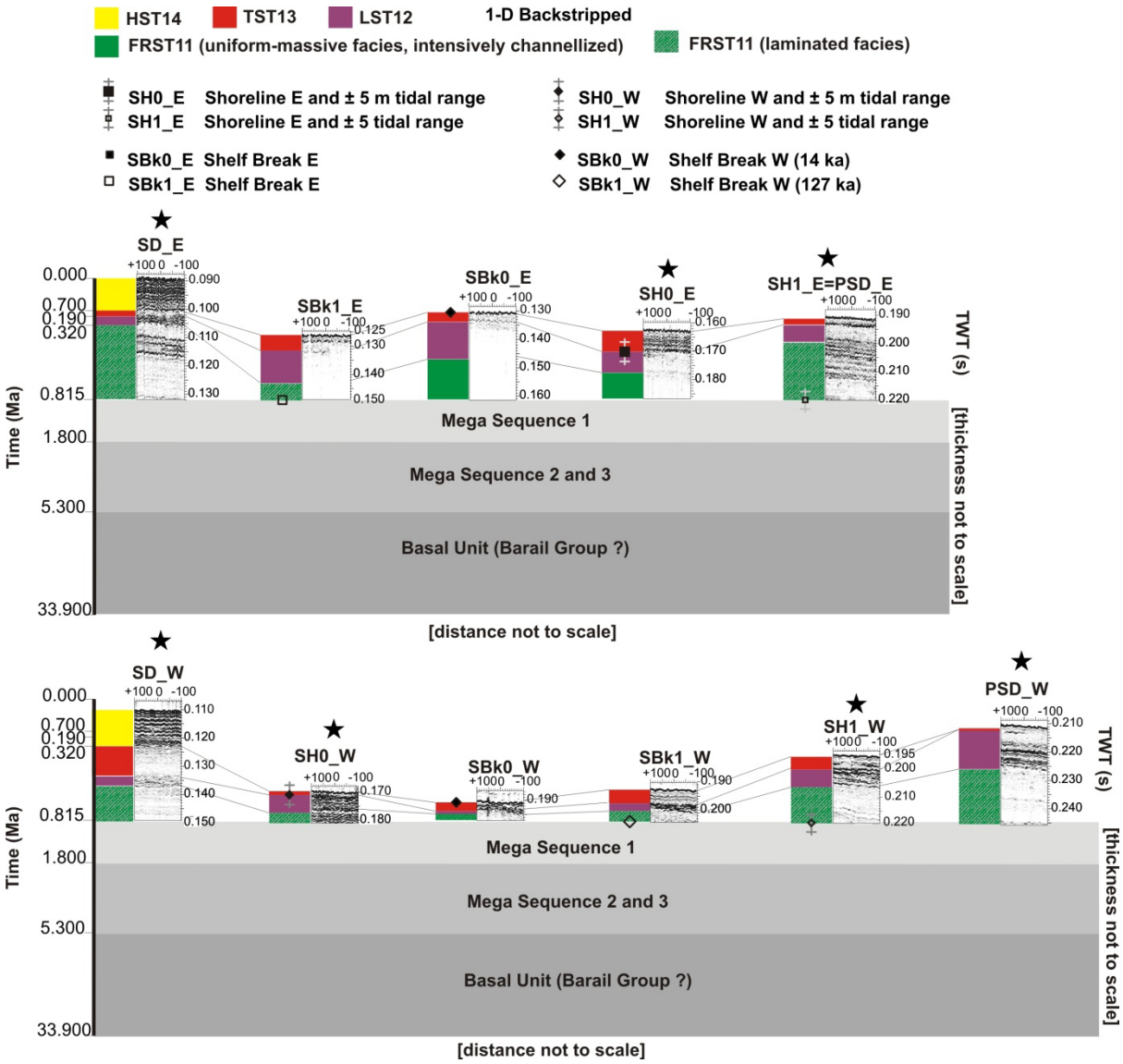

Figure 4.9. Illustration of the simplified chrono-stratigraphic succession of seven units from the basement to the surface adopted to perform a 1-D backstripping and to apply the Airy isostatic correction. Abbreviation: SD_E and SD_W are selected location for back stripping in the depocentre of the modern Subaqueous Delta (ca. 4-0 ka old); SH0_E and SH0_W are the shorelines and their tidal interval (Fig. 4.2) at MIS2 detected on the upper sequence boundary, SB0; SH1_E and SH1_W are the shorelines and their tidal interval (Fig. 4.2) at MIS6 detected on the lower sequence boundary, SB1; SBk0_E and SBk0_W are the shelf breaks during Termination I detected on the upper sequence boundary, SB0; SBk1_E and SBk1_W are the shelf breaks sculptured during Termination II after MIS6 detected on the lower sequence boundary, SB1; PSD_E and PSD_W are selected location for back stripping in the depocentre of the Paleo Subaqueous Delta (ca. 81.5-14 ka old).

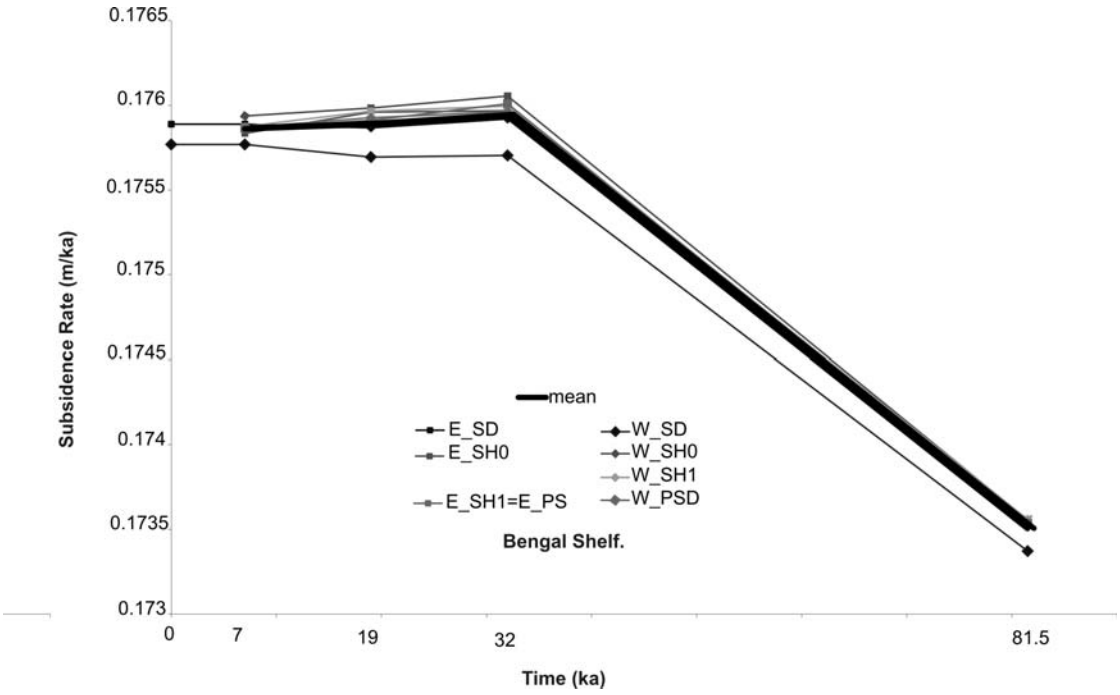

Figure 4.10. Eastern and western Bengal Shelf tectonic subsidence rate (m/ka).

modern (SbK0) and the paleo-shelf break (SbK1), the paleo-shorelines (SH0) of MIS 2 and MIS 6 (SH1) were also backstripped (Fig. 4.9). The subsidence rate derived does not differ significantly from that calculated at the BODC-3 site (Fig. 4.10). The variations re-enter within a millimetres dimension scale far beyond the seismo-acoustic measurements resolution and consequently the results here presented and discussed has to be considered as a thoughtful experiments with an error deriving primarily from the instrument accuracy (0.2 m) and in a manner which cannot be quantified from the used porosity trend. There are however some interesting details to notice:

(1) The deposition of the FRST11, LST12, TST13 and HST14 contributed to the lithostatic stress caused by the sedimentation of the last glacial-interglacial cycle composite sequence (10-35 m) has produced as much accommodation as the thickness of the sequence.

(2) The change in elevation from the compacted and decompacted thickness increases in the subaqueous delta on the western shelf where compaction has produced 20 cm of additional accomodation.

(3) The maximum rebound is necessary for the SB1 where 43 cm have been produced due to the effect of compaction.

(4) The prodelta area and the shelf margin are the regions where there is the maximum increment of porosity loss due to overburden pressure.

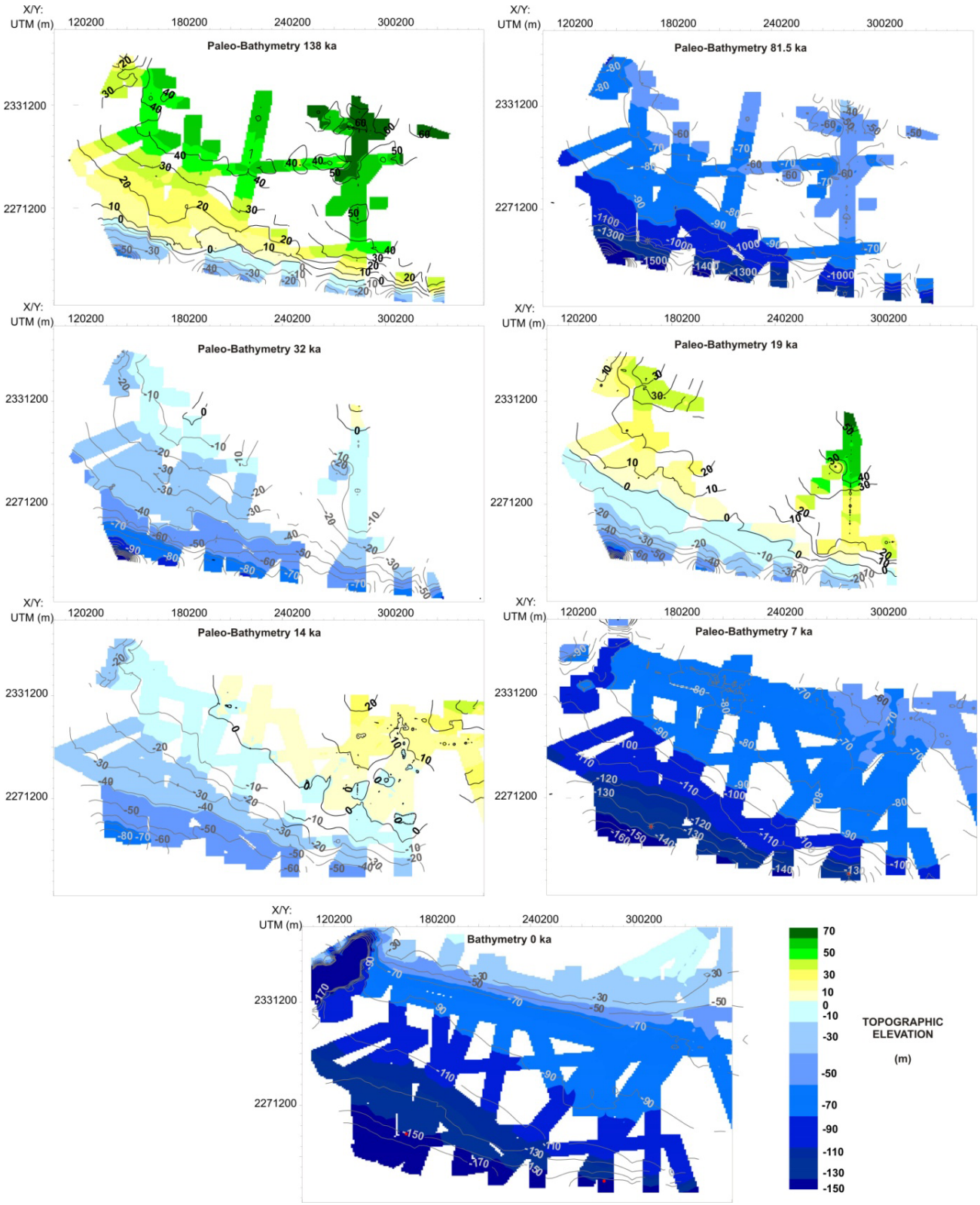

Figure 4.11. Paleobathymetric reconstruction at the top and bottom of each system tract of the last Glacial-Interglacial cycle. The subsidence correction is limited to the tectonic subsidence compensation as the accuracy of the Parasound depth measurements is inferior to the compensation effect derived by compaction. For image clarity reasons the survey lines net used to create the grids is not shown, please refer to Figure 4.1 for survey lines distribution.

4.4. Discussion: paleo-drainage reconstruction

The lithostatic pressure exerted on the basement from the uppermost composite sequence has been demonstrated to be significant; however, the porosity loss within its deposition is a much smaller component. The accuracy of the Parasound measurements (10-40 cm) is at the limit or below the effect of compaction which has not been included in the calculation of the paleo-bathymetric grids.

The bathymetric correction of the grids is therefore limited to the tectonic subsidence by applying a mean isostatic rebound derived from the interval mean subsidence rate. This has been applied to the top and bottom of each system tract. The bounding surfaces are correlated to a time (Fig. 4.9) by using a stratigraphical approach and the scattered dated cores on the shelf (Wiedecke et al., 1998).

The paleobathymetic reconstructions (Fig. 4.11) will be analyzed in order to identify the main depocentre formation and shift of each of the system tracts respect to the initial receiving basin.

4.4.1. Initial basin morphology at the onset of the Last Glacial-Interglacial cycle

4.4.1.1. Central Bengal Shelf

The presence of HST10 in the outermost reaches of the central Bengal Shelf outlines the across shelf extension of the incised valley (Figs. 4.2 and 4.3) created by the effects of base level fall. The depositional environments during the normal regression in the last Interglacial (MIS 5) must have shifted from distal to more and more proximal as HST14 is currently prograding. If the HST10 had prograded further offshore on the outer shelf is not possible to be unambiguously ascertained but the scarce recovery elsewhere than the central Bengal Shelf of a facies with a similar geometry seems to point also to the hypothesis that HST10 did not prograded much further than present day HST14.

The deep Indian Ocean circulation did not change significantly (Thomas et al., 2007) during Last Glacial-Interglacial cycle (140-0 ka). The climate during Last Interglacial Monsoon, based on stalagmite records of the atmospheric circulation from the Chinese loess plateau, initiated with a significant insolation decrease at the end of Monsoon Termination II when an insolation rise took place, indicating that the low Last Interglacial Monsoon ^{18}O values result from Northern Hemisphere insolation changes (Kutzbach, 1981; Yuan et al., 2004). Precipitations were already largely decreased at the end of the last Interglacial during MIS 5.1 and 5.3 and might have not supported a sediment supply sufficient to cover the transit time expected for the Brahmaputra to reach the shelf margin within relative sea level rise (Burgess and Hovius, 1998; Muto and Steel, 2002). Another possible explanation to the missed transit toward the shelf margin, which does not need to invoke external forcing, could be the distribution of the intra-basin accommodation. The plenty of space in the Swatch of No Ground shelf canyon could have created a sediment flux diversion toward the Bengal Fan sequestering large part of the subaqueous shelf deposition. The excavation processes of the SoNG

were already in act during the whole MIS 5 implying that similar shelf conditions as present day are largely possible (Palamenghi et al., in prep).

Many uncertainties derive from the subaerial component, however, at the onset of FRST11 the river graded profile could have significantly changed due to a very rapid seaward shift of the shoreline, if the slope angle of the topset beds was as flat as it is today (< 0.01°). Maximum sea level fall at MIS 4 was in the order of 80 mbsl which would have been largely sufficient to expose the topset. Once subaerially exposed the topset of HST10 could have became progressively dismantled and dissected by river course which redistributed the HST 10 sediments over a broader surface contributing significantly as source for the FRST11 deposits.

4.4.1.2. Outer Bengal Shelf and Margin

The paleo-shoreline positions at MIS 6 (W_SH1 and E_SH1) on the SB1 fall both seaward (Fig.s 4.9 and 4.11) to the respective shelf breaks (W_SBk1 and E_SBk1). The slope angle of the SB1 shorelines is very steep in this region (>3°) implying, when this was a shoreline, strong tides and/or very energetic waves (Fig. 4.11). The potential lithification of the MIS6 beach ridges (Fig.s 4.5 and 4.6) might have attenuated the effects of transgression associated to Termination II. The shelf breaks (W_SBk1 and E_SBk1) lying landward of the shoreline did not receive significant sedimentation during the TST9 (Hübscher and Spiess, 2005).

4.4.2. Base level changes during falling and low sea level

Sea level after MIS 5 did not fall uniformly towards MIS 2 level, but oscillated rapidly with amplitudes of 10–15 m about every 4,000 years. The cold stadials MIS 5.4 and 5.2, and, possibly MIS 4, occurred at the time of minima in insolation (Lambeck et al., 2002). Based on the paleobathymetric reconstruction (Fig. 4.11) and benthic assemblages, the laminated seismo-acoustic facies in FRST11 and LST12 is interpreted as subaqueous delta deposits of a mid-shelf (Fig. 4.12A) to shelf margin (Fig. 4.12B) delta (Porębski and Steel, 2003; Porębski and Steel, 2006). The massive-chaotic facies is interpreted as subaerial deposits and/or reworked deposits of the FRST11 during subaerial exposure within the MIS2.

Arid climate, weaker SW winds and altered sea surface circulation (Prell et al., 1980; Duplessy, 1982; Tierney et al., 2008) are typical for the Last Maximum Glacial (26-19 ka) in the tropical and equatorial regions of the Indian Ocean. Recent general circulation models of the Inter Tropical Convergence Zone response to Northern Hemisphere ice sheets during Last Glacial Maximum simulate decreased glacial precipitation in the Indian Ocean (Chiang and Bitz 2005; Broccoli et al., 2006).

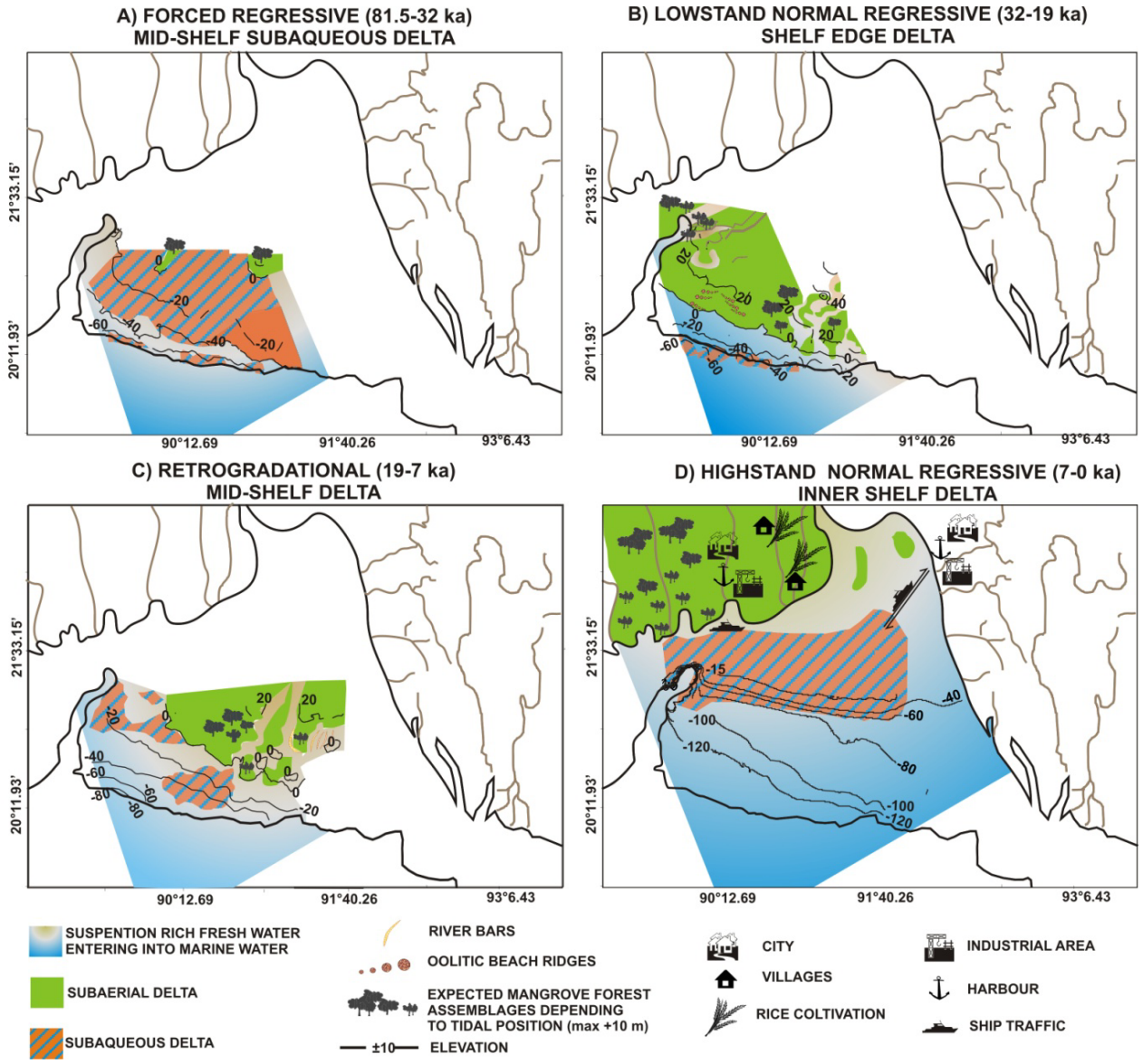

Figure 4.12. Paleo-drainage reconstruction of the Bengal Shelf during A) the forced regression phase, B) the normal regression during lowstand, C) the retrogradation of shoreline during transgression and D) present day condition.

The present day rainfall maxima associated to the monsoon occur in the frontal regions along the entire Himalaya (Bookhagen and Burbank, 2008) while at glacial time it increased in the southern Arakan coastal basin (Broccoli et al., 2006). The modeled shift in locus of precipitation is consistent with the details of the LGM salinity reconstructions (Duplessy, 1982; Cullen, 1981), which show that the salinity minimum moves from the northernmost Bay south to 15°N, consistent with shift in water influx from the Ganges–Brahmaputra to the Arakan coastal region. Despite the general pattern of modeled ITCZ migration between glacial and modern is supported by the εNd data, indeed the

magnitude of recorded variations in salinity and sediment flux are larger than modeled precipitation changes would suggest (Pierson-Wickmann et al.,2001; Stoll et al., 2006).

The discovery of a shelf margin delta on the eastern Bengal shelf (Fig. 4.12B) may explain the salinity variations and the excess of sediment flux and the significant differences across the Bengal Shelf can further contribute to outline the paleo-drainage during this climatic transition.

4.4.2.1. Eastern Shelf Margin

The prevailing occurrence on the eastern outer Bengal Shelf and margin of the broad U-shaped valleys and of the massive-chaotic facies of FRST11 and LST12 (Figs. 4.4 and 4.5) indicates a river course debouching close or at the slope. This river course might have formed a mid-shelf delta during falling sea level (Fig. 4.12A) and then, during maximum low sea level, a shelf margin delta (Fig. 4.12B). The massive-chaotic facies on the eastern Bengal Shelf has been deposited within a typical (Bristow and Best, 1993) braided deltaic plain. The U-shaped valleys widths, their lateral relationships and the scour depth, strongly support this interpretation (Fig. 4.3). One obvious hypothesis would be that this delta represents the Paleo-Brahmaputra delta. This hypothesis is strongly based on the similarity of the present day and paleo-braided regime. It is not obvious that the Brahmaputra must have always the same type of outflow within a normal regression under high-stand and low-stand relative sea level. Indeed, not only the slope of the receiving basin has changed being much steeper toward the end of base level fall (Fig. 4.11) when the SH0_E went beyond the SBk1_E. The atmospheric and oceanographic conditions associated to a glacial and interglacial phases are also not the same.

In a second hypothesis, this delta could have been formed and supplied by other rivers from the lesser Himalaya (Titsa, Atrai-Gur) or Indo-Burman (Meghna) or Northern Arakan (Karnaphuli, Sangu, Matamuhari, Naf) (Fig. 4.1). The sourcing region of the Titsa and the Atrai-Gur rivers underwent to the same precipitation reduction as the Ganges and Brahmaputra, as well as meander belt of interpreted late Pleistocene age are recognized in the alluvial plain and associated to these rivers (Coleman, 1969). If the Indo-Burman and Northern Arakan rivers (Fig. 4.1) instead benefitted from enhanced precipitations during falling and glacial time (Broccoli et al., 2006), they might have had increased sediment supply delivered to the shelf, particularly the Meghna, which is still today one of the mayor river in the Bengal Basin. The present day Meghna has a meandering regime, but due to slope gradient it may have developed a braided river on the shelf. The εNd increase throughout the Bay between 12° and 15°N (Colin, 1999; Pierson-Wickmann et al., 2001; Stoll et al., 2006) could be explained as carried from the inner shelf toward the margin via the mid-shelf and shelf margin delta possibly interpreted as the paleo-Meghna collecting the Norther Arakan Rivers as tributaries. In favour of this scenario, Holocene surface sediment samples retrieved in the Hatia Thought present the

same εNd anomalous signal (Personal Communication, France-Lanord/CRPG-CNRF) recorded in the margin during the Pleistocene and early Holocene. This evidence indicates the Northern Arakan rivers still have a different isotopic signature compared to the Himalayan rivers.

There are no studies about the Southern Arakan rivers, (Kaladan, Mayu and Laymro) falling and low stand conditions either about their geochemical signature. It is hard to imagine the Southern Arakan rivers flowing toward the north on the Bengal Shelf, and it is rather expected they connected to the Arakan Shelf (Myanmar). If they would present an εNd anomalous signal compatible to that recorded on the Bengal Shelf margin, this could have been carried along the shelf margin (Fig. 4.1) by a west or south-west oriented current. The existence of such current has been already postulated (Colin, 1999; Pierson-Wickmann et al., 2001; Stoll et al., 2006) but the suggested signal source is the Ayeyarwady Delta in the Andaman Sea which has well known compatible isotopic signature with the one recorded on the Bengal Shelf margin. When the NE winter monsoon (Ramaswamy et al. 2004) is enhanced during glacial time, it might be responsible for this contour current.

A broad spectrum of variations between these two hypotheses may exist. Potentially, after careful and regional provenance studies, it will be possible to establish a consequential succession of the impact the Indo-Burma Range tectonic and climatic influnce on the Bengal Basin. This study however highlighted for the first time, beyond the establishment if we are dealing with the Paleo-Brahmaputra or the Paleo-Meghna, that the signal could have been certainly transported through the shelf and only potentially along the Arakan and Bengal Shelf margin following the paleo-oceanographic transport pathways.

4.4.2.2. Western Bengal Shelf

The paleo geomorphological reconstruction on the western outer Bengal Shelf differs quite significantly from the eastern Bengal Shelf (Fig. 4.11). During late falling and lowstand (Wiedecke et al., 1998; Goodbred, 2003), oolitic beach ridges evolved as self-organized and autigenic deposits (Rankey et al., 2011) and the SH0 advance stopped prior to reach the SBk1_W (Fig 4.9). The V-shaped channels (Fig. 4.3) are confined in the central western Bengal Shelf and only the stratified deposits of the FRST11 oblique clinoforms are recovered on the outer shelf and interpreted as the subaqueous delta deposits of the V-shaped channels (Fig. 4.12B). The depth-width aspect ratio of the V-shaped channel in the prodelta area resembles a network of river distributaries channels and tidal inlets. The absence of any subaerial channel incision of the FRST11 on the outer western Bengal Shelf (Fig.s 4.4 and 4.5) indicates that such channel network was very close to the shoreline already in the central Bengal Shelf or even steered toward the canyon flank (Fig. 4.12B).

In the northern canyon some V-shaped valleys remained unaltered due to the fast filling of the canyon, point out there was at least an active bathymetric connection in the canyon northern head (Fig. 4.12B).

The progressive westward offset from the eastern shelf margin delta of the elongated body in FRST11 same as in the elongated- saddles bodies in LST12 (Fig. 4.7), and the absence of physical connection with the FRST11 oblique clinoforms (Fig. 4.8) on the western outer shelf suggest a different source region and sedimentary processes. The denser cloud rich of suspended sediment material in fresh water might have plunged very close to the river mouth due to the rapid density contrast when entering into oceanic saline water. During the SW summer monsoon, current-supported gravity flows might have dominated the offshore transport and caused the formation of this sedimentary isolated body. It is remarkable to notice how subtle would be in this scenario the difference between a subaqueous deltaic clinoform and an "extremely shallow" contourite deposit (Rebesco and Camerlenghi, 2008).

In this paleo-drainage reconstruction it has been discovered for the first time that the Bengal Basin, at least during last glacial Interglacial cycle, was a multiple source ramp margin (Reading and Richard, 1994; Stow et al., 1996). The presence of a shelf margin delta on the Eastern Bengal Shelf was indeed simoultaneous to a slope-channel system through the Swatch of No Ground canyon connected to the Bengal Fan (Weber et al., 1997; Curray et al., 2003; Schwenk and Spiess, 2010) in the Western Bengal Shelf.

4.4.3. Transgression, healing phase and final flood

Likewise the transition from MIS 6 to MIS 5, the end of the LGM coincides with an insolation minimum (Lambeck et al., 2002). In contrast with Termination II, Termination I has not developed as a continuous rise but rather as alternated phase of slow and rapid rise. Between 19.0 ky and 14.6 ky, sea level moderately rose from 114 m to 96 m at a rate of 0.41 m per 100 yr (Hanebuth et al., 2000). Wave ravinement deposits (T-C facies, Cattaneo and Steel, 2003) are found everywhere and clearly mark the onset of transgression which shaped the margin and sculptured the shelf break (SBk0_W and SBk0_E) as we can observe it today (Fig. 4.9).

A rapid rise globally registered by sea level curves, Melt Water Pulse 1A (Faibanks, 1989) is associated with the warm Bølling-Allerød interval. MWP-1A occurred from 14.6 ky to 14.3 ky, when mean sea level rose from -96 m to -80 m mostly due to the partial collapse of the Antarctic Ice Sheet (Hanebuth et al., 2000; Weaver et al., 2003; Deschamp et al., 2012).

The distributaries channel network on the western shelf in the prodelta area is first filled and then truncated (Fig. 4.12C). The integrity of their channels (Fig. 4.3) indicates not much material has been eroded.

The braided river course from the eastern Bengal Shelf margin detached within the Termination I and formed a retrogradational mid-shelf delta (Figs. 4.3 and 4.12C) on the eastern Bengal Shelf. This retrogradational delta fed from shoreface erosion and/or intensified sediment supply the lobate stratified body identified in TST13 on the central outer shelf (Fig. 4.8) which is therefore interpreted its subaqueous compartment (Fig. 4.12C). The subaqueous delta developed above the first wave ravinement surface in a low-gradient setting (T-C facies, Cattaneo and Steel, 2003; "healing phase deposits" in Posamentier and Allen, 1993). According to the sea level height at the end of the MWP-1A, it is expected an age of ca. 14 ka for the initiation this retrogradational mid-shelf delta. The thickening must have due to the transgression punctuation associated to Younger Dryass cold reversal (13-12 ka) during Termination I transgression. Intensified turbidites sedimentation on the Bengal Fan (Weber et al., 1997) and accelerated subaerial delta accretion (Goodbread and Kuehl, 2000) occurred ca. 11 ka ago at the Pleistocene to Holocene transition in concomitance with a second period of accelerated sea level rise, the MWP 1B. The ramp setting was therefore maintained during the early deglaciation and probably also trough the end of the Pleistocene. The magnitude and duration of MWP 1B is more controversy (Bard et al., 2010), however based on the estimated sea level of ca 50 mbsl at the onset of the Holocene, the retrogadational mid-shelf delta was flooded (Fig 4.11). Consequently this time represents the switch of the multiple source ramp margin to a point source margin system.

4.4.4. Highstand normal regression

Intensified monsoon precipitation was characteristic for the transition between Pleistocene and Holocene (Gasse et al., 1991; Goodbred and Kuehl, 2000). The subaerial drainage reconstruction is controversial (Coleman, 1969; Allison et al., 2003; Heroy et al., 2003; Youngs, 2011) and the landward most position of the shoreline has not been ascertained with sufficient details to be able to trace unambiguously the maximum flooding surface. The source points of the sediment supply to the Bengal Shelf has varied during sea level stabilization in the middle Holocene at the present day values. Both rivers exhibited extremely high course variability where the Brahmaputra avulsed numerous times east and west of the Mahdupur Terrace when the Ganges migrated eastward until it converged with the Brahmaputra in the early Nineteenth century (Fig. 4.1).

The subaqueous delta deposition (Fig. 4.12D) on the shelf started ca. 7 ka ago (Goodbread and Kuehl, 2000).

Through the Holocene, mass human migration into this area was discouraged for a long time due to the western highland and the forest cover, the tidal forest in the south, and the innumerable rivers. Expansion of human settlement and its distribution pattern in Bengal followed the navigable river channels (Dutt, 1906; Roychoudhury, 1963; Bakr, 1971).

The anthopogenic stress has increased progressively and in present day condition, with the exception of the Chittangong Hill Tracts and Sunderban mangrove forest, the country has been occupied by humans. Particularly, in the coastline and deltaic region, extensive crop and rice cultivation (Fig. 12D), after the deforestation, has requested always more bank re-enforcement and protection (Pearce, 1991).

The industrialization process has made Bangladesh one of the worldwide largest exporters of handicrafts and it grew the need to create big docking stations (Fig 12D). The Chittangong Harbour in the northern Bengal Bay and the Mogla Port located 48 km south of Khulna (Fig. 4.1) have been strongly potentiated. However, particularly the latter, often remained closed because it lost proper depth required for the ocean-going ships and every time it was reopened after dredging. Dredging of the Mogla Port entrance and offshore sediment dumping, right north of the head of the Swatch of No Ground canyon may represent a great peril for the seafloor and river floor stability.

4.4.5. Shoreline and shelf break trajectories

The shoreline trajectory (SH0 and SH1) is a basic concept for the description of the architecture of depositional cycles and their contained segments (Helland-Hansen and Gjelberg 1994; Helland-Hansen and Martinsen 1996). The shoreline is dynamic, as it continuously changes its position within the basin as a function of the local balance between accommodation and sedimentation. The reference curve of base level shifts should therefore describe the changes of accommodation at the shoreline wherever is within the basin at each time step (Catuneanu, 2006).

The SH1_E to SH0_E shoreline trajectory have a normal regression trend whereas the SH1_W to SH0_W trajectory is a partly accretionary transgression where the large part of the vertical growth occurred not at the shoreface (Fig. 4.13).

The infralittoral zone is however the ideal location to establish a trend in depocentre shift (Catuneanu, 2006) but it does not really says much of the real accommodation because of being the region of minor sedimentation due to the action of tides and waves which allows sediments to deposit only where their energy decreases. To better describe the attributes of the receiving basins, the subaqueous delta locations (SD and PSD) and the shelf breaks (SBk0 and SBk1) they are also presented as they represent the subaqueous depocentre and the zone of minimum deposition due to sediment bypass across the margin threshold (Steel and Olsen, 2002; Bullimore et al., 2005).

Both, the SBk1_E to SBk0_E and SBk1_W to SBk0_W have a negative shelf break trajectories trend whereas the western trajectory has even a degradation component as the negative trend is directed landward (Fig. 4.13). It is consequently excluded that bypass occurred within the western shelf break threshold. The eastern shelf break trajectory is negative but the margin is characterized by a minor horizontal progradatation. Bypass across this area occurred and the transfer to the margin formed a

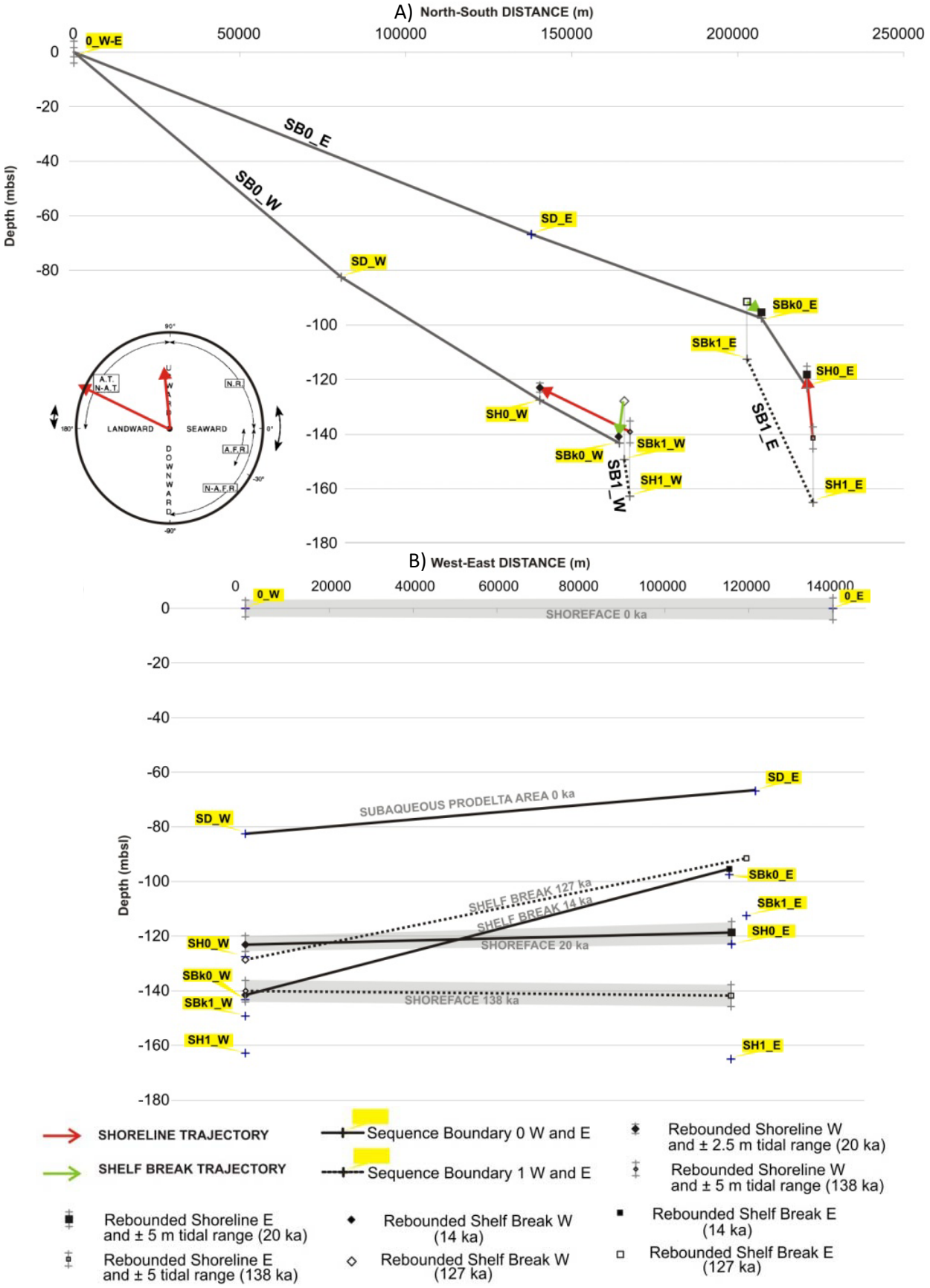

Figure 4.13. Shoreline and shelf break trajectories compensated of the tectonic subsidence and compaction on **A)** NS dip and **B)** EW cross section. The shoreline trajectory circle has been modified from Helland-Hansen and Martinsen (1996); A.T., accretionary transgression; N-A.T., non accretionary transgression; N.R., normal regression; A.F.R., accretionary forced regression; N- A.F.R., non accretionary forced regression.

subaqueous delta on the upper slope (elongated body in FRST11 and the saddle-elongated bodies in LST12; Figs. 4.11 and 4.12).

When the shorelines location are cross-correlated from east to west (SH1_E, SH1_W, SH0_E and SH0_W) (Fig. 4.13) they indicate a uniform level within the infralittoral zone. The cross-correlation fits quite well with the given mean sea level elevation from marine isotopes (Walbroek et al., 2002) showing that the experimental subsidence rate estimates quite realistic.

When instead the morphological relieves are compared from east to west (SD_E, SD_W, SBk0_E, SBk0_W, SBk1_E, SBk1_W, PSD_W and PSD_E), they are all dipping westward (Fig. 4.13). This is a completely unexpected result because the subduction zone is located eastward along the Arakan coast (Maurin and Rangin, 2009; Najman et al., 2010) and therefore more accommodation should be offered there due due to basement flexure in the subduction zone or duplexing in the form of syn- and anticline formation.

There are two possible explanations for this dicrepancy. The most logic explanation is an error in the assumption that the basement is flat which was used in the simplification of the sedimentary column (Fig. 4.9). An eastward inclination of the basement could eventually compensate the westward dipping. Another possible explanation could be that crustal deformation may have occurred at the continent-ocean margin between the Indian craton and the remnant of the initial Bengal Deep Basin (Alam et al., 2003). The transition from continental crust to oceanic crust may be an additional source for differential subsidence, for the first time revealed in this study.

4.5. Conclusions: shelf margin accretion during the Last Glacial Interglacial cycle

The paleo-drainage reconstruction has been made possible by applying a simplified experimental 1-D backstripping test at the BODC-3 date well site and on interpreted sedimentary succession at selected locations in the modern (SD) and the relict subaqueous delta (PSD), the modern (SbK0) and the paleo-shelf break (sbK1), the paleo-shorelines (SH0) of MIS 2 and MIS 6 (SH1). The values obtained where used to rebound (Airy Isostasy) the surfaces of the tectonic subsidence component estimated 0.17 m/ka during last Glacial-Interglacial cycle and 6.2 km of total accommodation within the last 33.9 Ma. The effect of the lithostatic stress exerted by the tentative sedimentary column (11.8 km) on the basement could have caused 1.3 km of additional accommodation. The lithostatic stress caused by the sedimentation of the last glacial-interglacial cycle composite sequence (10-35 m) has produced as much accommodation as the thickness of the sequence but the additional accommodation caused by the overburden pressure within the sequence is of max 0.4 m.

The present study has detailed analyzed the last 4th-order cycle of interpreted glacio-eustatic cyclicity in the sedimentary succession offshore the Ganges Brahmaputra Delta on the Bengal Shelf. During the last IV order eustatic cyclethe Bengal shelf behaved as a multi-source ramp setting with the

formation of a mid- to shelf margin delta on the eastern Bengal Shelf during fall and a retrogradational delta during rise simultaneous to a slope-channel system on the western Bengal Shelf. On the western Bengal Shelf a network of subaerial distributaries channels and tidal inlets was restricted to the inner shelf and connected to the northern head of the Swatch of No Ground Canyon until transgression. At the end of MWP-1A, the western Bengal Shelf was already drowned.

Beside through the canyon, sediment bypass toward the Bengal fan occurred along the eastern shelf margin before and through the end of base fall, and during early transgression due to the presence of a subaerial braided river delta. The subaqueous compartment of such braided river delta elongated along the Bengal Shelf margin possibly under the influence of an along shore current which may have transported the anomalous εNd increase detected on the western slope from the Southern Arakan Rivers or even from the Ayeyarwady.

However, the declining precipitation trend in the frontal regions along the entire Himalaya in favour of the Arakan coast may have potentiated the sediment flux from the Indo-Burma Ranges and contributed directly from the inner shelf via the eastern shelf margin braided river delta, leaving apart if this was the Paleo-Brahmaputra or the Paleo-Meghna, a sediment surplus derived from the Northern Arakan Rivers. The receiving basins morphological reliefs (subaqueous delta and shelf break) are all dipping toward the west with a slope angle which increased during the last Glacial Interglacial cycle. This unexpected result may indicate active tectonism in the area close to the canyon head.

The reconstruction of the drainage system demonstrates the great ‘resilience’ capability of the Bengal Basin mostly dependent on the total sediment supply rather than on sea level variability especially with the formation of a mid-shelf retrogradational delta during transgression. The majority of larger river on Earth drowned at the end of MWP 1A but on the eastern Bengal Shelf sedimentation kept on being active and especially significant at least until the onset of MWP 1B which finally drowned the Bengal Shelf. Present day shelf accretion and progradation is largely due to the highstand normal regressive subaqueous delta growth. The overlap of the natural delta development with the increasing anthropogenic pressure on the Ganges-Brahmaputra Delta may cause an intensified offshore sediment export in detriment of the subaerial storage to rapidly re-establish a new dynamic equilibrium profile.

Acknowledgements

This work was done within the Project ‘‘SO-188—Bengal Sea Level’’, funded by the German Ministry of Education and Science (BMBF), Grant no. 03G0188A and the DFG project ‘‘Bengal Shelf IODP’’, Grant no. SP296/31-1. An additional extension on the funding was kindly provided by the Family Support offered by the GLOMAR Bremen International Graduate School for Marine Science funded by the DFG under the Excellence Initiative by the German federal and state governments to promote science and research at German Universities.

We thank the captain and crew of the R.V. Sonne for excellent support and the scientific board party for their great collaboration.

We aknowledge Prof. S. Goodbred, Dr. M. Steckler, Dr. N. Seeber and Dr. A. Petter for the constructive discussions during the Bangla Pire Expedition. while sailing on the Ganges and Brahmaputra Rivers. A special mention is also for Prof. C. France-Lanord for his guidance and help in developing the concepts and in understanding the geo-chemistry of the system.

SO93-128SL

Depth [cm]	WBD [g/ccm] PP=0,6	porosity	dry bulk density	Depth [cm]	WBD [g/ccm] PP=0,6	porosity	dry bulk density	Depth [cm]	WBD [g/ccm] PP=0,6	porosity	dry bulk density
2	NaN	NaN	NaN	202	1.533	0.687	1.466	402	1.703	0.592	1.645
4	NaN	NaN	NaN	204	1.565	0.669	1.500	404	1.732	0.575	1.676
6	1.514	0.698	1.446	206	1.548	0.679	1.482	406	1.711	0.587	1.654
8	1.526	0.691	1.459	208	1.580	0.661	1.516	408	1.682	0.604	1.623
10	1.545	0.680	1.479	210	1.576	0.663	1.511	410	1.674	0.608	1.615
12	1.562	0.671	1.497	212	1.556	0.674	1.490	412	1.633	0.631	1.572
14	1.516	0.697	1.448	214	1.574	0.664	1.509	414	1.653	0.620	1.592
16	1.538	0.684	1.471	216	1.556	0.674	1.490	416	1.666	0.612	1.607
18	1.549	0.678	1.483	218	1.561	0.671	1.496	418	1.639	0.627	1.578
20	1.528	0.690	1.461	220	1.554	0.675	1.489	420	1.626	0.635	1.564
22	1.578	0.662	1.513	222	1.543	0.682	1.476	422	1.645	0.624	1.584
24	1.552	0.676	1.486	224	1.557	0.674	1.491	424	1.666	0.613	1.606
26	1.555	0.675	1.489	226	1.575	0.664	1.510	426	1.677	0.606	1.618
28	1.571	0.666	1.506	228	1.707	0.589	1.649	428	1.658	0.617	1.598
30	NaN	NaN	NaN	230	1.590	0.655	1.526	430	1.686	0.601	1.627
32	NaN	NaN	NaN	232	1.562	0.671	1.496	432	1.684	0.602	1.625
34	1.580	0.661	1.515	234	1.566	0.669	1.501	434	1.728	0.578	1.671
36	1.569	0.667	1.504	236	1.571	0.666	1.506	436	1.742	0.570	1.686
38	1.561	0.672	1.495	238	1.583	0.659	1.519	438	1.726	0.579	1.670
40	1.598	0.651	1.534	240	1.570	0.667	1.504	440	1.687	0.600	1.629
42	1.558	0.673	1.492	242	1.560	0.672	1.494	442	1.708	0.589	1.650
44	1.622	0.637	1.560	244	1.570	0.666	1.505	444	1.717	0.584	1.659
46	1.587	0.657	1.523	246	1.562	0.671	1.497	446	1.730	0.576	1.674
48	1.595	0.652	1.532	248	1.626	0.635	1.564	448	1.710	0.588	1.652
50	1.568	0.668	1.503	250	1.568	0.668	1.503	450	1.660	0.616	1.600
52	1.623	0.637	1.561	252	1.549	0.678	1.483	452	1.656	0.618	1.595
54	1.544	0.681	1.477	254	1.563	0.670	1.498	454	1.648	0.623	1.587
56	1.561	0.671	1.495	256	1.561	0.672	1.495	456	1.667	0.612	1.608
58	1.553	0.676	1.487	258	1.583	0.659	1.518	458	1.651	0.621	1.590
60	1.556	0.674	1.490	260	1.595	0.652	1.531	460	1.694	0.597	1.636
62	1.546	0.680	1.480	262	1.574	0.664	1.509	462	1.630	0.633	1.568
64	1.567	0.668	1.502	264	1.600	0.650	1.537	464	1.667	0.612	1.608
66	1.550	0.678	1.484	266	1.598	0.650	1.535	466	1.660	0.616	1.600
68	1.550	0.677	1.484	268	1.566	0.669	1.500	468	1.656	0.618	1.596
70	1.546	0.680	1.480	270	1.560	0.672	1.495	470	1.703	0.592	1.645
74	1.517	0.696	1.449	274	1.573	0.665	1.508				
76	1.522	0.693	1.454	276	1.599	0.650	1.535				
78	1.543	0.682	1.477	278	1.580	0.661	1.515				
80	1.538	0.684	1.472	280	1.557	0.674	1.491				
82	1.545	0.681	1.478	282	1.574	0.664	1.509				
84	1.547	0.680	1.480	284	1.562	0.671	1.496				
86	1.561	0.672	1.495	286	1.561	0.672	1.495				
88	1.564	0.670	1.499	288	1.571	0.666	1.506				
90	1.543	0.682	1.477	290	1.581	0.660	1.517				
92	1.561	0.671	1.496	292	1.545	0.680	1.479				
94	1.576	0.663	1.511	294	1.578	0.662	1.513				
96	1.547	0.679	1.481	296	1.563	0.670	1.498				
98	1.600	0.650	1.537	298	1.587	0.657	1.523				
100	1.586	0.657	1.522	300	1.561	0.672	1.495				
102	1.542	0.682	1.476	302	1.565	0.669	1.499				
104	1.583	0.659	1.519	304	1.578	0.662	1.513				
106	1.582	0.660	1.518	306	1.567	0.668	1.502				
108	1.581	0.660	1.517	308	1.575	0.664	1.510				
110	1.560	0.672	1.494	310	1.659	0.616	1.599				
112	1.540	0.683	1.473	312	1.563	0.671	1.497				
114	1.538	0.684	1.472	314	1.603	0.648	1.539				
116	1.573	0.665	1.509	316	1.570	0.666	1.505				
118	1.574	0.664	1.509	318	1.584	0.658	1.520				
120	1.541	0.683	1.474	320	1.570	0.666	1.505				
122	1.544	0.681	1.478	322	1.645	0.624	1.584				
124	1.559	0.672	1.494	324	1.597	0.651	1.533				
126	1.570	0.666	1.505	326	1.587	0.657	1.523				
128	1.569	0.667	1.504	328	1.557	0.674	1.491				
130	1.589	0.656	1.525	330	1.584	0.658	1.520				
132	1.594	0.653	1.531	332	1.566	0.669	1.501				
134	1.590	0.655	1.526	334	1.564	0.670	1.499				
136	1.592	0.654	1.528	336	1.553	0.676	1.487				
138	1.575	0.664	1.510	338	1.554	0.675	1.488				
140	1.563	0.671	1.497	340	1.606	0.646	1.543				
142	1.565	0.669	1.500	342	1.595	0.652	1.532				
144	1.579	0.661	1.514	344	1.602	0.649	1.538				
146	1.566	0.668	1.501	346	1.603	0.648	1.540				
148	1.559	0.673	1.493	348	1.594	0.653	1.530				
150	1.569	0.667	1.504	350	1.591	0.655	1.527				
152	1.565	0.669	1.500	352	1.586	0.657	1.522				
154	1.573	0.665	1.508	354	1.606	0.646	1.543				
156	1.580	0.661	1.515	356	1.589	0.656	1.525				
158	1.557	0.674	1.491	358	1.562	0.671	1.497				
160	1.564	0.670	1.499	360	1.585	0.658	1.521				
162	1.549	0.678	1.483	362	1.603	0.648	1.540				
164	1.555	0.675	1.489	364	1.614	0.642	1.551				
166	1.573	0.665	1.508	366	1.656	0.618	1.596				
168	1.539	0.684	1.473	368	1.623	0.637	1.561				
170	1.564	0.670	1.499	370	1.611	0.644	1.548				
174	1.533	0.687	1.466	374	1.615	0.641	1.552				
176	1.542	0.682	1.476	376	1.596	0.652	1.533				
178	1.546	0.680	1.479	378	1.627	0.635	1.565				
180	1.535	0.686	1.468	380	1.624	0.636	1.562				
182	1.538	0.685	1.471	382	1.628	0.634	1.566				
184	1.558	0.673	1.492	384	1.641	0.626	1.580				
186	1.566	0.669	1.500	386	1.643	0.625	1.582				
188	1.641	0.627	1.579	388	1.655	0.619	1.595				
190	1.643	0.625	1.582	390	1.657	0.617	1.597				
192	1.562	0.671	1.496	392	1.634	0.630	1.573				
194	1.547	0.679	1.481	394	1.668	0.612	1.608				
196	1.554	0.676	1.488	396	1.661	0.616	1.600				
198	1.551	0.677	1.485	398	1.676	0.607	1.617				
200	1.548	0.679	1.482	400	1.712	0.586	1.655				

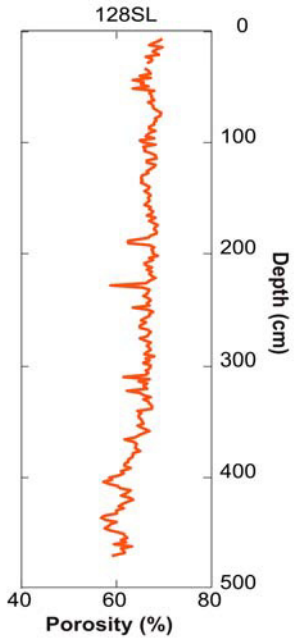

SO93-80SL

Depth [cm]	WBD [g/ccm]	PP=0.6	porosity	dry bulk density	Depth [cm]	WBD [g/ccm]	PP=0.6	porosity	dry bulk density	Depth [cm]	WBD [g/ccm]	PP=0.6	porosity	dry bulk density
2					201		1.745	0.568	1.690	401		1.833	0.519	1.782
2					203		1.778	0.549	1.725	403		1.774	0.552	1.720
6					205		1.749	0.566	1.694	405		1.784	0.546	1.731
8		1.715	0.585	1.658	207		1.763	0.558	1.709	407		1.800	0.537	1.747
10		1.749	0.566	1.693	209		1.804	0.535	1.752	409		1.813	0.530	1.761
12		1.744	0.568	1.689	211		1.770	0.554	1.716	411		1.801	0.536	1.749
14		1.808	0.532	1.756	213		1.756	0.562	1.701	413		1.797	0.539	1.744
16		1.760	0.559	1.706	215		1.748	0.566	1.692	415		1.816	0.528	1.764
18		1.818	0.527	1.766	217		1.727	0.578	1.670	417		1.807	0.533	1.755
20		1.820	0.526	1.768	219		1.818	0.527	1.767	419		1.828	0.521	1.777
22		1.876	0.494	1.828	221		1.779	0.549	1.725	421		1.845	0.512	1.795
24		1.885	0.489	1.837	223		1.816	0.528	1.764	423		1.814	0.529	1.763
26		1.743	0.569	1.687	225		1.807	0.533	1.755	425		1.782	0.547	1.728
28		1.788	0.544	1.735	227		1.780	0.548	1.727	427		1.807	0.533	1.755
30		1.780	0.548	1.727	229		1.806	0.534	1.754	429		1.818	0.527	1.767
32		1.780	0.548	1.727	231		1.791	0.542	1.738	431		1.794	0.540	1.741
34		1.887	0.488	1.839	233		1.776	0.551	1.722	433		1.796	0.539	1.744
36		1.808	0.533	1.756	235		1.778	0.549	1.725	435		1.785	0.545	1.732
38		1.818	0.527	1.767	237		1.789	0.543	1.736	437		1.786	0.545	1.733
40		1.792	0.542	1.739	239		1.804	0.535	1.752	439		1.799	0.538	1.746
42		1.783	0.547	1.730	241		1.799	0.538	1.746	441		1.800	0.537	1.747
44		1.745	0.568	1.690	243		1.805	0.534	1.753	443		1.798	0.538	1.746
46		1.788	0.544	1.734	245		1.796	0.539	1.743	445		1.798	0.538	1.746
48		1.823	0.524	1.772	247		1.781	0.548	1.727	447		1.798	0.538	1.745
50		1.794	0.540	1.742	249		1.779	0.549	1.725	449		1.791	0.542	1.738
52		1.895	0.484	1.848	251		1.735	0.574	1.679	451		1.799	0.538	1.746
54		1.869	0.498	1.820	253		1.734	0.574	1.678	453		1.797	0.539	1.744
56		1.915	0.472	1.869	255		1.790	0.543	1.737	455		1.798	0.538	1.745
58		1.919	0.470	1.873	257		1.773	0.552	1.719	457		1.785	0.546	1.732
60		1.844	0.512	1.794	259		1.747	0.567	1.692	459		1.778	0.550	1.724
62		1.871	0.497	1.822	261		1.745	0.568	1.690	461		1.777	0.550	1.723
64		1.819	0.526	1.768	263		1.784	0.546	1.731	463		1.815	0.528	1.764
66		1.804	0.535	1.752	265		1.737	0.573	1.681	465		1.786	0.545	1.733
68		1.808	0.533	1.756	267		1.745	0.568	1.689	467		1.789	0.543	1.736
70					269		1.748	0.567	1.692	469		1.778	0.550	1.724
73					273		1.765	0.557	1.711					
75		1.792	0.542	1.739	275		1.758	0.561	1.703					
77		1.807	0.533	1.755	277		1.792	0.542	1.739					
79		1.798	0.538	1.745	279		1.775	0.551	1.721					
81		1.953	0.451	1.909	281		1.789	0.543	1.736					
83		1.887	0.488	1.839	283		1.797	0.539	1.744					
85		1.793	0.541	1.740	285		1.792	0.542	1.739					
87		1.740	0.571	1.685	287		1.792	0.542	1.739					
89		1.756	0.562	1.701	289		1.802	0.536	1.749					
91		1.804	0.535	1.752	291		1.806	0.534	1.753					
93		1.815	0.529	1.763	293		1.771	0.553	1.717					
95		1.828	0.521	1.777	295		1.800	0.537	1.747					
97		1.808	0.533	1.756	297		1.797	0.539	1.744					
99		1.793	0.541	1.740	299		1.815	0.529	1.763					
101		1.742	0.570	1.686	301		1.789	0.543	1.736					
103		1.834	0.518	1.783	303		1.804	0.535	1.752					
105		1.831	0.520	1.780	305		1.801	0.536	1.749					
107		1.826	0.522	1.775	307		1.797	0.539	1.745					
109		1.813	0.530	1.761	309		1.767	0.556	1.713					
111		1.840	0.514	1.790	311		1.806	0.534	1.754					
113		1.812	0.530	1.760	313		1.779	0.549	1.726					
115		1.806	0.534	1.753	315		1.826	0.523	1.775					
117		1.819	0.526	1.768	317		1.802	0.536	1.750					
119		1.799	0.538	1.747	319		1.812	0.531	1.760					
121		1.836	0.517	1.786	321		1.818	0.527	1.767					
123		1.821	0.525	1.770	323		1.811	0.531	1.759					
125		1.823	0.524	1.772	325		1.812	0.530	1.760					
127		1.848	0.510	1.798	327		1.828	0.521	1.777					
129		1.837	0.516	1.787	329		1.839	0.515	1.789					
131		1.828	0.522	1.777	331		1.822	0.525	1.770					
133		1.823	0.524	1.772	333		1.807	0.533	1.755					
135		1.806	0.534	1.754	335		1.819	0.527	1.767					
137		1.817	0.527	1.766	337		1.828	0.521	1.777					
139		1.824	0.524	1.773	339		1.816	0.528	1.764					
141		1.831	0.520	1.781	341		1.829	0.521	1.778					
143		1.831	0.520	1.780	343		1.803	0.535	1.751					
145		1.789	0.544	1.736	345		1.811	0.531	1.759					
147		1.802	0.536	1.750	347		1.791	0.542	1.738					
149		1.803	0.536	1.750	349		1.814	0.529	1.762					
151		1.816	0.528	1.764	351		1.804	0.535	1.751					
153		1.784	0.546	1.731	353		1.770	0.554	1.716					
155		1.798	0.538	1.745	355		1.788	0.544	1.735					
157		1.799	0.538	1.747	357		1.786	0.545	1.733					
159		1.799	0.538	1.746	359		1.809	0.532	1.757					
161		1.805	0.534	1.753	361		1.791	0.542	1.738					
163		1.776	0.551	1.722	363		1.755	0.563	1.700					
165		1.773	0.552	1.719	365		1.741	0.571	1.685					
167		1.786	0.545	1.732	367		1.809	0.532	1.757					
169		1.796	0.539	1.743	369		1.786	0.545	1.733					
173		1.757	0.561	1.702	373		1.817	0.528	1.765					
175		1.763	0.558	1.708	375		1.786	0.545	1.732					
177		1.791	0.542	1.738	377		1.775	0.551	1.722					
179		1.790	0.543	1.737	379		1.686	0.601	1.628					
181		1.746	0.567	1.691	381		1.744	0.568	1.689					
183		1.758	0.560	1.704	383		1.845	0.512	1.795					
185		1.750	0.565	1.695	385		1.780	0.548	1.727					
187		1.782	0.547	1.728	387		1.822	0.525	1.770					
189		1.796	0.539	1.743	389		1.851	0.508	1.802					
191		1.804	0.535	1.751	391		1.866	0.500	1.817					
193		1.777	0.550	1.723	393		1.811	0.531	1.760					
195		1.766	0.556	1.711	395		1.815	0.529	1.763					
197		1.750	0.565	1.695	397		1.823	0.524	1.772					
199		1.763	0.558	1.709	399		1.818	0.527	1.767					

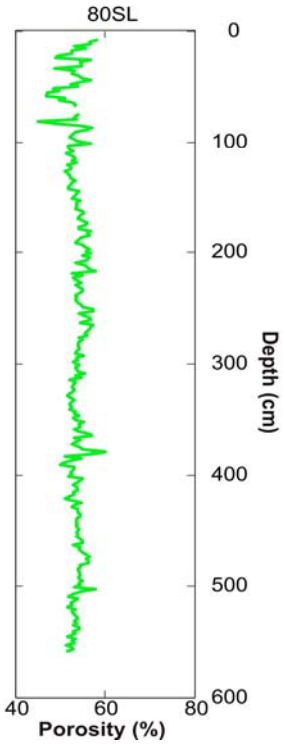

SO93-79SL

Depth [cm]	WBD [g/ccm] PP=0.6	porosity	dry bulk density	Depth [cm]	WBD [g/ccm] PP=0.6	porosity	dry bulk density	Depth [cm]	WBD [g/ccm] PP=0.6	porosity	dry bulk density
0	1.631	0.632	1.570	200	1.759	0.560	1.704	398	1.861	0.503	1.812
2	1.693	0.598	1.634	202	1.718	0.583	1.661	400	1.876	0.495	1.827
4	1.703	0.592	1.645	204	1.726	0.579	1.669	402	1.774	0.552	1.720
6	1.771	0.553	1.717	206	1.727	0.578	1.671	404	1.801	0.537	1.748
8	1.756	0.562	1.701	208	1.756	0.562	1.701	406	1.748	0.567	1.692
10	1.730	0.576	1.674	210	1.728	0.578	1.672	408	1.787	0.544	1.734
12	1.699	0.594	1.641	212	1.717	0.584	1.660	410	1.754	0.563	1.699
14	1.749	0.566	1.694	214	1.726	0.579	1.669	412	1.753	0.563	1.698
16	1.755	0.562	1.700	216	1.824	0.524	1.773	414	1.763	0.558	1.709
18	1.803	0.536	1.750	218	1.702	0.592	1.644	416	1.765	0.557	1.710
20	1.813	0.530	1.761	220	1.716	0.584	1.659	418	1.818	0.527	1.766
22	1.792	0.542	1.739	222	1.741	0.571	1.685	420	1.781	0.548	1.727
24	1.772	0.553	1.718	224	1.747	0.567	1.691	422	1.766	0.556	1.712
26	1.800	0.537	1.748	226	1.751	0.564	1.696	424	1.781	0.548	1.727
28	1.813	0.530	1.761	228	1.770	0.554	1.716	426	1.864	0.501	1.815
30	1.802	0.536	1.750	230	1.775	0.551	1.721	428	1.811	0.531	1.759
32	1.809	0.532	1.757	232	1.775	0.551	1.721	430	1.814	0.529	1.762
34	1.817	0.527	1.766	234	1.843	0.513	1.793	432	1.764	0.557	1.710
36	1.791	0.542	1.738	236	1.820	0.526	1.769	434	1.756	0.562	1.701
38	1.822	0.525	1.770	238	1.809	0.532	1.757	436	1.758	0.561	1.703
40	1.758	0.561	1.703	240	1.822	0.525	1.770	438	1.779	0.549	1.726
42	1.782	0.547	1.728	242	1.759	0.560	1.705	440	1.761	0.559	1.706
44	1.800	0.537	1.748	244	1.775	0.551	1.721	442	1.741	0.570	1.686
46	1.779	0.549	1.726	246	1.712	0.586	1.655	444	1.752	0.564	1.697
48	1.767	0.556	1.712	248	1.748	0.566	1.692	446	1.759	0.560	1.704
50	1.788	0.544	1.735	250	1.772	0.553	1.718	448	1.809	0.532	1.757
52	1.766	0.557	1.711	252	1.783	0.547	1.729	450	1.796	0.539	1.743
54	1.714	0.585	1.657	254	1.743	0.569	1.687				
56	1.689	0.599	1.631	256	1.741	0.570	1.685				
58	1.693	0.597	1.635	258	1.691	0.599	1.632				
60	1.681	0.604	1.622	260	1.745	0.568	1.690				
62	1.677	0.607	1.617	262	1.797	0.539	1.744				
64	1.713	0.586	1.656	264	1.859	0.504	1.810				
66	1.730	0.576	1.674	268	1.813	0.530	1.761				
68	1.729	0.577	1.672	270	1.837	0.516	1.786				
70	1.736	0.573	1.680	272	1.786	0.545	1.733				
72	1.724	0.580	1.667	274	1.829	0.521	1.778				
74	1.750	0.565	1.695	276	1.923	0.468	1.877				
76	1.744	0.569	1.688	278	1.834	0.518	1.783				
78	1.745	0.568	1.690	280	1.814	0.529	1.763				
80	1.762	0.559	1.707	282	1.876	0.494	1.828				
82	1.731	0.576	1.675	284	1.799	0.538	1.746				
84	1.717	0.584	1.660	286	1.854	0.507	1.805				
86	1.719	0.582	1.662	288	1.797	0.539	1.744				
88	1.700	0.593	1.642	290	1.784	0.546	1.730				
90	1.719	0.582	1.663	292	1.803	0.535	1.751				
92	1.751	0.565	1.695	294	1.783	0.547	1.729				
94	1.747	0.567	1.692	296	1.829	0.521	1.778				
96	1.739	0.572	1.683	298	1.835	0.517	1.785				
98	1.763	0.558	1.709	300	1.755	0.562	1.701				
100	1.780	0.548	1.727	302	1.791	0.542	1.738				
102	1.728	0.577	1.672	304	1.851	0.508	1.802				
104	1.727	0.578	1.671	306	1.819	0.526	1.768				
106	1.694	0.597	1.635	308	1.849	0.510	1.799				
108	1.748	0.566	1.692	310	1.831	0.520	1.780				
110	1.770	0.554	1.716	312	1.816	0.528	1.764				
112	1.746	0.567	1.691	314	1.810	0.531	1.759				
114	1.756	0.562	1.701	316	1.865	0.500	1.817				
116	1.722	0.581	1.666	318	1.824	0.524	1.773				
118	1.700	0.593	1.642	320	1.806	0.534	1.754				
120	1.711	0.587	1.654	322	1.720	0.582	1.663				
122	1.704	0.591	1.646	324	1.834	0.518	1.783				
124	1.737	0.572	1.682	326	1.839	0.515	1.789				
126	1.714	0.585	1.657	328	1.795	0.540	1.742				
128	1.688	0.600	1.629	330	1.821	0.525	1.770				
130	1.697	0.595	1.639	332	1.880	0.492	1.831				
132	1.651	0.621	1.590	334	1.840	0.515	1.790				
134	1.672	0.609	1.612	336	1.878	0.493	1.830				
136	1.692	0.598	1.633	338	1.837	0.516	1.786				
138	1.701	0.593	1.643	340	1.845	0.512	1.795				
140	1.703	0.592	1.645	342	1.871	0.497	1.823				
142	1.666	0.612	1.607	344	1.804	0.535	1.752				
144	1.684	0.602	1.626	346	1.794	0.541	1.741				
146	1.712	0.587	1.654	348	1.805	0.534	1.753				
148	1.740	0.571	1.684	350	1.755	0.562	1.701				
150	1.701	0.593	1.644	352	1.746	0.567	1.691				
152	1.672	0.609	1.613	354	1.867	0.500	1.818				
154	1.724	0.580	1.668	356	1.846	0.511	1.796				
156	1.678	0.606	1.618	358	1.795	0.540	1.742				
158	1.748	0.566	1.693	360	1.759	0.560	1.704				
160	1.741	0.570	1.686	362	1.786	0.545	1.733				
162	1.715	0.585	1.658	364	1.812	0.530	1.760				
164	1.718	0.583	1.661	366	1.843	0.513	1.793				
168	1.715	0.585	1.658	368	1.827	0.522	1.776				
170	1.704	0.591	1.646	370	1.849	0.510	1.799				
172	1.682	0.604	1.623	372	1.853	0.507	1.803				
174	1.683	0.603	1.624	374	1.888	0.488	1.840				
176	1.727	0.578	1.671	376	1.868	0.499	1.819				
178	1.703	0.592	1.645	378	1.861	0.503	1.812				
180	1.637	0.629	1.575	380	1.749	0.566	1.693				
184	1.648	0.622	1.588	382	1.817	0.528	1.766				
186	1.654	0.619	1.593	384	1.752	0.564	1.697				
188	1.713	0.586	1.656	386	1.824	0.524	1.773				
190	1.690	0.599	1.631	388	1.776	0.551	1.722				
192	1.750	0.565	1.695	390	1.805	0.534	1.753				
194	1.732	0.575	1.676	392	1.763	0.558	1.709				
196	1.732	0.575	1.676	394	1.793	0.541	1.740				
198	1.793	0.541	1.740	396	1.739	0.571	1.684				

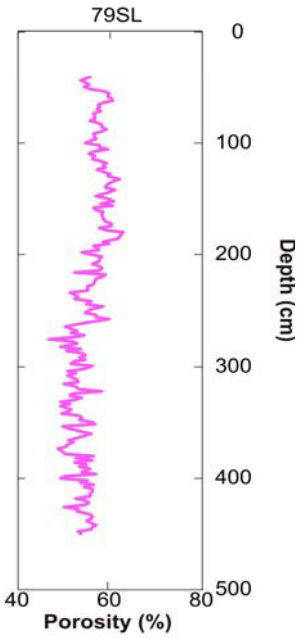

SO93-83KL

Depth [cm]	WBD [g/ccm] PP=0.6	porosity	dry bulk density	Depth [cm]	WBD [g/ccm] PP=0.6	porosity	dry bulk density	Depth [cm]	WBD [g/ccm] PP=0.6	porosity	dry bulk density
2	1.569	0.667	1.504	202	1.669	0.611	1.609	402	1.797	0.539	1.744
4	1.543	0.682	1.476	204	1.727	0.578	1.671	404	1.819	0.526	1.768
6	1.582	0.660	1.518	206	1.808	0.533	1.756	406	1.807	0.533	1.755
8	1.565	0.670	1.499	208	1.794	0.540	1.741	408	1.811	0.531	1.759
10	1.528	0.690	1.460	210	1.828	0.522	1.777	410	1.847	0.511	1.797
12	1.563	0.670	1.498	212	1.796	0.540	1.743	412	1.807	0.533	1.755
14	1.579	0.661	1.514	214	1.824	0.524	1.773	414	1.809	0.532	1.757
16	1.587	0.657	1.523	216	1.822	0.525	1.770	416	1.837	0.516	1.786
18	1.581	0.660	1.517	218	1.794	0.541	1.741	418	1.810	0.531	1.758
20	1.725	0.579	1.669	220	1.802	0.536	1.749	420	1.819	0.526	1.768
22	1.782	0.547	1.729	222	1.821	0.525	1.770	422	1.801	0.537	1.749
24	1.593	0.653	1.529	224	1.806	0.534	1.754	424	1.799	0.538	1.746
26	1.570	0.666	1.505	226	1.821	0.526	1.769	426	1.793	0.541	1.740
28	1.529	0.689	1.462	228	1.824	0.524	1.773	428	1.793	0.541	1.741
30	1.601	0.649	1.538	230	1.822	0.525	1.771	430	1.801	0.537	1.749
32	1.579	0.661	1.514	232	1.808	0.532	1.756	432	1.794	0.540	1.741
34	1.569	0.667	1.504	234	1.824	0.523	1.773	434	1.799	0.538	1.746
36	1.566	0.669	1.500	236	1.818	0.527	1.767	436	1.801	0.536	1.749
38	1.613	0.642	1.550	238	1.809	0.532	1.758	438	1.808	0.533	1.756
40	1.779	0.549	1.725	240	1.821	0.525	1.770	440	1.838	0.516	1.787
42	1.541	0.683	1.474	242	1.842	0.514	1.792	442	1.841	0.514	1.790
44	1.558	0.673	1.492	244	1.863	0.502	1.814	444	1.827	0.522	1.776
46	1.573	0.665	1.508	246	1.830	0.520	1.779	446	1.639	0.628	1.577
48	1.558	0.673	1.492	248	1.724	0.580	1.667	448	1.626	0.635	1.564
50	1.603	0.648	1.540	250	1.673	0.608	1.614	450	1.677	0.606	1.618
52	1.549	0.678	1.483	252	1.639	0.628	1.577	452	1.686	0.602	1.627
54	1.542	0.682	1.475	254	1.650	0.622	1.589	454	1.622	0.637	1.560
56	1.577	0.663	1.512	256	1.654	0.619	1.594	456	1.644	0.625	1.583
58	1.524	0.692	1.456	258	1.670	0.610	1.611	458	1.659	0.616	1.599
60	1.539	0.684	1.472	260	1.661	0.615	1.601	460	1.704	0.591	1.647
62	1.562	0.671	1.496	262	1.720	0.582	1.663	462	1.714	0.586	1.657
64	1.571	0.666	1.505	264	1.857	0.505	1.808	464	1.630	0.633	1.568
66	1.569	0.667	1.504	266	1.890	0.487	1.842	466	1.644	0.625	1.583
68	1.528	0.690	1.460	268	1.904	0.479	1.857	468	1.633	0.631	1.572
70	1.548	0.679	1.481	270	1.626	0.635	1.564	470	1.651	0.621	1.590
72	1.623	0.637	1.561	272	1.640	0.627	1.578	472	1.657	0.617	1.597
74	1.544	0.681	1.477	274	1.649	0.622	1.588	474	1.648	0.623	1.587
76	1.518	0.696	1.450	276	1.752	0.564	1.697	476	1.662	0.615	1.602
78	1.564	0.670	1.499	278	1.755	0.563	1.700	478	1.648	0.623	1.587
80	1.591	0.654	1.527	280	1.591	0.654	1.528	480	1.645	0.624	1.584
82	1.645	0.624	1.584	282	1.633	0.631	1.572	482	1.649	0.622	1.588
84	1.534	0.686	1.467	284	1.638	0.628	1.577	484	1.687	0.601	1.629
86	1.552	0.676	1.486	286	1.624	0.636	1.562	486	1.640	0.627	1.579
88	1.545	0.681	1.478	288	1.649	0.622	1.588	488	1.626	0.635	1.564
90	1.595	0.653	1.531	290	1.669	0.611	1.609	490	1.624	0.636	1.562
92	1.644	0.625	1.583	292	1.709	0.588	1.652				
94	1.582	0.660	1.517	294	1.645	0.625	1.584				
96	1.621	0.638	1.559	296	1.635	0.630	1.574				
98	1.624	0.636	1.562	298	1.622	0.637	1.560				
102	1.756	0.562	1.701	302	1.651	0.621	1.590				
104	1.673	0.609	1.613	304	1.638	0.628	1.576				
106	1.579	0.661	1.514	306	1.623	0.637	1.560				
108	1.635	0.630	1.573	308	1.646	0.624	1.585				
110	1.590	0.655	1.526	310	1.653	0.620	1.592				
112	1.588	0.657	1.524	312	1.691	0.598	1.633				
114	1.597	0.651	1.534	314	1.662	0.615	1.602				
116	1.601	0.649	1.538	316	1.635	0.630	1.574				
118	1.596	0.652	1.533	318	1.615	0.641	1.552				
120	1.607	0.645	1.544	320	1.647	0.623	1.586				
122	1.578	0.662	1.513	322	1.660	0.616	1.600				
124	1.550	0.678	1.484	324	1.630	0.633	1.568				
126	1.561	0.672	1.495	326	1.618	0.640	1.555				
128	1.576	0.663	1.511	328	1.620	0.638	1.558				
130	1.597	0.651	1.534	330	1.684	0.602	1.625				
132	1.616	0.641	1.554	332	1.639	0.628	1.578				
134	1.603	0.648	1.539	334	1.632	0.632	1.570				
136	1.599	0.650	1.536	336	1.644	0.625	1.583				
138	1.591	0.655	1.527	338	1.664	0.614	1.604				
140	1.603	0.648	1.540	340	1.668	0.611	1.609				
142	1.610	0.644	1.547	342	1.685	0.602	1.626				
144	1.664	0.614	1.604	344	1.678	0.606	1.619				
146	1.687	0.601	1.628	346	1.697	0.595	1.639				
148	1.723	0.580	1.667	348	1.731	0.576	1.675				
150	1.862	0.502	1.813	350	1.655	0.618	1.595				
152	1.628	0.634	1.566	352	1.689	0.599	1.631				
154	1.623	0.637	1.561	354	1.737	0.573	1.681				
156	1.630	0.633	1.568	356	1.632	0.632	1.570				
158	1.626	0.635	1.564	358	1.657	0.617	1.597				
160	1.622	0.637	1.560	360	1.653	0.620	1.593				
162	1.684	0.602	1.625	362	1.615	0.641	1.552				
164	1.711	0.587	1.654	364	1.612	0.643	1.550				
166	1.742	0.570	1.687	366	1.624	0.636	1.562				
168	1.714	0.586	1.657	368	1.637	0.629	1.576				
170	1.765	0.557	1.711	370	1.620	0.638	1.558				
172	1.692	0.598	1.634	372	1.642	0.626	1.581				
174	1.682	0.603	1.623	374	1.653	0.620	1.593				
176	1.690	0.599	1.631	376	1.713	0.586	1.656				
178	1.672	0.609	1.613	378	1.635	0.630	1.573				
180	1.657	0.617	1.597	380	1.667	0.612	1.607				
182	1.668	0.611	1.608	382	1.634	0.630	1.573				
184	1.675	0.607	1.616	384	1.645	0.625	1.584				
186	1.663	0.614	1.603	386	1.651	0.621	1.591				
188	1.686	0.601	1.627	388	1.657	0.617	1.597				
190	1.668	0.611	1.608	390	1.640	0.627	1.579				
192	1.670	0.610	1.610	392	1.622	0.637	1.560				
194	1.755	0.562	1.700	394	1.622	0.637	1.560				
196	1.688	0.600	1.629	396	1.662	0.615	1.602				
198	1.651	0.621	1.590	398	1.713	0.586	1.656				

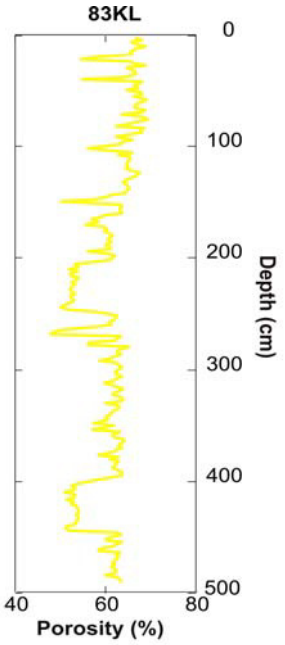

SO93-105KL

Depth [cm]	WBD [g/ccm] PP=0.6	porosity	dry bulk density	Depth [cm]	WBD [g/ccm] PP=0.6	porosity	dry bulk density
2	1.490	0.712	1.420	201	1.591	0.655	1.527
4	1.559	0.672	1.494	203	1.616	0.640	1.554
6	1.568	0.668	1.502	205	1.606	0.646	1.543
8	1.588	0.656	1.524	207	1.600	0.650	1.536
10	1.516	0.697	1.448	209	1.588	0.656	1.524
12	1.668	0.611	1.608	211	1.605	0.647	1.542
14	1.518	0.696	1.450	213	1.575	0.664	1.510
16	1.570	0.666	1.505	215	1.595	0.652	1.531
18	1.521	0.694	1.453	217	1.607	0.646	1.544
20	1.521	0.694	1.454	219	1.577	0.663	1.512
22	1.501	0.705	1.432	221	1.595	0.653	1.531
24	1.517	0.696	1.449	223	1.599	0.650	1.535
26	1.566	0.669	1.500	225	1.589	0.656	1.525
28	1.572	0.666	1.506	227	1.626	0.635	1.564
30	1.612	0.643	1.549	229	1.683	0.603	1.624
32	1.536	0.685	1.469	231	1.634	0.630	1.572
34	1.542	0.683	1.475	233	1.637	0.629	1.575
36	1.591	0.655	1.527	235	1.642	0.626	1.580
38	1.565	0.669	1.499	237	1.690	0.599	1.631
40	1.645	0.624	1.584	239	1.637	0.629	1.576
42	1.726	0.579	1.669	241	1.634	0.631	1.572
44	1.616	0.641	1.553	243	1.645	0.624	1.584
46	1.545	0.680	1.479	245	1.662	0.615	1.602
48	1.574	0.664	1.509	247	1.719	0.583	1.662
50	1.569	0.667	1.504	249	1.736	0.573	1.679
52	1.547	0.680	1.480	251	1.624	0.636	1.562
54	1.545	0.681	1.478	253	1.609	0.645	1.546
56	1.565	0.669	1.500	255	1.601	0.649	1.538
58	1.541	0.683	1.474	257	1.568	0.667	1.503
60	1.537	0.685	1.471	259	1.620	0.639	1.557
62	1.576	0.663	1.511	261	1.621	0.638	1.558
64	1.579	0.661	1.515	263	1.583	0.659	1.519
66	1.591	0.655	1.527	265	1.595	0.652	1.532
68	1.601	0.649	1.538	267	1.616	0.641	1.553
70	1.617	0.640	1.554	269	1.605	0.647	1.541
72	1.677	0.606	1.618	271	1.633	0.631	1.572
74	1.704	0.591	1.646	273	1.589	0.656	1.525
76	1.824	0.524	1.773	275	1.635	0.630	1.574
78	1.775	0.551	1.722	277	1.631	0.632	1.569
80	1.833	0.519	1.782	279	1.635	0.630	1.573
82	1.818	0.527	1.766	281	1.648	0.623	1.587
84	1.764	0.557	1.710	283	1.641	0.627	1.580
86	1.637	0.629	1.576	285	1.677	0.606	1.618
88	1.543	0.682	1.476	287	1.646	0.624	1.585
90	1.547	0.679	1.481	289	1.597	0.651	1.534
93	1.593	0.654	1.529	293	1.614	0.642	1.552
95	1.557	0.674	1.491	295	1.619	0.639	1.557
97	1.552	0.676	1.486	297	1.636	0.629	1.575
99	1.553	0.676	1.487	299	1.632	0.632	1.570
101	1.595	0.652	1.531	301	1.642	0.626	1.581
103	1.620	0.639	1.557	303	1.716	0.585	1.659
105	1.613	0.643	1.550	305	1.708	0.589	1.650
107	1.570	0.667	1.505	307	1.657	0.618	1.596
109	1.574	0.664	1.509	309	1.694	0.596	1.636
111	1.591	0.655	1.527	311	1.736	0.573	1.680
113	1.568	0.667	1.503	313	1.622	0.637	1.560
115	1.578	0.662	1.513	315	1.637	0.629	1.576
117	1.620	0.638	1.558	317	1.648	0.622	1.588
119	1.603	0.648	1.540	319	1.683	0.603	1.624
121	1.581	0.660	1.517	321	1.723	0.581	1.666
123	1.629	0.633	1.567	323	1.692	0.598	1.633
125	1.598	0.651	1.535	325	1.715	0.585	1.657
127	1.596	0.652	1.532	327	1.699	0.594	1.641
129	1.627	0.635	1.565	329	1.650	0.622	1.589
131	1.597	0.651	1.534	331	1.692	0.598	1.634
133	1.609	0.644	1.546	333	1.637	0.629	1.576
135	1.638	0.628	1.576	335	1.650	0.622	1.589
137	1.690	0.599	1.631	337	1.676	0.607	1.617
139	1.717	0.584	1.660	339	1.681	0.604	1.622
141	1.614	0.642	1.551	341	1.697	0.595	1.639
143	1.600	0.650	1.537	343	1.656	0.618	1.596
145	1.613	0.642	1.550	345	1.620	0.638	1.558
147	1.609	0.645	1.546	347	1.610	0.644	1.547
149	1.631	0.632	1.570	349	1.613	0.643	1.550
151	1.572	0.665	1.507	351	1.641	0.627	1.580
153	1.576	0.663	1.512	353	1.660	0.616	1.600
155	1.596	0.652	1.532	355	1.722	0.581	1.665
157	1.560	0.672	1.494	357	1.605	0.647	1.542
159	1.581	0.660	1.517	359	1.642	0.626	1.581
161	1.565	0.670	1.499	361	1.626	0.635	1.563
163	1.563	0.670	1.498	363	1.615	0.641	1.553
165	1.561	0.671	1.496	365	1.580	0.661	1.516
167	1.570	0.666	1.505	367	1.601	0.649	1.538
169	1.588	0.656	1.524	369	1.597	0.651	1.534
171	1.589	0.656	1.525	371	1.583	0.659	1.518
173	1.603	0.648	1.540	373	1.602	0.648	1.539
175	1.602	0.648	1.539	375	1.584	0.659	1.519
177	1.639	0.628	1.577	377	1.581	0.661	1.516
179	1.580	0.661	1.515	379	1.574	0.664	1.509
181	1.613	0.642	1.550	381	1.577	0.663	1.512
183	1.617	0.640	1.554				
185	1.600	0.650	1.536				
187	1.603	0.648	1.540				
189	1.635	0.630	1.573				
193	1.598	0.651	1.535				
195	1.572	0.665	1.507				
197	1.570	0.666	1.505				
199	1.579	0.661	1.515				

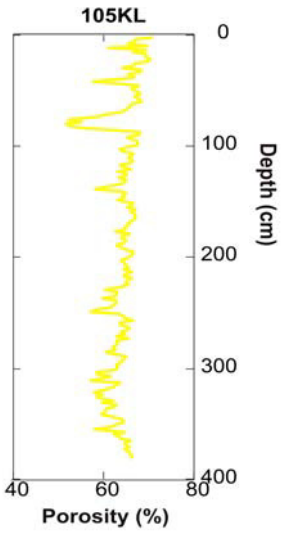

~ Chapter 5~

Seismostratigraphic Analysis with Centennial to Decadal Time Resolution of the Sediment Sink in the Ganges-Brahmaputra Subaqueous Delta.

Luisa Palamenghi[1,2,*], Tilmann Schwenk[3], Volkhard Spiess[4], Hermann R. Kudrass[5]

[1-3-4] Department of Geosciences, University of Bremen, Klagenfurter Str. 28359 Bremen, Germany.
[1] lupala@uni-bremen.de, [3] tschwenk@uni-bremen.de, [4] vspiess@uni-bremen.de

[2] GLOMAR — Bremen International Graduate School for Marine Sciences, University of Bremen, Leobener Str., 28359 Bremen, Germany

[5] MARUM — Center for Marine Environmental Sciences, University of Bremen, Leobener Str., 28359 Bremen, Germany
kudrass@gmx.de

* corresponding author

5.1. Introduction

The hydrology of all megadeltas in Southeast and East Asia is dominated by the monsoonal cycle, and all rivers in the region have their origin in the Himalayas and the Tibetan Massif. In contrast to other deltas which have been formed on tectonically stable platforms, the Ganges Brahmaputra Delta is situated in a very active, plate-tectonic area, which has severe consequences for long-term stability. The delta is built by the complex interaction of subduction and monsoonal variability. Today significant transformations of the landscape and water use by humans both play a significant role in governing the system (Crutzen, 2002). The expected global sea level rise will, in fact, soon exceed natural aggradation (Syvitski et al., 2009), and projected values are very likely to result in significant losses of coastal land, ecosystems, agriculture, economic activities and infrastructure (Cruz et al., 2007). This is of primary socio-economic relevance, as the Ganges-Brahmaputra alluvial and deltaic plain support the livelihood of more than 110 million people, a number destined to grow in the near future (Ericson et al., 2006; Woodroffe et al., 2006). Sea level intrusion due to sea level rise will worsen the effects of storm surge inundation during cyclones; a higher sea level will also reduce the drainage capacity of the river's fresh water during monsoon floods (Han and Webster, 2002).

According to previous onshore and offshore investigations, the suspended sediment supply is thought to be partitioned between the subaerial delta, the shallow subaqueous delta and the submarine canyon from where episodic turbidity currents feed the deep sea Bengal Fan (Kuehl et al., 1989; Kuehl et al., 1997; Weber et al., 1997; Michels et al., 1998; Goodbred and Kuehl, 1999; Curray et al., 2003; Schwenk et al., 2005).

In this study of the Ganges-Brahmaputra subaqueous delta, it has been used for the first time an integrated seismo-acoustic stratigraphic approach within millennial, centennial and decadal time scales in order to understand and quantify the seaward sediment accumulation. The volume of sediment in the foreset beds is calculated and, wherever reliable chronostratigraphic boundaries are defined, mean annual storage rates are estimated to evaluate long and short term dynamics. The partitioning in various depositional centres is related to the major forcing factors on the deltaic source-to-sink system. A main goal of this research is to contribute to a better risk assessment of the alluvial and deltaic plains of Bangladesh by defining the offshore sediment transport from the subaerial delta to the depocentres on the shelf.

5.2. Background

The source-to-sink system of the Himalayas-Bengal Basin-Bengal Fan is fed by the rivers Ganges and Brahmaputra, together with their Trans-Himalaya tributaries. They spring from the western Himalayas and central Tibet, respectively, and merge 190 km inshore from the coastline in the Bengal Basin, in the Bangladesh alluvial plain. The merged river enters the sea in the former estuary of a river draining the adjacent Sylhet Basin, the Meghna. The latter gives the name Meghna Estuary to the deltaic system that lies at the north-eastern edge of the Bengal Bay. The Meghna Estuary is tidally dominated

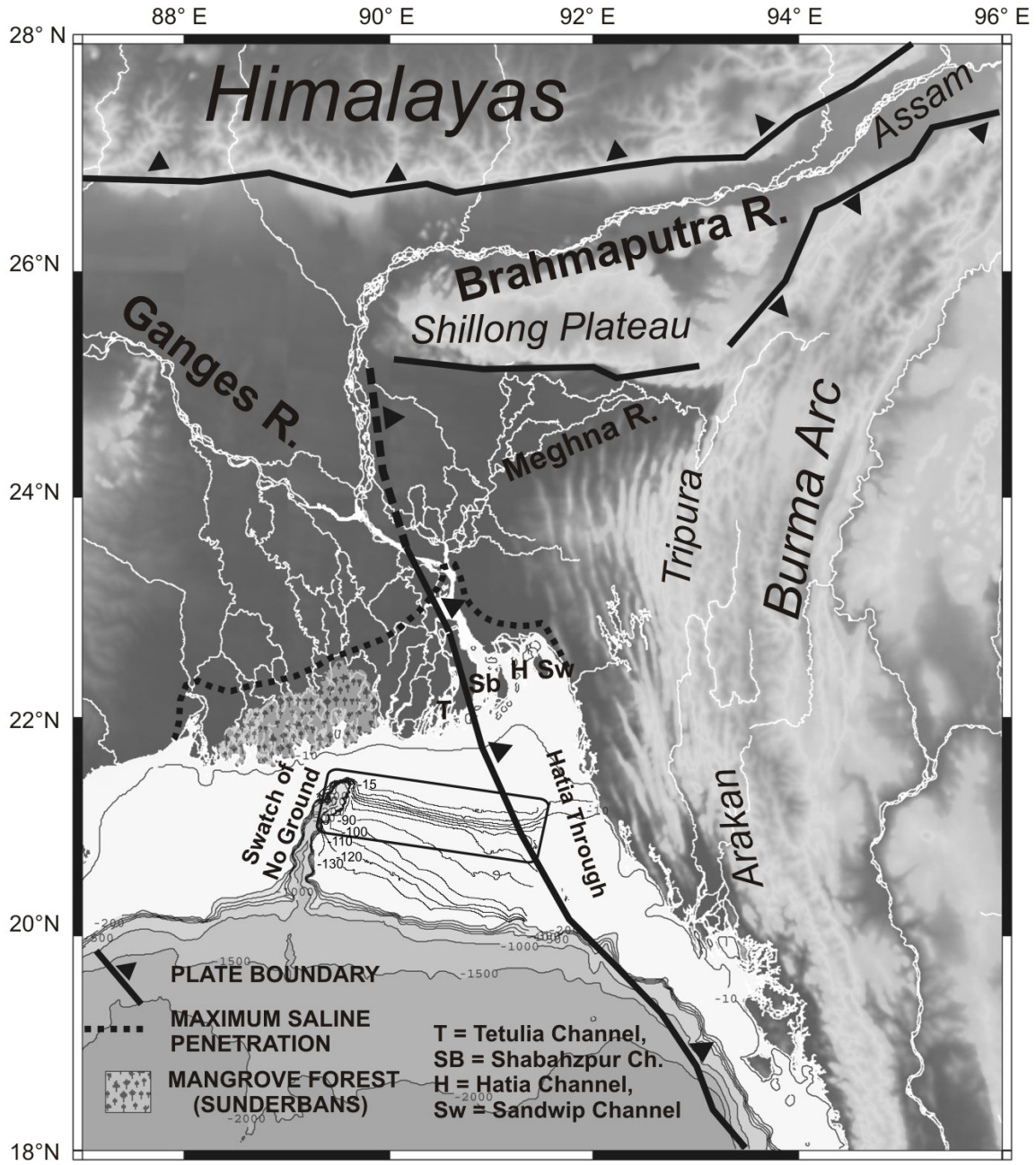

Figure 5.1 Basemap of the Bengal Basin showing the Ganges–Brahmaputra Delta and the study area. The tide influenced region (modified from Allison et al., 2003) and the plate boundaries (modified from Steckler et al, 2008) are also shown. Bathymetric lines from -15 m to -130 m are gridded from the SO93, SO126 and SO188 Parasound profiles with five seconds resolution (~150 m); bathymetry from -150 m to -1000 m is plotted from the GEBCO-08 One Minute Grid.

(Galloway, 1975) and formed by four major channels (Fig. 5.1): Tetulia, Shahbazpur, Hatia and Sandwip.

A subaqueous delta (Coleman and Write, 1975) has developed offshore. Within the near mouth area, the shallow sandy topset beds are unusually wide and extend from -5 m until -15 to -20 m water depth to ~100 km offshore distance. The delta front is located between -20 and -80 m water depth where the foreset bed grain size decreases to silty-clayey and slope steepens. In the prodelta area, the bottomset

are even finer grained beds and extend seaward from -80 m to a maximum -100 m water depth (Kuehl et al., 1997; Allison, 1998; Hübscher et al., 1998; Michels et al., 1998). The eastern limit of the subaqueous delta is at the Hatia Trough while at its western margin, a deeply incised canyon, the Swatch of No Ground, cuts into the shelf and the topset beds (Fig. 5.1).

Regardless of their dimension, transport mechanism and location, the formation of sigmoidal clinoforms is a worldwide common phenomenon like in the Atchafalaya near mouth area (Neill and Allison, 2005), in the Amazon (Hübscher et al., 2003) or in the Fly (Walsh et al., 2004) delta fronts, in the Yangtze alongshore deposits (Liu et al., 2006) and in the Taiwan Strait from a multiple river source (Liu et al., 2008).The hydrodynamic characteristics of the water column result in sediment dispersal patterns ultimately determining the shape of the sedimentation rate profile across the clinoform surface (Pirmez et al., 1998; Friedrichs and Wright, 2004; Swenson et al., 2005; Wolinsky and Pratson, 2007). The gravity-driven across-shelf and along-shelf transport of mud moving down slope may deposit sediment in response to decreases in wave or current induced near-bed velocity shear stress, bed slope or both (Wright and Friedrichs, 2006).

In the Indian Ocean, the shelves offshore the mouths of Indus, Ganges- Brahmaputra and Ayeyarwady-Salweel are intersected by shelf canyons. However, while the Ganges-Brahmaputra Swatch of No Ground and the Martaban canyons act at present as major conduits actively channelling turbidity currents to the Bengal Deep-Sea Fan (Weber et al., 1997; Curray et al., 2003) and to the deep Andaman Sea (Ramaswamy et al., 2004), sedimentation in the Indus Canyon is presently inactive (Giosan et al., 2006).

5.2.1. Tectonic of the Bengal Basin

The Bengal Basin is a forearc basin located at the junction of three interacting plates: the Indian, Burmese and Tibetan (Eurasian) Plates. Most of the Bengal Basin is formed over the north-eastern rim of the Indian Plate, which is subducted to the north under the Eurasian Plate and to the east under the Burmese Plate (Fig. 5.1). The Tripura Fold Belt, characterized by north-south trending anticlines in the eastern basin, was formed by the subduction-related collision (Alam et al. 2003). The deformation front is located at the foot of the fold belt and crops out at the continental slope offshore of eastern Myanmar, crossing the shoreline in the Meghna Estuary. A Wadati–Benioff Zone of earthquakes illuminating the subducted oceanic lithosphere characterizes the entire India–Sunda boundary and some of the plate-boundary earthquakes are huge (Steckler et al, 2008).

On the continental shelf, space is made available by tectonic subsidence, in addition to sediment compaction (Table 1). Different locations in the basin show spatially variable tectonic subsidence rates. Estimates for the Holocene in the alluvial and deltaic plain give 2-4 mm a^{-1} (Goodbred and Kuehl, 2000a). On the outer shelf, subsidence rate estimated since the Middle Pleistocene averages to ~0.4 mm a^{-1} (Hübscher and Spiess, 2005). No data are so far known on the contribution of compaction to subsidence.

5.2.2 Climate and oceanography of the northern Bengal Bay

Monsoon affects the climate of the Bengal Basin, in terms of intensity of precipitation and of wind (Table 1). Holocene centennial and multi-decadal-scale monsoon variability is significant (Dykoski et al., 2005) and related to the 11 years Schwabe Cycle of solar activity, the fluctuations of the Indian Dipole and ENSO variability (Wang et al., 2005a and references therein).

Precipitation estimated from oxygen isotope ratio in stalagmites has gradually weakened since 7 ka (Wang et al, 2005b and references therein; Breitenbach, 2009). Arid/wet monsoon episodes are not in perfect agreement with the minima and maxima of reduced solar activity (Versteegh, 2005). However, the 1.5 ka old stalagmite KRUM-3 from the Krem Umsynrang Cave in the SE Shillong Plateau (Fig. 5.1) reports a wetter period from 1670 to 1840 (Breitenbach, 2009). From the 19^{th} to 20^{th} century, oxygen isotope records report drier climate conditions (Breitenbach, 2009).

Oceanic surface circulation in northern Bengal Bay is driven by the seasonal migration of the Inter-Tropical Convergence Zone (ITCZ). During the summer monsoon, the N-NW displacement of the ITCZ generates a SW wind inducing an anticlockwise surface current (Shetye et al., 1991) and intense precipitation in the drainage area of the Ganges and Brahmaputra, which in turn can cause catastrophic floods as in 1987, 1988 and 1998. Vice versa, in winter, a NE monsoon induces a weaker clockwise oceanic current and dry conditions onshore (Shetye et al., 1996). Pre monsoon periods, spring and autumn, coincide with tropical cyclone formation. Cyclones hit land in northern Orissa, West Bengal, Bangladesh and part of northern Myanmar, often causing dramatic storm surges (Murty and El-Sabh, 1992).

Equatorial wind variability, rather than river run-off, is responsible for a positive sea level anomaly of 0.1-0.25 m in the coastal region and 0.05-0.15 cm in the interior bay, from May to September (Han and Webster, 2002).

Coastal waters respond to semi-diurnal tidal forcing (Table 1). Maximum amplitudes of 5 m have been registered in the eastern estuary region of the Hatia and Sandwip Channels. In the western channels, Shahbazpur and Tetulia, lower amplitudes create a net export of river water (Fig. 5.1). Westward of the Meghna Estuary, in the Sunderban mangrove forest (Fig. 5.1), tide amplitude is about 2 m (Murty and Henry, 1983). The lower delta plain is less than 3 m above sea level and saline water from the Bengal Bay may penetrate inland by 100 km or more (Fig. 5.1) along the distributaries channels during the winter monsoon, while during summer this region is flooded (Allison et al., 2003). On the shelf, tidal amplitude decreases from 0.8 m in the topset beds to 0.5 m in the foreset-bottomset beds and becomes negligible on the outer shelf (Murty and Henry, 1983).

5.2.3 Transport and Sedimentation on the Bengal Shelf

Maximum discharge peaks of water and sediment are reached during the summer monsoon. River bed sediments are coarser than suspended sediments and fall in the range of pure sand. Surface suspended sediments are the finest and fall in the range of pure silt. The proportion of clay (<2 μm) is always

limited and reaches a maximum of appx. 10 % in surface suspended sediments (Galy et al., 2008). The Ganges-Brahmaputra total suspended sediment load is estimated to be 1 x 10^9 t a^{-1} (Delft Hydraulics, 1996).

The main transport vector is driven by the SW monsoon and is directed westward along the shelf toward the Swatch of No Ground (Table 1). Tides are an important mean of transport as well as resuspension, and suspended sediment concentration is higher during spring tides and lower during neap tides (Kuehl et al., 1989; Barua et al., 1994). Remobilization and transport of sediments, however, is also caused by the passage of the tropical cyclones in a significant way. An 11 m long core was taken at the head of the canyon at 217 mbsl recording all the cyclones crossing the shelf from 1969 to 1993 as graded sequences (Kudrass et al., 1998**).** In the North Indian Ocean basins, satellite data have been used to determine number and intensity of cyclones during the last 35 years (Table 1). The proportion of hurricanes reaching categories 4 and 5 increased, while the total number of cyclones and cyclone days decreased during the past decade (Webster et al., 2005).

Sedimentation rates estimated by ^{210}Pb and ^{137}Cs gamma spectrometry show highest sedimentation rates of about 5 to 10 cm a^{-1} occurring at the foreset beds (Michels et al., 1998; Suckow et al., 2001). Sedimentation rate at the bottomset is estimated to be less than 0.3 cm a^{-1} (Kuehl et al., 1997). According to dated cores from the subaerial deltaic plain, ~8.5 × 10^{12} m^3 of sediments have accumulated since 11 ka estimated as the onset of deltaic development (Goodbred and Kuehl, 2000b). During the last 7 ka, 1.97 × 10^{12} m^3 have been deposited in the subaqueous delta by storing 0.42 × 10^9 t a^{-1} equivalent to 42 % of the yearly total suspended sediment load (Kuehl et al., 1997; Allison, 1998; Goodbred and Kuehl, 1999). According to the distribution of the sedimentation rate over the last 50 years, the sediment volume deposited annually in the foreset beds is 1.31 × 10^8 m^3, equivalent to 20 % of the total sediment load (Michels et al., 1998).

5.2.4 Holocene subaqueous delta reconstructions and progressive intensification of the anthropogenic stress

During the middle Holocene highstand (Geyh et al., 1979; Lambeck and Chappell, 2001) the Ganges's main course started an eastward migration, while the Brahmaputra was confined to the eastern region, following a similar course to the present one, joining the Meghna (Allison et al., 2003). The Sunderbans mangrove forest (Fig. 5.1) was formed during the Ganges eastward migration. Catastrophic floods at the turn from the 18th to the 19th century caused famines (http://www.banglapedia.org/httpdocs/HT/F_0103.HTM), and lead to the Brahmaputra avulsion and merger of the Ganges and Brahmaputra (Rennell 1786; Allison et al., 2003).

Table 5.1. Evidences and consequences on the sediment transport and deposition in the Ganges-Brahmaputra subaqueous delta

	EVIDENCES	CONSEQUENCES	References
NATURAL FACTORS:			
Tectonic Subsidence:	Offshore rate 0.4 mma^{-1}.[1]	Seaward export of sedim. by creating accommodation	[1]Hübscher and Spiess, 2005
Earthquakes:	Huge plate-boundary earthquakes. [2]	Post-depositional processes with formation of liquefaction flows in the delta front.* After-shock altered subsidence may favor the seaward export of sedim. by creating temporary additional accommodation.*	[2]Steckler et al, 2008 *This study
Compaction:	Unknown	Seaward export of sedim. by creating accommodation	
Precipitation:	Have gradually been weakening since ca 7 ka BP.[3] A wetter period between 1670-1840 is followed in 19th to 20th century by drier climate conditions.[4]	The storage rate in the foreset beds is progressively reduced especially in the eastern foreset beds.*	[3]Wang et al., 2005b and references therein [4]Breitenbach, 2009 *This study
Floods and Droughts:	Catastrophic floods occurred at the transition of the 18th to the 19th century.[5]During the past 50 years, 29 major floods. Floods of 1987, 1988, and 1998 were exceptional both in areal extent and in terms of destruction.[6] The number of droughts has been increasing over the last two decades.[7]	Floods: seaward export of sedim. with increased sedim. yield in the eastern foreset beds.* Droughts: decrease of the total suspended sediment flux	[5]http://www.banglapedia.org/httpdocs/HT/F_0103.HTM [6]Choudhury et al., 2004 [7]http://www.banglapedia.org/httpdocs/HT/D_0284.HTM *This study
SW Monsoon Wind Driven Current Field:	Suspended sediment transport directions are seaward and westward from May-December with an order of magnitude of higher transport in July-August during the high-discharge period.[8,9]	Constant storage rate during last three centuries in the western delta front foreset beds.*	[8]Barua et al., 1994 [9]Kuehl et al., 1997 *This study
Frequency and Magnitude of Cyclones:	In the North Indian Ocean basins during the last 35 years the number of cyclones and cyclone days has decreased while a large increase was seen in the proportion of hurricanes reaching categories 4 and 5.[10]	Seaward export of sedim. with a prevalence of the canyon as sink.	[10]Webster et al., 2005
Tide:	Semi-diurnal tide. [11]	Suspended sediment concentration is higher during spring tides and lower during neap tides.[12]	[11]Murty and Henry, 1983 [12]Kuehl et al., 1989
Sea Level:	Rise of 8-18 mma^{-1}.[13]	Inland intrusion of saline water and seaward export of sedim.	[13]Syvitski et al., 2009

Table 5.1. Continues

ANTHROPOGENIC FACTORS:			
Landscape modification:	From 1870 to 1970, Bangladesh experienced an expansion of human and animal populations, the conversion and reclamation of land for sedentary agriculture and settlement, and the depletion of all non-agricultural types of vegetation[14] with the exception of the Sunderbans mangrove forest.	Initial seaward export of sedim. followed by a decreased sedim. load	[14]Richards et al., 1985
Coastal and river embankment:	During the last few decades, under the programme of flood control and drainage improvement, embankment (including coastal embankments and hydraulic structures like sluices, river regulators, river closures and drainage channels) have been built.[15]	Embankments and polders have partly reduced floodplain storage capacity during floods, leading an increase in water levels and discharges in many rivers[16] but also detrimental effect on land elevation in the western Sunderbans by reducing the influx of sedim. during tidal and cyclonic floods.[17]	[15]http://www.banglapedia.org/httpdocs/HT/E_0049.HTM [16]Chowdhury, 1998 [17]Allison and Kepple, 2001
Water Management:	In order to prevent siltation of Kolkata Harbour, the Indian Government built (1961-1971) the Farakka Barrage to divert the Ganges flux during the dry season.[18] Water is massively exploited in the lower delta plain	Numerous and dramatic problems arised regarding ecologic sustainability and trans-boundary water management.[18] Decrease of the total suspended sediment flux.	[18]Bandyopadhyay, 2010
Gas Exploitaion:	Sangu offshore field in block 16 of the Bay of Bengal has been producing natural gas since 1998.[19]	Expected seaward export of sedim. by creating accommodation	[19]Kuo, 1998.

The anthropogenic influence on the delta (Table 5.1.) has caused intensive landscape modifications (Richards et al., 1985), systematic development of large-scale embankments and polders for flood control (http://www.banglapedia.org/httpdocs/HT/E_0049.HTM), exploitation of fresh **water** (Bandyopadhyay, 1995) and gas (Kuo, 2003). The annual decrease in sediment volume of 6.3×10^7 t a^{-1} (Allison, 1998) in the western Sunderbans has been attributed to polders which are being constructed along the lower delta plain shoreline (Allison and Kepple, 2001) but also an increase in water level and discharge has been observed due to embankments (Chowdhury, 1998). On the contrary the Meghna Estuary has experienced both, shoreline accretion and aggradation of the lower delta plain surface during the last 200 years (Allison et al., 2003).

5.3. Material and Methods

The R/V SONNE Expedition SO188 (BENGAL SEA LEVEL) in 2006 was the fourth Sonne cruise to the Bay of Bengal. Previous cruises took place in 1993-1994 (SO93) and 1997 (SO125 and SO126). During the second leg of the SO188 Expedition, the shelf area was extensively studied by means of seismo-acoustic methods with EW regional lines and NS crossing transects from a water depth of -15 m to maximum -85 m (Fig. 5.2).

In two main study areas in the west and east foreset beds, respectively, denser spaced surveys were already carried out during SO93 and SO126 (Fig. 5.2). They were revisited to improve the coverage, add seismic data and investigate changes within the previous 12 years.

5.3.1 Multichannel Seismic

High-resolution Multichannel Seismic (MCS) data acquisition was performed with a GI Gun (^{TM}SODERA, France) with reduced chamber volumes of 2 x 0.4 l, and a specially designed 50 m long shallow water streamer, with 48 single hydrophones of 1 m spacing. The main frequency was 100–500 Hz. Seismic data were recorded with MaMucs acquisition software, developed by Dr H. Keil (Bremen University), with a sampling rate of 125 μs, and recording length of 3 s. The data set was processed with the Vista (Gedco Co.) seismic processing software package. After velocity analysis and normal move out (NMO) correction, geo-referenced common midpoints (CMP) stacking were carried out with 5 m binnig distance. Before stack, a manual post-processing static correction was adopted to remove residual static induced by oceanic waves. Data were migrated with the FD method. For displaying and interpretation of MCS data the commercial software package Kingdom Suite (SMT Co.) was used.

5.3.2 Parasound echosounder

The Parasound sediment echosounder system DS-2, designed by ATLAS Hydrographic, is hull mounted and ran in a 24 hour schedule. The system utilizes the parametric effect, generating a secondary frequency of 4 kHz by the interaction of two sound waves of high energy emitted simultaneously (18 kHz and 22 kHz). The signal length of the Parasound echosounder is 5 x 10^{-4} s. Seismograms were sampled at a frequency of 40 kHz, with a registration length of 133 ms or 266 ms for a depth window of ~100 m or ~200 m, respectively. The data digitized by the ParaDigMa software (Spiess, 1993), was converted to the SEG-Y standard format to load them into the interpretation software. The vertical resolution ranges from 0.1 m to maximum 0.2 m and it is in the same order of magnitude as the error of ±0.5 m induced by the tidal range on the middle shelf (Murty and Henry, 1983) to sum

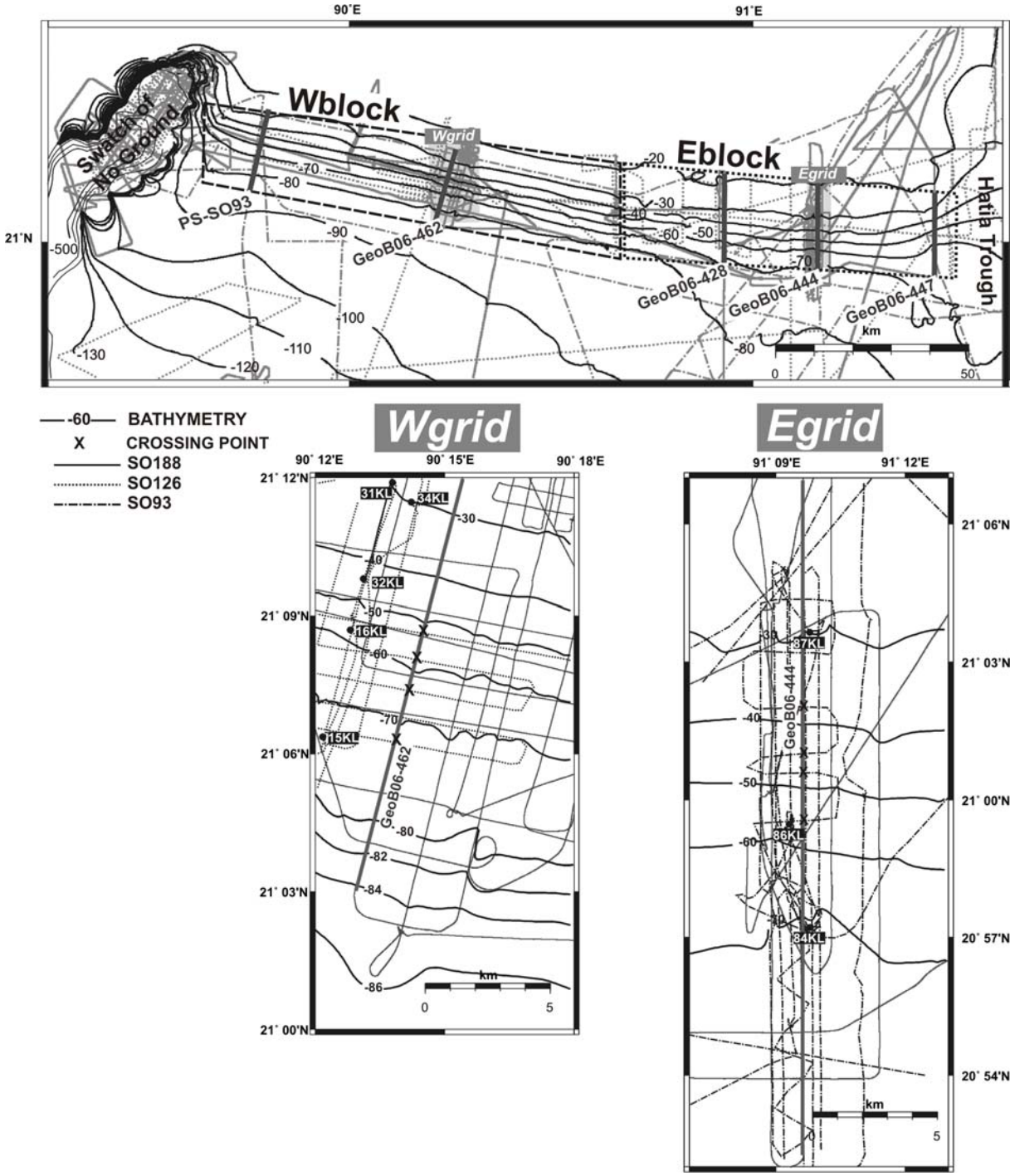

Figure 5.2. Bathymetry and cruise tracks on the Bengal Shelf for the Eblock and Wblok with detailed enlargement of Egrid and Wgrid. Cruise track of SO93 is a dot-dashed line, SO126 is a dotted line and SO188 is a continuous line. Bathymetric lines from -15 m to -130 m are gridded from the SO93, SO126 and SO188 Parasound profiles with five seconds resolution (~150 m); bathymetry from -150 m to -1000 m is plotted from the GEBCO One Minute Grid. Crossing points where thickness variations have been evaluated are marked with a cross. Cores 15KL, 16KL, 31KL, 32KL and 34KL in the Wgrid were collected during SO126 expedition while cores 84KL, 86KL and 87KL in the Egrid during SO93.

to the inter-annual sea level variability of ±0.15 m (Han and Webster, 2002). Therefore the maximum error associated to the depth values is ±0.75 m.

Depths for slope analysis ware sampled every 5-10 m along the profiles. Residual heave was eliminated by a running average of 50 steps applied to horizontal and vertical measures. For time-depth conversion a standard velocity of 1500 m s^{-1} was used to calculate the thickness. Where surveys from different years crossed each other, the difference of thickness within the stratigraphic sequence (Fig. 3) was used instead of the depth value so as to eliminate the errors associated to them. In addition, these thickness measurements give an estimate of the accumulation rate. Years have been counted as complete monsoon seasons which occurred in the time intervals.

5.3.3. Volume calculation methodologies

The data collected during the three expeditions are used for volume calculations by three procedures:

1. Calculations utilizing prominent reflections in the two main study areas.

The depth of picked horizons in the two main study areas has been gridded to create isopach maps using a gradient projection algorithm. Increment values of 150 m equivalent to 5'' of latitude, and maximum projection distance of 450 m are the best fit spatial data distribution. The resulting grids are hereafter referred to as Wgrid and Egrid (Fig. 5.2). Volumes are calculated in m^3 and transformed into tons using an average bulk density of 1.67 t m^{-3} from sediment cores of the foreset beds (Michels at al., 1998).

2. Extending the grid results to the entire foreset.

The entire foreset beds were divided into two polygon blocks, Wblock and Eblock, covering water depths between -20 m and -80 m (Fig. 5.2). The Wblock extends from the canyon margin until the seaward projection of the westward termination of the Meghna Estuary; the Eblock reflects the offshore foreset portion in front of the Meghna Estuary (Fig. 5.2). The volume of each *i*-th unit is calculated using the following equation:

$$Volume_i = \left[\left(\frac{Wblock\ Area}{Wgrid\ Area}\right) \times Wgrid\ volume_i\right] + \left[\left(\frac{Eblock\ Area}{Egrid\ Area}\right) \times Egrid\ volume_i\right] \quad (5.1.)$$

3. Volume calculation for the last decade.

Thickness differences (Fig. 5.3) as described in section 3.2 have been used to build the following finite integral:

$$Volume_{Egrid\ (or\ Wgrid)} = \left(\sum_{j,k=0}^{N} h_j\, x_k\right)(\varphi_2 - \varphi_1) \quad (5.2.)$$

where h_j is the thickness of the last 12 and 9 years measured at each *j*-th selected crossing point on Line GeoB06-462 in the Wgrid and Line GeoB06-444 in the Egrid (Fig. 5.2); h_0 has been set at the top and at the toe of the foreset beds where changes are negligible and approximated to zero. x_k is the horizontal distance of each *k*-th crossing point covered by the profile calculated from the UTM profile coordinates, φ is the UTM longitude taken at the extremes of the grid. Volumes obtained were extended to the entire foreset beds using equation (1).

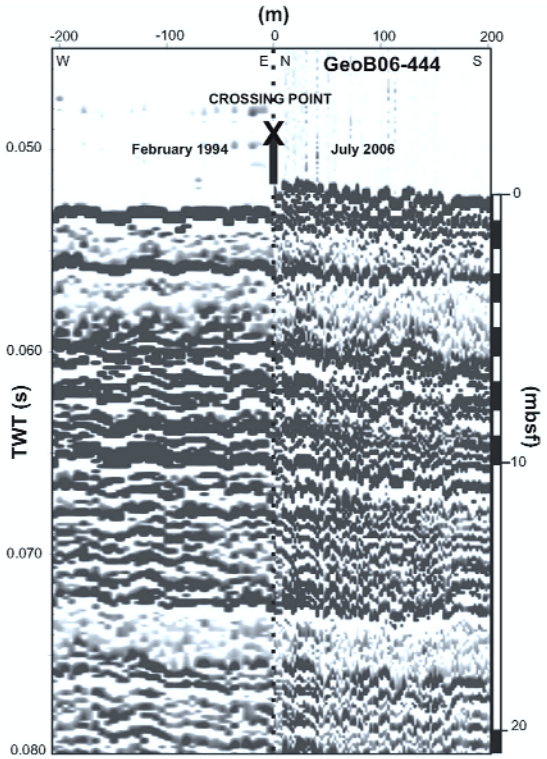

Figure 5.3. Selected Parasound example of the crossing of Lines GeoB06-444 from SO188 survey in July 2006 with a survey from SO93 in February 1994. Note the increase of 90 cm in the thickness of the sediments.

5.4. Results

5.4.1 Spatial variability of the subaqueous delta slope

Typical cross sections of the subaqueous delta are characterized by a sigmoidal surface represented by the seafloor and a base. The seafloor is steepest in the foreset and is conformable to nearly horizontal with the underlying base at the top in the topset and at the toe in the bottomset beds (Fig.s 4 and 5).

A very pronounced regional unconformity has been identified as a base by combination of Parasound and MCS profiles. The base of the subaqueous delta deepens to the west at a regional scale while it is horizontal in NS sections. The base is located at the edge of the canyon (Fig. 5.1) at 95 mbsl and shallows toward the east on the central shelf between 90 and 80 mbsl, where reflections predominantly have toplap termination (Fig. 5.5). In the eastern shelf at the Hatia Trough, the base is exposed at the seafloor at 50-60 mbsl. In the all NS sections multiple reflections and acoustic blanking due to the presence of shallow gas obscure its landward extension. In the western shelf, it is possible to trace it a bit further inland where it is recorded at a minimum depth of 75 mbsl. The base merges with the seafloor on the outer shelf.

Five representative profiles have been analyzed in detail to evaluate the spatial variability of the subaqueous delta slope in the foreset beds (Fig. 5.6). The inflection points of the sigmoidal clinoform, where the shape changes from convex to concave, can be unequivocally recognized on Lines PS-SO93, GeoB06-462 and-447, where slope angles reach maximum values of 0.28°, 0.30° and 0.31°. On Lines GeoB06-428 and -444, the average slope angle is modified by a sequence of peaks due to minor local relief caused by sub-seafloor structures. In these cases, the highest angle has not been chosen as the inflection point but rather the one that also has the higher gradient in comparison to its landward portion. The selected slope values on Lines GeoB06-428 and -444 are 0.29° and 0.28°. The rollover

point estimated by the highest slope curvature landward of the inflection remains almost constant at ~26 mbsl (Fig. 5.6). The slope angle reveals a variable asymmetry between the convex and concave section of the foreset beds. In the western Lines PS-SO93 and GeoB06-462, the mean values are 0.21° and 0.19° for the convex section from the rollover point to the inflection point, and 0.12° and 0.14° for the concave part, from the inflection point to 80 mbsl. In the eastern Lines GeoB06-428,-444 and -447, the slope mean values in the convex section are 0.15°, 0.13° and 0.16°, while in the concave section, from inflection point to 70 mbsl, they are 0.17°, 0.22° and 0.08°. No consistent trend of convergence of the rollover and the inflection point (Fig. 5.6) was observed, and the average distance is 7500 m.

5.4.2. Seismic and acoustic facies

In the foreset beds, two main seismic facies types can be identified from the MCS profiles: normal stratified and complex stratified facies (Fig.s 4a and 5a). The normal stratified seismic facies is a layered sequence with medium to low amplitude. Internal reflections are mostly parallel to the base or, rarely, downlap onto the base in the bottomset beds in the distal tail of the subaqueous delta. Such aggrading to prograding seismic facies is found in a low-gradient wedge thinning eastward. The complex stratified seismic facies type is composed of a layered sequence where internal reflections are disrupted and frequent amplitude changes are accompanied by phase reversals. It appears in a clinoform–shaped lens with internal reflections dipping down in the foreset and in the bottomset beds.
A comparison of seismic facies in MCS profiles with the acoustic facies derived from Parasound data clearly relate the complex pattern in the MCS with interlayered normal stratified sub-sequences, and acoustically transparent units in Parasound data (Fig.s 4b and 5b). In the topset beds, many transparent lenses apper, but lacking lateral continuity. Four main acoustic transparent units, Transparent Units 1-4 (TUs), can be traced continuously from east to west within the foreset beds. TU1, TU2 and TU4 appear most prominent, while TU3 is a much thinner unit, directly overlying TU2. In the MCS profiles, TUs often display negative reflection polarity (Fig.s 4a and 5a). In Parasound profiles (Fig.s 4b and 5b), the upper boundary is mostly regular with sub-horizontal or slightly seaward inclined surfaces. The upper boundary of the TUs has been described as a “staircase” by Michels et al. (1998). The lower boundary is square or round-edged.

5.4.3. Seismostratigraphy of the foreset beds

The lower boundary of TU1 is used as internal conform surface (or conformity *lato sensu* Mitchum, 1977) to separate the foreset into two sub-units, displaying: (1) a normally stratified seismo-acoustic facies and (2) a complex stratified seismo-acoustic facies, respectively (Fig.s 4c and 5c). In Sub-Unit 1, there are some reflections with a negative polarity indicating a similar pattern to Sub-Unit (2), but no cross check with the Parasound is possible due to its limited penetration.

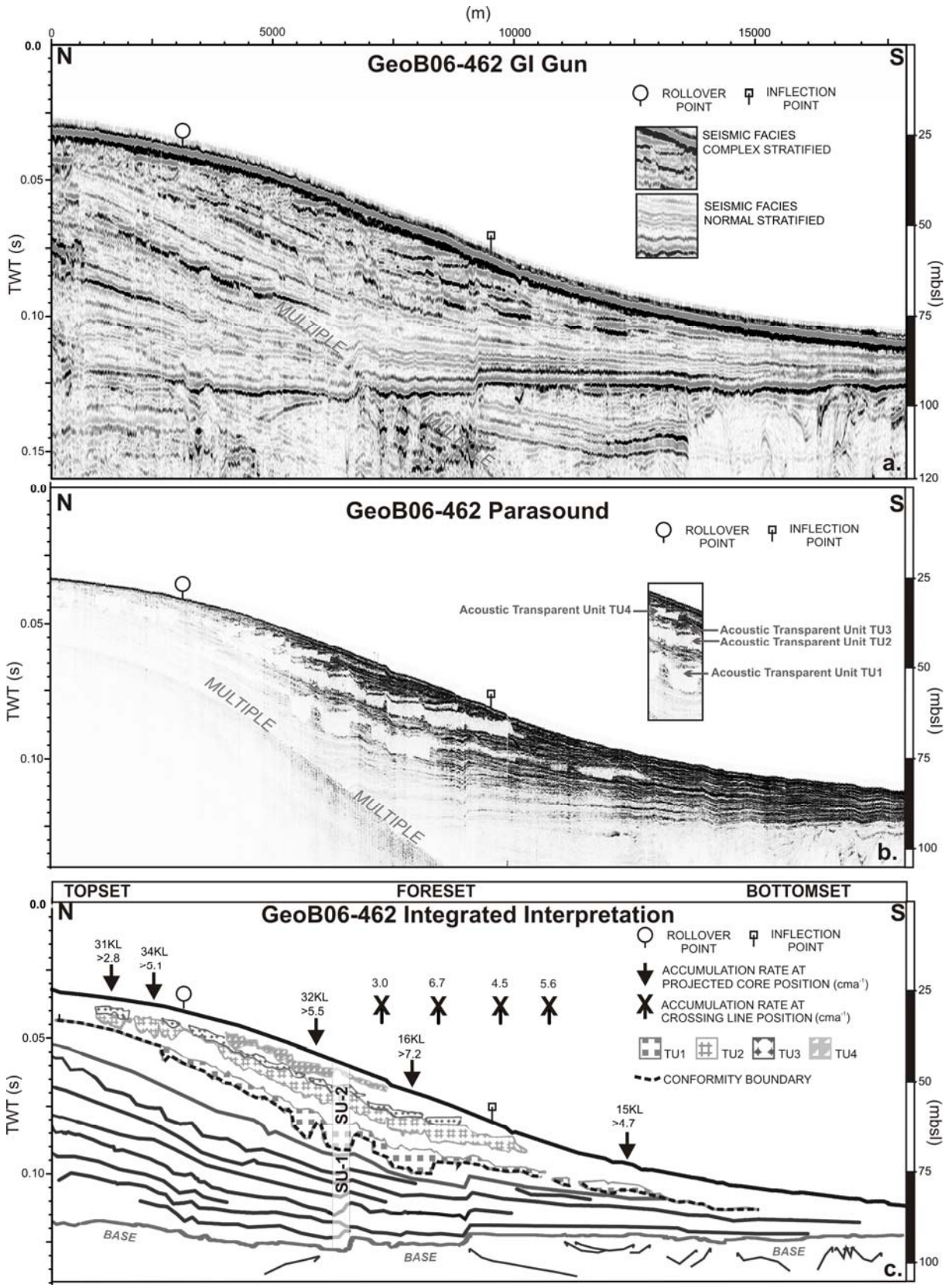

Figure 5.4. Foreset beds NS sections of Line GeoB06-462 from the Wgrid. (a.) GI Gun data, (b.) Parasound echosounder and (c.) integrated interpretation (see Fig. 5.2 for profile, grid, crossing points and cores locations).

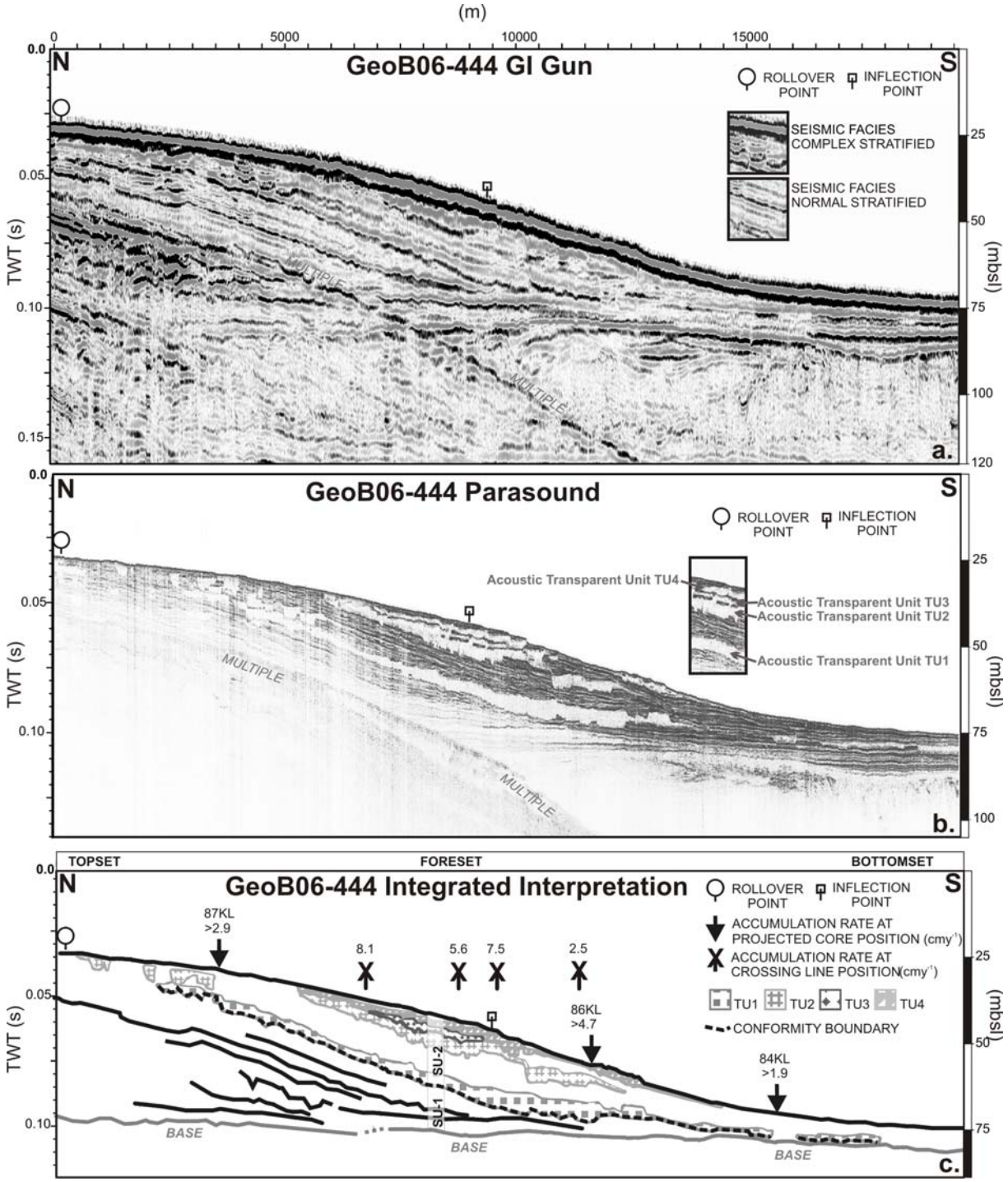

Figure 5.5. Foreset beds NS sections of Line GeoB06-444 from the Egrid. (a.) GI Gun data, (b.) Parasound echosounder and (c.) integrated interpretation (see Fig. 5.2 for profile, grid, crossing points and cores locations).

Based on this internal subdivision, isopach maps of the foreset beds stratigraphic sequence have been created in Wgrid and Egrid to evaluate thickness distribution and identify the depocentres.

The mean thickness of Sub-Unit 1 is about 50 m in the Wgrid and 25 m in the Egrid. The maximum thickness is found landward of the rollover point.

The isopachs of Sub-Unit 2 (Fig. 5.7) reveal a sedimentary depocentre in the foreset beds between 30 mbsl and 60 mbsl. Sub-Unit 2 reaches a maximum thickness of 20-25 m, both in the Wgrid and Egrid in the depth interval of 40 to 50 mbsl.

Individual isopach maps for the TUs have also been produced. Maximum thickness of TU1 is up to 7 m in the Wgrid, while in the Egrid, it does not exceed 6 m (Fig. 5.8). Maximum thickness of TU2 is on the order of 5 m in both grids. The uppermost TU4 has an average thickness of 3 to 4 m. It is thicker in the Egrid than in the Wgrid. Toward the West, TU4 thins and it almost disappears near the canyon margin.

The TUs terminate seawards in digitate lobes (Fig. 5.8). TU1 lobes extend down to 80 mbsl, TU2 lobes reach the transition from foreset to bottomset beds at 60 to 70 mbsl, and TU4 terminates at 50 to 60 mbsl. Such retrogradational vertical stacking explains the dipping down surfaces of the complex stratified seismic facies.

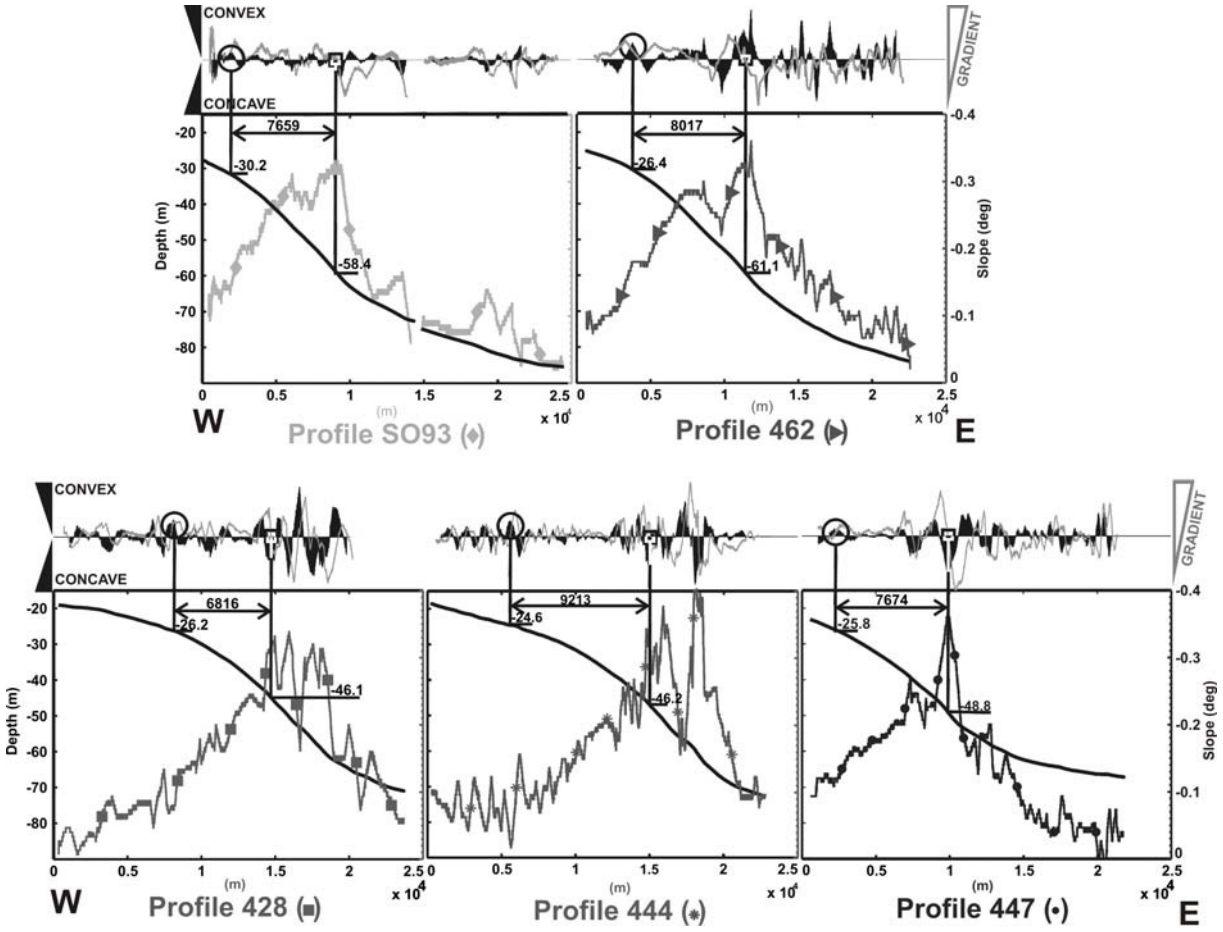

Figure 5.6. Foreset beds NS representative depth sections compared to slope angle of Lines PS-SO93, GeoB06-462, -428, -444 and 447 (see Fig. 5.2 for profiles locations). Rollover points (circle) and inflection points (square) are identified by calculation of the 1st derivate of the slope (gradient) and 2nd derivate of the slope (curvature) shown in the graphics above each depth-slope profile. Relative distance between rollover and inflection point in m is also indicated. Note the accentuated convexity seaward of the inflection point in Lines GeoB06-428 and 444.

5.4.4. Accumulation of the foreset over the last decade

Accumulation for the last decade was analyzed for Sub-Unit 2 using the thickness between seafloor and the upper boundary of TU1. Thicknesses were calculated at the crossing points of Line GeoB06-462 with an SO126 survey (December 1996) for the Wgrid and of Line GeoB06-444 with an SO93 survey (February 1994) for the Egrid (Fig. 5.3). The decimetre-scale prograding geometry of the newly deposited sediment develops in two phases (Fig. 5.9). First, aggrading sediments are accommodated on the sub-horizontal surfaces of the upper boundary of TU4. When the staircase like structure is smoothed, the normally stratified pattern continues. “Tips of the stairs” are preserved and progressively buried by the prograding sediments (Fig. 5.9).

Based on the determination of the thickness, accumulation rates were estimated. The values were compared to the slope angles (Fig. 5.10). On Line GeoB06-444, a higher accumulation rates coincided with a decrease in slope angle (Fig. 5.10a), while on Line GeoB06-462, accumulation rate and slope angle changes occur in phase (Fig. 5.10b).

Dividing the thickness of Sub-Unit 2 by the maximum recorded accumulation rate at the crossing points, an age of Sub-Unit 2 of ~216 years and ~219 years for Lines GeoB06-462 and -444 is determinate for the entire unit.

5.4.5. Sediment Volumes

Volumes were calculated for the entire stratigraphic sequence and individually for Sub-Units 1 and 2, TU1, TU2 and TU4 in Wgrid and Egrid by the interpretation software and then extended to the Wblock and Eblock (Table 2) by using Equation (1). The constraining surfaces of the entire sequence are the base of the subaqueous delta and the seafloor. The volume of Sub-Unit 1 was calculated between the regional unconformity (the base) and the conformity boundary (the lower boundary of TU1). The volume of Sub-Unit 2 was calculated between the conformity boundary and the seafloor. It is important to note that the calculation of volume for the entire sequence is not the sum of both sub-units, as the constraining boundaries are not the same. Additionally, volumes between the major reflections of TUs were also calculated.

The volume contained in the entire stratigraphic sequence of the Ganges-Brahmaputra subaqueous delta from 20 to 80 mbsl adds to 9.03×10^{10} m^3. Sub-Unit 1 contains one order of magnitude more sediment in the Wblock than in the Eblock (Fig. 5.11). On the contrary, the volumes of Sub-Unit 2 are very similar in both blocks for a total volume of 4.35×10^{10} m^3. 20 % of the sediment mass in Sub-Unit 2 is constituted by the TUs (Fig. 5.11). The direct sum of Sub-Unit 1 + 2 underestimates the total volume by 3.3 %.

The volumes calculated from Equation (2) record the trend for the last decade. During the last 12 years, when in the Wblock 3.93×10^8 m^3, while in the Eblock, 5.22×10^8 m^3 have been deposited. The mean annual storage rate for the foreset beds is 0.82×10^8 m^3 or 0.138×10^9 t a^{-1}, equivalent to 13.8 % of the total suspended sediment flux per year.

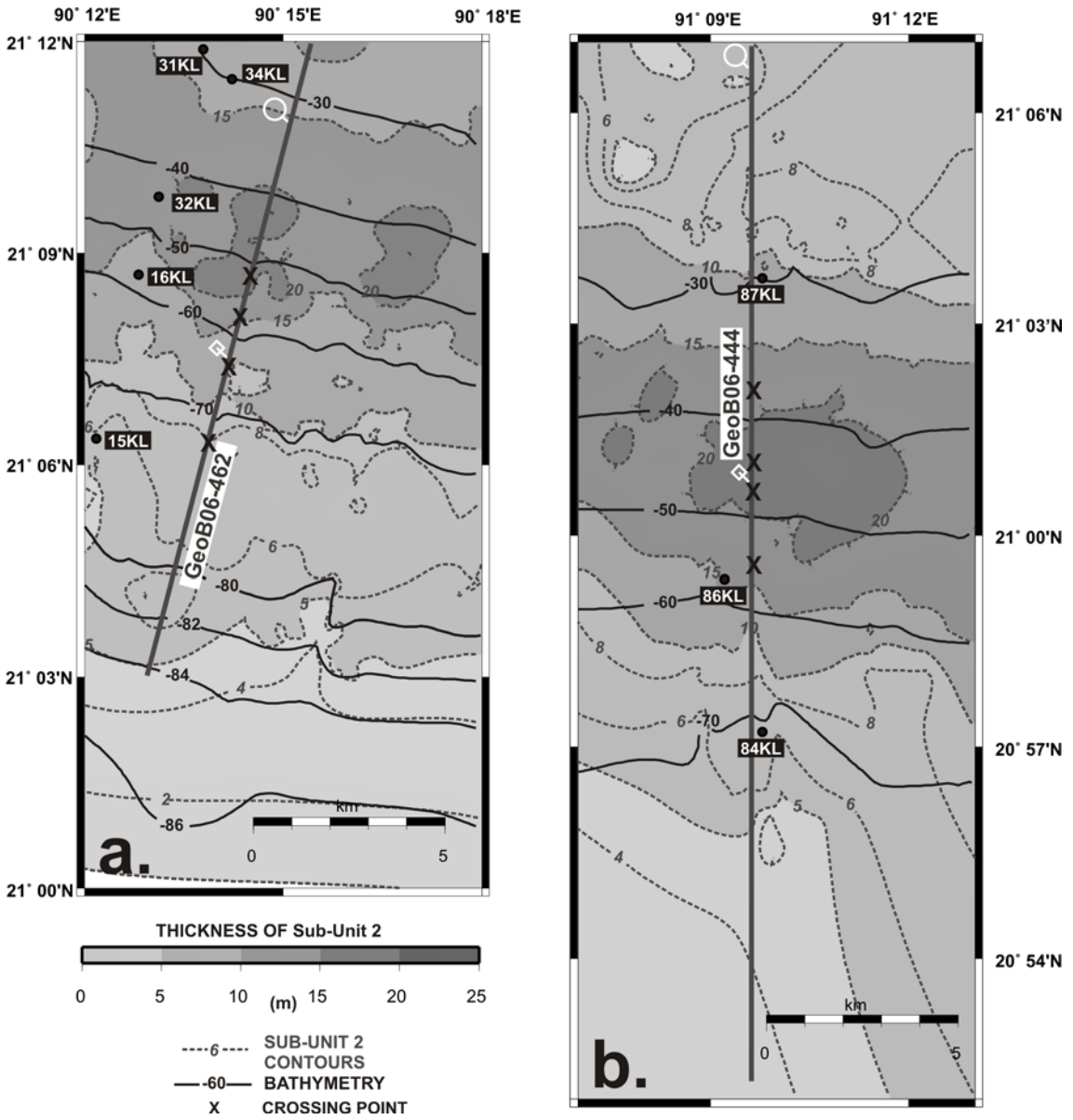

Figure 5.7. Isopach map of Sub-Unit 2, in Wgrid (a.) and Egrid (b.) (see Fig. 5.2 for grids locations). Rollover points are identified as circles and inflection points as squares. Bathymetric lines are gridded from the SO93, SO126 and SO188 Parasound profiles with five seconds resolution (~150 m). The Sub-Unit 2 depocentre is located between -40 m and -60 m water depth.

5.5. Discussion

5.5.1. Chronostratigraphy of the foreset beds

5.5.1.1. Subaqueous delta initiation and development of Sub-Unit 1

At the termination of the last ice age (Termination 1), the development of the Ganges-Brahmaputra high-stand delta started prior to the formation of other world's modern deltas (Goodbred and Kuehl, 2000b) which was caused by a deceleration of sea level rise 8-7 ka ago (Stanley and Warne, 1994; Hori and Saito, 2007). During this deceleration, the Ganges-Brahmaputra delta changed from an aggradational to a progradational system (Umitsu, 1993). The sea level rise eroded the former low-stand deltaic plains and produced a transgressive ravinement surface (*sensu* Catuneanu et al., 2009) which is the base of the subaqueous delta at a regional scale (Fig.s 4 and 5).

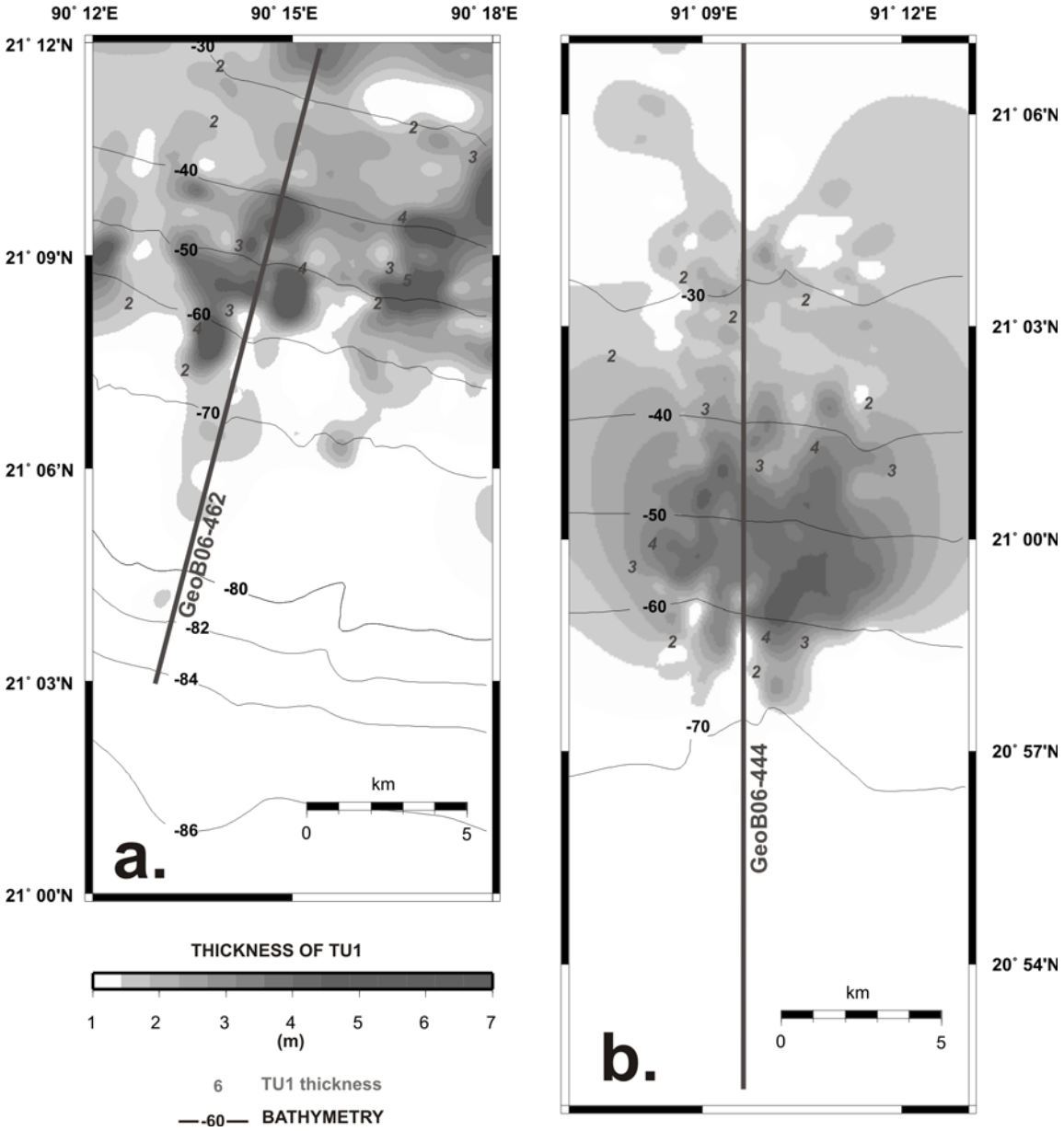

Figure 5.8. Isopach map of the Transparent Unit 1, TU1, in Wgrid (a) and Egrid (b) (see Fig. 2 for grid locations). Bathymetric lines are gridded from the SO93, SO126 and SO188 Parasound profiles with five seconds resolution (~150 m). The TU1 lobes extent seaward to -70 m in the Wgrid and -60 m water depth in the Egrid.

The observed westward deepening of the base may be explained by a locally higher subsidence rate, but it might be also caused by increased erosion of the low-stand tidal flats due to the proximity of the canyon margin. The time lag between the subaerial delta initiation 11 ka ago (Goodbred and Kuehl, 2000b) and subaqueous delta initiation 7 ka ago (Kuehl et al., 1997; Goodbred and Kuehl, 1999) suggests a hiatus in the sedimentary succession. The time span of the hiatus in the study area between the base and Sub-Unit 1 initiation cannot be quantified. The aggrading to prograding vertical stacking of the normally stratified seismic facies, however, reflects a sedimentary environment from distal to

more and more proximal. This suggests that during deposition of Sub-Unit 1 the coastline was moving seaward.

During the mid-Holocene sea level high-stand (Geyh et al., 1979; Lambeck and Chappell, 2001), the Brahmaputra River switched to its eastern course in the Sylhet Basin and drained into this large and rapidly subsiding basin. The missing sediment supply to the eastern shelf prolonged the transgression by 1-2 ka, in contrast with the progradation of the western Bengal coastline (Goodbred and Kuehl, 2000a). The sediment deposited in Sub-Unit 1 could have been deposited during the progradation of the Ganges Delta, from approximately < 4 to 0.2 ka (Allison at al., 2003) in the region north of the Wblock (Fig. 5.11). The mean depth of the base made more space available to accomodate sediment on the western shelf and explains why Sub-Unit 1 is significantly thicker in the western foreset beds. In addition, the suspected presence of acoustically transparent units indicates that the Sub-Unit 1

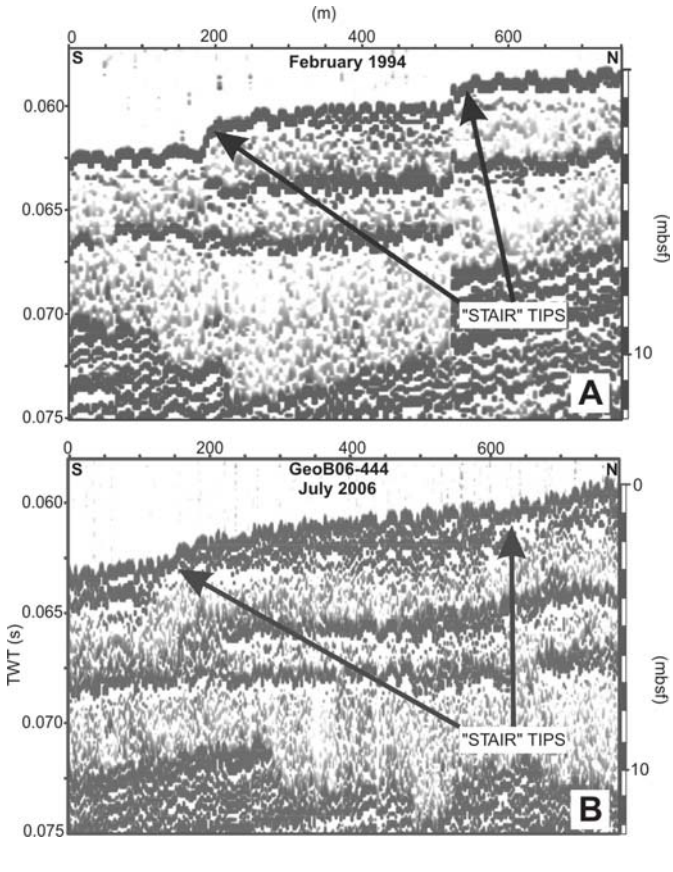

Figure 5.9. Selected Parasound examples of the decimetre scale prograding geometry of the newly deposited sediment from SO93 survey in February 1994 (A) with Line GeoB06-444 collected in July 2006 (B). In (A) initially aggrading sediments are accommodated on the surfaces offered by the TU4 upper boundary described as a "staircase" by Michels et al., (1998). In (B) "stair tips" are preserved 12 years later and progressively buried by the prograding sediments.

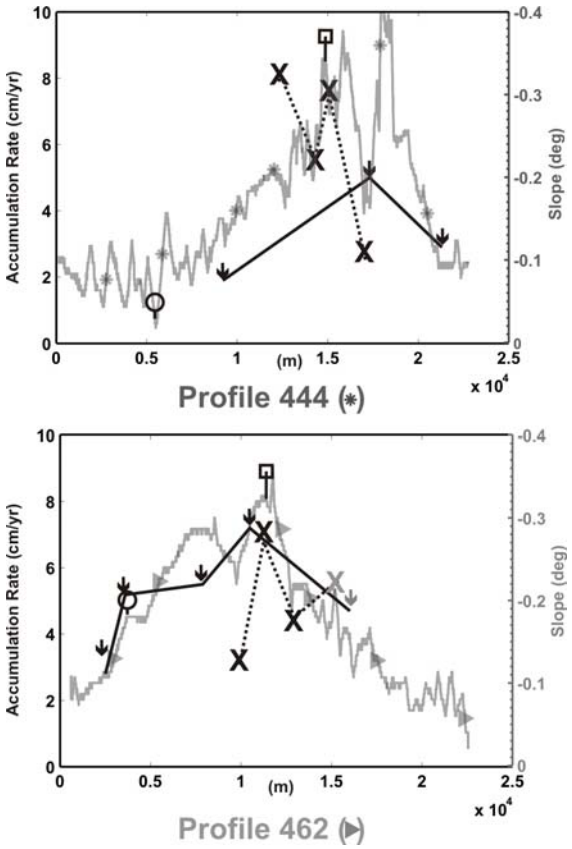

Figure 5.10. Slope angle on Lines GeoB06-444 and -462 (see Fig. 2 for profiles locations) compared to the accumulation rate derived from the thickness variations at the crossing point (X). Accumulation values calculated with the ^{137}Cs measurements (Michels et al., 1998; Suckow et al., 2001) are projected on the profiles and indicated by a small arrow (see Fig. 2 for cores locations). Rollover points are marked with a circle and inflection points are marked with a square. In Line GeoB06-444 accumulation rate increases where slope diminish, while on Line GeoB06-462 they increase and decrease in-phase.

consists of a mixed sequence of bottomset and incoming foreset beds. The uneven distribution of Sub-Unit 1 may be also caused by a different setting of river mouths which is an important factor controlling the subaqueous delta formation and evolution together with accommodation.

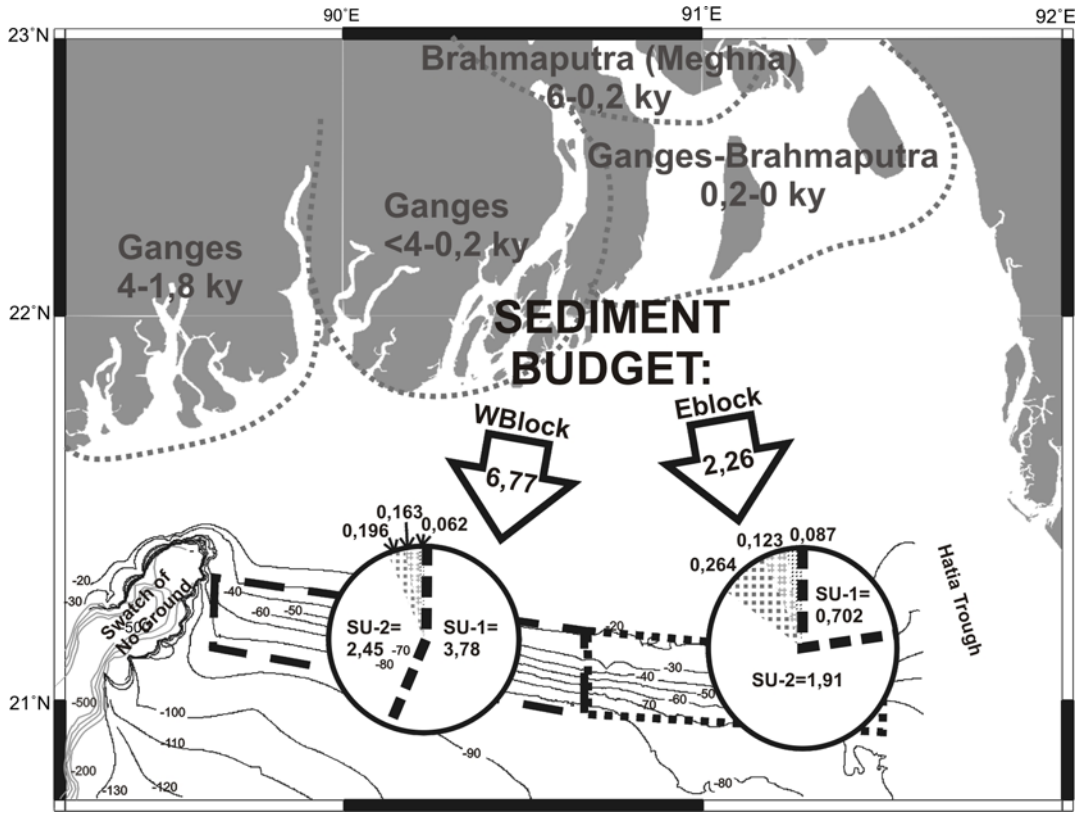

Figure 5.11 Sediment volumes for Wblock and Eblock and internal sediment partition. The significant increment of volume in Wblock of Sub-Unit 1 is caused by a different deltaic configurations (modified from Allison et al., 2003 and their Fig. 13). See Table 2 for the values of the pie slices.

5.5.1.2. Sub-Unit 2 development in relation to river courses

Historical maps from the 18th century (Rennell, 1786) show the Ganges discharging through the Tetulia channel while the Brahmaputra was following its eastern Sylhet–Meghna route (Fig. 5.1). This situation was changed by the confluence of the Ganges and the Brahmaputra around 1830 (Rennell 1786; Allison et al., 2003; http://www.banglapedia.org/httpdocs/HT/F_0103.HTM). Probably Sub-Unit 2 has been deposited since the last phase of convergence of the rivers. The uniform distribution of Sub-Unit 2 (see section 4.3) along the foreset beds (Fig. 5.7 and Table 2) strongly suggests a sediment source of the combined Ganges Brahmaputra river flux (Pierson-Wickmann et al., 2001; Allison at al., 2003, their Fig. 5.13). Sub-Unit 2 is therefore an individual sigmoidal clinoform building block of the prograding Ganges-Brahmaputra subaqueous delta and the complex stratified facies is thus interpreted as proper foreset beds.

5.5.1.3. Sub-Unit 2 development in the last decade

The sigmoidal clinoform shape fits the right half of a Gaussian distribution and landward of the inflection point, the shape is convex, while it is concave seaward (Adams and Schlager, 2000). In the profiles of the surveyed area, roughness of the seafloor masks the idealized curve (Fig. 5.6). The acoustically derived accumulation rates of the last decade compared to those calculated with the ^{137}Cs measurements (Michels et al., 1998; Suckow et al., 2001) projected on the two selected profiles are in good agreement (Fig. 5.10). Accumulation rate is locally influenced by the presence of the TUs in the subsurface, particularly in the eastern clinoform (Fig.s 6 and 10). An initial vertical component of accretion precedes the normal progradation (Fig. 5.9). In order to compare the five representative depth profiles (Fig. 5.6), running only approximately perpendicular to the slope, they have been normalized (Fig. 5.12) as suggested by Pirmez et al. (1998).

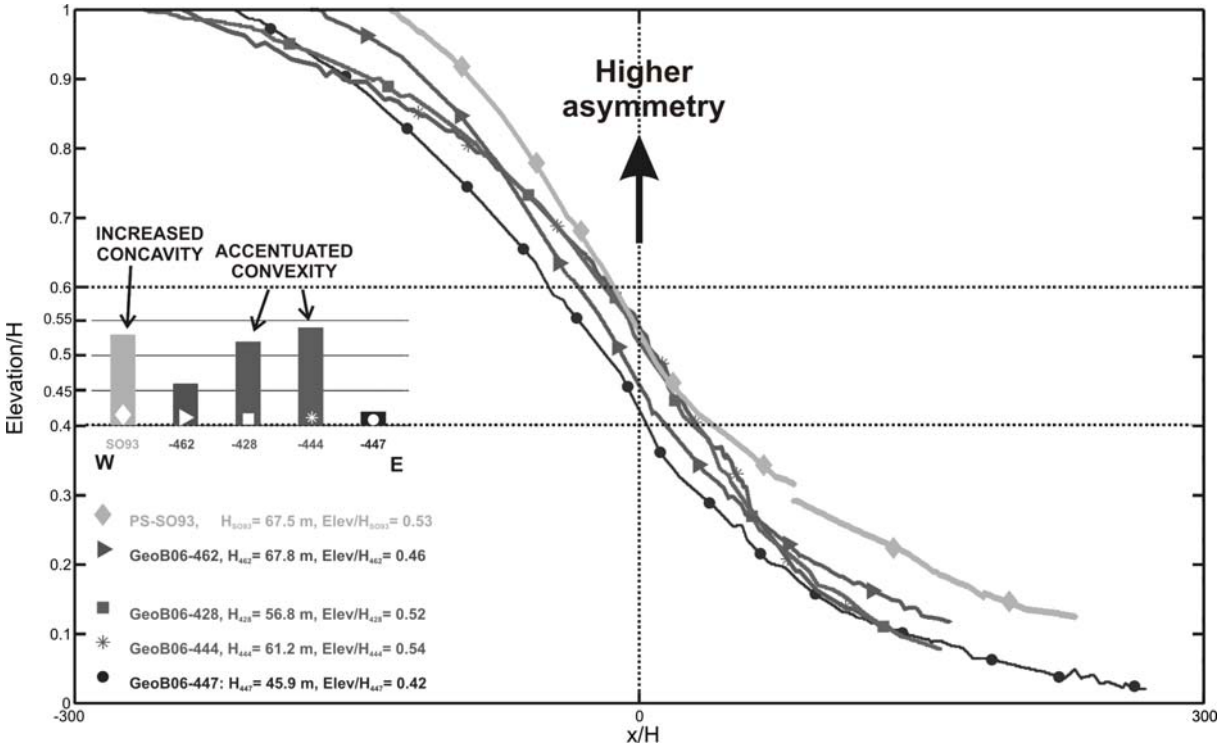

Figure 5.12 Normalized topographic elevation of the NS **representative** depth sections of Lines PS-SO93, GeoB06-462, -428, -444 and -462 (see Fig. 5.2 for profiles locations).

The toe elevation (zero) is determined at the point where the seafloor becomes horizontal or conformable with the underlying regional unconformity identified as the base of the entire sequence. The top is defined as the shallowest point at the topset surface of the clinoform. The elevation differences between the top and the toe, H, is taken at the seafloor and the base of the entire sequence and it decreases from west to east as Sub-Unit 1 is thicker to the west. At the inflection point of Lines PS-SO-93, -462 and GeoB-447, the normalized elevation of the foreset beds thickness, elevation/H, progressively decreases. Instead, Lines GeoB06-428 and -444 have a very similar normalized depth profile and elevation/H is 0.5 for both. The inflection point deepens toward the west, where the

uppermost TU3 and TU4 are less pronounced. The asymmetry between the convex and concave portion of the clinoform and its spatial variability also depends on the presence of the TUs, especially for Lines GeoB06-428 and -444. However, the main processes responsible for the asymmetry during a phase of relatively stable sea level are: (1) offshore transport processes, especially the interplay of fluvial input with tidal energy, wave/current field (Walsh et al., 2004, Swenson et al., 2005; Ma et al., 2010) and (2) space available to accommodate the sediment (Pirmez et al., 1998).

(1) The central-eastern clinoform is in front of the active delta (Fig. 5.1) but main transport is directed toward the west (Barua et al., 1994; Kuehl et al., 1997). Tide-supported gravity flows may dominate the transport of suspended sediment deriving from the river flood peaks. This process is probably dominated by individual pulses rather than occurring continuously. In the Amazon and Fly River discrete decimetre-scale sediment-supply events are responsible for clinoform progradation (Sternberg et al., 1996; Walsh et al., 2004) and a similar mechanism caused the asymmetry found in the Lines GeoB06-444 and GeoB06-428 (Fig.s 6 and 12).

In the western clinoform, the tidal energy has an additional component derived by the SW monsoon wind driven current, generating tide+current-supported gravity flows. The combined action of tide and current keeps accumulation active over the entire monsoon floods periods as current-supported gravity flows can operate in deeper water and carry sediment further offshore with deposition where bed slope decreases (Fig. 5.6). Such deposition pattern has been observed also in the Waiapu River in New Zeeland (Ma et al., 2010). The intersection of the canyon in the topset beds interrupts the westward alongshore transport because, with the increase of depth, the current velocity and therefore the transport capacity is reduced. The sediments are consequently trapped in the canyon head. However, in absence of the Swatch of No Ground the suspended sediment load would migrate further to the west and accumulate in alongshore clinoform deposits like offshore the mouth of the Yangtze River in the East China Sea (Liu et al., 2006).

The effect of cyclonic waves on the clinoform is discussed in section § 5.2.2.

(2) As less space is available over time to accommodate the sediment flux, the clinoforms, to remain in equilibrium, tend to grade (Fig. 5.12) into a convex shape in the central-eastern beds (Lines GeoB06-428 and -444), and to a concave shape at the margins (Lines PS-SO93, -462 and GeoB06-447). In general, convex clinoforms experience a decreased accumulation rates over time, while concave clinoforms increased accumulation rates (Wolinsky and Pratson, 2007). Therefore, the accumulation rate in the central eastern foreset beds of the Ganges-Brahmaputra is decreasing, whereas toward the western margin of the clinoform an increase in accumulation rate over time is more characteristic.

5.5.2. Acoustic Transparent Units

5.5.2.1. Sedimentary processes

Grain-size analyses and thin-section photomicrographs indicate that the acoustically transparent units, referred as TUs in this study, are unsorted and homogeneous (Kuehl et al., 2005). In the same cores, unusually high P-wave velocities have been measured within the homogenized sediments (Spiess et al., 1998). This explains the phase reversal of the reflection observed in the MCS records (Fig.s 4a and 5a), as produced by the interface from TUs and the underlying normally stratified sediments which have lower P-wave velocities.

The process responsible for TUs formation in the clinoform were “mudflow deposits which are caused by liquefaction and subsequent gravitational flow (...) with down slope relatively small movement but bedding sediments were destroyed or contorted by the movement of overlying sediments” (Michels et al., 1998).

The Ganges-Brahmaputra subaqueous delta is located above the clay liquefaction line (Wolinsky and Pratson, 2007) and the slope angle never reaches the critical value of 0.5° (Fig. 5.6) where gravity flows may go into autosuspension (Friedrichs and Wright, 2004). Therefore, the collapsed beds may have changed to their actual stair-case structure (Fig.s 4 and 5) after deposition by liquefaction flow, as described by Lee et al. (2007). In conclusion, the formations of the TUs are now interpreted as follows: once the already deposited and unconsolidated beds are subjected to a cyclic load, the excess of pore pressure dewaters or degases (where gas is also present) the surface beds and destroys the internal stratification. This post-depositional and in-situ process is associated with a small down slope movement, recognisable in the lobed terminations at the transition between foreset and bottomset beds.

5.5.2.2. Trigger mechanism for liquefaction flow generation

Waves and currents inducing velocity shear within near-bed layers may support hyperpycnal layers as thick as a meter or more, initially formed by sediment flux convergence like in the Amazon shelf (Sternberg et al., 1996; Wright and Friedrichs, 2006). If the stratigraphic sequences of the Amazon clinoform (Hübscher et al., 2003) and of the Ganges-Brahmaputra, both surveyed with the Parasound system, are compared, some lenses with an acoustically transparent facies could be seen also in the Amazon but only in the topset beds. It can be then excluded that in Ganges-Brahmaputra foreset beds, waves or currents have deposited the sedimentary bodies identified in the seismo-acoustic records as TUs.

Earthquake and/or cyclone activity, in combination with high accumulation rates, were formerly suspected to have triggered gravity flows in the foreset beds of the Ganges Brahmaputra subaqueous delta (Michels et al., 1998; Kuehl et al., 2005).

Some tempestite deposits in the foreset beds, caused by cyclonic wave-supported gravity flows, have been identified as decimeter-thick graded and ungraded sand+silt layers (Michels et al., 1998). The

close relationship between cyclones and tempestites is not found in foreset beds in contrary to the Swatch of No Ground (Kudrass et al., 1998). The depths of the TUs are mostly below wave base; however, cyclone waves may have caused a liquefaction flow in the topset-foreset transition which would then flow down the foreset slope. On the other hand, removing up to 0.15 x 10^{10} m^3 of sediment during a single flow event should have produced a prominent scar which could not be observed. Additionally, major cyclones influence the area about once a year, whereas only four TUs have been observed, as was already noted by Kuehl et al. (2005). Therefore it is suggested the widespread presence of only four TUs in the foreset and their meter scale thickness can attribute the origin of the liquefaction flows to the passage of the compressional waves generated by earthquakes.

An acoustically transparent unit in the depth range of appx. -50 to -60 m is visible in the Taiwan Strait clinoform which is predominantly derived from the Taiwanese Choshui River (Liu et al., 2008). Lateral continuity has not been studied yet, but it is remarkable that it occurs in an extremely active tectonic region (Liu et al., 2008).

The retrogradational stacking pattern in the longitudinal distribution of the TUs in the foreset beds (Fig.s 4 and 5) might be related to the location of the earthquake, the depth of the ipocentre, the way compressional waves propagate through sediments and the shear strength of the sediment. Especially where accumulation rate was higher, it is expected that the liquefaction flow is thicker because of the initially higher water content of the uppermost sediments. The relative sand content in the foreset might also play a role in the sensitivity of the sediments to liquefaction, as the thinning of the uppermost TU4 toward the west is accompanied by a net decrease in sand content, revealed by grain size analyses in the uppermost beds (Kuehl et al., 1997; Michels et al., 1998).

Geo-technical measures should be conducted on the TUs to validate the hypothesis on their formation as liquefaction flows and their initiation by earthquakes.

5.2.3 Earthquake records in the stratigraphic sequence

The age attributed to TU1 based on the ^{137}Cs accumulation rate is ~250 years (Michels et al., 1998). The accumulation rates for the last decade of 6.7 cm a^{-1} and 8.1 cm a^{-1} for Lines GeoB06-462 and -444, provide an age between 1786 and 1789 to TU1. However, there is an uncertainty in projecting a centennial scale from a decadal accumulation rate especially on a prograding sequence. Therefore, TU1 is interpreted to be caused by the plate-boundary earthquake along the Arakan Coast in 1762 (8.8 magnitude as worst scenario in Cummins, 2007), TU2 may be related to the Great India Earthquake (8.7 magnitude) in 1897 and TU4 to the Assam Earthquake (8.4 magnitude) in 1950. The minor event of TU3, directly above TU2 could be attributed to the Srimangal earthquake in the Sylhet Basin in 1918, which had a magnitude of 7.6. The boundary between TU2 and TU3 is preserved (Fig.s 4 and 5) indicating that the previously mobilized sediments during the first earthquake were not remobilized by the following earthquake. A possible explanation is that once the beds are dewatered they can probably not experience any further liquefaction. The transition from Sub-Unit 1 to 2 has been altered

by the liquefaction flow caused by the 1762 earthquake but there is no physical evidence of erosion or non-deposition and it is not expected any significant hiatus. However the linking of TUs to specific earthquakes now reveals an internal chronostratigraphy in Sub-Unit 2 and, thus, a new opportunity to establish a mean annual storage rate for the last two centuries at a higher temporal resolution.

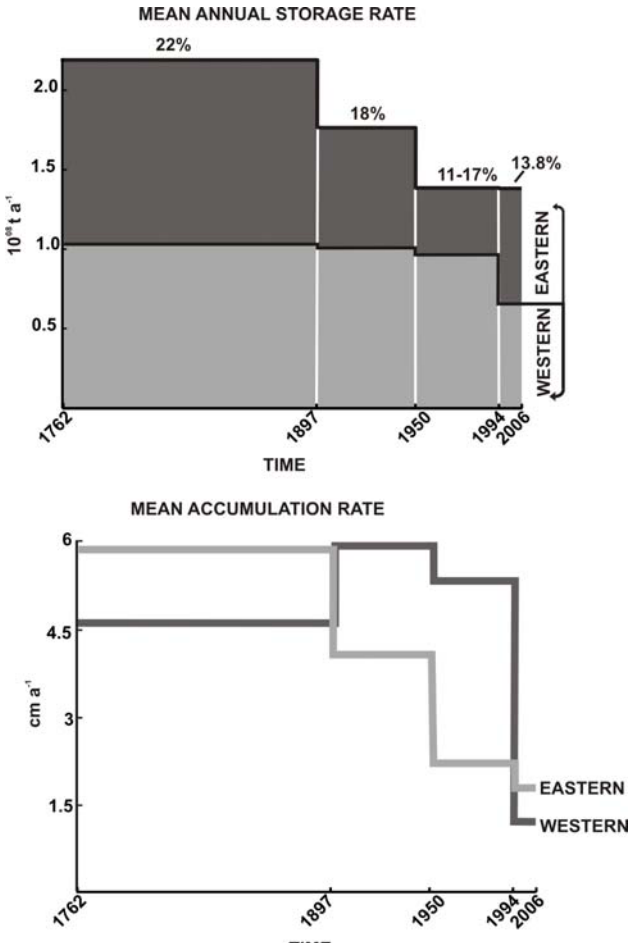

Figure 5.13. Mean annual storage rates and mean accumulation rates for Sub-Unit 2 calculated with 1,67 g cm^{-3} of density (Michels et al., 1998). Internal repartition from 1762 to 1897, from 1898 to 1950 and from 1951 to 1993 is derived by the attribution of specific earthquakes to TU1, TU2 and TU4 until the SO93 expedition. The last decade values (1994-2006) are derived by comparison of thickness variations in different surveys. Indicated in percentages is the partition with respect to the total suspended sediment load. Note the higher mean annual storage and mean accumulation rates in the interval 1762-1897 probably due to intensified monsoon precipitations inland in the eastern clinoform possibly due to post seismic deformation.

5.5.3. Sediment budget

The mean annual storage rate of 13.8 % over the time period 1994-2006 in the foreset beds, compared to ~20 % since the subaqueous delta initiation (Kuehl et al., 1997; Goodbred and Kuehl, 1999) and for the last 50-60 years (Michels et al., 1998; Suckow et al., 2001), gives a new dynamic perspective, and highlights the net decrease in the sediment sink of the foreset beds compartment in the Himalaya-Bengal Basin source-to-sink system. This decrease becomes even more evident when considering each interval defined by the TUs in Sub-Unit 2. Using the upper boundary of each TU as time marker horizon, volumes, and consequently mean annual storage rates (Table 3)*, have been calculated. Based on the attribution of TUs to specific earthquakes (see section 5.2.3), the mean annual storage rate in Sub-Unit 2 in the interval 1762-1897 was 22 % of the total river input, and decreases to 18 % between 1897 and 1950. It further decreased from 1950 to 2006 to 11-17 % of the total river load (Fig. 5.13). The decrease of mean annual storage rate in the entire foreset beds since the convergence of Ganges with Brahmaputra is mainly due to a progressive decrease in the eastern clinoform (Table 3 and Fig. 5.13). Mean annual storage rates were identical between east and west in the oldest time interval. The eastern clinoform mean storage rates significantly decreased over time while the western clinoform approximately maintained a constant

mean annual storage rate from 1762 to 2006 (Table 3 and Fig. 5.13). The annual average land loss of 6.7×10^7 t a^{-1} in the western delta from 1840 to 1990 (Allison, 1998) accounts for only a very small contribution to the mean annual storage rate in the foreset beds, though the coastal land loss did not supply significantly to the constant mean annual storage rate in the western clinoform.

The mean annual storage rates on a local scale indicate that the mean accumulation rate was 5.9 cm a^{-1} in the eastern clinoform and 4.6 cm a^{-1} in the western clinoform from 1762 to 1897 (Table 3 and Fig. 5.13). The explanation for the higher mean accumulation rate in the eastern foreset beds could be a mix of climatic and tectonic forcing. In the immediate post seismic phase, the mean annual storage rates could have been indeed influenced by deformation processes that might have resulted in an altered subsidence and/or sediment supply. Intensified subsidence rates have been clearly demonstrated as being due to tectonic deformation after the Sunda Megathrust Earthquake in 2005 (Briggs et al., 2006). Historical reports describe significant deformations along the Arakan coast up to Chittagong after the 1762 event (Cummins, 2007) accompanied by a wetter period from 1670 to 1840 (Breitenbach, 2009). Anomalous floods occurred also after the 1897 event (Gahalaut and Chandler, 1992). A minor deformation was reported after the 1950 Assam Earthquake (Reddy et al., 2009). A temporarily higher subsidence rate together with sediment pulses due to severe floods contributed to the higher mean annual storage rate for the interval 1762-1897. The local higher mean accumulation rate in the eastern clinoform suggests that there was more space available to accommodate the sediment accompanying the increased sediment load. The anomalous floods after the 1897 Great India Earthquake would have contributed to keep the mean annual storage rate high despite the decreasing trend of the monsoon precipitation. On the contrary, the 1950 Assam earthquake might have had a negative feedback on the mean annual storage rate. In fact, landslides following the 1950 earthquake released millions of tons of debris from the Himalaya Mountains to the Brahmaputra main valley and some tributary valleys, causing river clogging (Murty and El-Sahb, 1992; http://earthquake.usgs.gov/earthquakes/world/events/1950_08_15.php).

In the last decade, the mean accumulation rate increased again distinctly in the eastern clinoform (Table 3 and Fig. 5.13). Despite the number of droughts has been increasing over the last two decades (http://www.banglapedia.org/httpdocs/HT/D_0284.HTM) a catastrophic flood occurred in 1998. It is expected that this flood is the suspended sediment source responsible for individual sediment pulses which resulted in a higher mean accumulation rate in the eastern clinoform for the last decade (Table 3, Fig.s 10 and 13). Based on these evidences, it could be generally reassumed that the accumulation rate in the eastern clinoform is more sensitive to discharge peaks caused by floods. The constant mean annual storage rate over the last two centuries in the western clinoforms is instead derived from constant SW monsoon wind driven oceanic currents resulting in wind induced tide+current-supported gravity flows.

*The gridding of the seafloor has a 12 years maximum error associated which gives a 20 % error in the calculation of the mean annual storage rate for the last interval of 56 years.

5.5.4. Dynamics of the subaqueous delta as sink for sediment

The present day configuration of the subaqueous delta is the result of a complex interaction between the forcing factors on the Ganges-Brahmaputra deltaic system. Modeling the clinoform development attributes the natural partitioning of sediment between subaerial and subaqueous deltas mostly to the frequency and magnitude of floods and storms (Swenson et al., 2005), but in the Bengal Basin other forcing factors, such as tide, long-term current field, sea level, subsidence and anthropogenic stress also play a significant role in growth rates. Table 1 summarizes the evidences on the different factors and the possible consequences expected on the deltaic system.

The decrease in the mean annual storage rate in the eastern clinoform located directly south of the active river mouths, which is also reflected in the accentuated convexity of the clinoform surface, has been caused by a decrease in monsoon precipitation. The SW trade winds in combination with the tides instead support a constant delivery of sediment to the western clinoform, as shown by the increasing concavity toward the west. Intensified magnitude of storm events, landscape modifications, river embankments and poldering all favor the seaward export of sediment. Accelerated subsidence due to gas exploitation together with natural subsidence, caused by both tectonic and compaction effect, and expected sea level rise will provide additional space to accommodate the sediments in the foreset beds, also favoring seaward export. Unless it is the result of a decreased sediment load transported by the river due to inappropriate water management and poldering especially in the coastal areas, the decrease in the mean annual storage rate suggests that the system is favoring the Swatch of No Ground canyon as sink.

Based on available data, the quantification of the anthropogenic impact on the clinoform of such huge land conversion, river course stabilization, damming, water and/or gas exploitation is yet not possible, due the lack of a continuous and accessible monitoring of bed and suspended sediment load.

If the subaerial delta is disadvantaged as sink, it is of high socio-economical importance as it will lead to intensified coastal erosion and saline intrusion into the lower delta plain. While the sink of sediment in the subaqueous delta might represent an intermediate state between land and sea sediment domain with a positive effect on mitigation of oceanic and tsunamis waves, the sink in the canyon means a definitive loss of sediment for the coastal system.

5.5.5. The subaqueous delta as high resolution archive

The stratigraphic sequence in the eastern foreset beds is more sensitive to discharge peaks caused by floods and thus it contains a high-resolution archive recording the frequency and intensity of monsoon precipitation and of extreme flood events. The stratigraphic sequence in the western clinoform provides instead a high-resolution archive of current variability and therefore, indirectly of the SW monsoon wind intensity. In general, the sediments of the clinoform can be used as a high-resolution

archive to reconstruct the response on the deltaic system to the anthropogenic stress during the pre and post-industrialization time.

Drilling the Ganges-Brahmaputra clinoform could be a useful tool to understand also other river systems and their response to external forcing. In particular this study could be set as a future scenario for the impact of the planned and ongoing damming projects on the mainstream of the Salween (Hedley et al., 2010).

5.6. Summary and Conclusion

The seismostratigraphic approach to reconstruct the sedimentary paleo-environment has been successfully applied to the high resolution acoustic and seismic data collected in the Ganges Brahmaputra subaqueous delta in water depth from -20 to -80 m.

Reflection terminations, internal geometry and seismo-acoustic facies identification divided the stratigraphic sequence into two sub-units. Sub-Unit 1 is interpreted as a mixed sequence of bottomset and incoming foreset beds, and Sub-Unit 2 is composed of an individual sigmoidal clinoform building block of the prograding stratigraphic sequence of the Ganges-Brahmaputra subaqueous delta and, therefore, proper foreset beds. Sub-Unit 1 was estimated to have been deposited between < 4 and 0.2 ka, and Sub-Unit 2 since the Ganges final convergence and confluence with the Brahmaputra ~300 years ago.

Mapping of Transparent Units (TUs) has confirmed their spatial extent across the entire clinoform. Based on their meter-scale thickness, their restricted number, their wide-spread distribution and especially their timing, they have been interpreted as liquefaction flows generated by cyclic loading from compressional waves of major plate-boundary earthquakes.

The sediment volume of the analyzed subaqueous delta sequence is 9.03×10^{10} m^3. Sub-Unit 1 contains one order of magnitude more sediment in the western foreset than in the eastern due to more accommodation availability. The volume of Sub-Unit 2 is 4.35×10^{10} m^3. Attribution to specific earthquakes of each TU provides the time frame for a centennial scale mean annual storage rate. The mean annual storage rate was 22 % in the interval 1762-1897 with a higher mean accumulation rate on the eastern clinoform. A decrease to 18 % between 1897 and 1950 was followed by a decrease to 11-17 % from 1950 to 2006 (Table 3). In the last decade (1994-2006), based on thickness variations in the stratigraphic sequence, it results that only 13.8 % of the total suspended sediment load has been deposited in the clinoform.

Surface slope angle variability of the clinoform confirms these findings with a variable degree of asymmetry between the convex and concave portion of the sigmoidal shape. The tendency to grade into a convex clinoform toward the east is attributed to frequency and intensity of floods and episodic tide-supported gravity flows. Toward the west, the clinoform surface tends to grade into a concave shape, which is attributed to a sediment transport governed by SW monsoon wind, inducing more regular tide-current-supported gravity flows.

The subaqueous delta deposits, and in particular Sub-Unit 2, have a great potential as a high-resolution archive, recording the response of the deltaic system during the last centuries to monsoon floods and SW monsoon wind intensity. Additionally, the stratigraphic sequence has recorded post seismic deformations but, above all, the time span coincides with the progressive intensification of the anthropogenic impact on the alluvial and deltaic plain. The sink of sediments in the Ganges Brahmaputra subaqueous delta is not constant due to decreased flood frequency and intensity, increased magnitude of cyclone and scarcer accommodation. More information is however needed on the bed and suspended load, on the current velocity fields, on the dispersal patterns with different relative sea level scenarios and on the compaction effects to ascertain if the natural processes are prevailing on the anthropogenic stress and if the Swatch of No Ground canyon has become the main depocentre on the Bengal Shelf.

Acknowledgements

This work was done within the Project "SO-188 - Bengal Sea Level", funded by the German Ministry of Education and Science (BMBF), Grant No. 03G0188A and the DFG project "Bengal Shelf IODP", Grant SP296/31-1. We thank the captain and crew of the R.V. Sonne for excellent support and the scientific board party for their great collaboration. We acknowledge Prof. S. Goodbred and Prof. C. France-Lanord for their guidance and help in developing the concepts and methods. Special thanks go to Dr D. Heslop for the mathematical support in the slope analysis and to Dr V. B. Ernstsen's review that contributed with valuable improvements to the manuscript and figures. The moderation of Dr M. Strasser was very important during discussion of the origin of the transparent units. The quality of this manuscript has been significantly improved by the comments and suggestions of two anonymous reviewers.

~ Chapter 6~

Import, accumulation, and export of sediments into a shelf canyon: Insights from the head of the Swatch of No Ground offshore the Ganges-Brahmaputra Delta, (Bangladesh).

Luisa Palamenghi[1,2,*], Tilmann Schwenk[3], Volkhard Spiess[4], Hermann R. Kudrass[5]

[1-3-4] Department of Geosciences, University of Bremen, Klagenfurter Str. 28359 Bremen, Germany.
[1] lupala@uni-bremen.de, [3] tschwenk@uni-bremen.de, [4] vspiess@uni-bremen.de

[2] GLOMAR — Bremen International Graduate School for Marine Sciences, University of Bremen, Leobener Str., 28359 Bremen, Germany

[5] MARUM — Center for Marine Environmental Sciences, University of Bremen, Leobener Str., 28359 Bremen, Germany
kudrass@gmx.de

* corresponding author

Introduction

6.1. The head of channel-levee complexes

Canyons are very common geomorphologic features on continental margins, but nowadays they are only in a small percentage associated with a canyon head, which is incised into the shelf (Pratson et al., 2007; Harris et al., 2011). An even smaller number occurs pn passive margins, however, in this group some of the biggest conduits channelizing sediments to large deep sea fans are found, such as in front of the Missisippi, Congo, Indus, Ganges (Wynn et al., 2007) and Ayeyarwady.

In their treaty on submarine canyons, Shepard and Dill (1963) distinguished these canyons from others as 'delta-front troughs' where sediments have been building up the shelf and maintaining progradation while concurrently gravity flows were crossing the shelf through the canyons (Shepard and Dill, 1963; Galloway et al., 1991; Gerber et al., 2009).

The canyon's head is addressed as a key determining factor for the architectural style of the deposits generated in deepwater environments (Pirmez et al., 2000). The reconstruction of the depositional history of siliciclastic sequences, going beyond sea level controls, would be of great help in the understanding of the tectonic and climatic forcing inherent to a continental margin and its terrestrial sediment source (Posamentier et al., 1991; Allen and Allen, 2005; Covoult and Graham, 2010).

6.1.1 Architectural style

Time series analysis on the thickness of event beds such as of turbidite deposits that show minimal basal erosion and amalgamation, may obey a power law (Rothman et al., 1994): the larger an event is the rarer it is, while the size of each individual event cannot be predicted. A small disturbance can trigger an event, big or small, and as a result, the system is restored to a marginally stable state (Turcotte, 1997; Weedon, 2003). Successive analyses of the same database revealed instead that the turbidite sequence likely reflects a stochastic thickness distribution in which the magnitude of successive events is uncorrelated (Beattie and Dade, 1996).

Turbidites represent single beds (events) whose vertical structure is associated with the energy of the tubidity current passing over the sampled location and waning with time (Bouma, 1962; Parson et al., 2007). Turbidity currents are a specific type of non-conservative gravity flow capable of deposition on the peripheral flow and erosion in its core. While eroding, the hydrostatic pressure due to the addition of particles increases and drives a horizontal pressure gradient that supports runout distances of hundreds of kilometers (Stow et al., 1989; Parsons et al, 2007). This results in the formation of levees beside a central channel that acts as container (Imran et al., 1998). On longer time scales, the development of many slope channel systems involve the generation of container by large scale initial erosion, or a canyon, that is subsequently infilled, finally leading to a spillover from the erosional container (Kneller et al., 2003). Commonly, the channel container represents a 3rd-order bounding surface (1–2 Ma) and the smaller scale erosional cuts within it to be 4th- and 5th-order surfaces (Mayall et al., 2006). When sediment flows that cut these passages, promote slope failure frequent

enough to induce upslope erosion of the failure headwall along sediment flow passages up to their source, the canyon may indent into the shelf (Pratson and Coakley, 1996). The time scale of this updip erosion are unknown, however, in a slope system where channel activity switches over time, periods of abandonment may result from autocyclic events rather than be directly controlled by high-order eustatic cycles. Hence, if autocyclic processes dominate, the fill of any 3rd-order channel complex may be purely a combination of stacked high-frequency events deposited during periods when the given channel system was acting as an active conduit (Mayall et al., 2006).

The sediment supply to deep water has been linked to dominant types of gravity flows for specific stages of shoreline positions by Posamentier and Kolla (2003). Deep-water basin-floor successions are commonly characterized by mass transport deposits at the base, overlain by turbidite frontal-splay deposits and subsequently by leveed-channel deposits. The cap of this succession is another mass transport unit, ultimately overlain and draped by condensed-section deposits of hemi-pelagic and pelagic origin.

The sedimentology of canyon heads, being incised into the margin or not, is largely unexplored. Canyons could be supplied from the head and the flanks, and the fills are characterized by muddy sediment. Sand, where present, tends to be heavily compartmentalized and aligned with distributary axes that lies updip and extend over the canyon axes onto the shelf (Galloway et al., 1991). Resulting deposits may range from those formed under the influence of a single dominant process to those influenced by an admixture of many processes (Syvitski and Hutton, 2001; Piper and Normack, 1993; Parson et al., 2007). Recent pioneer studies have focused on the generation of gravity flows since the onset of the last interglacial normal regression (Stanley and Warne, 1994) using a wide range of sedimentological and oceanographic observations. Trigger mechanism of gravity flow initiation are addressed to climate and sea level changes (Förster et al., 2009; Heinrich et al., 2010), dense water cascading (Shapiro et al., 2003; Canals et al., 2006), floods (Puig et al., 2003) and storms (Kudrass et al., 1998; Puig et al., 2004). Although often earthquakes are invoked for gravity flow generation, an unequivocal link had been rarely established where a specific event could be associated with a deposit (Goldfinger et al., 2007; Bourget et al., 2009).

6.1.2 Filling Architecture

Due to the repetitive nature of gravity flows, reworking of the same material may occur several times causing a high degree of complexity for seismostratigraphic interpretation (Catuneanu, 2006).

The depositional architecture preserved in slope channel-levee systems is interpreted to be in principle controlled by cyclic changes of accommodation in response to slope equilibrium profile variability (Kneller 2003). Depth profiles tend to adjust to a base level, the deepest point that can be reached by a sediment gravity flow, such that the prevailing sediment discharge is carried with minimum

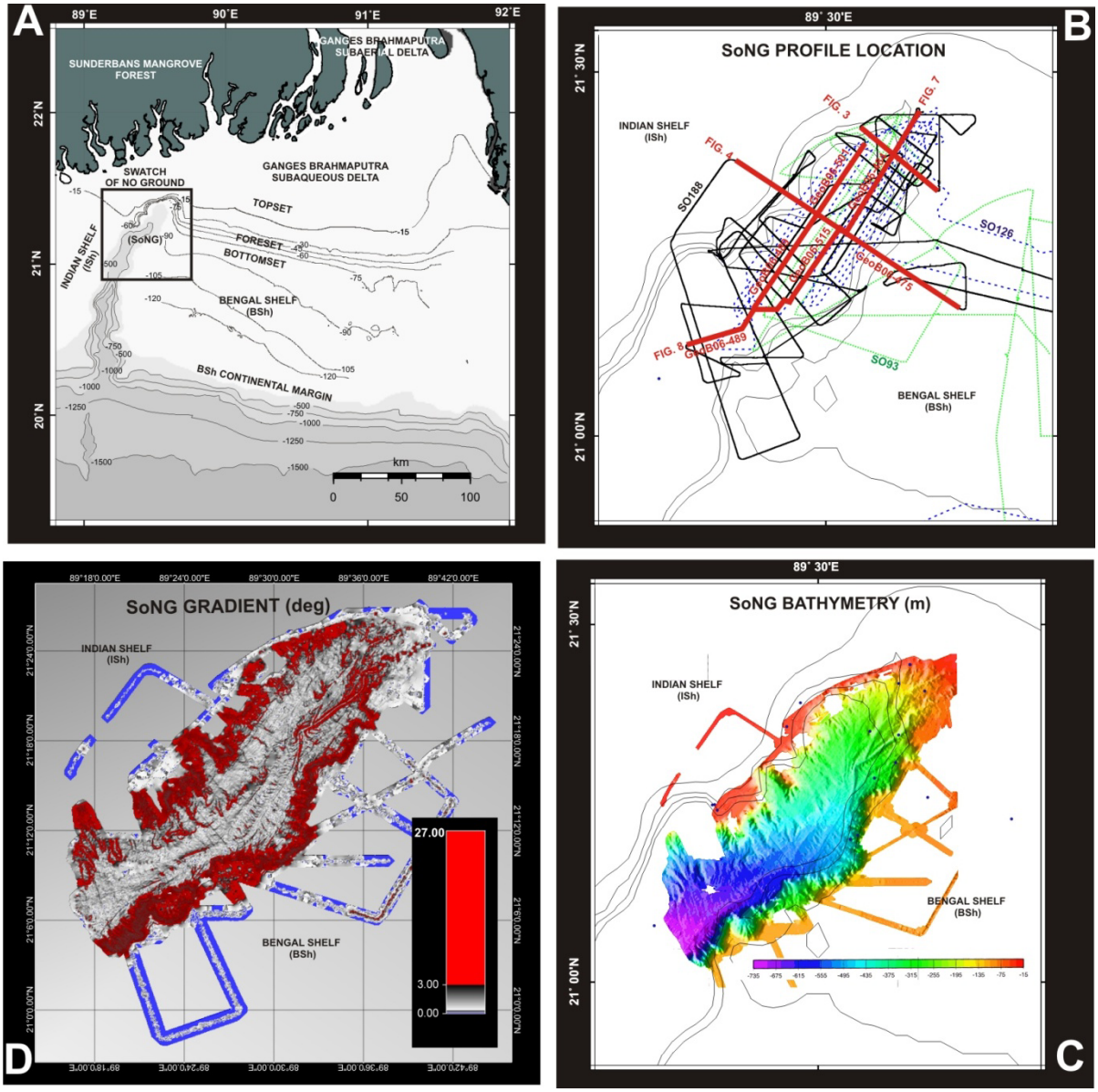

Figure 6.1. General map of the northern Bay of Bengal and location of the mayor depositional elements the the Bengal Shelf (BSh) and Indian Shelf (ISh). The Swatch of No Ground (SoNG) is located in a central position of the bay while the Ganges Brahmaputra Delta (GBD) lies at the northern most edge. Bathymetric lines from -15 m to -130 mbsl are gridded from the SO93, SO126 and SO188 Parasound profiles with five seconds resolution (~150 m); bathymetry from -150 m to -2000 is plotted from the GEBCO-08 One Minute Grid. The study area is indicated in the square and the surface morphology detailed profile location (B), bathimethy (C) and gradient (D) are derived from the integration of the Hydroseep survey (SO93 and SO126) collected in 1993 and 1996 and Simrad EM120 and Multichannel Seismic (SO188) in 2006. The blue color indicates where the shelf gradient is <0.1°but they aren't reliable values as Simrad EM120 is not designed for <100 mbsl.

aggradation or degradation (Carter, 1988; Pirmez et al. 2000). Low accommodation drives initial slope degradation and sediment bypass while increased accommodation leads to slope aggradation with vertical stacking of component channels and internal levee development, and ultimately system abandonment (Hübscher et al., 1997; Hodgson et al., 2011). The thickness of the channel-levee system deposits associated with the base level forced regression is often much greater than the overlying shale-prone sections related to base level transgression and normal regression (Cotuneanu,

2006; Mayall et al., 2006). Basin base level changes have drastically changed amplitude at the transition from greenhouse to icehouse conditions at the Plio-Pleistocene transition (Lisiecki & Raymo 2005; Naish and Wilson, 2009; Sømme et al.,, 2009). Since then significant sediment delivery to the outer shelf, slope, and basin floor might have occurred mostly in periods of falling sea level and lowstands (Vail et al., 1977; Posamentier et al., 1988) and only in minor proportion during highstand (Burgess and Hovius, 1998; Muto and Steel, 2002) and transgression (Weber et al., 1998; Cattaneo and Steel, 2005; Palamenghi et al., in prep).

Canyons are usually recognized as zones of sediment bypassing and little sediment accumulation (Stow et al., 1996; Normack and Carlson, 2003). However, in response to the ongoing depth profile adjustment, available space leads to the formation of internal levees or limited space promotes overspill deposits, which may appear superficially similar to terrace deposits (Hübscher et al., 1997; Deptuck et al., 2003; Hodgson et al., 2011; Kane et al., 2011).

This study is intended to provide a seismostratigraphic framework integrating multi-frequency seismo-acoustic data (30-200 Hz, 100-500 Hz and 4 kHz) for a shelf incised canyon (delta front troughs) filling architecture and to characterize the seismo-acoustic facies of different architectural styles. The case study (Fig. 6.1) will focus on the delta front trough Swatch of No Ground (SoNG) one of the main Quaternary canyon heads of the Bengal Fan channel levee complex. It is fed by the Ganges-Brahmaputra Delta (GBD) and is located on the Bengal Shelf between the Bengladesh Shelf (BSh) and the Indian Shelf (ISh).

The study area is restricted on the SoNG section belonging to the Bangladesh territorial waters.

6.2. Location and settings

The GBD is located in Bangladesh in the northeasternmost edge of the Bay of Bengal and delivers appx. 1 Gt of suspended sediment (Delft Hydraulics, 1996), originating from the Northern and Southern Himalaya flanks (Fig. 6.1). Almost two thirds are expected to be stored in the subaerial and subaqueous delta (Goodbred and Kuehl, 2000). A declining trend toward reduced sediment storage in the subaqueous delta has been, however, recognised in the sigmoidal clinoform shape. On the eastern BhS, the subaqueous delta clinoform is grading toward an overall convex shape, while on the western BhS, in proximity of the SoNG's head, concavity is more pronounced (Palamenghi et al., 2011). The offshore export prevails during SW monsoon rainy peaks (June-september) by tide and ambient waves supported-gravity flows directed south-westward. Storm wave supported-gravity flows characterize the deposits during pre- and post-monsoon times (April-May and October-November) (Barua et al., 1996; Kuehl et al., 1997; Michels et al, 1998).

The Swatch of No Ground (SoNG) is located between 89° and 90° E and from 20° to 22° S. It contains saline water with an oxygen minimum zone with very low oxygen concentration starting at 150 m (Kudarss et al., 2010). In the Quaternary, the Bengal Shelf (BSh) has accumulated several hundred meters (Maurin and Rangin, 2003), while the Bengal Fan has been fed by mostly channelized

turbidity currents (Hübscher et al., 1997; Weber et al., 1998; Curray et al., 2003; Schwenk et al., 2005; Schwenk et al., 2009) building a vertical succession of channel levee systems or channel levee complex (Flood et al., 1991). During the Quaternary, the shelf switched from a multi-source to a single canyon configuration (Alam et al., 2003; Curray et al., 2003).

Sedimentation rate varies significantly along the margin. It peaks at and around the inflection point of the sigmiodal clinoform subaqueous delta which results in a mean accumulation rate of 2 cm/yr (Palamenghi et al., 2011) but ceases on the outer BSh. In the SoNG thalweg sedimentation rates can

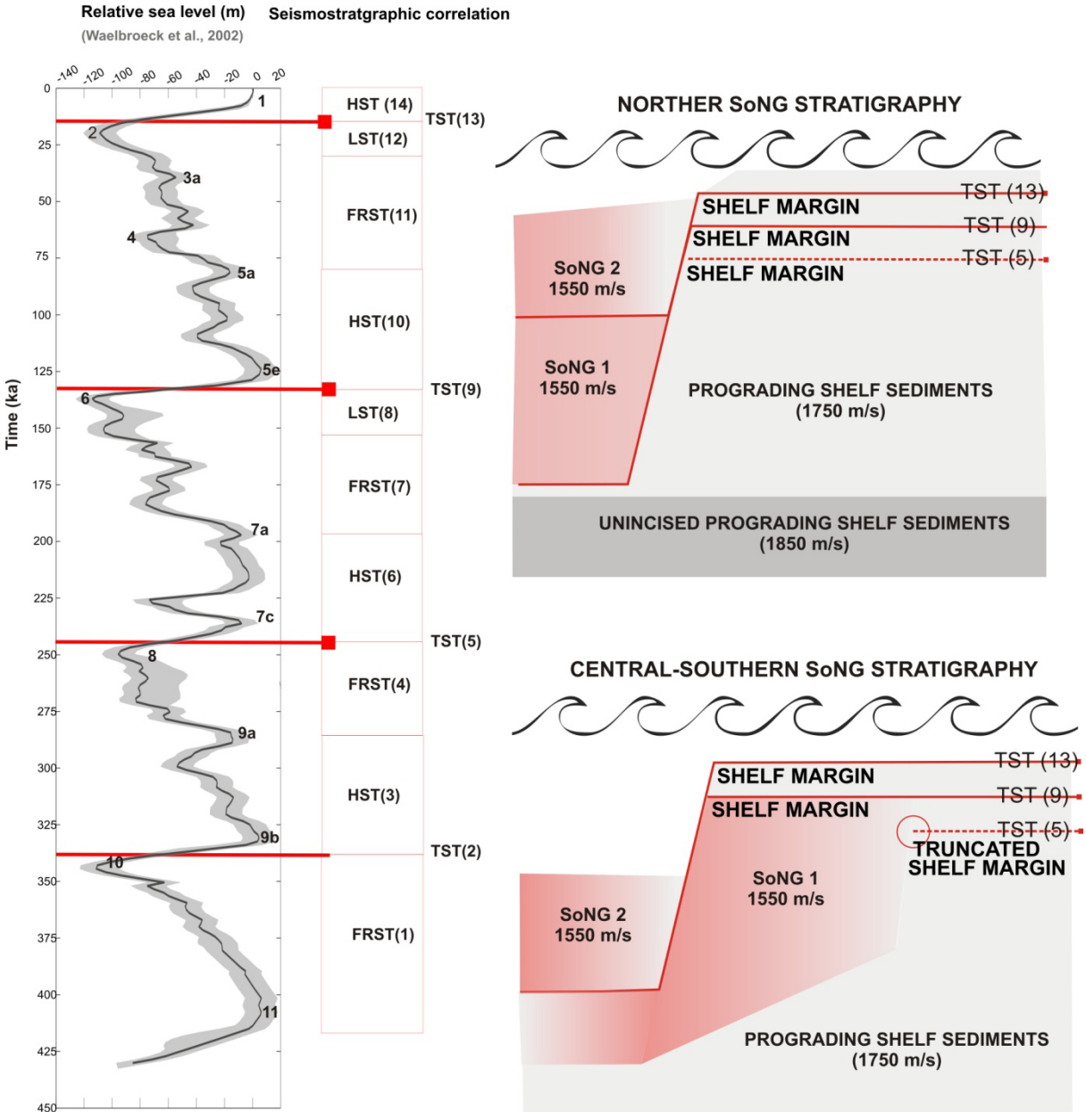

Figure 6.2. Seismostratigraphic correlation with the Relative Sea Level Curve modified from Walbroeck et al., (2002) based on benthic foraminifera isotopic records from North Atlantic, Equatorial Pacific Ocean and Southern Indian Ocean; confidence intervals in gray are derived from the SPECMAP compilation in Martinson et al., (1993). Seismostratigraphic units have been adjusted to the integration of the High Stand System (Palamenghi et al., in prep). The sketches illustrate a simplified vertical succession from the Northern and Central-Southern SoNG and the stratal geometry relationship of the canyon filling with the prograding shelf.

be locally exceptionally high. Cores 96KL and 23KL, collected in 228 m and 564 m water depth in undisturbed and well-stratified sediments (Kottke et al., 2003), have 50 cm/yr and 15 cm/yr accumulation rate respectively (Suckow et al., 2001; Michels et al., 2003). Based on grain size distributions and X-ray photographs, the near surface SoNG thalweg deposits (facies Ia, Kottke et al., 2003) consist of succession of graded sequences of clayey-silty fine sand, mm-thick laminae of clayey silt, and a final layer of silty clay. that closely correlate with the historical record of cyclones (Kudrass et al., 1998; Michels et al., 2003; Mayer et al., 2012). According to the estimates of sedimentation rate, the undisturbed sequence must have been deposited during the last 200 to 300 years with an average sedimentation rate of 20 cm/yr. Such value would be sufficient to fill the canyon within fairly 1000 years (Weber et al., 1997).

While monsoon precipitation is decreasing since the middle Holocene (Breitenbach, 2009), in the North Indian Ocean basins, it was determined from satellite data that the proportion of hurricanes reaching categories 4 and 5 increased, while the total number of cyclones and cyclone days had decreased during the last 35 years (Webster et al., 2005). After the passage of the Sidr cyclone in 2007, category 5 on the Saffir-Simpson Scale, flank failures, deformation, disruptions, faulting and degassing have been reported from the canyon's head (Rogers and Goodbred, 2010).

Some of the plate-boundary earthquakes in the nearby India–Sunda arc are huge (Steckler et al, 2008) and liquefaction flows caused by cyclic loading produced by plate boundary earthquakes have been identified and measured in the foreset beds of the subaqueous delta for the last 300 years (Palamenghi et al., 2011). Besides a large number of acoustically transparent units, TUs, are present especially at the transition from topset to foreset beds, TU1, TU2 and TU4 (Kuehl et al., 2005; Palamenghi et al., 2011) could be associated to the Chittagong Earthquake (1762), the Great India Erathquake (1897) and the Assam Earthquake (1950) based on lateral continuity, number And age estimation from the surface accumulation rate.

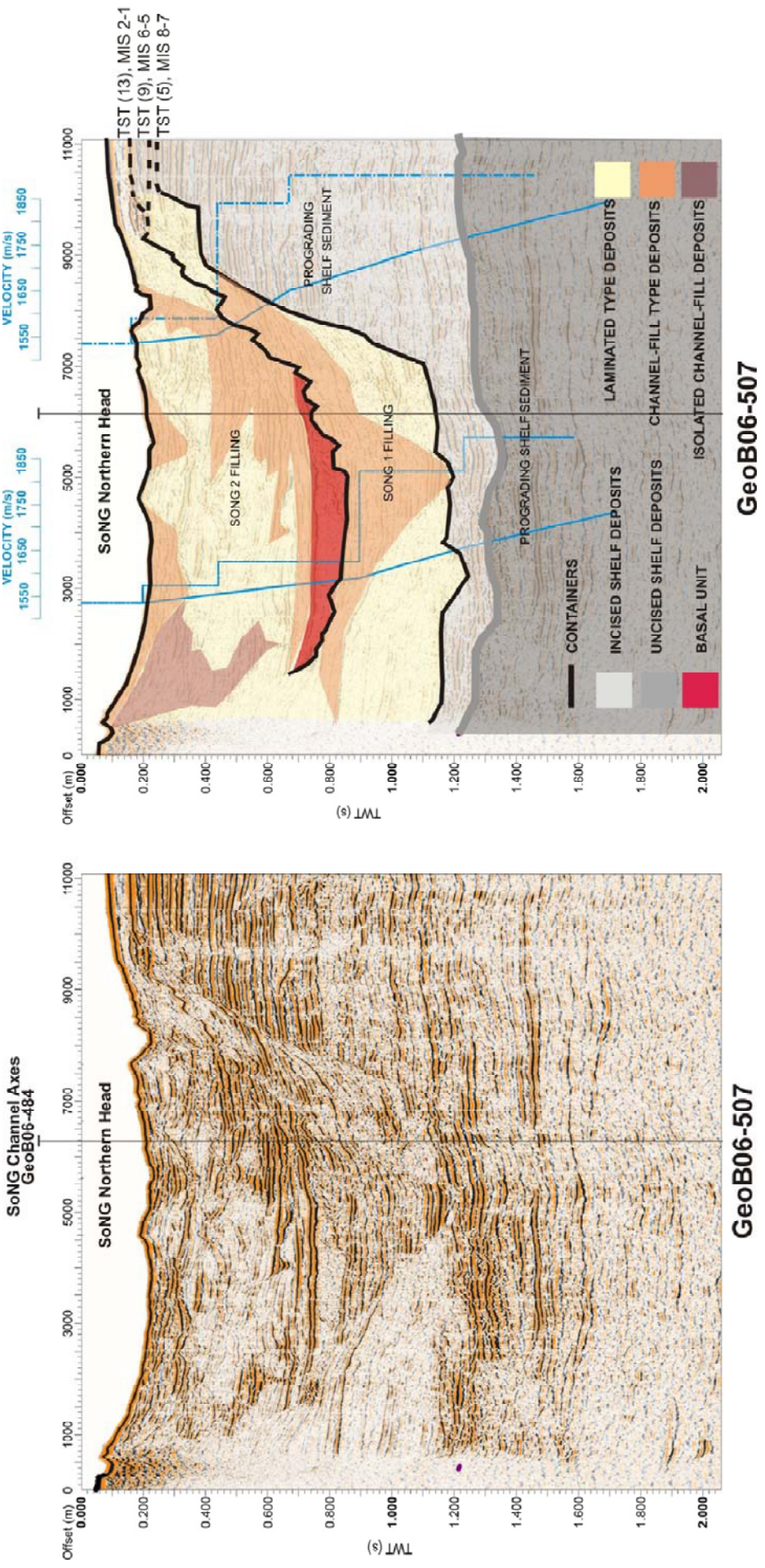

Figure 6.3. Seismic line GeoB06-507 from the Northern SoNG and its seismo-acoustic integrated interpretation. See Fig.6.1. for profile location

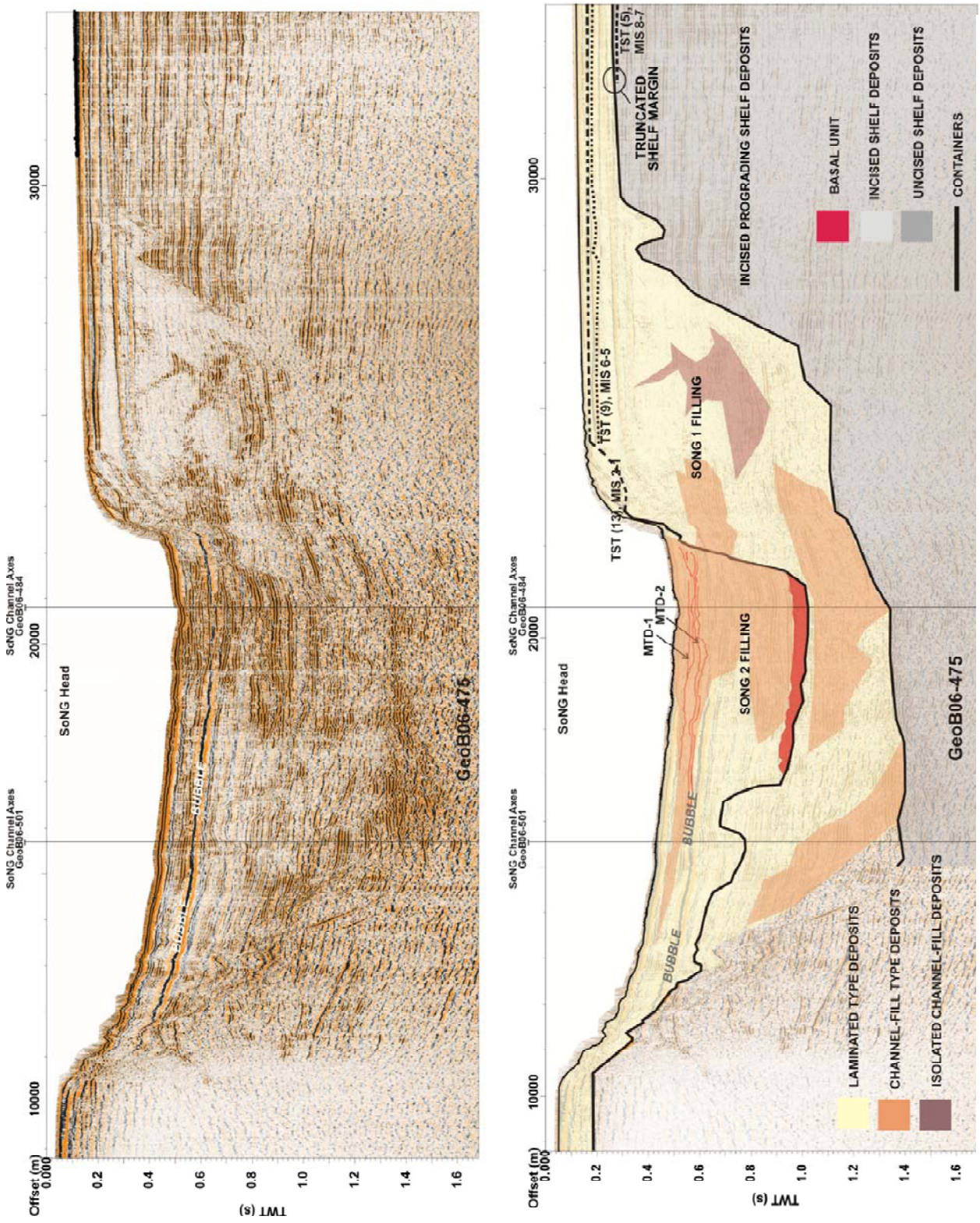

Figure 6.4. Seismic line GeoB06-475 from the Central-Southern SoNG and its seismo-acoustic integrated interpretation. See Fig.6.1 for profile location.

Material and methods

6.3. Seimoacoustic data processing

Bathymetric (Hydroseep and Simrad EM120), sediment echosounder (Parasound) and multichannel seismic data have been collected during SO93 (1993), SO126 (1998) and SO188-2 (2006) expeditions with R/V SONNE (Fig. 6.1). An extensive interpretation description of the surface morphology and a near sur face acoustic facies characterization was presented by Kottke et al. (2003). In this study we will discuss only some of the new features which became evident from higher quality data using an EM120 multibeam system and from the larger survey area in 2006.

As MCS sources a 4.1 L and a 0.4 L GI gun were fired in an alternating mode and recorded by two different receivers sets. The larger offsets were received by 4-section streamer recording equipment, with a total active length of 300 m and the shallow water data were collected with a specially designed 50 m long streamer, with 48 single hydrophones of 1 m spacing. The dominant frequency range of the collected data set is 30–200 Hz and 100-500 Hz, respectively. The data were processed with a multichannel seismic processing method, using the Vista seismic processing software package (Gedco & Co.). The profiles were binned with 2.5 m common midpoint (CMP) spacing to optimize imaging of steeper horizons at the canyon flanks. Data were filtered with broad band-pass filters of 10/20–300/600 Hz and 50/100-500/1000, respectively. The binned data were then normal move out (NMO) corrected and stacked, based on carefully picked velocities. Stacked profiles were time migrated using the finite difference method.

The Parasound sediment echosounder system DS-2, designed by ATLAS Hydrographic, is hull mounted and utilizes the parametric effect, generating a secondary frequency of 4 kHz by the interaction of two simultaneously emitted sound waves of high energy (18 and 22 kHz). The data digitized by the ParaDigMa software (Spiess, 1993), was converted to the SEG-Y standard format to load them into the interpretation software. For display and interpretation of MCS data the commercial software package Kingdom Suite (IMT Co.) was used.

Results

6.4. Canyon morphology

The Swatch of No Ground canyon break is the slope region where the maximum curvature is found with respect to the surrounding BSh and ISh mean slope angle (0.01°). For a large part of the study area, the canyon break coincides with the subaqueous GBD clinoform rollover. The transition from topset to foreset beds increases slope angle from 0.1° to a maximum of 0.3° at the inflection point. A progressive outstripping of the clinoform rollover from the canyon break occurs where the subaqueous delta maximum curvature region bends toward the BSh sigmoidal clinoform. The ISh margin beds are concave clinoforms with a gradient which is too steep to develop bottomset beds in the form of directly connected sheet deposits (Fig. 6.1). Channel formation starts at appx 40 mbsl. Along the Ish concave margin, appx. 20 channels developed on the western flank. Three distinct V-

shaped channels occur on the sigmoidal clinoform on the Northern BSh. The gradients in the channel regions largely exceed that of the maximum curvature of the canyon breaks due the negative relief of the incisions. The maximum channel depth found is appx. 45 m and depth-width ratio ranges from 3.5% to 5% maximum (Fig. 6.1). The slope gradient in the SoNG thalweg is characterized by different amplitude and frequency fluctuations. Sediment waves oriented downward regional dip with an arcuate planform are found in the northern and central canyon axes. On the western side of the central canyon axes, slope gradient experiences a smaller seafloor roughness and terraces elevate above the base level.

The three channels originating from the northern SoNG converge and merge in the central SoNG (Fig 1). The canyon axes decreases in depth and broadens with a depth-width of 1.5%. In the southern most region of the SoNG study area, the mean gradient in the canyon axes is smaller and the depth-width ratio is 0.6%.

6.5. The SoNG containers

The middle Pleistocene to Holocene sedimentary sequence on the Bengal Shelf (Fig. 6.2) is built of rhythmic stacked composite sequences consisting of clinoform beds interrupted by regional transgressive surfaces of clear glacio-eustatic cycle origin (Hübscher et al., 1998; Hübscher and Spiess, 2005; Palamenghi et al., 2011). The early Pleistocene boundary on the shelf margin (1.8 Ma) is 1.4 s TWT deep or ~1400 m for an interval velocity of 1996 m/s (Maurin and Rauger, 2009). Within the vertically aggrading stacking pattern, the transgressive surfaces formed by the wave ravinement are truncated by the SoNG container which has a smooth surface (Fig. 6.3). The continental margin deposits have vertically accreted and prograded into the SoNG, which causes incisions on the flanks, and the fill is demarked by convex upward onlap surfaces. The SoNG container nests two broad U-shaped valleys, the SoNG1 and SoNG2 containers.

6.5.1. SoNG1

The northern SoNG1 container is completely filled at its rim. The deposition of TST (9) marks the conclusion of the filling phase (Fig. 6.3). The transgressive surface of erosion at the base of TST (9) was formed at Termination II (Fig. 6.2) from the glacial MIS 6 to the interglacial MIS 5 (Hübscher and Spiess, 2005). In the central SoNG1, the TST (5) beds deposited one 4^{th}-order transgression prior to TST (9) are heavily incised. The prograding margin has been excavated during falling after MIS 7 and the subsequent maximum regressive phase at MIS 6. In the time lag from TST (5) to TST (9) a full 4^{th}-order cycle has elapsed and possibly deposited in the SoNG1 (Fig. 6.2). Nothing is known so far about the fate of the HST (6) beds corresponding to the MIS 7. Sea level seems to have not risen as much as the successive MIS 5 and MIS 1, however, several highstand peaks succeeded (7a and 7c) within a moderate mean value of appx. -20 m below present day zero (Fig. 6.2). On the BBSh, the

FRST (7) and LST (8) have prograded toward the shelf break region whereas the TST (9) retrograded landward (Hübscher and Spiess, 2005).

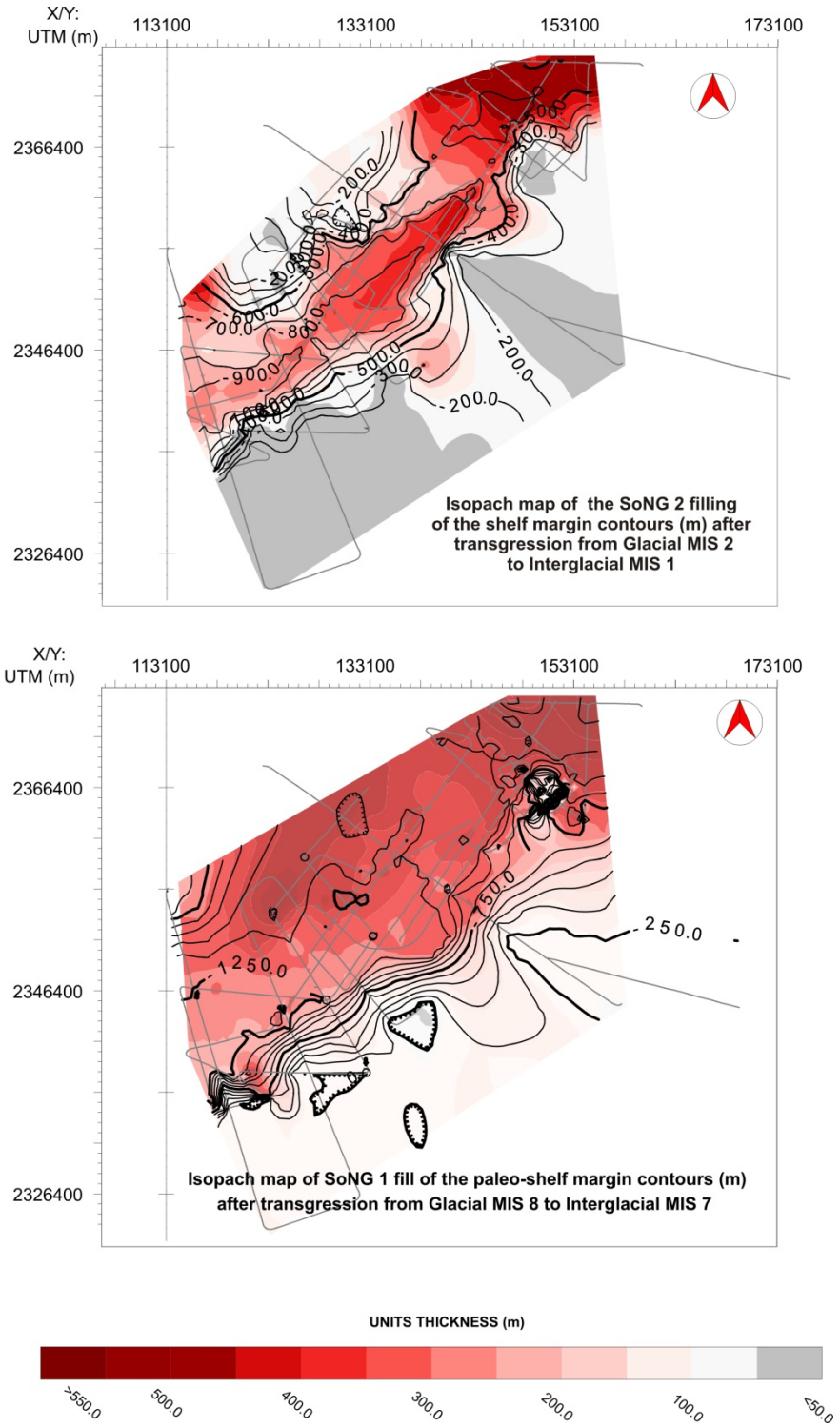

Figure 6.5. Contours (m) of the paleo-geomorphological relief of the SoNG 1 (1.6 m/s) and SoNG (2) and isopach map (m) of the SoNG 1 and SoNG 2 filling for 1.55 m/s velocity for time-depth conversion. Note the dislocation of the SoNG 1 and SoNG 2 main depocentre and the narrowing of the SoNG 2.

6.5.2. SoNG2

After the fill of SoNG1 a new full 4th-order composite sequence (Fig. 6.3) has been deposited: HST (10), FRST (11), LST (12) and TST (13). The distribution and thickness of this composite sequence on the shelf has been treat in detail in Palamenghi et al., (in prep). The lower boundary of the TST (13) may potentially be conformable with the maximum regressive surface in the canyon which would make it the 4th order sequence boundary (Posamentier et al., 1988; Hunt and Tucker, 1992; Catuneanu, 2006). The maximum regression occurred appx. 20 ka ago falling to -120 mbsl, but then the wave action could no longer be a direct source of erosion, as the thalweg is positioned well below the sea level minimum (Fig. 6.5).

Along the northern SoNG2, the MIS 2 sea level minimum would have been sufficient to expose the northern rim SoNG2to the action of the waves and atmospheric erosion (Fig. 6.5). The depth of the SoNG2 incisions, however, largely exceeds the maximum regressive depth. Thus, exceptionally high slope gradients in the northern rim of SoNG2 may have developed in response to base level readjustment in an inner shelf subaqueous environment, attributing their formation to a subaqueous portion of a subaerial low stand delta. To compare this situation with a modern analogue, in the Zaire River estuary, the submarine canyon begins at the estuary head and distinctly increases in depth from appx. 90 m near to the river shore to 450 m at the mouth of the estuary.

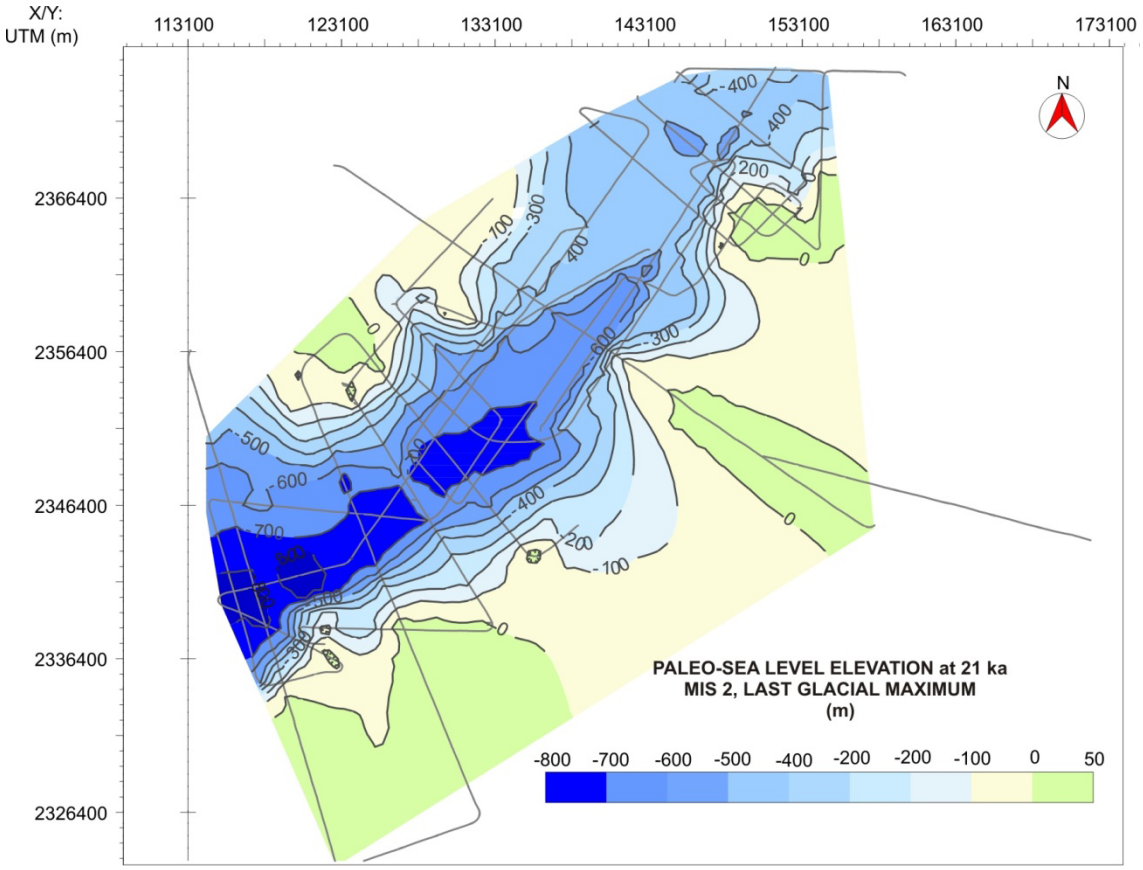

Figure 6.6. Contours (m) of the paleo-geomorphological relief of SoNG (2) at the local Last Glacial Maximim minimum depth of 127.5 mbsl. Paleo-depth is uncorrected for subsidence and compaction.

Such high gradients could also develop in response to large mass wasting events. The SoNG2 container has incised into the SoNG1 main valley juxtaposing it with a swerve more to the west (Fig. 6.4). This might be the reason for the generation of large mass wasting events when the steep flanks of the SoNG1 become locus of fluvial incision, oversteepen and subsequently fail.

During the time of deposition of TST (13), sea level rose very rapidly around 14 ka and large parts of the western BSh were flooded while an eastern delta still delivered sediments on the central shelf, possibly until the Younger Dryas 11 ka (Palamenghi et al., in prep). The HST (14) did not accumulate on the inner BSh shelf before 7 ka ago (Goodbrea and Kuehl, 2000). The sediment above the lower boundary of the TST (13) must have been therefore deposited in the SoNG2 in the interval from 19 ka to recent as a continuous sequence or with some time lag between the upper boundary of TST (13) and the onset of deposition of the HST (14) beds (Fig. 6.2).

6.6. Depositional elements of the canyon fill

Beyond their stratal termination and stacking pattern, the age of the fills determine a different velocity fields (Fig. 6.3). The young fills of SoNG1 and SoNG2 are characterized by low velocities of ~1550 m/s with a sharp transition toward the shelf deposits. Unincised shelf deposits reveal higher interval velocities between 1750 m/s and 1850 m/s (Fig. 6.3).

The SoNG1 fill appears widespread and homogeneous, but the incision of SoNG2 seems to have largely dismantled the western SoNG1 flank (Fig. 6.6). The depocentre of the SoNG1 fill lies on the BSh margin and the fill thickness reaches maximum values of 400 m in the northern section, while thinning toward the south (Fig.s 6, 7 and 8). Lacking stratigraphic constraints, the development of the SoNG1 on the ISh margin has larger uncertainties. It seems, however, that the container of SoNG1 was wider and SoNG2 has developed narrower. The depocentre of the SoNG2 fill is located more toward the ISh canyon margin. The thickness is significantly higher in the northern SoNG2 reaching 500 m, and decreases gradually toward to a minimum of 250 m in the south (Fig.s 6.6, 6.7 and 6.8). A distinct mound appears in the central SoNG2 (6.6), where the three V-shaped incisions, connecting the northern SoNG to the subaqueous delta foreset beds, merge (Fig. 6.1).

The onlap surfaces of the partially concordant vertical fill (Ricci Lucchi, 1980) on the SoNG2 container indicate that the northern part is close to fill up to the rim (Fig. 6.2). Sharp onlap surfaces associated to high amplitude seismic horizons demark the central SoNG2 fill on the BSh margin. The onlap surfaces on the ISh margin have weaker amplitude but is not straightforward that the high amplitude reflection termination on the BSh and ISh can be correlated from one to the opposite side (Fig.s 6.3. and 6.4.).

As a strategy to develop a conceptual model for the filling evolution, the distribution and thickness of major seismo-acoustic bodies have been traced.

6.6.1. Basal unit

In the basal part of the SoNG2 container, the seaward extension of the lower boundary of the TST (13) is conformable to the maximum regressive surface. However, scouring may have occurred due to the change in shoreline at the onset of transgression, when the balance between sediment load and the hydrodynamic energy of the receiving marine environment is changing (Galloway, 1989). Along the flanks of the BSh southern section, the bottom of TST (13) and the top of LST (12) overlap. In the thalweg the onlap trend against the top of LST (12) is interrupted (Fig. 6.3) and the SoNG2 container describes a convex upward surface with smooth topography.

The earliest filling of the SoNG2 consists of a sedimentary body with lenticular shape in cross section. Seismic facies appears chaotic with Grooves at the basal surface in the northern SoNG2 (Fig. 6.3). The mean thickness of this body is appx. 40 m at the base of the mound in the central SoNG2 region (Fig. 6.7) and it is well localized in a trough which resembles the shape of a channel (Fig.s 6.3 and 6.4). The upper boundary is also very flat, but mimics locally the topography of the lower boundary. The upper boundary extends as a high amplitude horizon across the remaining SoNG2 thalweg and marks an erosional surface (Fig. 6.8.).

It is not possible to define the landward most updip section of such basal unit and therefore the sourcing region must be further inland either connected to the base level at the time of the unit formation, or to a large scar on the margin, or the margin itself has become ubiquitously the source region. The latter hypothesis contradicts to the lower boundary of the TST (13) to be correlative with the maximum regressive surface and therefore might not be a good representation of the paleo-seafloor at the end of forced regression because of a drastic alteration of the paleo-morphological relief created during falling and low sea level stands.

6.6.2. Channel-fill type deposits

The basal unit of the SoNG2 is the thickest event bed which appears in the fill sequence of SoNG1 and SoNG2 but it is not the only one. The deposition of the basal unit of SoNG2 has not distinctly changed the seismic facies which reveals a succession of high amplitude sub-horizontal horizons, separated by chaotic to transparent seismic facies (Fig. 6.7). Basal surfaces grooves are not always present but indeed internal sub-horizontal reflections are occasionally visible. The majority of the units have flat basal surfaces and thicknesses up to 15 m. The near-surface stratigraphy of the channel-fill ‘type’ deposits consists of a stacked parallel to subparallel sequence of approximately 10 units (Fig. 6.9). These stacked sequences are bounded by a condensed section and the thickness of each individual unit ranges from 1 to 3 m. Two larger events, MTD-1 and MTD-2, exceed locally a thickness of 25 m. The internal acoustic facies is persistently transparent. By comparing the same type of unit recorded with different frequencies (Fig. 6.9) it becomes evident from deep penetration of the Parasound signal of 80 m that deposits must be basically fine-grained, and higher amplitudes in lower

frequency data may be associated with thin coarser layers. Similar to the basal unit of SoNG2, the upper boundary extends as a high amplitude horizon across the unchannelized beds and marks an erosional surface.

The mapping of the transparent zone of the largest event (MTD-2) using the 4 kHz Parasound data outlines the channel morphology at that time (Fig. 6.10). Its thickest part in the upstream end lies in a strictly confined region but further downstream the thickest deposits distribute over a wider area suggesting a transition from entrenched to less confined flow (Fig. 6.10). This transition occurred just downstream of the confluence zone the three V-shaped incisions (Fig. 6.10).

The same channel-fill type deposits also occur in the channelized regions along the Ish canyon break (Facies III, Kottke et al., 2003) but the number of acoustically transparent units distinctly increases upstream and mapping of the MTD-2 becomes impossible with the available 2D seismic data. Facies III is isolated in depositional niches where it is not possible to follow the acoustic transparent units from one to the other.

6.6.3. Laminated type deposits

Along the rim of the channel-fill type deposits, the near surface unit in SoNG2 consists of densely laminated parallel beds. In the seimic record, the acoustic appearance of lamination depends on the seismic wavelength. If the acoustic impedance of the contrast between laminae is not sufficient to generate a reflection or if it is too thin then such deposits will appear homogeneous and almost transparent in lower frequency data. The higher frequency and resolution are, the larger the number of visible laminae is (Fig. 6.9). In analogy to the near-surface deposits, the wide zones of weaker amplitude and semitransparent seismic facies at the rim of the channel-fill deposits at depth are therefore interpreted as sequences of laminated ‘type’ deposits (Fig.s 6.7 and 6.8).

Some high amplitude reflector segments found within the laminated type deposits are associated with the upper boundaries of the discrete units within the channelized type deposits (Fig.s 6.8 and 6.9).

Other recurrent regions of vertical amplitude anomalies in the laminated type deposits are isolated zone of channelization along the ISh margin (Fig. 6.1). The negative relief in the surface expression of these amplitude anomalies is minor and the seafloor gradient does not change significantly too. However the amplitude anomalies vertical persistence in the sedimentary succession of the SoNG2 indicate a relative stable location of this’ isolated’ channel type deposits from the ISh margin and regularly active at least since the onset of the fill (Fig. 6.8).

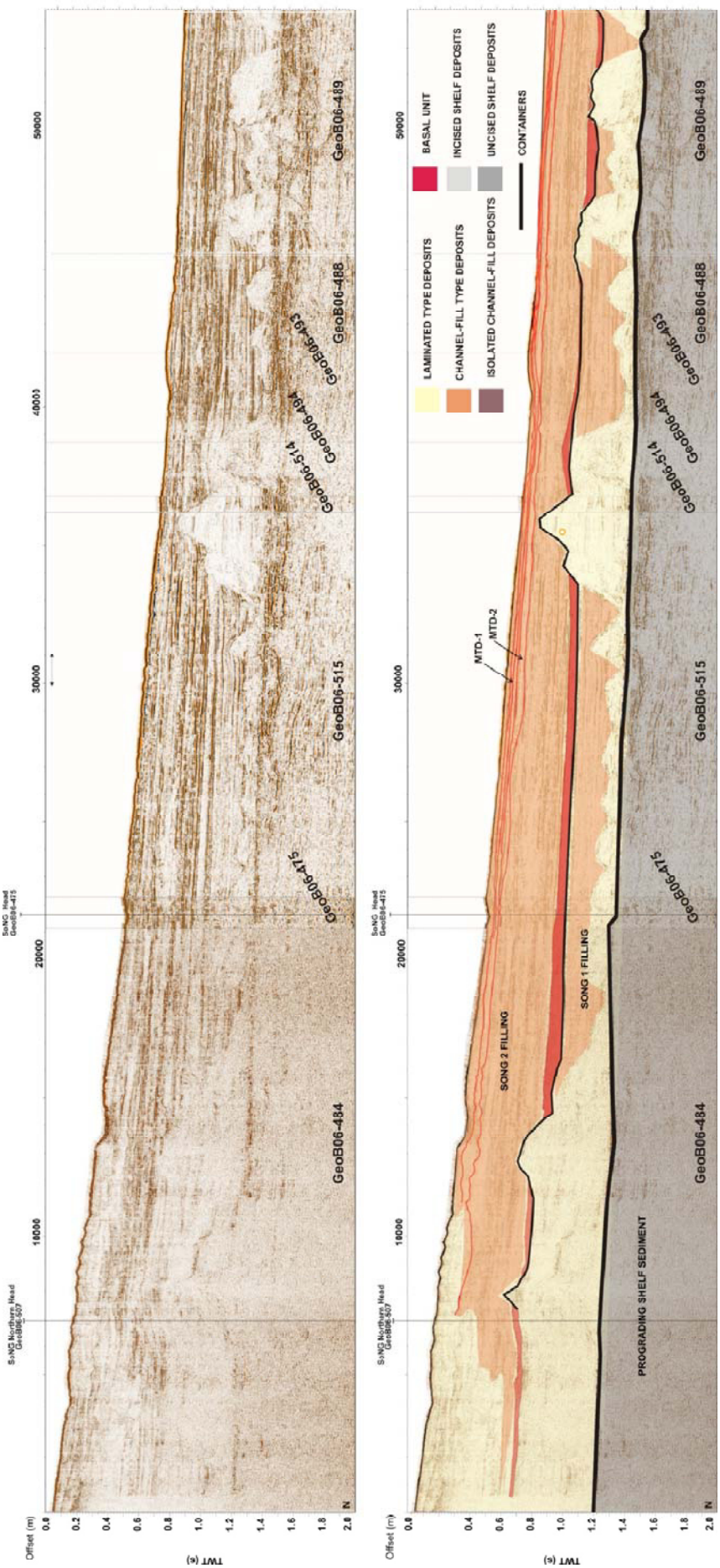

Figure 6.7. Seismic line GeoB06-484,-475,-515,-514,-494,-493,488 and -489 in the channel-fill type deposits in the SoNG. See Fig.6.1. for profiles location.

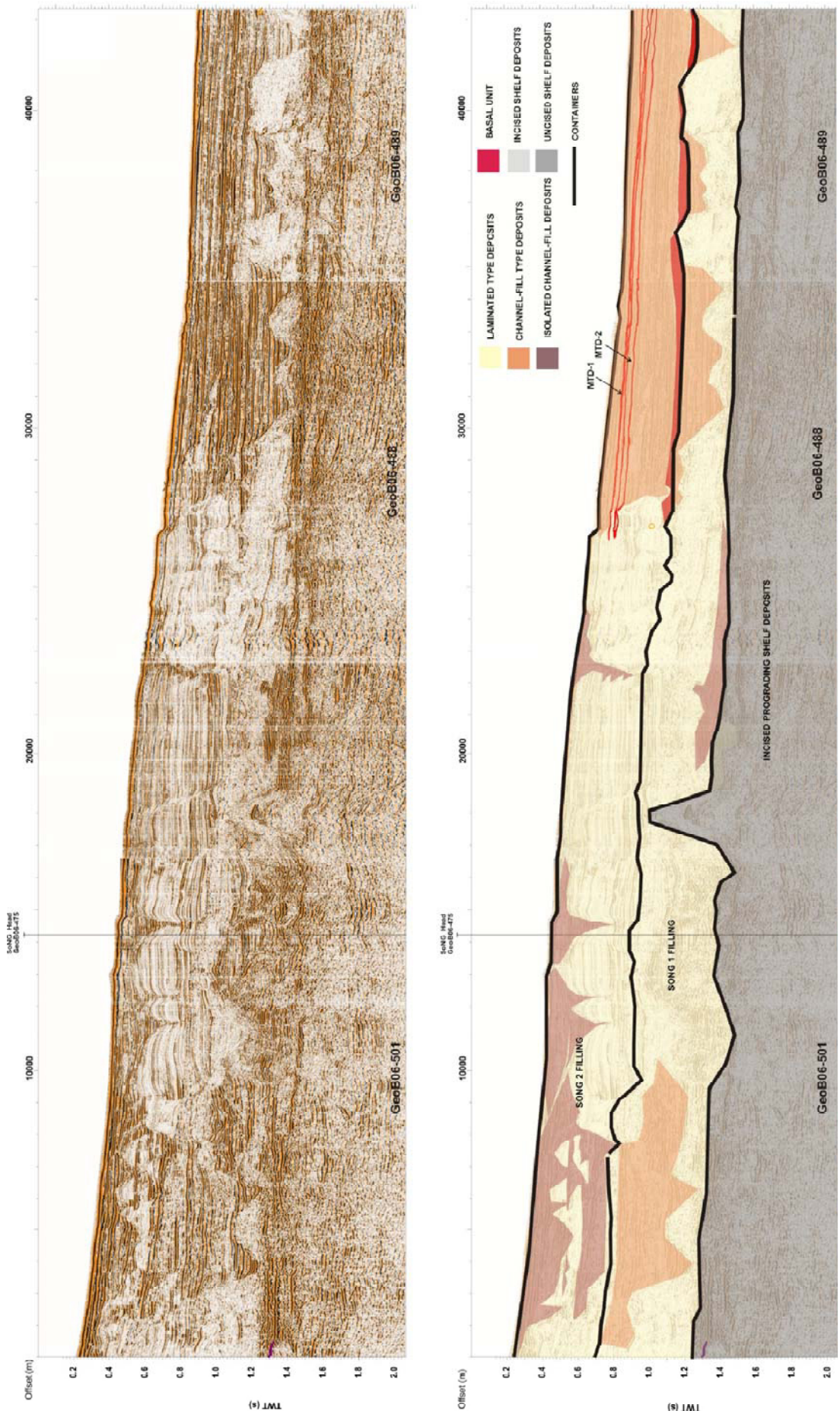

Figure 6.8. Seismic line GeoB06-501,488 and -489 in the depocentre of the laminated type deposits in the SoNG. See Fig.6.1. for profiles location.

Discussion

6.7. SoNG excavation processes

The westward shift of the main depocentre of SoNG2 has left part of the central-eastern beds of SoNG1 unaltered. Whether such shift occurred by updip erosion from the shelf margin or by downdip fluvial erosion is unclear. The amount of material remobilized is unknown however the accommodation created by the SoNG2 incision is very rapidly replaced by new sediment. The SoNG2 container reveals 4th-order cyclicity and contains at least two 5th-order cycles: TST (13) and HST (14). If the sedimentary system did not change, the SoNG2 may gradually infill from the head toward the margin.

The filling time of SoNG1 in the study area ranged from the lower boundary of TST (5) to the lower boundary of TST (9) which covers four system tracts of the second-last 4th-order cycle. However it is hard to establish whether the second-last 4th-order cycle was sufficient to completely fill SoNG1 incision from the head to the shelf break as it not in our survey.

If SoNG1 filling was completed within the cycle, the plug of the SoNG2 could have occurred at the shelf margin and migrated updip by fluvial incision and consequent retrogressive failures along the main axis. If the second-last 4th-order cycle has indeed terminated by leaving any kind of depression or re-entrant, this would be the most favourable region where subaqueous delta progradation of the HST (10) would have taken place, and, if not still full, where the fluvial incision of FRST (11) would have occurred first. During the regional transgressive flooding accompanying TST (13), the submerged shelf space is made available by growth toward the canyon head. The hydrodynamic regime had appx. 10’000 years time to erosionally enlarge the SoNG2 container and to trap shelf currents, internal waves and turbidity flows along the canyon (Farre et al., 1983). Once formed, re-entrants in the shelf margin focus internal waves, storm driven currents and low density gravity driven flows enlarging the head by headward erosion and thalweg incision (Galloway, 1991). The frequency and magnitude of these processes determines ultimately the thickness and spatial distribution of the depositional types.

6.8. Architectural variability of the filling

In channel-levee systems, a canyon develops when the erosional fairway is too deeply incised to allow overbank flow. In turn, the basal incision rate will be significant for its architecture (Deptuck et al., 2003). The deeper the incision is, the more confined the flow will be, promoting the formation of internal rather than external levees. The SoNG2 channel-fill type and the laminated type with isolated channel type deposits do not spill over the banks. Instead, both types of deposits are related to the prograding subaqueous delta through deposition of finely laminated beds or discrete bodies of variable thickness. Only with the complete fill of the incision, sediment would deposit on the canyon ‘bank’ in a form of a subaqueous prodelta. The incision down to the lower boundary of TST (13) marks the onset of the filling of SoNG2 with TST (13) and HST (14) beds. The deposits within

SoNG1 reveal similar seismic facies types as SoNG2 suggesting a comparable sediment flux and filling during both phases. Although the excavation processes have not yet been clarified, facies analysis may indicate the SoNG1 fill to be deposited during the last interglacial MIS 5 associated to HST (10) or during the second-last interglacial MIS 7-HST (6). If the latter is the case, the SoNG 1 was filled during two 4th-order cycles.

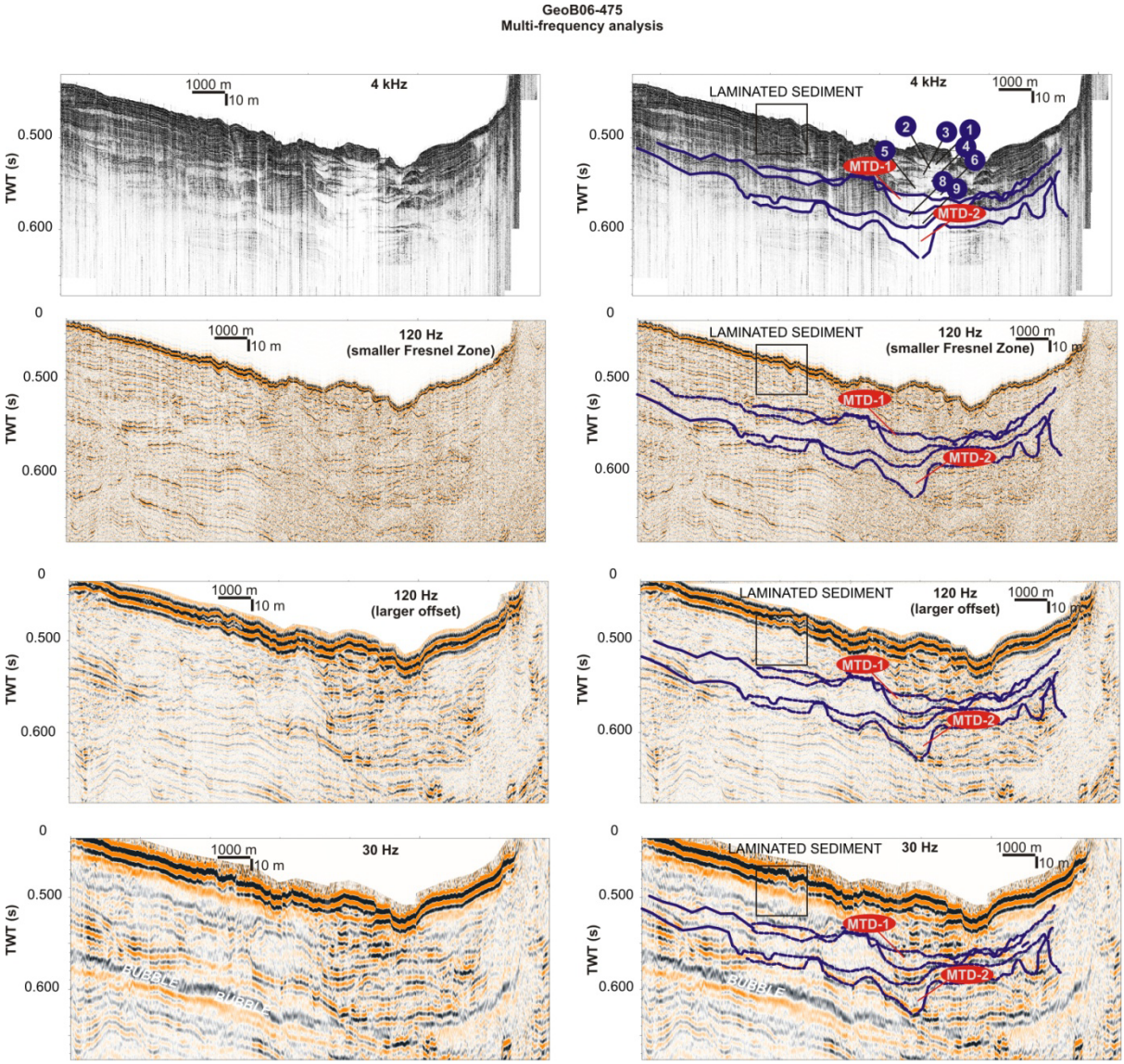

Figure 6.9. Example of multifrequency analisys of the seismic line GeoB06-475 where the amplitude responses of the 30 Hz, the 120 Hz and 9 kHz signals are compared and integrated. See Fig. 6.1. for profile location.

If seismic facies is not directly dependent on relative sea level but rather on the depth of the wave boundary layer, the canyon might then also contain a large portion of the late FRST (11) and LST (12). Once the bathymetric connection of the littoral cell to the canyon break is established, a drainage system will develop and filling will start. The SoNG1 filling would contain three 4th-order cycles with a minimum of erosion. When not much erosion took place the lower boundary of the TST (13)

and the upper boundary of the LST (12) might be conformable and consequently the SoNG2 be the paleo-geomorphological reflief at the onset of transgression.

However, it must be always kept in mind that cooling stages are usually associated with a change in fluvial discharge with respect to provenance, composition (Pierson and Wieckman, 2001; Stoll et al., 2006) and drainage pattern (Palamenghi et al., in prep), possibly causing large deviations from the standard stratigraphic model (Blum and Price, 1998).

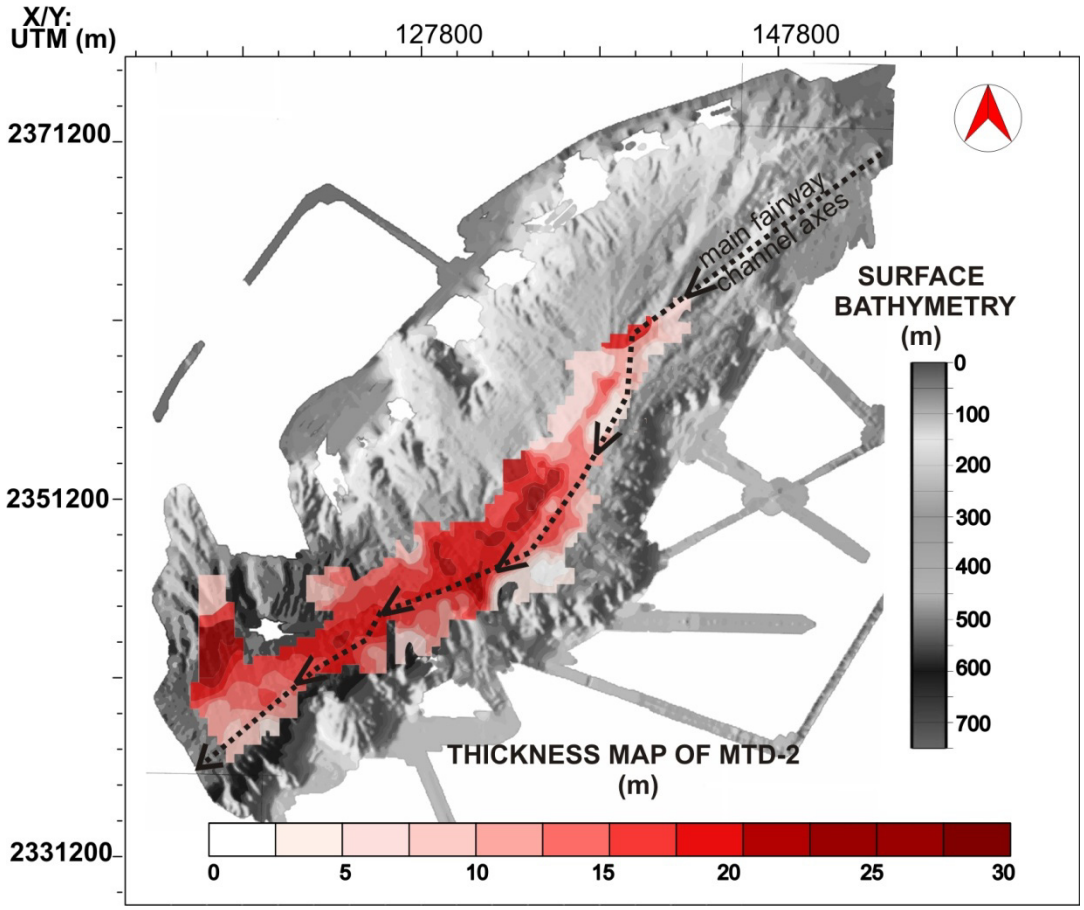

Figure 6.10. Surface bathimetry (m) compared to the buried MTD-2 thickness (m) distribution. The main erosional fairway is indicated by the arrows. Note the diversion of the main erosional fairway from a straight channel where the MTD-2 extrudes from a confined flow to unconfined.

6.9. Facies association and events duration

The restriction of the main canyon axes in the vertical stacking pattern from SoNG1 to SoNG2 (Fig. 6.6) may also indicate a meandering pattern due to the continuous entrenchment. As much as the base level aggrades, it first adjusts to shelf margin gradient changes, which generates a straight channel, subsequently deviating from the original course in response to obstacles along his path or upstream channel piracy. This could mean that the duration of such changes determines the magnitude of the incision independently of regressive or transgressive phases. The longer a change is, the more it will cause a landward penetration of the base line to reconcile with the moving shoreline position. If the

sediment supply is variable, the landward incision of the base line will be rapidly filled and a new incision will be eroded elsewhere initiating there a new landward regression and/or altering the main fairway direction. This is what happened indeed on event scale after the deposition of MTD-2, when the transition from entrenched to unchannelized flow provoked the formation of a small mound (knick-point) which hindered the fairway and needed to be overtaken (Fig. 6.10). It therefore generated a distinct deviation from the straight channel and the flow is now captured in a bend close to the BSh margin (Fig.s 1 and 10). The successive discrete units in the channelized type deposits follow this trend of extrusion from the channelized section and enlargement but it causes the majority of the units to decelerate enough to deposit. MTD-1 instead reaches down to the southern section like the laminated type deposits do with yearly frequency (7^{th} order) in association to the passage of tropical and severe cyclones.

According to the average sedimentation rate of 20 cm/yr, derived from the upper 10 meters, MTD-1 could have formed 170 years ago, MTD-2 320 years ago and the basal unit could have deposited 1.5 ka ago. This may indicate a decadal periodicity of the event beds in the channel-fill type deposits (6th-order) where outsized ones may have a centennial periodicity (5th-order). The singularity of the size of the basal unit in the SoNG2 fill, based on the maximum estimated time of initial formation of the excavation processes 19 ka ago, might indicate 4th-order cyclicity. However, based on the surface sedimentation rate, it could have been deposited also within 2 ka which would indicate 5th-order cyclicity. The SoNG1 container could be a segmented surface comprehending at least two but maximum three 4th-order cycles which are sufficient to elevate it just to a 4^{th} of a 3rd-order cycle.

6.10. Flow regime characterization

The variety and distribution of the amplitude anomalies in the seismo-acoustsic facies associations of the deposit types largely reflects the local characteristics of the flow which generated them but some insights on their lithology may be derived, too.

6.10.1. Channelized debris flow

The homogeneity in the event beds in the channel type deposits indicate a mixing where any original bedding has been destroyed. Insights on the rheology of these beds could be derived from the thinning of the majority of the near surface events in response to the deceleration provoked by the creation of a bend after the deposition of the MTD-2 (Fig. 6.10). When they exceeded their critical shear threshold, they seem to have stopped, which is a typical property of pseudo-plastic flow: when they overcome discrete shear strength they are able to move and, when available transport energy drops, they ‘freeze’ (Lowe, 1979). In the absence of cohesion, the critical shear stresses of pseudo-plastic flows decrease with grain diameter, however, the range of critical shear stress values necessary to initiate the transport of mixed grain size beds can be smaller than the one for well sorted beds (Miller et al., 1977; Wheatcroft et al., 2007). Deceleration and termination of transport depend on the initial coherence of

SEISMO-ACOUSTIC PROPERTIES			SEISMO-ACOUSTIC SIGNAL FREQUENCY				TRANSPORT PROCESSES		
TYPE DEPOSITS	DESCRIPTION	LITHOLOGAL INSIGHT	4 kHz	120 Hz	120 Hz	30 Hz	EVENT	FREQUENCY(a^{-1})	ORDER
LAMINATED	mm-cm scale events laminations	intecalted fine (silty clay) and coarser grain (silty sand)	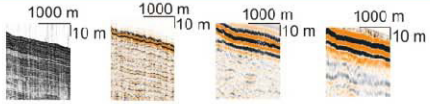				TURBIDITY FLOW	1	VII tropical and severe cyclone varibility
CHANNEL-FILL	1-5 m scale event succession (no or rare basal grooves)	fine grained (or mixed)	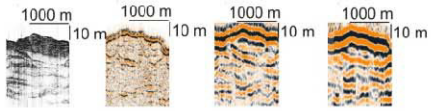				DEBRIS FLOW degenerated from turbidity flow (slurry flow)	0.1	VI severe cyclone
ISOLATED CHANNEL-FILL IN LAMINATED	mm-cm scale events laminations with scattered 1-5 m scale events (no basal grooves)	fine grained potentially sandier (or mixed)	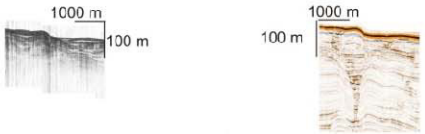				DEBRIS FLOW degenerated from turbidity flow (slurry flow)	0.1	VI severe cyclone
OUTSIZED EVENT BEDS IN CHANNEL-FILL	5-20 m scale event no or rare basal grooves	fine grained (or mixed)	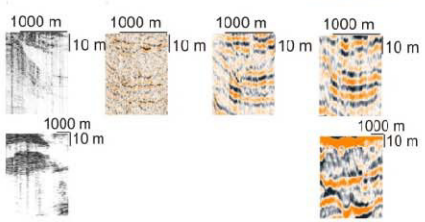				DEBRIS FLOW	0.01	V severe cyclone or earthquake
OVERSIZED EVENT BEDS IN CHANNEL-FILL	>40 m scale event vistous basal grooves	coaeser or mixed			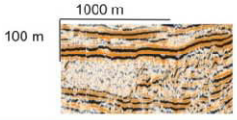		DEBRIS AVALANCHE	0.2-19x10^{-4}	V-IV collapse or eustasy

Figure 6.11. Summary of the main type-deposits.

the failed material which determines to what extent the frontal part of the flow will be subjected to ambient fluid entrainment (dilution) or grain-to-grain erosion (Mohring et al., 1998). Based on their short runout distance, where the gravity forces exerted its influence, it does not seem that buoyancy played a significant role, which would apply for more fine-grained material.

Moderate to strong coherent pseudo-plastic flows of mixed grain size are largely known as debris flow, depositing as debrite. Channel-axis restricted debrites have been recognized in the Mississippi Fan (Kastens and Shor, 1985) and the Niger Fan (Deptuck et al., 2007). Channelized debris flows tend to be associated with lower sinuosity than most leveed turbidity-flow channels. In few instances channelized flows are associated with levees, whereas in other instances levees are absent (Posamentier and Kolla, 2003), but it is an apparent form of channelization which is not representative for the style of transport (Catuneanu, 2006). The shape of the body resembles that of the confining channel at the base of SoNG2 while on an open slope the vertical succession of debris flows would not necessarily be that close.

6.10.2. Turbidity flow

Surface samples within the laminated type deposits indicate a close correlation between the beds and the frequency of cyclone events which affiliated them to the genetic term of tempestite (Seilacher and Aigner, 1991; Kudrass et al., 1998; Michels et al., 2003). Tempestites are beds formed as a result of the passage of a turbulent flow generated by storms (Seilacher and Aigner, 1991).This implies that the main flow is controlled by the wave base boundary layer, and by the deepest region that this layer could reach. Beneath this depth, the advective processes characteristic for the foreset region (Pirmez et al., 1998) are replaced by the convective processes which cause deposition in the bottomset. During a storm, falling particles in the turbulent medium tend to migrate toward areas of diminished vorticity where they concentrate (Maxey, 1987). If the concentrated sediment in these regions becomes unstable, it might start moving initially solely due to gravity. Again depending on the internal coherence, flows might accelerate or decelerate due to the seafloor topography. It is not unlikely that the turbulent water entraining into the initial flow, may initiate erosion of a channel in the region of maximum clinoform slope between 30 and 60 mbsl, as observed on the ISh and BSh margin.

The sediment waves in the seascape of the central SoNG thalweg surface (Fig. 6.1) indeed glimpse the presence of forms of spillover and flowstripping from the channel region of the predominantly dilute fine-grained upper part of turbidity flows.

6.10.3. Transitional flow

Horizon geometry and concurrent deposition seems to indicate a close relationship between channel-fill and laminated type deposits. When turbidity flows undergo significant transformations during its depositional stage, short lived debris flows may form as a degenerate flow or slurry flow (Lowe and Guy, 2000; Sylvester et al., 2002). The velocity of the turbidity current varies locally with the

topographic relief. Erosional potential depends on velocity and, in turn, on lateral or vertical confinement. In the presence of unconsolidated unstable layers, these may become incorporated into the flow as an isolated dense and viscous unit dragged at the base of the turbidity flow without disperse into it. The turbidity flow peel off while the slurry flow would rapidly deposit within a relatively short runout distance (Ricci Lucchi, 1980).

The concurrent development of channel-fill and laminated type deposits moderated by a transitional flow may indicate that cyclone activity provides a trigger mechanism. The slurry flows may potentially be formed during the most severe storms when the wave boundary layer deepens enough to mobilize sediment from the concave portion of the sigmoidal clinoforms of the subaquous delta prograding into the SoNG. When the main axes of the isolated channel fill type deposits in the laminated facies on the ISh margin, aggrades due to the sediment flux from the north-eastern head, a similar process to aggradational gullies on open slope margin (Pratson et al., 2009) occurs. This process restricted in the canyon thalweg may significantly contribute to the canyon filling. The sandy topset beds on the ISh extend much further south compared to the BSh topset and the thickness of sand layers on the ISh decreases towards the south suggesting a southerly net sand transport((Malik et al., 1976). The isolated channel-fill type deposits intercalated into laminated beds may be connoted as fine grained units with a higher potentiality for larger percentage of sand recovery.

.

6.10.4. Mass transport deposits

The two outsized events MTD-1 and MTD-2 and the oversize basal unit largely fall into the category of debris flows, but the acoustic appearance distinctly differs from other event beds in the succession. Grooves and a chaotic texture are accentuated in the basal unit. The degree of erosion associated with MTD-1 and MTD-2 is comparitively small with respect to the basal unit.

An age of 19 ka may be assigned to the basal unit, if the TST (13) basal surface is correlative with the upper boundary of the LST (12). On the other hand, extrapolating surface sedimentation rates would provide an approximate age of only 2-1.5 ka. In that case, the SoNG2 container cannot represent a sequence boundary, but rather a sub-stage within HST (14). Seismically transparent deposits of 5-7 m thickness, associated to regional liquefaction flow (in situ shock deformation) have profoundly destabilized the subaqueous delta foreset region on the BSh during the last 300 years (Palamenghi et al., 2011). Two very large subduction earthquakes occurred in 1892, Great India Earthquake (Magnitude 8.7), and in 1762, Chittagong Earthquake (Magnitude 8.8), which have been recognized as possible origin of such a liquefaction flow, leading to deposits called seismite according to Seilacher (1991). As to the much steeper slopes of a shelf canyon as well as the much larger reservoir of material, which could be potentially mobilized, it can be hypothesized, that the large earthquakes could also have caused the deposition of large scale mass transport deposits within the SoNG, as MTD-1 and MTD-2. The steeper slope of the SoNG would have favoured longer runout distances

whereas in the subaqueous delta the liquefaction flow initiated at the clinoform roll over and reach maximum the bottomset beds.

Thickness, amalgamation, erosive and deformation characteristics of the basal unit seem to indicate that a major remobilization of material occurred. Thickening may result from a combination of failed material and subsequent deposition of reworked sediment. Deposits of this type have been termed debris avalanches (Moore, 1989). Although the formation of debris avalanches had been mostly recognized in response of the process of flank collapse in the growth and evolution of volcanic islands (Deplus, 2001), the process may also occur in other environments. Debris avalanches run very fast and they do not require the pre-existence of a channel. However, being caught in a depression, their erosion potential would likely be sufficient to alter the seafloor morphology and to lead to a major modification of the drainage pattern.

6.11. The Swatch of No Ground and the Bengal Sedimentary Fan

Within the Swatch of No Ground, sediments are temporarily stored but subsequent remobilization may deliver a major proportion to the deep-water sedimentary fan system. On the other hand, the significant fill of the SoNG also reveals that sediment accumulation occurs on relatively short time scales documenting ongoing and past sediment dynamics of delta and shelf environments. The dating of the basal unit is a crucial point in this discussion to be able to relate the active transport through the SoNG, if stratigraphically assigned to the LST (12) top, to the deposits in the younger channel-levee systems on the Bengal fan as their deep-sea counterpart.

Since the onset of the current interglacial when the shoreline has initiated to move seaward, the delta has first aggraded while subaqueous delta formation onshore started ca. 7 ka ago and is now overlaid by deltaic deposits (Goodbred and Kuhel, 2000). The precise location of the landward most position reached by the shoreline (maximum flooding surface) it is still under debate as well as the river course variability exhibited during Termination I is not fully understood (Coleman, 1969; Allison et al., 2003; Heroy et al., 2003; Youngs, 2011). However the sedimentation rate on the Bengal Shelf and consequently also in the canyon must have increased through the Holocene and especially variable in response to river course switching, making the extrapolation of the age of the basal unit from the modern surface sedimentation rate doubtful.

The staging (Posamentier and Kolla, 2003) of sediments in the SoNG's head is nowadays sequestering large part of the sediment flux, but to which extent a gravity flow, initiated in the head's canyon break is not oltrepassing the shelf margin, it cannot be ascertained. In a slope channel-levee systems, high stand periods are associated with hemi-pelagic and pelagic drapes, but, on the Bengal Fan, seen the dimension and the flux to the system, channel-levee sedimentation might well be already again active if it ever really interrupted.

6.12. Delta front trough evolution

The SoNG excavation and fill processes differ from the evolution of slope channel-levee complexes not only by mechanism of sediment mobilisation but also in the stratigraphic hierarchical rank. Large containers in slope channel-levee complexes are 3rd-order bounding surface (Mayall et al., 2006) and the SoNG in the study area contains nearly two and half 4th-order cycles: the present one, the last glacial-interglacial and the second-last. This is nearly sufficient to cover one quarter of a 3rd-order cycle. Within the Quaternary, the first long glaciation in the Pleistocene in coincidence with a global temperature minimum in SST records occured 920 ka ago (Clark et al., 2006) at the intervening interglacial MIS 23, being markedly colder than previous odd numbered stages. During the late Pleistocene, eleven glaciations succeeded but the SoNG excavation processes in the study area only accounts for the last two. Between 960 to 465 ka, the Upper Bengal fan had as many as four canyons supplying the fan according to Curray et al. (2003), but it is not known if they were simultaneously or sequentially active. When mud-rich submarine fan systems have multiple sources in the upslope region, the broad constructional area of the slope and base-of-slope is termed ‘ramp’ (Reading and Richard, 1994; Stow et al., 1996). During the last glacial-interglacial cycle the BSh has proven to develop a ‘ramp’ with a shelf margin delta on the eastern BSh coexisting with a canyon margin delta in the central region (Fig. 6.5). When a ‘ramp’ environment influenced the excavation and fill processes, the birth of the SoNG might belong to a more regional shelf geo-morphological evolution. It becomes then more plausible that the accommodation available in a pre-existing fluvial incision or simply an embayment or a re-entrant in the coastal zone after a phase of transgression has become the depocentre of the subaqueous delta deposition. The establishment of a drainage system in the head is very rapid and extremely dynamic and in absence of an allocyclic force that unplug drastically the drainage from the head, it will tend to cut-and-fill until it is full. The SoNG excavation processes might be therefore the result of a downdip incision prevented by complete fill by the vertical aggradation of the BSh and ISh which causes the base level to be always in adjustment. Tectonic might be responsible also of the initial location of the incision as long as the ratio of the time scales describing lateral channel mobility to tectonic deformation is sufficiently large (Kim et al., 2010).

6.14. Summary and concluding remarks

The delta front trough Swatch of No Ground, which connects the Ganges-Brahmaputra Delta to the Bengal Fan, is a major depositional element on the Bengal and Indian Shelves and it includes channel-fill type deposits, laminated type deposits and isolated channel-fill within laminated type deposits.

Each type deposit might be up to 800 meter thick and contains discrete event beds of different frequency and size. The near surface mm-to-cm scale laminated type deposits are genetically associated to graded sequences, closely correlated to the frequency and magnitude of tropical and severe cyclones in the northern Bay of Bengal passing during pre- and post-monsoon seasons. The interface of the wave boundary layer with the canyon break is therefore addressed as a key location in

the generation of turbidity flows and as a fundamental geo-morphologic threshold. The event beds in the channel-fill type deposits, based on their seismo-acoustic properties, are fine grained or mixed debrites with potentially higher proportions of sand in the isolated channel-fill type deposits. The vertical distribution of the debrites resembles that of a channel but the upper boundary of outsized and oversized event beds truncate the laminated type deposits.

The waning and waxing processes occuring between the type deposits may indicate significant transformations of gravity flows during their depositional stages transient over a large spectrum of turbulent states from their degenerate products (e.g. slurry slows) toward more massive events which may apex into collapses (e.g. debris avalanche). The frequency of events decreases with their size, being the laminated type deposits the most frequent (7th-order) and debris avalanches the rarer.

The discrepancy of the age derived from extrapolation of near surface sedimentation rates with the age attributed to this unit based on seismo-stratigraphic correlation with the Bengal Shelf deposits cannot be resolved here and leaves an age uncertainty between 2-19 ka.

The strata relationship of the SoNG depositional element with the rhythmic stacked composite sequences of the Bengal Shelf consisting of clinoform beds interrupted by regional transgressive surfaces of clear glacio-eustatic cycles origin, determines the excavation processes of the thalweg initiated ~245 ka ago at the onset of TST (5). The large container of the SoNG could be therefore be a composite segmented sequence of the recent cycle, the last and the second-last glacial-interglacial cycles. The excavation and fill processes might belong to a regional shelf geo-morphological evolution where from a ramp margin the drainage system that was optimally located in time and space is erosionally enlarged to form a singular, mature canyon (Galloway, 1991), which is permanently entrenched. The delta front trough evolution is therefore largely a down-dip incision of the margin by fluvial incision due to limited accommodation as a response to excess sediment supply.

The filling architecture largely resembles that of slope channel-levee systems where flow confinement provokes entrenchment (Hodgson et al., 2011). In the case of the SoNG the formation of internal levees (laminated type) on the side of debris channels (channel-fill type) is promoted not by external levee outbuilding but by the convergent sediment flux from the surrounding shelf.

The SoNG gives the exceptional possibility to be able to discern the multi-millennial, centennial and decadal scale accommodation variability with yearly resolution. The paucity of observations of active systems hampers the development of channel and seascape evolution models and limits the ability to reconstruct past environmental states using deep-water stratigraphy (Mohring, 1998). Consequently the Swatch of No Ground despite the large difficulties that might arise in the sedimentological characterization and cross-correlation, might be addressed as a high priority target for future explorations. If a causal relationship derived from the frequencies of external forcing events (monsoon climate and earthquakes) and the internal re-organization in form of gravity flow generation toward deep-sea could be established, there would be a great benefit for basin scale perspectives.

Acknowledgements

This work was done within the Project ‘‘SO-188—Bengal Sea Level’’, funded by the German Ministry of Education and Science (BMBF), Grant no. 03G0188A and the DFG project ‘‘Bengal Shelf IODP’’, Grant no. SP296/31-1. An additional extension on the funding was kindly provided by the Family Support offered by the GLOMAR Bremen International Graduate School for Marine Science funded by the DFG under the Excellence Initiative by the German federal and state governments to promote science and research at German Universities. We thank the captain and crew of the R.V. Sonne for excellent support and the scientific board party for their great collaboration.

~Chapter 7~
Synthesis and Outlook

7.1. Summary and conclusions

The aim of this study was to focus on the impact of tectonic and sea level changes on a sedimentary basin and to examine in detail the event succession within the sedimentary sequences during last glacial-interglacial cycle (123-0 ka). In this case study, work concentrated on the Bengal Basin and in particular the Ganges-Brahmaputra Delta. The stated objectives have been achieved by processing a seismoacoustic data set not only with conventional steps, but also including additional, time-consuming enhancements for very shallow water depth (15 to 700 mbsl) and large reflection angles. The data set has been interpreted applying general principles of process stratigraphy, particularly seismic stratigraphy, sequence stratigraphy and lithostratigraphy. A framework for basin development at the highest resolution available is obtained from a preliminary chronostratigraphy.
Main achievements are summarized below.

7.1.1. The depocentre shift in response to different sea level stands

The diversion of the theoretical seismostratigraphic model for system tract identification based on sinusoidal curves applied on a real global sea level curve with centennial to millennial resolution has been successfully reconciled. The depositional sequences have been coupled to marine isotope stages as derived from benthic oxygen isotopes and their correlation with oxygen isotope stratigraphy from ice cores. This has created a robust and coherent chronostratigraphic framework from which it became evident that the subaqueous portion of the Ganges Brahmaputra has continuously supplied sediment to the Bengal Basin throughout the last glacial-interglacial cycle. The fundamental building blocks of the accretion on the Bengal Shelf are subaqueous wedges of laminated beds with an overall clinoform geometry which grades depositional surfaces in response to environmental changes. From subtle to significant sea level changes, the clinoforms have registered the overall trend varying from oblique during the falling phase of the last glacial-interglacial cycle, toward a sigmoidal in the lowstand and, unexpectedly, also during transgression in Termination I, which led present day again to a sigmoidal subaqueous delta. An uneven curvature of the present day sigmoidal subaqueous delta has been highlighted and addressed as a precursor of an incoming variation in the subaqueous drainage.
The action of the tides in combination with the ambient waves and the preferentially SW directed shelf current have been also constantly accompanying the Bengal Basin accretion. Sedimentation has turned out to be strongly depth dependent and, beyond the location of the shoreline, the depocentre will always occur in depths between 30 and 60 mbsl and the highest sedimentation rate is in the

interval between -40 and -50 mbsl. This implies that the sediment flux is largely controlled by the oceanographic conditions in the Bay of Bengal, particularly by the wave base boundary layer and the deepest region affected by waves. Beyond this depth, advective processes, characteristic for the foreset region, are replaced by the convective processes which cause the deposition of the finer tail in the bottomset. Where the slopes become too steep, where sedimentation rate are too high or in concomitance with too rapid sea level changes, as it occurred during the accelerated sea level rise periods also kwon as Melt Water Pulses, the core of the depocentre becomes unstable. It has been shown in this PhD Thesis that channelization processes activate at appx. 40 mbsl, establishing a subaqueous drainage pattern. If this drainage is maintained in time, it may initiate first a subaqueous channel (with or without levee) and, if sufficiently persistent in time and optimally located on the shelf, this channel may become entrenched due to the continuous shelf vertical accretion, which in turn leads to the development of a canyon. This process of canyon generation is driven by the very efficient sediment supply to the shelf. Available sediment supply drove the development of a shelf ramp or a multi-source setting indeed on the Bengal Shelf during falling, lowstand and early transgression when a mid- to shelf margin delta formed on the eastern Bengal Shelf and contemporaneously gravity flows channelled through the canyon in the west. A ramp seems to be an indispensable pre-requisite for this type of canyon evolution which relies also on the flanks where shoreface processes act (top-down canyon-genesis) as much as shelf margin stability play a role, as is generally perceived (bottom-up canyon-genesis).

7.1.2. Depocentre anomalous distribution along and across the continental shelf

Sedimentation occurred at any time during the sea level cycle leading to a different overall geometry, but the distribution of clinoform sedimentary bodies is not uniform. The control of sea level stands on the location of the depocentre core is not sufficient to explain why a mid-shelf to shelf margin delta solely formed on the eastern Bengal Shelf, why an environment incompatible with deltas formed on the western Bengal Shelf such as the formation of oolitic beach ridges and why the canyon is not filled despite sedimentation rate in the head is on the order of 50 cm/yr. Sea level changes did not create a preferential debouching area on the eastern Bengal Shelf, as sea level action is ubiquitous. Instead, the depth where sedimentation occurs in the canyon is below the shoreface and is therefore only in its initial pulse related to the wave boundary layer, but further seaward gravity is the major controlling factor on slope stability. The formation of oolitic beach ridges during last glacial is instead clearly related to the falling and low stands of sea level. The development of this type of sedimentary environment might be not an isolated episode, as another set of beach ridges of unknow lithology formed during the second-last glacial. The boundary conditions for the formation of this type of carbonatic sedimentary environment necessitate a drastic diversion of the suspended sediment load.

Other factors must have then exerted their influence, as alongshore contour currents and particularly climate, as arid conditions and high evaporation are required for oolitic ridges formation. If these climatic conditions were reached, also the overall sediment supply to the mid-shelf to shelf margin delta, derived from the usual source region, must have been affected. And indeed it was. The majority of the sediments deposited on the shelf are contained in the system tract associated to the falling phase but a large portion of it probably is derived from sediment recycling by the action of the wave interface on previously deposited sequences. The sediments could have been dismantled from the last interglacial subaqueous delta with the creation of a broad shelfwide regressive incised valley. A contribution from the Northern and Central Arakan Coast rivers to the sediment load from the mid-shelf to shelf margin delta is also hypothesized as the εNd content in a core from the western continental slope has an Indo-Burma provenance.

Therefore, if sediment supply was maintained by such recycling action plus an additional contribution from the Indo-Burman Range, and sea level cannot be addressed as a fulfilling explanation for the uneven depocentre distribution on the shelf, the forcing inherent to the formation of a multi-source shelf ramp setting has to be searched elsewhere.

7.1.3. The tectonic subsidence and its differential component

Decompaction and backstripping, very useful tools for unravelling and reconstructing the geodynamic evolution of sedimentary basins, are normally applied to wells and under favourable conditions, reliable curves could also be obtained from outcrops. For the first time in this PhD thesis, this method is applied to a seismostrigraphic reconstruction as a thoughtful experiment to evaluate the potential magnitude of the effect of lithostatic stress and of the tectonic subsidence on millennial scale.

The tectonic subsidence component estimated is 0.175 m/ka during last glacial-interglacial cycle and 5.9 km of total accommodation within the last 33.9 Ma. The effect of the lithostatic stress exerted by the experimental sedimentary column (11 km) on the basement could have caused 0.935 km of additional accommodation. The lithostatic stress caused by the sedimentation of the last glacial-interglacial cycle composite sequence (10-35 m) has produced as much accommodation as the thickness of the sequence but the additional accommodation caused by the overburden pressure within the sequence is of maximum 0.4 m. As an application of the obtained values, the shoreline and shelf breaks locations during the last and second-last glacial-interglacial cycles were rebounded. The shoreline trajectory is that of a normal regression on the eastern Bengal Shelf whereas the shoreline trajectory on the western Bengal Shelf is a partly accretionary transgression where the large part of the vertical growth occurred not in the shoreface but on the inner shelf and shelf margin.

The shelf break trajectories on the eastern and western shelf are both negative whereas the western trajectory has even a degradation component as the negative trend is directed landward. It is

consequently excluded that bypass occurred within the western shelf break threshold. The eastern shelf break trajectory is negative but the margin experienced only a minor horizontal progradation. Bypass across this area occurred but the transfer was limited to the margin and the formation of subaqueous delta clinorform beds along the upper slope. The westward elongation of this clinoform body and its physical disconnection with the regressive and lowstand western shelf deposits strongly invokes the existence of a long shore shelf margin contour current.

The receiving morphological relieves of the Bengal Basin are all dipping toward the west with a slope angle which increased during the last Glacial-Interglacial cycle. This unexpected result might be an error in the assumption that the basement is a semi-horizontal surface because an eastward inclination of the basement could eventually compensate the obtained inclination. However may possibly indicate active tectonism in the area at the continent-ocean margin between the Indian craton and the remnant of the initial Bengal Basin developed on oceanic crust. Active tectonic processes on the Bengal Shelf might have contributed to the initial formation and consolidation of the Swatch of No Ground canyon as a preferential conduit toward the Bengal Fan by keeping a knick point constantly located close or at the canyon head. This could have diverted the drainage during falling and low sea level stands from the western shelf toward the canyon and have prevented any river or tidal inlet to go beyond the present day prodelta area of the subaqueous delta. On the eastern Bengal Shelf, a constant accommodation supply instead leaded to the connection of a delta with the shelf margin contemporaneously with the channelization of turbidity currents in the canyon, realizing the observed multi-source ramp setting.

7.1.4. Architectural style and individual strata, genetically related, traced for considerable distance across the basin

The near surface mm-cm laminated fundamental type deposits in both major deposition elements of the Bengal Basin on the Bengal Shelf, the subaqueous delta and the Swatch of No Ground canyon, are graded sequences. The graded beds are locally close correlated to the frequency and magnitude of tropical and severe cyclone in the northern Bay of Bengal during periods of pre- and post-monsoon seasons. The genetic term of these deposits is tempestites. The close correlation of the tempestites with the cyclones historical record is not found in the foreset beds of the Ganges-Brahmaputra subaqueous delta. According to the decadal slope analysis, to the centennial scale mass budget and to the millennial trend this is because the effect of the current on the wave-tide-supported gravity flows becomes prevalent toward the west. The eastern foreset beds in the modern subaqueous delta are grading toward a convex shape witnessing a decrease in sedimentation rate. The global late Holocene decrease in monsoon precipitation could be an explanation when the eastern foreset beds are more subjected to the influence of the alternating phases of high precipitation and droughts during the

Anthropocene.. The western subaqueous delta foreset beds are grading toward a concave clinoform indicating instead an increasing trend in sediment supply. The intensification of the magnitude of cyclone events might accelerate such trend producing over-sedimentation on the canyon head and large potential for mass wasting events while channelization already occurs establishing a permanent bathymetric connection between the two depositional elements.

Together with the graded bed tempestites, massive sediments wasting occurred from the head and the flanks to the canyon fill as well as in the subaqueous foreset beds. In the subaqueous delta the mass wasting events are acoustically transparent units, TUs. Based on their meter-scale thickness, their restricted number, their wide-spread distribution and especially their timing with respect to the accumulation rate, TUs have been interpreted as liquefaction flows generated by cyclic loading from compression waves of some of the last major plate-boundary earthquakes (1762, 1857, 1950). The projection of the surface accumulation rate in the canyon also indicates two major episodes of thicker transparent units (MTD-1 and MTD-2) extending through the canyon thalweg and beyond the study area. They are preliminarily interpreted as seismites. The number and thickness of transparent units in the canyon is much larger. Some thinner debrites, terminating within the study area, could be formed by cyclic loading generated by transient gravity flows as short lived basal debris flows (slurry flows). If the causal mechanism is a turbid flow, when this is generated during a severe cyclone, such slurry flows may be part of the record of the same cyclone event and be coeval with a tempestite.

In conclusion, both depositional regions, the subaqueous delta and the Swatch of No Ground canyon fill, may contain valuable records of allocyclic forcing on the Bengal Basin on time scale necessary for anthropocenic studies.

7.2 Outlook

The publication of this study will be soon completed to make it available to the scientific community and to cooperative enterprise such as the IGP, International Geoscience Programme, which is promoted by UNESCO and the International Union of Geological Sciences (IUGS) to stimulate comparative studies in the Earth Sciences as they are holding numerous project dealing with the East, South and South-East Asia.

The seismic data processing could benefit from a systematic time-depth conversion. With the integration of the two missing working areas, area 4 and area 5 (Fig. 3.1.), it could emerge how much material has passed the shelf break threshold and reached the upper Bengal Fan through the slope, the third mayor depositional element of the shelf.

The natural continuation of this study is therefore the extension of the used methods, through the whole imaged sedimentary succession. A Quaternary development of the Bengal Shelf would then become consistent and contribute to the ensemble vision on the evolution of the Bengal Basin with

respect to the regional geology and global eustasy. The strategy should be implemented by using an appropriate drilling strategy to ground truth the seismo-acustic record and to derive lithological, geo-chemical and geo-technical measures on the shelf sediments. The shelf sediments properties may indeed be very different from deep sea records as the subaerial exposure might have accelerated early diagenetic processes as well as the removal of surface sediments during erosive events might have produced spontaneous decompaction. Compaction tests should be made to better evaluate its importance on a centennial scale and also in response to mass wasting events when thick strata are deposited in a short time interval producing a sudden excess of lithostatic stress. Compaction should also be carefully evaluated in the canyon as there decompaction due to the frequent passage of gravity flows, may occur indeed spontaneously.

The shelf correlation of different events must be tested keeping in mind that the same causal trigger mechanism might produce different sedimentary records depending on the type of depositional element. The data should be also integrated with oceanographic studies for a better understanding of the direct influence of climate on sedimentary dynamics. There is an urgent need for precise and continuous records of the bed load and suspended load released offshore, together with current velocity fields and detailed dispersal models with different relative sea level scenarios.

The integration of the climatic forcing into the tectonic and sea level variability will finally reveal the accommodation trend and ultimately the Anthropogenic impact may emerge and potentially be quantified.

~ Chapter 8~

References

Acharyya, S.K., 1998. Break-up of the greater Indo-Australian continent and accretion of blocks framing south and east Asia. J. Geodyn. 26, 149– 170.

Adams, E.W., Schlager, W., 2000. Basic types of submarine curvature. Journal of Sedimentary Research 70, 814-828.

Alam, M.M., 1991. Paleoenvironmental study of the Barail succession exposed in northeastern Sylhet, Bangladesh. Bangladesh J. Sci. Res. 9, 25– 32.

Alam, M., Alam, M. M., Curray, J. R., Chowudhury, M. L. R., Gani, M. R., 2003. An overview of the sedimentary geology of the Bengal Basin in relation to the regional tectonic framework and basin-fill history. Sedimentary Geology 155 179–208.

Allen, P.A., Allen, J.R., 1990. Basin Analysis: Principles and applications. Blackwell Scientiphic Publications, Cambridge, 451 pp.

Alley, R.B., 2002. Climate change: enhanced: on thickening ice? Science, 295, 451-452.

Allison, M.A., 1998. Historical changes in the Ganges–Brahmaputra delta front. Journal of Coastal Research 14, 1269– 1275.

Allison, M.A., Kepple, E.B., 2001. Modern sediment supply to the lower delta plain of the Ganges-Brahmaputra River in Bangladesh. Geo-Marine Letters 21, 66-74.

Allison, M.A., Khan, S.R., Goodbred Jr, S.L., Kuehl, S.A, 2003. Stratigraphic evolution of the late Holocene Ganges–Brahmaputra lower delta plain. Sedimentary Geology 155, 317–342.

Arrigoni, A. S., Greenwood, M. C., Moore, J. N., 2010. Relative impact of anthropogenic modifications versus climate change on the natural flow regimes of rivers in the northern Rocky Mountains, United States, Water Resour. Res., 46, W12542.

As-Salek, J.A. and Yasuda, T., 2001. Tide–surge interaction in the Meghna Estuary: most severe conditions. American Meteorological Society 31, 3059-3072.

Athy, L.F., 1930. Density, porosity, and compaction of sedimentary rocks. AAPG Bulletin, 14, 1–24.

Bakr, A., 1971. Human settlement in the Bengal Basin in relation to geological setting. Journal of the Asiatic Society of Pakistan, 16(1).

Bandyopadhyay, J., 1995. Water management in the Ganges-Brahmaputra Basin: emerging challenges for the 21st Century. International Journal of Water Resources Development 11, 411-442.

Bard, E., Hamelin, B., Delanghe-Sabatier, D., 2010. Deglacial Meltwater Pulse 1B and Younger Dryas sea levels revisited with boreholes at Tahiti. Science 327, 1235-1237.

Barua, D.K., Kuehl, S.A., Miller, R.L., Moore, R.S., 1994. Suspended sediment distribution and residual transport in the coastal ocean off the Ganges–Brahmaputra River mouth. Marine Geology 120, 41– 61.

Barua, D. K., 1997. The active delta of the Ganges-Brahmaputra Rivers: dynamics of its present formations. Marine Geodesy 20, 1-12.

Beattie, P.D., Dade, W.B., 1996. Is scaling in turbidite deposition consistent with forcing by earthquakes? J. Sed. Res. 66, 909-915.

Berner, U., Poggenburg, J., Faber, E., Quadfasel, D. & Frische, A., (2003). Methane in ocean waters of the Bay of Bengal: Its sources and exchange with the atmosphere. Deep sea Res. II 50, 925–950.

Bookhagen, B., Burbank, D.W., 2006. Topography, relief, and TRMM-derived rainfall variations along the Himalaya. Geophisical Research Letters 33, L08405Muto, T., Steel, R.J., 2002. In defense of shelf-edge delta development during falling and lowstand of relative sea level. Journal of Geology 110, 421-436.

Blum, M.D., Price, D.M., 1998. Quaternary alluvial plain construction in response to glacio-eustatic and climatic controls, Texas Gulf Coastal Plain. In: Shanley, K.W., McCabe, P.J., (Eds.), Relative Role of Eustasy, Climate, and Tectonism in Continental Rocks: Society for Sedimentary Geology Special Publication 59, 31–48.

Bouma, A.H., 1962. Sedimentology of some flysch deposits: a graphic approach to facies Interpretation. Elsevier, Amsterdam.

Bourget, J., Zaragosi, S., Ellouz-Zimmermann, S., Ducassou, E., Prins, M.A., Garlan, T., Lanfumey, V., Schneider, J.-L., Rouillard, P., Giraudeau, J., 2010. Highstand vs. lowstand turbidite system growth in the Makran active margin: Imprints of high-frequency external controls on sediment delivery mechanisms to deep water systems. Marine Geology 274,187–208.

Breitenbach, S., 2009. Changes in monsoonal precipitation and ptmospheric circulation during the Holocene reconstructed from stalagmites from northeastern India. Dissertation zur Erlangung des Akademischen Grades Doktor der Naturwissenshaften in der Wissenschaftdiziplin Geologie. Potsdam Universität, Scientific Technical Report STR10/06.

Briggs, R., Sieh, K., Meltzner, A., Natawidjaja, D., Galetzka, J., Suwargadi, B., Hsu, Y-j., Simons, M., Hananto, N., Suprihanto, I., Prayudi, D., Avouac, J.-P., Prawriodirdjo, L., Bock, Y., 2005. Deformation and slip along the Sunda megthrust during the great March 2005 Nias-Simeulue earthquake. Science 311, 1897-1901.

Bristow, C.S., Best, J. L., 1993. Braided rivers: perspectives and problems. Geological Society, London, Special Publications. 75, 1-11.

Broccoli, A.J., Dahl, K.A., Stouffer, R.J., 2006. Response of the ITCZ to Northern Hemisphere cooling, Geophys. Res. Lett. 33.

Brunnschweiler, R.O., 1966. On the geology of the Indoburman Ranges. Geol. Soc. Aust. J., 13, 127–194.

Brunnschweiler, R.O., 1974. Indoburman ranges. In: Spencer, A.M. (Ed.), Mesozoic– Cenozoic Orogenic Belts. Geol. Soc. London, Spec. Publ., vol. 4, 279– 299.

Brusova, O., 2011. Compaction of deep sea siliciclastic sediments based on log data. MS at Geoscience, University of Utah, 260 pp.

Bullimore, S., Henriksen, S., Liestøl, F.M., & Helland-Hansen, W., 2005. Clinoform stacking patterns, shelf-edge trajectories and facies associations in Tertiary coastal deltas, offshore Norway: Implications for the prediction of lithology in prograding systems. Norwegian Journal of Geology 85, 169-187.

Burgess, P.M., Hovius, N., 1998. Rates of delta progradation during highstands; consequences for timing of deposition in deep-marine systems. Journal of the Geological Society of London 155, 217-222.

Canals, M., Puig, P., de Madron, D.X., Heussner, S., Palanques, A., Fabres, J., 2004. Flushing submarine canyons. Nature 444, 354-357.

Carter, R.M., 1988, The nature and evolution of deep-sea channel systems. Basin Research 1, 41-54.

Cattaneo, A., Steel, R. J., 2003. Transgressive deposits: a review of their variability. Earth-Science Reviews 62, 187–228.

Catuneanu, O., 2006. Principles of Sequence Stratigraphy. Elsevier, Amsterdam, 375 pp.

Catuneanu, O., Abreu, V., Bhattacharya, J.P., Blum, M.D., Dalrymple, R.W, Eriksson, P.G., Fielding, C.R., Fisher, W.L., Galloway, W.E., Gibling, M.R., Giles, K.A., Holbrook, J.M., Jordan, R., Kendall, C.G., Macurda, B., Martinsen, O.J., Miall, A.D., Neal, J.E., Nummedal, D., Pomar, L., Posamentier, H.W., Pratt, B.R., Sarg, J.F., Shanley, K.W., Steel, R.J., Strasser, A., Tucker, M.E., Winker, C., 2009. Towards the standardization of sequence stratigraphy. Earth-Science Review, 92, 1-33.

Chen, Y., Courtillot, V., Cogne´, J.P., Besse, J., Yang, Z., Enkin, R.,1993. The configuration of Asia prior to the collision of India:Cretaceous paleomagnetic constraints. J. Geophys. Res. 98, 21.927– 21.941.

Chiang, J.C.H., Bitz, C.M., 2005. Influence of high latitude ice cover on the marine Intertropical Convergence Zone, Clim. Dyn. 25, 477–496.

Choudhury, N.Y., Paul, A., Paul, B. K., 2004. Impact of costal embankment on the flash flood in Bangladesh: a case study. Applied Geography 24, 241-258.

Chowdhury, J., 1998. Some hydraulic aspects of floods in Bangladesh and their implications in planning. In: Ali, M. A., Hoque, M. M., Rahman, R., and Rashid, S., 1998 (Eds), Bangladesh Floods – Views from Home and Abroad, Dhaka, United Press Limited, 209-17.

Clark, P., Archer, D., Pollard, D., Blum, J., Rial, J., Brovkin, V., Mix, A., Pisias, N., and Roy, M., 2004. The middle Pleistocene transition: characteristics, mechanisms, and implications for long-term changes in atmospheric pCO2. Quaternary Science Reviews 25, 3150–3184.

Coffin, M.F., 1992. Emplacement and subsidence of Indian Ocean plateaus and submarine ridges, in Duncan, R.A., D.K. Rea, R.B. Kidd, U. von Rad, and J.K. Weissel, eds., Synthesis of Results from Scientific Drilling in the Indian Ocean, Geophysical Monograph 70, American Geophysical Union, (Washington, D.C.): 115-125.

Coleman, J. M. 1969. Brahmaputra river. Channel processes and sedimentation. Sed. Geol. 3, 129-239.

Coleman, J.M., Wright, L.D., 1975. Modern river deltas. variability of processes and sand bodies. Im: Broussard, M.L., (Ed), Deltas, Models for Exploration. Houston Geological Society, 99–149.

Covault, J.A., Graham, S.A., 2010. Submarine fans at all sea-level stands: Tectono-morphologic and climatic controls on terrigenous sediment delivery to the deep sea. Geology 38, 939–942.

Cruz, R.V., Harasawa, H., Lal, M., Wu, S., Anokhin, Y., Punsalmaa, B., Honda, Y., Jafari, M., Li, C., Huu Ninh, N., 2007. Asia. Climate Change 2007: Impacts, Adaptation and Vulnerability. Contribution of Working Group II to the Fourth Assessment Report of the Intergovernmental Panel on Climate Change. In: Parry, M.L., Canziani, O.F., Palutikof, J.P., van der Linden, P.J., Hanson, C.E. (Eds.), Cambridge University Press, Cambridge, UK, 469-506.

Crutzen, P.J., 2002. Geology of mankind. Nature 415, 23.

Cullen, J.L., 1981. Microfossil evidence for changing salinity patterns in the Bay of Bengal over the past 20,000 years. Palaeogeogr. Palaeoclimatol. Palaeoecol. 35, 315–356.

Cummins, P.R., 2007. The potential for giant tsunamigenic earthquakes in the northern Bay of Bengal. Nature 449, 75-78.

Curray, J. R., Moore, D. G., 1971. Growth of the Bengal deep-sea fan and denudation in the Himalayas. Geological Society of America Bulletin, 82, 563–572.

Curray, J.R., Emmel, F.J., Moore, D.G., Raitt, R.W., 1982. Structure, tectonics and geological history of the northeastern Indian Ocean. In: Nairn, A.E.M., Stehli, F.G. (Eds.), The Ocean Basins and margins. The Indian Ocean, vol. 6. Plenum, New York, pp. 399– 450.

Curray, J. R., 1994. Sediment volume and mass beneath the Bay of Bengal.Earth and Planetary Science Letters, 125, 371–383.

Curray, J.R., Emmel, F.J., Moore, D. G., 2003. The Bengal Fan: morphology, geometry, stratigraphy, history and processes. Marine and Petroleum Geology 19, 1191-1223.Watts and Ryan, 1976.

Darwin, C.M.A., 1859. On the origin of species by means of natural selection, or the preservation of favoured races in the struggle for life. J. Murray Ed., London, 813 pp.

Delft Hydraulics, 1996. River Survey Project, Flood Action Plan 24, Special Report No.18: Sediment Rating Curves and Balances. Dhaka, Water Resources Planning Organization.

Deplus, C., Le Friant, A., Boudon, G., Komorowski, J.-C., Villemant, B., Harford, C., Ségoufin, J., Cheminée, J.-L., 2001. Submarine evidence for large-scale debris avalanches in the Lesser Antilles Arc. Earth Planet. Sci. Lett., 192, 333–354.

Deptuck, M.E., Steffens, G.S., Barton, M., Pirmez, C., 2003. Architecture and evolution of upper fan channel-belts on the Niger Delta slope and in the Arabian Sea. Marine and Petroleum Geology 20, 649–676.

Deptuck, M.E., Sylvester, Z., Pirmez, C. & O'Byrne, C. 2007. Migration–aggradation history and 3D seismic geomorphology of submarine channels in the Pleistocene Benin-major Canyon, western Niger Delta slope. Marine and Petroleum Geology 24, 1–28.

Deschamps, P., Durand, N., Bard, E., Hamelin, B., Camoin, G., Thomas, A.L., Henderson, G. M., Okuno, J., Yokoyama, Y., 2012. Ice-sheet collapse and sea-level rise at the Bølling warming 14,600 years ago. Nature 483, 559-564.

Du, B.L., Zhang, J.W., 2000. Adaptation strategy for sea-level rise in vulnerable areas along China's coast. Acta Oceanologica Sinica, 19, 1-16.

Duplessy, J.C., 1982. Glacial to interglacial contrasts in the northern Indian Ocean, Nature 295, 494–498.

Dutt, R.C., 1906. The Economic History of India under Early British Rule, Paul, Trench, and Trubner, London.

Dykoski, C.A., Edwards, R.L., Cheng, H., Yuan, D., Cai, Y., Zhang, M., Lin, Y., Qing, J., An, Z., Revenaugh, J., 2005. A high-resolution, absolute-dated Holocene and deglacial Asian monsoon record from Dongge Cave, China. Earth and Planetary Science Letters 233, 71- 86.

Emery, D., Myers, K.J., 1996. Sequence Stratigraphy. Blackwell, Oxford. 297 pp.

Ericson, J.P., Vorosmarty, C.J., Dingman, S.L., Ward, L.G., Meybeck, M., 2006. Effective sea-level rise and deltas: causes of change and human dimension implications. Global Planet Change 50, 63-82.

Fairbanks, R. G., 1989. A 17,000-year glacioeustatic sea level record: Influence of glacial melting rates on the Younger Dryas event and deep-ocean circulation. Nature 342, 637– 642.

Farre, J.A., McGregor, B.A., Ryan, W.B.F., Robb, J.M., 1983. Breaching the shelf break; passage from youthful to mature phase in submarine canyon evolution. In: Stanley, D.J., Moore, G.T., (Eds), The Shelf Break; Critical Interface on Continental Margins, Society of Economic Paleontologists and Mineralogists Special Publication 33, 25–39.

Flood, R.D., Manley, P.L., Kowsmann, R.O., Appi, C.J., Pirmez, C., 1991. Seismic facies and late Quaternary growth of Amazon submarine fan. In: Weimaer, P., Link, M.H. (Eds), Seismic Facies and Sedimentary Processes of Submarine Fans and Turbidite Systems. Springer-Verlag, New York, 415−433.

Förster, A., Ellis, R.G., Henrich, R., Krastel, S., Kopf, A.J., 2010. Geotechnical characterization and strain analyses of sediment in the Mauritania Slide Complex, NW-Africa. Marine and Petroleum Geology 27, 1175-1189

France-Lanord C., Derry L.A., Michard A., 1993. Evolution of the Himalaya since Miocene time: Isotopic and sedimentologic evidence from the Bengal Fan. In: Treloar, P.J., Searle, M. (Eds) Himalayan Tectonics, Geological Society of London Special Publication 74, 605-623.

Friedrichs, C.T., Wright, L.D., 2004. Gravity-driven sediment transport on the continental shelf: implications for equilibrium profiles near river mouths. Coastal Engineering 51, 795– 811.

Gahalaut, V.K., Chander, R., 1992. A rupture model for the great earthquake of 1897,northeast India. Tectonophysics 204, 163-174.

Galloway, W.E., 1975. Process framework for describing the morphologic and stratigraphic evolution of deltaic depositional systems. Im: Broussard, M.L. (Ed.) Deltas--Models for Exploratio, Houston Geological Society, 87-98.

Galloway W.E., Dingus, W. F., Paige, R. E., 1991. Seismic and depositional facies of Paleocene-Eocene Wilcox Group submarine canyon fills, northwest Gulf Coast, U.S.A. In: Weimaer, P., Link, M.H. (Eds), Seismic Facies and Sedimentary Processes of Submarine Fans and Turbidite Systems. Springer-Verlag, New York, 247-271.

Galy, A., France-Lanord, C., Derry, L.A., 1999. The strontium isotopic budget of Himalayan Rivers in Nepal and Bangladesh. Geochimica et Cosmochimica Acta 63, 1905-1925.

Galy, A., France-Lanord, C., 2001. Higher erosion rates in the Himalaya: Geochemical constraints on riverine fluxes. Geology 29, 23-26.

Galy, V., France-Lanord, C., Lartiges, B., 2008. Loading and fate of riverine particulate organic carbon from the Himalaya to the Ganga–Brahmaputra delta. Geochimica et Cosmochimica Acta 72, 1767–1787.

Gani, M.R., Alam, M.M., 1999. Trench-slope controlled deep-sea clastics in the exposed lower Surma group in the southeastern fold belt of the Bengal Basin, Bangladesh. Sediment. Geol. 127, 221– 236.

Gani, M.R., Alam, M.M., 2003. Sedimentation and basin-fill history of the Neogene clastic succession exposed in the southeastern fold belt of the Bengal Basin, Bangladesh: a high-resolution sequence stratigraphic approach. Sediment. Geol. 155, 227– 270.

Gasse, F., Arnold, M., Fontes, J.C., Fort, M., Gibert, E., Huc, A., Li, B.Y., Li, Y.F., Lju, Q., Melieres, F., Vancampo, E., Wang, F.B., Zhang, Q.S., 1991. A 13,000-year climate record from western Tibet. Nature 353, 742–745.

Gerber, T.P., Amblas, D., Wolinsky M.A., Pratson, L., and Canals, M. 2009. A model for the long-profile shape of submarine canyons. Journal of Geophysical Research 114, F03002.

Geyh, M.A., Kudrass, H.-R., Streif, H., 1979. Sea-level changes during the late Pleistocene and Holocene in the Strait of Malacca. Nature 278, 441–443.

Giosan, L., Constantinescu, S., Clift, P.D., Tabrez, A.R., Danish, M., Inam, A., 2006. Recent morphodynamics of the Indus delta shore and shelf. Continental Shelf Research 26, 1668–1684.

Goldfinger, C., Morey, A.E., Nelson, C.H., Gutiérrez-Pastor, J., Johnson, J.E., Karabanov, E., Chaytor, J., Eriksson, A., Shipboard Scientific Party, 2007. Rupture lengths and temporal history of significant earthquakes on the offshore and north coast segments of the Northern San Andreas Fault based on turbidite stratigraphy. Earth and Planetary Science Letters 254, 9–27

Goodbred Jr., S.L., Kuehl, S.A., 1999. Holocene and modern sediment budgets for Ganges–Brahmaputra river: evidence for highstand dispersal to floodplain, shelf, and deep-sea depocenters. Geology 27, 559–562.

Goodbred, S.L., Kuehl, S.A., 2000a. Late Quaternary evolution of the Ganges–Brahmaputra River delta: significance of high sediment discharge and tectonic processes on margin sequence development. Sedimentary Geology 133, 227– 248.Hays, J. D., Imbrie J., Shackleton N. J., 1976. Variations in the Earth's Orbit: Pacemaker of the Ice Ages. Science 194, 1121-1132.

Goodbred, S.L., Kuehl, S.A., 2000b. Enormous Ganges–Brahmaputra sediment load during strengthened early Holocene monsoon. Geology 28, 1083-1086.

Goodbred, S.L., JR., 2003, Response of the Ganges dispersal system to climate change: a source-to-sink view since the last interstade. Sedimentary Geology 162, 83–104.

Hamilton, E.L., 1976. Variations of density and porosity with depth in deep sea sediments. Journal of Sedimenrara Petrology 46, 280-300.

Hamilton, A. C., Taylor, D., 1991. History Of climate and forest in tropical Africa during the last 8 million years. Climatic Change 19, 65-78.

Han, W., Webster, P.J., 2002. Forcing Mechanisms of Sea Level Interannual Variability in the Bay of Bengal. Journal of Physical Oceanography, 216-239.

Hanebuth, T., Stattegger, K., Grootes, P.M., 2000. Rapid flooding of the Sunda shelf: A late-glacial sea-level record, Science 288, 1033–1035.

Haq, B U, HardenboJl , Vail PR. 1987.Chronology of fluctuating sea levels since the Triassic. Science 235: 1156-67.

Harris, P.T., Whiteway, T., 2011. Global distribution of large submarine canyons: Geomorphic differences between active and passive continental margins. Marine Geology 285, 69-86.

Hedberg, H. D., 1936. Gravitational compaction of clays and shales. Am. J. Sci. 31, 241–287.

Hedley, P.J., Bird, M.I., Robinson, R.A.J, 2010. Evolution of the Irrawaddy delta region since 1850. The Geographical Journal 176, 138-149.

Helland-Hansen, W., Gjelberg, J.G., 1994. Conceptual basis and variability in sequence stratigraphy: a different perspective. Sedimentary Geology 92, 31– 52.

Helland-Hansen, W., Martinsen, O.J., 1996. Shoreline trajectories and sequences: description of variable depositional-dip scenarios. Journal of Sedimentary Research 66, 670– 688.

Henrich, R., Cherubini, Y., Meggers, H., 2010. Climate and sea level induced turbidite activity in a canyon system offshore the hyperarid Western Sahara (Mauritania): The Timiris Canyon. Marine Geology 275, 178–198.

Heroy, D.C., Kuehl, S.A., Goodbred Jr., S.L., 2003. Mineralogy of the Ganges and Brahmaputra Rivers: implications for river switching and Late Quaternary climate change. Sedimentary Geology 155, 343-359.

Hodgson, D.M., Di Celma, C.N., Brunt, R. L., Flint, S.S, 2011. Submarine slope degradation and aggradation and the stratigraphic evolution of channel–levee systems. Journal of the Geological Society, London, 168, 625–628.

Hori, K., Saito,Y., 2007. An early Holocene sea-level jump and delta initiation. Geophysical Research Letters 34.

Hübscher, C., Breitzke, M., Michels, K., Kudraß, H.R., Spieß, V., Wiedicke, M., 1998. Late Quaternary seismic stratigraphy of the Eastern Bengal Shelf. Marine Geophysical Research 20, 57– 71.

Hübscher, C. Figueiredo, Jr, A.G., Kruse, L., Spiess, V., 2003. High-resolution analysis of the deposition pattern on the Amazon sub-aquatic delta and outer continental shelf. Marine Geophysical Research 23, 209-222.

Hübscher, C., Spieß V., 2005. Forced regression systems tracts on the Bengal Shelf. Marine Geology 219, 207–218

Hulbe, C.L., Payne, A.J. , 2001: Numerical modelling of the West Antarctic Ice Sheet. Antarctic Research Series, 77, 201-220.

Hunt, D., Tucker, M.E., 1992. Stranded parasequences and the forced regression wedge systems tract: deposition during baselevel fall. Sediment. Geol. 81, 1– 9.

Hunt, D., Tucker, M.E., 1995. Stranded parasequences and the forced regression wedge systems tract: deposition during baselevel fall—reply. Sediment. Geol. 95, 147–160.

Hutchison, C.S., 1989. Geological evolution of South-East Asia. Clarendon Press, London, 368 pp.

Imbrie, J., 1982. Astronomical theory of the Pleistocene Ice Ages: a brief historical review. Icarus 50, 408-422.

Imran, J., Parker, G., Katopodes, N., 1998. A numerical model of channel inception on submarine fans. J. Geophysical Research 103, 1219-1238.

Inam, A., Ali Khan, T.M., Tabrez, A.R., Amjad, S., Danishb, M., Tabrez, S.M., 2003. Natural and man-made stresses on the stability of Indus deltaic Eco region. Extended Abstract, 5th International Conference on Asian Marine Geology, Bangkok, Thailand (IGCP475/APN).

Ingersoll, R.N., Graham, S.A., Dickinson, W.R., 1995. Remnant ocean basins. In: Busby, C.J., Ingersoll, R.V. (Eds.), Tectonics of Sedimentary Basins. Blackwell, Oxford, pp. 363–391.

IPCC, 2007, Climate Change 2007: The physical science basis, Contribution of Working Group I to the fourth assessment report of the Intergovernmental Panel on Climate Change, edited by S.D. Solomon et al., Cambridge University Press, Cambridge, United Kingdom and New York, New York, USA.

Jervey, MT. 1988. Quantitative geological modelling of siliciclastic rock sequence and their seismic expression. In: Wilgus, C.K., Hastings, B.S., Kendall, C.G.S.C., Posamentier, H.W., Ross, C A,, Van Wagoner, J.C. (Eds). Sea-Level Changes: An Integrated Approach. Soc. Econ. Paleontol. Mineral. Spec.Publ. No. 42., 47-69.

Kaila, K. L., Reddy, P. R., Mall, D., Venkateswarlu, M. N., Krishna, V. G., Prasad, A. S. S. S. R. S., 1992. Crustal structure of the west Bengal basin, India from deep seismic sounding investigations. Geophys. J . Int. 111, 45-66.

Kane, I., Hodgson, D.M. 2011. Submarine channel levees: nomenclature and criteria to differentiate subenvironments. Exhumed examples from the Rosario Fm. (Upper Cretaceous) of Baja California, Mexico, and the Laingsburg Fm. (Permian), Karoo Basin, S. Africa. Marine and Petroleum Geology 28, 807–823.

Kastens, K.A., Shor, A.N., 1985. Depositional processes of a meandering channel on Mississippi fan. AAPG Bulletin 69, 190–202.

Kim, W., Sheetsz, B.A., Paola, C., 2010. Steering of experimental channels by lateral basin tilting. Basin Research 22, 286–301.

Klootwijk, C.T., Gec, J.S., Peirce, J.W., Smith, G.M., McFadden, P.L., 1992. An early India– Asia contact: paleomagnetic constraints from Ninetyeast Ridge, ODP Leg 121. Geology 20, 395–398.

Kottke, B., T. Schwenk, M. Breitzke, M. Wiedecke, H.R. Kudrass, and V. Spiess (2003) Acoustic facies and depositional processes in the upper submarine canyon Swatch of No Ground (Bay of Bengal). Deep-Sea Research II 50, 979-1001.

Kneller, B., 2003. The influence of flow parameters on turbidite slope and channel architecture. Marine and Petroleum Geology 20, 901–910.

Kudrass, H.R., and Scientific Shipboard Party, 2010. Cruise Report SO188-2. Bundesanstalt für Geowissenschaften und Rohstoffe, Hannover.

Kudrass, H. R., Hofmann, A., Doose, H., Emeis, K., Erlenkeuser, H., 2001. Modulation and amplification of climatic changes in the Northern Hemisphere by the Indian summer monsoon during the past 80 k.y. Geology 29, 63–66.

Kudrass, H.R., Michels, K.H., Wiedicke, M., Suckow, A., 1998. Cyclones and tides as feeders of a submarine canyon off Bangladesh. Geology 26, 715–718.

Kudrass, H.R., and Scientific Shipboard Party, 1994. Cruise Report SO93/1-3. Bundesanstalt für Geowissenschaften und Rohstoffe, Hannover.

Kuehl, S.A., Hariu, T.M., Moore, W.S., 1989. Shelf sedimentation off the Ganges– Brahmaputra river system: Evidence for sediment bypassing to the Bengal fan. Geology 17, 1132–1135.

Kuehl, S.A., Levy, B.M., Moore, W.S., Allison, M.A., 1997. Subaqueous delta of the Ganges–Brahmaputra river system. Marine Geology 144, 81–96.

Kuehl, S.A., Allison, M.A., Goodbred, S.L., Kudrass, H.R., 2005. The Ganges-Brahmaputra Delta. In: Giosan, L., Bhattacharya, J.P., (Eds), River Deltas—Concepts, Models, and Examples., SEPM Special Publication No. 83., 413-434.

Kutzbach, J. E., 1981. Monsoon climate of the Early Holocene: Climate experiment with the Earth's orbital parameters for 9000 years ago. Science, 214, 59–61.

Kustu, M. D., Fan, Y., Rodell, M., 2011. Possible link between irrigation in the U.S. High Plains and increased summer streamflow in the Midwest.Water Resour. Res., 47, W03522.

Lambeck, K, Chappell, J., 2001. Sea Level Change through the Last Glacial Cycle. Science 292, 679-686.

Lambeck, K., Esat, T.M., Potter, E-K., 2002. Links between climate and sea levels for the past three million years. Nature 419, 199–206.

Liu, J.P., Li, A.C., Xu, K.H, Velozzi, D.M., Yang, Z.S., Milliman, J.D., DeMaster, D.J., 2006. Sedimentary features of the Yangtze River-derived along-shelf clinoform deposit in the East China Sea. Continental Shelf Research 26, 2141–2156.

Liu, J.P., Liu, C.S. , Xu, K.H., Milliman, J.D., Chiu, J.K., Kao, S.J., Lin, S.W., 2008. Flux and fate of small mountainous rivers derived sediments into the Taiwan Strait. Marine Geology 256, 65-76.

Lee, T.T., Lawver, L.A., 1995. Cenozoic plate reconstruction of Southeast Asia. Tectonophysics 251, 85– 138.

Lee, H.J., Locat, J., Desgagnes, P., Parsons, J.D., McAdoo, B.G., Orange, D.L., Puig, P., Wong, F.L., Dartnell, P., Boulanger, E., 2007. Submarine Mass Movements on Continental Margins. In: Nittrouer, C.A., Austin, J.A., Field, M.E., Kravitz, J.H., Syvitski, J.P.M., and Wiberg, P.L. (Eds), Continental-Margin Sedimentation: from Sediment Transport to Sequence Stratigraphy, IAS special publication 37, Blackwell Publishing Ltd., Oxford, 213-275.

Leopold, L. B. and Bull, W. B. 1979. 'Base level, aggradation and grade', Proceedings ofthe American Philosophical Society, 123,168-202.

Li, C.X., Yang, S.Y., Fan, D.D., Zhao, J., 2004. The change in Changjiang suspended load and its impact on the delta after completion of Three-Gorges Dam. Quaternary Sciences, 24, 495-500 (in Chinese with an English abstract).

Lisiecki, L. E., Raymo, M. E., 2005. A Pliocene–Pleistocene stack of 57 globally distributed benthic d18O records. Paleoceanography 20, PA1003.

Lowe, D.R., 1979. Sediment gravity flows: their classification and problems of application to natural flows and deposits. In: Doyle, L.J., Pilkey, O.H., (Eds), Geology of Continental Slopes, Spec. Publ. Soc. Econ. Paleont. Miner. 27, 75-82.

Lowe, D. R., Guy, M., 2000. Slurry-flow deposits in the Britannia Formation (Lower Cretaceous), North Sea: a new perspective on the turbidity current and debris flow problem. Sedimentology 47, 31-70.

Ma, Y, Friedrichs, C.T., Harris, C. K., Donelson Wright, L., 2010. Deposition by seasonal wave- and current-supported sediment gravity flows interacting with spatially varying bathymetry: Waiapu shelf, New Zealand. Marine Geology 275, 199-211.

Mallik, T.K., 1976. Shelf sediments of the Ganges-Brahmaputra delta with special emphasis on the mineralogy of the western part, Bay of Bengal, Indian Ocean. Marine Geology, 22, l-32.

Martinson, D.G., Pisias, N.G., Hays, J.D., Imbrie, J., Moore, T.C., Shackleton, N.J., 1987. Age dating and the orbital theory of the ice ages —development of a high-resolution – 0 to 300,000 – year chronostratigraphy. Quat. Res. 27, 1–29.

Maurin, T., Rangin, C., 2009. Structure and kinematics of the Indo-Burmese Wedge: recent and fast growth of the outer zwedge. Tectonics, 28, TC2010.

Maxey, M.R., 1987. The gravitational settling of aerosol particles in homogeneous turbulence and random flow fields. J. Fluid Mech. 174, 441-465.

Mayall, M., Jones, E., Casey, M., 2006. Turbidite channel reservoirs—key elements in facies prediction and effective development. Marine and Petroleum Geology 23, 821–841.

Mayer, I., Palamenghi, L., Kudrass, H.-R., Spiess, V., 2012. Sediment transfer and deposition in the shelf canyon off the Ganges Brahmaputra Delta, Bangladesh. Accepted abstract, Geologische Vereinigung e.V. (GV), 23-28 September 2012, Hamburg.

Miall, A.D., 1991. Stratigraphic sequences and their chronostratigraphic correlation. Journal of Sedimentary Petrology 61, 497–505.

Miall, A.D., 1992. Exxon global cycle chart: An event for every occasion? Geology 20, 787-790,

Miall, A.D., 1996. The geology of fluvial deposits: sedimentary facies, basin analysis and petroleum geology: Berlin Springer-Verlag Inc 582 p.

Miall, A.D., 2000. Principles of Sedimentary Basin Analysis, 3rd ed., Springer-Verlag, Berlin, 616 pp.

Michels, K.H., Kudrass, H.R., Hubscher, C., Suckow, A., Wiedicke, M., 1998. The submarine delta of the Ganges – Brahmaputra: cyclone-dominated sedimentation patterns. Marine Geology 149, 133–154.

Michels, K.H., Suckow, A., Breitzke, M., Kudrass, H.-R., Kottke, B., 2003. Sediment transport in the shelf canyon "Swatch of No Ground" (Bay of Bengal). Deep-Sea Research II 50, 1003–1022.

Miller, M.C., McCave, I.N. and Komar, P.D., 1977. Threshold of motion under unidirectional currents. Sedimentology 24, 507–527.

Mitchell, A.H.G., 1989. The Shan Plateau and western Burma: Mesozoic– Cenozoic plate boundaries and correlations with Tibet. In: Sengor, A.M.C. (Ed.), Tectonic Evolution of the Tethyan Region. Kluwer Academic Publishing, 567–583.

Mitchum Jr., R.M., 1977. Seismic stratigraphy and global changes of sea-level, Part 11: glossary of term used in seismic stratigraphy. In: Payton, C.E. (Ed.), Seismic Stratigraphy—Applications to Hydrocarbon Exploration. Memoir, vol. 26. American Association of Petroleum Geologists, pp. 205–212

Mitchum, R. M.J., Van Wagoner, J. C., 1991. High-frequency sequences and their stacking patterns: sequence-stratigraphic evidence of high-frequency eustatic cycles. Sedimentary Geology 70, 131-160.

Mitra, S., Bhattacharya, S. N., Nath, S. K., 2008. Crustal Structure of the Western Bengal Basin from Joint Analysis of Teleseismic Receiver Functions and Rayleigh-Wave Dispersion. Bulletin of the Seismological Society of America 98, 2715–2723.

Mohrig, D., Whipple, K.X., Hondzo, M., Ellis, C., and Parker, G., 1998. Hydroplaning of subaqueous debris flows. Geological Society of America Bulletin 110, 387-394.

Moore, J.G., Clague, D.A., Holcomb, R.T., Lipman, P.W., Normark, W.R., Torresan, M.E., (1989). Prodigious submarine slides on the Hawaiian Ridge. J. Geophys. Res., 94, 465–17,484.

Mukhopadhyay, M., Dasgupta, S., 1988. Deep structure and tectonics of the Burmese arc: constraints from earthquake and gravity data. Tectonophysics 149, 299–322.

Murty, T.S., Henry, R.F., 1983. Tides in the Bay of Bengal. Journal of Geophysical Research 88, 6069-6076.

Murty, T.S., El-Sabh, M., 1992. Mitigating the Effects of Storm Surges Generated by Tropical Cyclones: A Proposal. Natural Hazards 6, 251-273.

Naish, T.R., Wilson G.S., 2009. Constraints on the amplitude of Mid-Pliocene (3.6-2.4?Ma) eustatic sea-level fluctuations from the New Zealand shallow-marine sediment record. Phil. Trans. R. Soc. 367, 169-187.

Nicholls, R.J., P.P. Wong, V.R. Burkett, J.O. Codignotto, J.E. Hay, R.F. McLean, S. Ragoonaden and C.D. Woodroffe, 2007: Coastal systems and low-lying areas. Climate Change 2007: Impacts, Adaptation and Vulnerability. Contribution of Working Group II to the Fourth Assessment Report of the Intergovernmental Panel on Climate Change, M.L. Parry, O.F. Canziani, J.P. Palutikof, P.J. van der Linden and C.E. Hanson, Eds., Cambridge University Press, Cambridge, UK, 315-356.

Neill, C. F., Allison, M.A., 2005. Subaqueous deltaic formation on the Atchafalaya Shelf, Louisiana. Marine Geology 214, 411-430.

Najman, Y., Bicke, M., Boudagher-Fadel, M., Carter, A., Garzenti, E., Paul, M., Wijbrans, J., Willett, E., Oliver, G., Parrish, R., Akther, H., Allen, R., Ando, S., Christy, E., Reisberg, L., Vezzoli, G., 2008. The 'missing' record of Himalayan erosion, Bengal Basin, Bangladesh. Earth Planet. Sci. Lett., 273, 1–14.

Najman,Y., Allen, R., Willett, E. A. F., Carter, A., Barfod, D., Garzanti, E., Wijbrans, J., Bickle M. J., Vezzoli, G., Ando, S., Oliver, G., Uddin, M. J., 2010. The record of Himalayan erosion preserved in the sedimentary rocks of the HatiaTrough of the Bengal Basin and the Chittagong Hill Tracts, Bangladesh. Basin Research 24, 1–21.

Normark, W.R., Carlson, P.R., 2003. Giant submarine canyons: is size any clue to their importance in the rock record? In: Chan, M.A., Archer, A.W. (Eds.), Extreme Depositional Environments: Mega End Members in Geologic Time Geological Society of America Special Paper 370, 175-190.

O'Grady, D.B., Syvitski, J.R.M., Pratson, L.F., Sarg, J.F., 2000. Categorizing the morphologic variability of siliclastic passive continental margins. Geology 28, 207-210.

Palamenghi, L., Schwenk, T., Spiess, V., Kudrass, H.-R., 2011. Seismostratigraphic Analysis with Centennial to Decadal Time Resolution of the Sediment Sink in the Ganges-Brahmaputra Subaqueous Delta. Continental Shelf Research 31, 712-730.

Parsons, J.D., Friedrichs, C.T., Traykovski, P.A., Mohrig, D., Imran, J., Syvitski, J.P.M., Parker, G., Puig, P., Buttles, J.L., and Garcia, M.H., 2007. The mechanics of marine sediment gravity flows. In: Nittrouer, C.A., Austin, J.A., Field, M.E., Kravitz, J.H., Syvitski, J.P.M., Wiberg, P.L., (Eds.), Continental margin sedimentation: From sediment transport to sequence stratigraphy, International Association of Sedimentologists Volume 37. Malden, Massachusetts, Blackwell Publishing,275–337

Pearce, F., 1991. The rivers that won't be tamed. New Scientist, 38-41.

Peltier, W.R., 2001, Global glacial isostatic adjustment and modern instrumental records of relative sea level history, in Douglas, B.C., Kearney, M.S., and Leatherman, S.P., eds., Sea-Level Rise: History and Consequences: International Geophysics Series, vol. 75, Academic Press, New York, New York, pp. 65-95.

Peterson, R., 1958. Rebound in the Bearpaw shale, Western Canada. Geol. Sac. America Bull. 69, 1113-1124.

Pierson-Wickmann, A.-C., Reisberg, L., France-Lanord, C., Kudrass, H.-R., (2001). Os-Sr-Nd results from sediments in the Bay of Bengal: Implications for sediment transport and the marine Os record. Paleoceanography 16, 435–444.

Piper, D.J.W., Normark, W.R., 1983. Turbidite depositional patterns and flow characteristics, Navy submarine fan, California Borderland. Sedimentology 30, 681–694.

Pirmez, C., Pratson, L.F., Steckler, M.S., (1998). Clinoform development by advection-diffusion of suspended sediment: Modeling and comparison to natural systems. Journal of Geophysical Research 103, 24,141-24,157.

Pirmez, C., Beaubouef, R.T., Friedmann, S.J., 2000. Equilibrium profile and baselevel in submarine channels: examples from Late Pleistocene systems and implications for the architecture of deepwater reservoirs. In: Weimer, P., Slatt, R.M., Coleman, J.L., Rosen, N., Nelson, C.H., Bouma, A.H., Styzen, M., Lawrence, D.T. (Eds.), Global Deep-Water Reservoirs: Gulf Coast Section SEPM Foundation 20th Annual Bob F. Perkins Research Conference, pp. 782–805.

Porobski, S.J., Steel, R. J., 2003. Shelf-margin deltas: their stratigraphic significance and relation to deepwater sands. Earth-Science Reviews 62, 283-326.

Porobski, S.J., Steel, R. J., 2006. Deltas and sea level change. J. Sedim. Research 76, 390-403.

Posamentier, H.W., Vail, P.R., 1988. Eustatic controls on clastic deposition: II. Sequences and systems tract model. In: Wilgus, C.K., Hastings, B.S., Kendall, C.G.St.C., Posamentier, H.W., Ross, C.A., Van Wagoner, J.C. (Eds.), Sea-Level Changes—An Integrated Approach. SEPM Special Publication, vol. 42, 125– 154.

Posamentier, H.W., Erskine, R.D., Mitchum R.M.J., 1991. Models for submarine-fan deposition within a sequence-stratigraphic framework. In: Weimaer, P., Link, M.H. (Eds), Seismic

Facies and Sedimentary Processes of Submarine Fans and Turbidite Systems. Springer-Verlag, New York, 127–136.

Posamentier, H.W., Allen, G.P., James, D.P., Tesson, M., 1992. Forced regressions in a sequence stratigraphic framework: concepts, examples, and exploration significance. Am. Assoc. Pet. Geol. Bull. 76 (11), 1687– 1709.

Posamentier, H.W., Allen, G.P. (Eds.), 1999. Siliciclastic Sequence Stratigraphy—Concepts and Applications. SEPM Concepts in Sedimentology and Paleontology, vol. 7. 216 pp.

Posamentier, H.W., Kolla, V., 2003. Seismic geomorphology and stratigraphy of depositional elements in deep-water settings. Journal of Sedimentary Research 73, 367–388.

Pratson, L.F., Coakley, B.J., 1996. A model for the headward erosion of submarine canyons induced by downslope-eroding sediment flows. Geol. Soc. Am. Bull. 108, 225–234.

Pratson, L.F., Nittrouer, C.A., Wiberg, P.L., Steckler, M.S., Swenson, J.B., Cacchione, D.A., Karson, J.A., Murray, A.B., Wolinsky, M.A., Gerber, T.P., Mullenbach, B. L., Spinelli, G.A., Fulthorpe, C. S., O'Grady, D.B., Parker, G., Driscoll, N.W., Burger, R.L., Paola, C., Orange, D.L., Field, M. E., Friedrichs, C.T., Fedele, J.J., 2007. Seascape evolution on clastic continental shelves and slopes. In: Nittrouer, C.A., Austin, J.A., Field, M.E., Kravitz, J.H., Syvitski, J.P.M., Wiberg, P.L., (Eds.), Continental margin sedimentation: From sediment transport to sequence stratigraphy, International Association of Sedimentologists Volume 37. Malden, Massachusetts, Blackwell Publishing, 339–380.

Prell,W. L., Hurso, W. H., Williams, D. F., Be', A.W.H., Geitzenauer, K., Molfino, B., 1980. Surface circulation of the Indian Ocean during the Last Glacial Maximum, approximately 18,000 yr B.P. Quaternary Research 14, 309-336.

Prell, W. L., Imbrie, J., Martinson, D. G., Morley, J. J., Pisias, N. G., Shackleton, N. J., Streeter, H. F., 1986. Graphic correlation of oxygen isotope stratigraphy application to the late Quaternary. Paleoceanography 1, 137– 162.

Preston, B.L., Suppiah, R., Macadamand, I., Bathols, J., 2006. Climate change in the Asia/Pacific region. Report prepared for the Climate Change and Development Roundtable, Commonwealth Scientific and Industrial Research Organisation, CSIRO Publishing, Collingwood, Victoria, 89 pp.

Puig, P., Ogston, A.S., Mullenbach, B.L., Nittrouer, C.A., Sternberg, R.W., 2003. Shelf-to-canyon sediment transport processes on the Eel continental margin (northern California). Mar. Geol. 193, 129–149.

Puig, P., Ogston, A.S., Mullenbach, B.L., Nittrouer, C.A., Parsons, J.D., Sternberg, R.W., 2004. Storm-induced sediment gravity flows at the head of the Eel submarine canyon, northern California margin. J. Geophys. Res., 109, C03019.

Ramaswamy, V., Rao, P.S., Rao, K.H., Thwin, S., Srinivasa Rao, N., Raiker, V., 2004. Tidal influence on suspended sediment distribution and dispersal in the northern Andaman Sea and Gulf of Martaban. Marine Geology 208, 33-42.

Rankey, E. C., Reeder, S. L., 2011. Holocene oolitic marine sand complexes of the Bahamas. Journal of Sedimentary Research 81, 97–117.

Reading, H. G., Richards, M., 1994. Turbidite systems in deep-water basin margins classi®ed by grain size and feeder system. Bull. Am. Ass. Petrol. Geol., 78, 792±822.

Reddy, P.R., Prasad, A.S.S.S.R.S., Sarkar, D., 1998. Velocity modelling of Bengal Basin refraction data—refinement using multiples. Journal of Applied Geophysics 39, 109–120.

Reddy, D.V , Nagabhushanam, P., Kumar, D., Sukhija, B.S., Thomas, P.J., Pandey, A. K., Sahoo, R.N., Ravi Prasad, G.V., Datta, K., 2009. The great 1950 Assam Earthquake revisited: Field evidences of liquefaction and search for paleoseismic events. Tectonophysics 474, 463-472.

Rennell J., 1786. F.R.S., late Surveyor Genl. in Bengal. London: printed for W. Faden, Geographer to the King, Charing Cross.

Ricci Lucchi F., 1980. Sedimentologia, vol.II. Processi e meccanismi. CLUEB Bologna, 2nd Ed, 210 pp.

Richards, J. F., Haynes, E. S., Hagen J. R., 1985. Changes in the land and human productivity in Northern India, 1870-1970. Agricultural History 59, 523-548.

Rogers, K.G., and Goodbred, S.L. Jr, 2010. Mass failures associated with the passage of a large tropical cyclone over the Swatch of No Ground submarine canyon (Bay of Bengal). Geology 38, 1051-1054.

Rossi, A., Massei, N., Laignel, B., Sebag, D., Copard, Y., 2009. The response of the Mississippi River to climate fluctuations and reservoir construction as indicated by wavelet analysis of streamflow and suspended-sediment load, 1950–1975, J. Hydrol., 377, 237–244.

Rothman, D.H., Grotzinger, J.P., and Flemings, P., 1994. Scaling in turbidite deposition. J. Sed. Res. 64, 59-67.

Roychoudhury, H.C., 1963. Physical and historical geography. In Majumdar ed.

Saito,Y., 2005. Mega-deltas inAsia: characteristics and human influences.Mega-Deltas of Asia: Geological Evolution and Human Impact, Z.Y. Chen, Y. Saito, S.L. Goodbred, Jr., Eds., China Ocean Press, Beijing, 1-8.

Schilling, K. E., Chan, K., Liu, H., Zhang, Y., 2010. Quantifying the effect of land use land cover change on increasing discharge in the Upper Mississippi River. J. Hydrol., 387, 343–345.

Schwenk, T.A., Spiess, V., 2009. Architecture and stratigraphy of the Bengal fan as response to tectonic and climatic revealed from high resolution seismic data. In: •Kneller, BC.,

McCaffrey, W. & Martinsen, O., (Eds.), External Controls on Deep-Water Depositional Systems, SEPM Special Publication No. 92, 107-131.

Schwenk, T., Spiess, V., Breitzke, M. & Hubscher, C., 2005. The architecture and evolution of the Middle Bengal Fan in vicinity of the active channel-levee system imaged by high-resolution seismic data. Marine Petroleum Geology 22, 637–656.

Seilacher, A., 1991. Events and their signatures-an overview. In: G. Einsele, W. Ricken and A. Seilacher (Eds.), Cycles and Events in Stratigraphy. Springer-Verlag, Berlin, 222-226.

Seilacher, A., Aigner, T., 1991. Storm deposition at the bed, facies, and basin scale: the geologic perspective. *In*: Einsele, G., Ricken, W., Seilacher, A., (Eds.), Cycles and Events in Stratigraphy. Springer-Verlag, Berlin, 249-267.

Shapiro, G. I., Huthnance, J. M., Ivanov, V. V., 2003. Dense water cascading off the continental shelf. J. Geophys. Res. 108, 3390,

Shepard, F.P., Dill, R.F., 1966. Submarine Canyons and Other Sea Valleys. Rand McNally, Chicago, p. 381.

Shetye, S.R., Shenoi, S.S.C. A., Gouveia, D., Michael, G.S., Sundar, D., Nampoothiri, G., 1991. Wind-driven coastal upwelling along the western boundary of the Bay of Bengal during the southwest monsoon. Continental Shelf Research 11, 1397-1408.

Shetye, S., Gouveia, A., Shankar, D., Shenoi, S., Vinayachandran, P., Sundar, D., Michael, G., Nampoothiri G., 1996. Hydrography and circulation in the western Bay of Bengal during the northeast monsoon. Journal of Geophysical Research 101, 14011-14026.

Shipboard Scientific Party, 1989b. Site 718: Bengal Fan. In Cochran, J. R., Stow, D.A.V., et al., Proc. ODP, Init. Repts., 116: College Station, TX (Ocean Drilling Program), 91-154.

Shipboard Scientific Party, 1989c. Site 719: Bengal Fan. In Cochran, J. R., Stow, D.A.V., et al., Proc. ODP, Init. Repts., 116: College, Station, TX (Ocean Drilling Program), 155-196.

Sloss, LL., 1950. Paleozoic stratigraphy in the Montanaa rea. Am. Assoc. Petrol. Geol. Bull.34:423-51

Sloss, L.L., 1962. Stratigrahic models in exploration. Journal of Sedimentary Petrology 32, 415-422.

Sloss, LL., 1963. Sequences in the cratonic interior of North America. Geol. soc. Am. Bull 74:93-114.

Socquet, A., Vigny, C., Chamot-Rooke, N., Simons, W., Rangin, C., Ambrosius, B., 2006. India and Sunda plates motion and deformation along their boundary in Myanmar determined by GPS. J. Geophys. Res. 111.

Sømme, T.O., Helland-Hansen, W., Granjeon, D., 2009. Impact of eustatic amplitude variations on shelf morphology, sediment dispersal, and sequence stratigraphic interpretation: Icehouse versus Greenhouse systems. Geology 37, 587-590.

Spieß, V., 1993. Digitale Sedimenttechographie - Neue Wege zu einer hochaufösenden Akustostratigraphie. Ber. Fachbereich Geowiss. Universität Bremen 35, 1–199.

Spieß, V., Hübscher, C., Breitzke, M., Böke, W., Krell, A., von Larcher, T., Matschkowski, T., Schwenk, T., Wessel A., Zühlsdorff, L., 1998. Report and preliminary results of R/V Sonne Cruise 125, Cochin—Chittagong, 17.10.–17.11.97. Berichte, Fachbereich Geowissenschaften, Universität Bremen, No. 123, 128 pp.

Springer, J., 1993. Decompaction and backstripping with regard to erosion, salt movent, and interlayering bedding. Computer and Geoscience 19, 1115-1125.

Stanley, D.J., Warne, A.G., (1994). Worldwide initiation of Holocene deltas by deceleration of sea-level rise. Science 265, 228–231.

Steckler, M.S., Watts, A.B., 1978. Subsidence of the Atlantic-type continental margin of New York. Earth Planet. Sci.Lett., 41, 1-13.

Steckler, M.S., Akhter, S.H., Seeber, L., 2008. Collision of the Ganges–Brahmaputra Delta with the Burma Arc: Implications for earthquake hazard. Earth and Planetary Science Letters 273, 367–378.

Steckler, M.S., Nooner, S.L., Akhter S.H., Chowdhury, S.K., Bettadpur, S., Seeber, L., Kogan, M.G., 2010. Modeling Earth deformation from monsoonal flooding in Bangladesh using hydrographic, GPS, and Gravity Recovery and Climate Experiment (GRACE) data. Journal of Geophysical research, 115, B08407.

Steel, R., Olsen, T., 2002. Clinoforms, Clinoform Trajectories and Deepwater Sands. In: Armentrout, J.M., Rosen, N.C., (eds.), Sequence Stratigraphic models for exploration and production: Evolving Methodology, Emerging Models and Application Histories. Special Publication GCS- Society of Economic Paleontologists and Mineralogists, 367-381.

Steel, R.J., Carvajal, C., Petter, A., Uroza, C., 2006. Shelf and shelf-margin growth in rising and falling sea-level scenarios. In: Hampson, G.J., Steel, R., Burgess, P., Dalrymple, R. (Eds.), Recent advances in shallow-marine stratigraphy. SEPM Special Publication.

Sternberg, R.W., Cacchione, D.A., Paulson, B., Kineke, G.C., Drake, D.E., 1996. Observations of sediment transport on the Amazon subaqueous delta. Continental Shelf Research 16, 697–715.

Stoll, H. M., Vance, D., Arevalos, A., 2006. Records of the Nd isotope composition of seawater from the Bay of Bengal: Implications for the impact of Northern Hemisphere cooling on ITCZ movement. Earth and Planetary Science Letters 255, 213–228.

Stow, D.A.V., Cochran, J. R., ODP Leg 116 Shipboard Scientific Party, 1989. The Bengal Fan: Some Preliminary Results from ODP Drilling. Geo-Marine Letters 9, 1-10.

Stow, D. A. V., Reading, H. G., Collinson, J. D., 1996. Deep seas. In: Reading, H.G., (Ed.), Sedimentary Environments, 3rd ed., Blackwell Science.

Syvitski, J.P.M., Hutton, E.W.H., 2001. 2D Sedflux 1.0. An advanced process–response numerical model for the fill of marine sedimentary basins. Comput. Geosci., 27, 731–754.

Syvitski, J.P.M., Kettner, A.J., Overeem, I., Hutton, E.W.H., Hannon, M.T., Brakenridge, J., Day, G.R., V¨or ¨ osmarty, C., Saito, Y., Giosan, L., Nicholls, R.J., 2009. Sinking deltas due to human activities. Nature Geoscience 2, 681–685.

Suckow, A., Morgenstern, U., Kudrass, H.-R., 2001. Absolute dating of recent sediments in the cyclone-influenced shelf area off Bangladesh: comparison of gamma spectrometric (137Cs, 210Pb, 228Ra) radiocarbon and 32Si ages. Radiocarbon 43, 917–927.

Swenson, J.B. , Paola, C., Pratson, L.F., Voller, V.R., Murray, A.B., 2005. Fluvial and marine controls on combined subaerial and subaqueous delta progradation: morphodynamic modeling of compound-clinoform development. Journal of Geophysical Research-Earth Surface, 110, F02013.

Sylvester, Z., LOWE, D.R., 2004. Textural trends in turbidites and slurry beds from the Oligocene flysch of the East Carpathians, Romania. Sedimentology 51, 945–972.

Tapponnier, P., Peltzer, G., Le Dain, A.Y., Armijo, R., Cobbold, P., 1982. Propagating extrusion tectonics in Asia: new insights from simple experiments with plasticine. Geology 10, 611–616.

Tapponnier, P., Peltzer, G., Armijo, R., 1986. On the mechanics of the collision between India and Asia. In: Coward, M.P., Ries, A.C. (Eds.), Collision Tectonics. Blackwell, Oxford, pp. 115–157.

Terzaghi, K., 1936. The shear resistance of saturated soils. Proceedings for the 1st. International Conference on Soil Mechanics and Foundation Engineering (Cambridge, MA), 1, 54 - 56.

Terzaghi, K., Peck, R.B., 1948. Soil Mechanics in Engineering Practice, John Wiley and Sons, New York.

Thanh, T.D., Saito, Y., Huy, D.V., Nguyen, V.L., Ta, T.K.O., Tateish, M., 2004. Regimes of human and climate impacts on coastal changes inVietnam. Reg. Environ. Change, 4, 49-62.

Thomas, A.L., Henderson, G.M., McCave, N. I., 2007. Constant bottom water flow into the Indian Ocean for the past 140 ka indicated by sediment 231Pa/230Th ratios. Paleoceanography 22, PA4210.

Tierney, J.E., Russell, J.M., Huang, Y., Sinninghe Damsté, J.S., Hopmans, E.C., Cohen, A.S., 2008. Northern Hemisphere Controls on Tropical Southeast African Climate During the Past 60,000 Years. Science 322, 252.255.

Turcotte, D.L., 1997. Fractals and chaos in geology and geophysics. 2nd edn, Cambridge University Press, pp 398.

Uddin, A., Lundberg, N., 1999. A paleo-Brahmaputra? Subsurface lithofacies analysis of Miocene deltaic sediments in the Himalayan-Bengal system, Bangladesh. Sed. Geol. 123, 239–254.

Uddin, A. & Lundberg, N., 2004. Miocene sedimentation and subsidence during continent-continent collision, Bengal Basin, Bangladesh. Sed. Geol., 164, 131–146.

Umitsu, M., 1993. Late Quaternary sedimentary environments and landforms in the Ganges delta. Sedimentary Geology 83, 177– 186.

Vail, P.R., Mitchum, R.M.J., Todd, R.G., Widmier, J.M., Thompson S.III, 1977. Seismic stratigraphy and global change of sea level. In: Payton C.E., (Ed) Seismic Stratigraphy-Applications to Hydrocarbon Exploration. Am. Assoc. Petrol. Geol. Mem. 26, 49-212

Van Wagoner JC, Posamentier HW, Mitchum RM Jr, Vail PR, Sarg JF, 1988. An overview of the fundamentals of sequence stratigraphy and key definitions. In: Wilgus, C.K., Hastings, B.S., Kendall, C.G.S.C., Posamentier, H.W., Ross, C A,, Van Wagoner, J.C. (Eds). Sea-Level Changes: An Integrated Approach. Soc. Econ. Paleontol. Mineral. Spec.Publ. No. 42., 39-45

Van Wagoner, J.C., Mitchum, R.M., Campion, K.M., Rahmanian, V.D., 1990. Siliciclastic sequence stratigraphy in well logs, cores, and outcrops. American Association of Petroleum Geologists Methods in Exploration Series 7 (55 pp.).

Veevers, J.J., 1982. Western and northwestern margin of Australia. In: Nairn, A.E.M., Stehli, F.G., (Eds.), The Ocean Basins and M. Alam et al. / Sedimentary Geology 155 (2003) 179–208 207 Margins: The Indian Ocean, vol. 6, Plenum Press, New York, pp. 513–544.

Versteegh, G.J.M., 2005. Solar Forcing of Climate. 2: Evidence from the past. Space Science Reviews 120, 243-286.

Vörösmarty, C. J. , Green, P., Salisbury, J., Lammers, R. B., 2000. Global Water Resources: Vulnerability from Climate Change and Population Growth. Science 289, 284-288.

Von Lom-Keil, H., Spiess, V., Gerriets, A., Schwenk, T., Zühldorff, L., Krastel, S., (2005). A very high resolution multichannel seismic system for operation in shallow marine evironments, lakes and rivers. Geophysical Research Abstracts, Vol. 7, 10279.

Walsh, J.P., Nittrouer, C.A., Palinkas, C.M., Ogston, A.S., Sternberg, R.W., Brunskill, ,G.J., 2004. Clinoform mechanics in the Gulf of Papua, New Guinea. Continental Shelf Research 24, 2487–2510.

Waelbroeck, C., Labeyrie, L., Michel, E., Duplessy, J.C., McManus, J.F., Lambeck, K., Balbon, E., Labracherie M., 2002: Sea-level and deep water temperature changes derived from benthonic foraminifera isotopic records. Quaternary Science Reviews 21, 295-305.

Wang, D., Cai, X., 2010. Comparative study of climate and human impacts on seasonal base flow in urban and agricultural watersheds. Geophys.Res. Lett., 37, L06406.

Wang, D., and Hejazi, M., 2011. Quantifying the relative contribution of the climate and direct human impacts on mean annual streamflow in the contiguous United States. Water Resource Research 47.

Wang, P., Clemens, S., Beaufort, L., Braconnot, P., Ganssen, G., Jian, Z., Kershaw, P., Sarnthein, M., 2005a. Evolution and variability of the Asian monsoon system: state of the art and outstanding issues. Quaternary Science Reviews 24, 595-629.

Wang, Y., Cheng, H., Edwards, R. L., He, Y., Kong, X., An, Z., Wu, J., Kelly, M. J., Dykoski, C. A., Li, X., 2005b. The Holocene Asian Monsoon: Links to Solar Changes and North Atlantic Climate. Science 308, 854-857.

Watts, A.B., Ryan, W.B.R., 1976. Flexure of the lithosphere at continental margin basins. Tectonophysics 36, 25–44.

Weaver, A.J., Saenko, O.A., Clark, P.U., Mitrovica, J.X., 2003. Meltwater pulse 1A from Antarctica as a trigger of the Bølling-Allerød warm interval. Science 299, 1709 – 1713.

Weber, M.E., Wiedicke, M.H., Kudrass, H.R., Hübscher, C., Erlenkeuser, H. 1997. Active growth of the Bengal Fan during sea-level rise and highstand. Geology 25, 315–318.

Webster, P. J., Holland, G. J., Curry, J. A., Chang H.-R., 2005. Changes in Tropical Cyclone Number, Duration, and Intensity in a Warming Environment. Science 309, 1844-1846.

Weedon, G., 2003. Time-Series Analysis and Cyclostratigraphy: Examining Stratigraphic records of Environmental Cycles. Cambridge University Press, pp 259.

Wheatcroft, R.A., Wiberg, P.L., Alexander, C.R., Bentley, S.J., Drake, D.E., Harris, C.K., Ogston, A.S., 2007. Post-depositional alteration and preservation of sedimentary strata. In: Nittrouer, C.A., Austin, J.A., Field, M.E., Kravitz, J.H., Syvitski, J.P.M., Wiberg, P.L., (Eds.), Continental margin sedimentation: From sediment transport to sequence stratigraphy, International Association of Sedimentologists Volume 37. Malden, Massachusetts, Blackwell Publishing, 101-155.

Weiskel, P. K., Vogel, R. M., Steeves, P. A., Zarriello, P. J., DeSimone, L. A., and Ries, K. G., 2007. Water use regimes: Characterizing direct human interaction with hydrologic systems. Water Resour. Res., 43, W04402.

Wiedicke, M., Kudrass, H.R., Hubscher, C., 1999. Oolitic beach barriers of the last Glacial sea-level lowstand at the outer Bengal shelf. Mar. Geol. 157, 7–18.

Wilgus, C.K., Hastings, B.S., Kendall, C.G.S.C., Posamentier, H.W., Ross, C A,, Van Wagoner, J.C., 1988. Sea-Level Changes: An Integrated Approach. Soc. Econ. Paleontol. Mineral. Spec.Publ. No. 42. 407 pp.

Wolanski, E., 2007: Protective functions of coastal forests and trees against natural hazards. Coastal protection in the aftermath of the Indian Ocean tsunami: what role for forests and trees? Proc. FAO Regional TechnicalWorkshop, Khao Lak, Thailand, 28-31August 2006. FAO, Bangkok.

Wolinsky, M.A., Pratson, L.F., 2007. Overpressure and slope stability in prograding clinoforms: Implications for marine morphodynamics. Journal of Geophysical Research, 112, F04011.

Woodroffe, C.D., Nicholls, R.J., Saito, Y., Chen, Z., Goodbred, S.L., 2006. Landscape variability and the response ofAsianmegadeltas to environmental change. Global Change and Integrated CoastalManagement: The Asia-Pacific Region, N. Harvey, Ed., Springer, 277-314.

Wright, L.D., Friedrichs, C.T., 2006. Gravity-driven sediment transport on continental shelves: A status report. Continental Shelf Research 26, 2092-2107.

Wynn, R.B., Cronin, B.T., Peakall, J., 2007. Sinuous deep-water channels: genesis, geometry and architecture. Marine and Petroleum Geology 24, 341e387.

Yilmaz, O., 1991. Seismic Data Processing, Soc. of Explor. Geophys., Tulsa.

Youngs, P., 2010. Provenance and Weathering of Holocene Ganges-Brahmaputra Sediments: Applications of Sr Geochemistry to Late Quaternary Delta Evolution. PhD Thesis, 142 pp.

Yuan, D., Cheng, H., Edwards, R.L., Dykoski, C.A., Kelly, M. J., Zhang, M., Qing, J., Lin, Y., Wang, Y., Wu, J., Dorale, J. A., An, Z., Cai, Y., 2004. Timing, Duration, and Transitions of the Last Interglacial Asian Monsoon. Science 304, 575-578